Volumetric Constitutive Behaviour of an Unsaturated Basaltic Expansive Clay Stabilised Using Lime

By

Asmaa Younus Al-Taie

A thesis submitted in total fulfilment of the requirements for the degree of Doctor of Philosophy

2018

Centre for Sustainable Infrastructure
Faculty of Science Engineering and Technology
Swinburne University of Technology, Melbourne, Australia

ABSTRACT

The constitutive volumetric behaviour, in terms of a void ratio (e)-moisture ratio (e_w)-net stress (σ) space, for a compacted untreated and lime-treated expansive clay was investigated. The studied expansive clay was a residual soil derived from a weathered Quaternary Basalt deposit located in the Victoria, Australia. Expansive soils, which are also referred to as unsaturated soils, moved from expansive clay to unsaturated soil display swelling or collapse behaviours relying on the state paths including loading-wetting-unloading. The Monash Peradeniya Kodikara (MPK) framework proposed by Kodikara (2012) describes the volumetric behaviour of unsaturated soil using void ratio-moisture ratio-net stress space. The virgin compression surface known as the Loading Wetting State Boundary Surface is established using traditional compaction curves. This framework suggests that moisture content is a practical approach in explaining most state paths relevant to practice, such as the deformation of clays under loading/unloading paths and wetting under constant stress. Therefore, this framework was adopted to describe the volumetric behaviour of an unsaturated compacted expansive clay, as well as an expansive clay stabilised with lime at the optimum lime content (OLC). The question raised in this research is whether collapse potential can be obtained in this condition, or whether the swelling potential will be close to zero if a soil is stabilised with lime at the OLC.

A suite of tests was conducted to investigate the behaviour of stabilised basaltic expansive clays, which were collected from Braybrook and Whittlesea sites (western and northern suburbs of Melbourne, Australia) over the curing period, and to find the OLC. These tests included determining the pH concentration at various curing periods, Atterberg limit, linear shrinkage strain, swelling potential, and Unconfined Compressive Strength (UCS). Furthermore, X-Ray Diffraction (XRD) and Scanning Electron Microscopy (SEM) tests were conducted to investigate the mechanism of soil–lime reaction. These test results indicated that the longer the curing time, the larger the drop in pH concentration. As ASTM-D6276 (1999) recommends using the method by Eades and Grim (1966) that relies on measuring the pH 1 hr after stabilisation (the curing time is neglected), a new method to determine the OLC for basaltic expansive clays was

proposed. The mechanism of lime stabilisation and the analysis of the above tests were the major factors in establishing this method. This method depends on measuring the pH concentration at different lime contents and curing periods.

To check the validity of the MPK framework on the untreated (Braybrook clay) and lime-treated clays, a comprehensive series of tests were performed on statically compacted soils. Firstly, the virgin compression surfaces in the e-e_w-σ space were generated for both soils by establishing the compaction curves at different net stress levels. Secondly, different state path tests were applied to investigate the volumetric behaviour of the untreated and lime-treated expansive clays for cycles such as loading-wetting, loading-wetting-loading, loading-unloading-wetting, and loading-unloading-wetting-unloading-wetting. Finally, collapse and swelling potential were measured using the one-dimensional deformation test. The results showed that the behaviour of all clay specimens tested followed the MPK framework proposed by Kodikara (2012). However, in this study, the MPK framework was found not to be valid for specimens prepared at very low moisture contents and compacted at low net stresses. For these samples, the virgin compression surface was found to be divided into two parts. Part A, where the MPK was valid and Part B, where the MPK did not extend. As a result of this finding, a new method was proposed to estimate collapse and swelling potential using the virgin compression surface. This study also concluded that the hydrated lime contributed to improving the collapsibility of the expansive clay specimens tested from very high to high collapsibility or from high to medium collapsibility. This means that the collapse potentials were significantly reduced after stabilisation and that these values should be considered. Additionally, a significant swelling occurred when the specimens were prepared at low moisture content and OLC.

Although suction is not essential for the practical application of the MPK framework in many scenarios, the suction profile within the $e-e_w-\sigma$ space is essential to complete the hydro-mechanical picture in the volumetric space. This extension will allow the development of constitutive models, as well as Soil Water Characteristic Curves (SWCC), to be more rational in the future. The Hyprop, filter paper and Chilled Mirror Hygrometer (WP4C) were all used to measure the SWCC at and below the virgin compression surface at different net stress levels for the untreated and lime-treated expansive clay samples.

Finally, to investigate the effect of the climate on the volumetric behaviour (long-term), a set of cycles of swell-shrink tests were conducted on the untreated and lime-stabilised expansive clays at different initial lime contents, moisture contents and net stress levels. The results showed that the maximum swelling occurred in the second cycle, when specimens were prepared with the OMC, MDD and lime contents less than the OLC. Thus, it is important to measure swelling from the first cycle, for short-term, to simulate the field condition after compaction. It is also important to consider the climate cycles to simulate the field condition for the long-term. However, for specimens prepared at the OLC and with moisture contents less than the OMC, the results showed that the maximum swelling occurred in the first cycle for all specimens tested. This suggests that the effect of the climate can be neglected for such design procedures.

ACKNOWLEDGMENT

Firstly, I would like to express my sincere gratitude to my supervisors, Dr. Mahdi Miri Disfani at the University of Melbourne and Dr. Robert Evans at the Swinburne University of Technology, for their constant support and for providing me with the opportunity to carry out this research and publish my findings in journals and conference papers. I am also indebted to my associate supervisors, Prof. Arul Arulrajah at the Swinburne University of Technology and Prof. Suksun Horpibulsuk at the Suranaree University of Technology, for their vital technical advice and invaluable support. Prof. Jayantha Kodikara from Monash University is acknowledged for the productive conversations we had during the review of some of the state path results and also for his insightful comments.

I would also like to extend my thanks to the University of Baghdad/ Department of Civil Engineering for giving me the opportunity to study at an advanced academic level through financial support from the Ministry of Higher Education.

I wish to give my best thanks to Mr. Alec Papanicolaou at the Swinburne University of Technology for his technical help and guidance in designing the complementary laboratory test devices successfully. My thanks are extended to Dr. Aruna Karunarathne, Dr. Hamed Haghighi and Mr. Farshid Maghoolpilehrood for their valuable assistance during my laboratory work. I would also like to give my thanks to my colleague Dr. Ehsan Yaghoubi for useful discussions to improve this work.

I am indebted to my husband (Muataz Al-Dabbagh) for his patience, encouragement, sacrifice and prayers for me. My grateful thanks are also extended to my mother, sisters (Wafaa, Warkaa, and Eanas), brother (Adil), my children (Shahad, Abdullah and Rowan) and my best friends, Dr. Balqees Abdulwahid Ahmed and Dr. Bushra Albusoda. They deserve special mention for their support, love and prayers throughout the course of my life.

Finally, I would like to thank everybody who was important in the successful realisation of this thesis.

DECLARATION

The candidate herein declares that the research work presented in this thesis contains no material that has been accepted for the award of any other degree or diploma in any university or other institutions. I affirm that to the best of my knowledge, the thesis contains no material previously published or written by another person, except where due reference is made in the text in the thesis.

Asmaa

Asmaa Younus Al-Taie

March 2018

PUBLICATIONS

The following papers were produced by the candidate and are based on the work presented in this thesis:

Journal Papers

- Al-Taie, A, Disfani, MM, Evans, R, Arulrajah, A & Horpibulsuk, S 2016, 'Swell-shrink Cycles of Lime Stabilised Expansive Subgrade', Procedia Engineering, vol. 143, pp. 615-622.

- Al-Taie, A, Disfani, M, Evans, R, Arulrajah, A & Horpibulsuk, S 2018, 'Impact of curing on behaviour of basaltic expansive clay', Road Materials and Pavement Design, vol. 19, No. 3, pp. 624-645, DOI: 10.1080/14680629.2016.1267660

- Al-Taie, A, Disfani, M, Evans, R, Arulrajah, A & Horpibulsuk, S, 'Volumetric Behavior and Soil Water Characteristic Curve of Untreated and Lime Stabilised Reactive Clay'. ASCE International Journal of Geomechanics, Accepted 31 July 2018. DOI: 10.1061/(ASCE)GM.1943-5622.0001336.

- Al-Taie, A, Disfani, M, Evans, R, & Arulrajah, A, 'Collapse and Swell of Lime Treated and Untreated Expansive Clays in Void Ratio-Moisture Ratio-Net Stress Space'. Submitted to ASCE International Journal of Geomechanics.

Conference Papers

- Al- Taie, AY, Disfani, MM, Evans, RP, Arulrajah, A & Horpibulsuk, S 2015, 'Determination of Optimum Lime Content for Volcanic Expansive Clays', From Fundamentals to Applications in Geotechnics: Proceedings of 15th Pan-American Conference on Soil Mechanics and Geotechnical Engineering (15th PCSMGE), Edited by Manzanal, D. and O.Sfriso, Alejo., Buenos Aires; Argentina; 15-18 November, pp. 1623-1630.

- Al-Taie, A, Disfani, M, Evans, R, Arulrajah, A & Horpibulsuk, S 2017., 'Collapse Prediction Using Static Compaction Curves for Untreated and Treated Basaltic Expansive Clays'. Proceedings of the First MoHESR and HCED Iraqi Scholars Conference in Australasia 2017, Melbourne, Australia, 5-6 December.

TABLE OF CONTENTS

LIST OF FIGURES

LIST OF TABLES

NOTATIONS AND ABBREVIATIONS

Notations

υ	specific volume
β	$(\frac{\partial e}{\partial w})$ at constant net stress
χ	Bishop's effective stress parameter
ξ	positive variable representing bonding effects due to suction
κ	slope of the unloading-reloading line
λ	slope of compression line
$\lambda(s)$	slope of compression line at specific suction
λ_0	gradient of compression line at e_w=e_{w0}
λ_1	compression index for saturated soil
λ_2	compression index for dry soil
$\lambda_{v\sigma}$	coefficient of compressibility
κ_s	stiffness parameter for changes in suction
G_s	specific gravity
H_0	Initial specimen height
h_0	osmotic suction
Pc_1	Preconsolidation pressure at initial condition
Pc_2	Preconsolidation pressure at saturation
ε_p	deviatoric strain
S_r	degree of saturation
e	void ratio
e_0	initial void ratio
e_0'	initial void ratio at σ, e_{w0} and S_r
e_0^*	void ratio under nominal stress for dry soil
$e_0^{*\prime}$	initial void ratio at σ= σ_i , e_{w0} ($e_{w0} < e_{w0i}^*$)
e_{com}	void ratio at a certain compaction stress
e_{cs}	critical void ratio
e_{omc}	void ratio of a specimen compacted at an optimum moisture content
e_s	void ratio at saturation under net stress σ

e_s'	void ratio on NCL and at stress σ
e_{s0}	void ratio at saturation under nominal stress
e_{so}^*	void ratio on NCL and at stress σ_i
e_w	moisture ratio
e_{w0}	initial moisture ratio
e_{w0}	initial moisture ratio at σ and S_r
e_{w0i}^*	moisture ratio at S_r and $\sigma = \sigma_i$
e_{wi}	initial moisture ratio
u_a	pore air pressure
u_w	pore water pressure
γ_d	unit weight of dry soil
γ_ω	unit weight of water
δ_h	Kronecker's delta
σ	net stress
σ'	effective stress
σ_h	total stress
σ^c	reference stress state
σ_i	nominal stress in modified MPK
σ_m	mean stress
ΔH	change in height due to swelling or shrinkage
a, b, a^*, b^*, $e_r{}^*$, m^*, $\emptyset$, d, f, g, h, c	fitting parameters
N(s)	specific volume at reference net stress
Pc	compaction stress
q	deviatoric stress
R	gas constant
T	absolute temperature
φ	model parameter in compaction curve equation
M	slope of the critical state line
W	rate of work input per unit volume
$d\varepsilon_v$	volumetric strain
n	porosity

s	suction
w	gravimetric moisture content
α	hydric coefficient $\left(\frac{\partial e}{\partial e_w}\right)$ at constant net stress
ψ	total suction

Abbreviations

AS	Australian Standards
ASCE	American Society of Civil Engineers
ASTM	American Society for Testing and Materials
BBM	Barcelona Basic Model
CAH	Calcium Aluminate Hydrate
CEC	Cation Exchange Capacity
CH	Clay of high plasticity
CH-MH	Silty Clay-Clayey Silt with high plasticity
CRT	Cathode Ray Tube
CSH	Calcium Silicate Hydrate
LC	Loading Collapse
LEED	Low Energy Electron Diffraction
LL	Liquid Limit
LOO	Line of Optimum
LS	Linear Shrinkage
LUW	Loading-Unloading-Wetting
LUWUW	Loading-Unloading-Wetting-Unloading-Wetting
LV	constant void ratio line
LW	Loading-Wetting
LWL	Loading-Wetting -Loading
LWSBS	Loading Wetting State Boundary Surface
MC	Moisture content
MDD	Maximum Dry Density
MPK	Monash-Peradeniya-Kodikara
NCL	Normally Consolidated Line

OLC	Optimum Lime Content
OMC	Optimum Moisture Content
PI	Plasticity Index
PL	Plastic Limit
RH	Relative Humidity
SEM	Scanning Electron Microscopy
SFG	Sheng Fredlund Gens
SWCC	Soil Water Characteristic Curve
USC	Unconfined Compressive Strength
XRD	X-Ray Diffraction

CHAPTER 1. **INTRODUCTION**

1.1 Problem Statement

The performance of lightly loaded foundations on expansive clays has been an ongoing challenge for geotechnical engineers, as these soils experience significant volume change in response to changes in soil moisture content. This volume change occurs as swelling or collapse during wetting, or shrinkage during drying. Considerable ground movements can arise from non-uniform soil moisture changes, which can lead to cracking and damage (Houston et al. 2001; Li & Cameron 2002). Approximately 20 per cent of the surface soils in Australia can be categorised as moderate to highly expansive (Richards et al. 1983), with approximately 50 per cent of the surface soils in Victoria falling under this expansive category (Northcote 1962). Such soils are mainly distributed in the west part of Melbourne (Karunarathne et al. 2014a).

Different methods are available to stabilise the engineering properties of problematic soils. These include adding chemicals to the soil, pre-wetting the soil, moisture control techniques, surcharge loading thermal methods, reinforcement, and replacement of the soil with compaction control (Muhmed & Wanatowski 2013; Nelson & Miller 1992). Additives are commonly used to enhance the performance of expansive clays, which include salt, polymers, cement, lime, fly ash and, in some cases, a mixture of these additives. Lime has been more commonly used to reduce swelling and improve the workability of the soil. Furthermore, it is economical and is widely available in many parts of the world (Al-Mukhtar et al. 2012). Lime can be applied either in the form of quicklime (CaO) or hydrated lime ($Ca(OH)_2$) (Zhao et al. 2014b).

The optimum lime content (OLC) is a concept extensively applied to the lime stabilisation design of soils in the road-building industry. ASTM-D6276 (1999) recommends using the method by Eades and Grim (1966), which depends on measuring the pH 1 hr after stabilisation. This method has been adopted and followed in many studies (Al-Mukhtar et al. 2012; Ciancio et al. 2014; Ismaiel 2006; Little 1999; Manasseh & Olufemi 2008; Muhmed & Wanatowski 2013; Saride et al. 2013).

However, this method does not consider the time effect of curing, which causes a reduction in pH concentration over time. Therefore, there is merit in pursuing research that takes into account the effect of curing on estimating the OLC.

Several studies have investigated the importance of using lime as a binder to change the properties of expansive soils, including a reduction in plasticity, swelling and collapse potential, and an increase in shear strength. However, the majority of these studies, which confirm the suitability of lime in reducing swell potential and increasing soil strength, obtain their results from samples prepared at Optimum Moisture Content (OMC) and Maximum Dry Density (MDD) (Al-Mukhtar et al. 2012; Bell 1996; Ciancio et al. 2014; de Brito Galvão et al. 2004; Elkady 2015; Gueddouda et al. 2011; Huat et al. 2005; Manasseh & Olufemi 2008; Ramesh et al. 2012; Saride et al. 2013; Schanz & Elsawy 2015; Zhao et al. 2014b). At these conditions, the main limitation is that the soil's behaviour on the dry side of OMC (unsaturated zone) and the behaviour of the lime-stabilised soil under different operational stresses are not considered. The question raised here is whether collapse potential can be obtained in this condition, or whether the swelling potential will be close to zero if a soil is stabilised with lime at the OLC and prepared at a lower moisture content than optimum. Some studies have considered a certain state located at the dry side of the OMC (Al-Rawas et al. 2005; de Brito Galvão et al. 2004), but the question remains whether results obtained for one particular state of unsaturated soil condition can represent the behaviour of unsaturated soil at different moisture contents and operational stresses. To explain the volumetric behaviour of unsaturated compacted soil stabilised with lime, it is important to select a relevant constitutive model.

Soil mechanics can be divided into saturated and unsaturated soil mechanics (Fredlund & Rahardjo 1993). Soils commonly found in nature are unsaturated. Unsaturated soil behaviour is more complicated, and the ability to model this behaviour is still under development. The cost of not considering this behaviour in reference to light structures is significant. In the USA alone, the total damage has been estimated to be $U15 billion per year (Jones & Jefferson 2012), which is more than twice the damage caused by floods, hurricanes, tornadoes and earthquakes combined. Most of these damages are caused by the response of unsaturated soil to the wetting or drying path. Therefore, over the past half century, numerous studies have focused on modelling the hydromechanical behaviour of unsaturated soil (Alonso et al. 1990; Bishop 1959; Fredlund & Morgenstern 1976; Gallipoli et al. 2003a; Khalili et al. 2000; Lloret et al. 2003; Matyas & Radhakrishna 1968; Sivakumar & Wheeler 2000; Wheeler et al. 2003; Wheeler & Sivakumar 1995). These studies have used suction, defined as the difference between pore air pressure and pore water pressure at the water meniscus, to express the effective stress that dominates the behaviour of the unsaturated soil. However, it is very difficult to measure suction accurately in the laboratory, as well as in the field. Therefore, there exists a significant gap between developed theoretical models and their practical applications. It has been recently suggested that in describing the behaviour of an unsaturated soil, evaluating only the suction parameter is not enough; a moisture content or a degree of saturation parameter needs to be incorporated into the constitutive modelling, usually referred to as hydromechanical coupling (Islam 2015; Kodikara 2012). Thus, researchers have attempted to incorporate the hydromechanical coupling in constitutive models in an attempt to make unsaturated soil models more practical (Islam & Kodikara 2015; Kodikara 2012).

Kodikara (2012) suggested a new framework called the Monash-Peradeniya-Kodikara (MPK) framework to interpret the volumetric behaviour of unsaturated compacted soils. This framework deals with net stress (σ), void ratio (e), and moisture ratio ($e_w = w \times G_s$, where w is gravimetric moisture content and G_s is specific gravity). A significant feature of the MPK framework is the generation of a direct relationship between traditional compaction curves and the constitutive deformation behaviour of soil. In principle, any variable with the potential for considerable effect on the mechanical behaviour can be taken as a state variable (Lu 2008). Thus, both suction and moisture content could be considered a state variable, since these could influence the volume change of soils (Fredlund & Rahardjo 1993). In this model, the suction parameter is used as the fourth variable, and it is a dependent variable on moisture content. The MPK framework suggests that moisture content is a practical approach in explaining most state paths relevant to practice, such as the deformation of soil under loading/unloading path, wetting under constant stress, and deformation resulting from swell-shrink cycles (environmental stabilisation of soil) (Kodikara et al. 2014). For example, for compacted fills, suction is important in identifying and measuring collapse potential caused by a reduction in suction throughout the project life. As most field requests are based on moisture content, which geotechnical engineers commonly, there are merits in pursuing practical approaches to field analysis and design while avoiding the use of more complicated suction parameters. However, it is important to mention that suction controls the behaviour of an unsaturated soil and cannot be neglected, especially for unsaturated water flow conditions (such as slope stability applications). Using suction as potential in the water flow equation is necessary; however, the water flow that uses the moisture diffusivity as well can be modelled where the entire equation is written using water content without suction. One limitation of this approach is that only single materials can be modelled, since the interface between two materials (like clay and sand) will have the same suction but not the same water content. Therefore, the Soil Water Characteristic Curve (SWCC) will be necessary if two layers using the water diffusion equation are needing to be modelled. The MPK theory is not a complete theory when suction is not considered, but ignoring it is not theoretically incorrect. It makes only a partial theory. In fact, the MPK directly considers hydro-mechanical coupling by directly getting moisture ratio without going through suction. In more so-called “complete” models, it is necessary to go through the SWCC to couple water content through suction. Advocating the usage of the moisture ratio does not undermine the work that can be done on hysteresis with suction, but it is important to develop a method where some difficulties can be avoided. The question raised is whether the MPK framework can be applied to explain the volumetric behaviour of lime-stabilised soil, particularly if a soil is stabilised with lime at the OLC.

This research investigates the effect of curing on estimating the OLC for basaltic expansive clay. The OLC based on swelling potential is selected to study the volumetric behaviour of lime-stabilised clay. To explain the volumetric behaviour, the MPK framework proposed by Kodikara (2012) is adopted and the incorporation of the role of suction within the framework is investigated. This study considers the behaviour of unsaturated soil at different moisture contents and operational stresses. Furthermore, the deformation of stabilised clay is addressed in the short- and long-term. The short-term represents the volumetric behaviour of stabilised clay immediately after compaction, whereas the long-term represents the volumetric behaviour of environmentally-stabilised soil, which is achieved when the soil has been exposed to an adequate number of wet-dry cycles and reaches a stable soil structure. Finally, if the framework proposed by Kodikara (2012) is found not to be valid in describing the volumetric behaviour of unsaturated stabilised clay, a new model will be investigated.

1.2 Research Aim and Scope

The aim of this research project is to enhance the understanding of the volumetric behaviour of an unsaturated expansive clay after lime stabilisation by using net stress, void ratio and moisture ratio, and by using the parameter of suction as a dependent variable on moisture ratio. In this study, the MPK framework, proposed by Kodikara (2012), was adopted as the starting point for developing a new model.

1.3 Research Objectives

To achieve the aim of this study, four main objectives were programmed, as shown in **Figure 1.1**:

- The first objective included measuring the optimum lime content for expansive clays according to swelling potential. To achieve this objective, an extensive suite of laboratory tests, including conventional classification, deformation and soil strength tests, accompanied by pH measurement, X-Ray Diffraction (XRD) and Scanning Electron Microscopy (SEM), were performed on treated and untreated samples.

- The second objective included the application of the MPK framework on untreated and treated clay to assess the framework's validity. To achieve this objective, the following goals were set:
  - Loading Wetting State Boundary Surface (LWSBS) is generated for both untreated and treated specimens by establishing the compaction curves at different stresses. Each curve was developed by using the static compaction test.

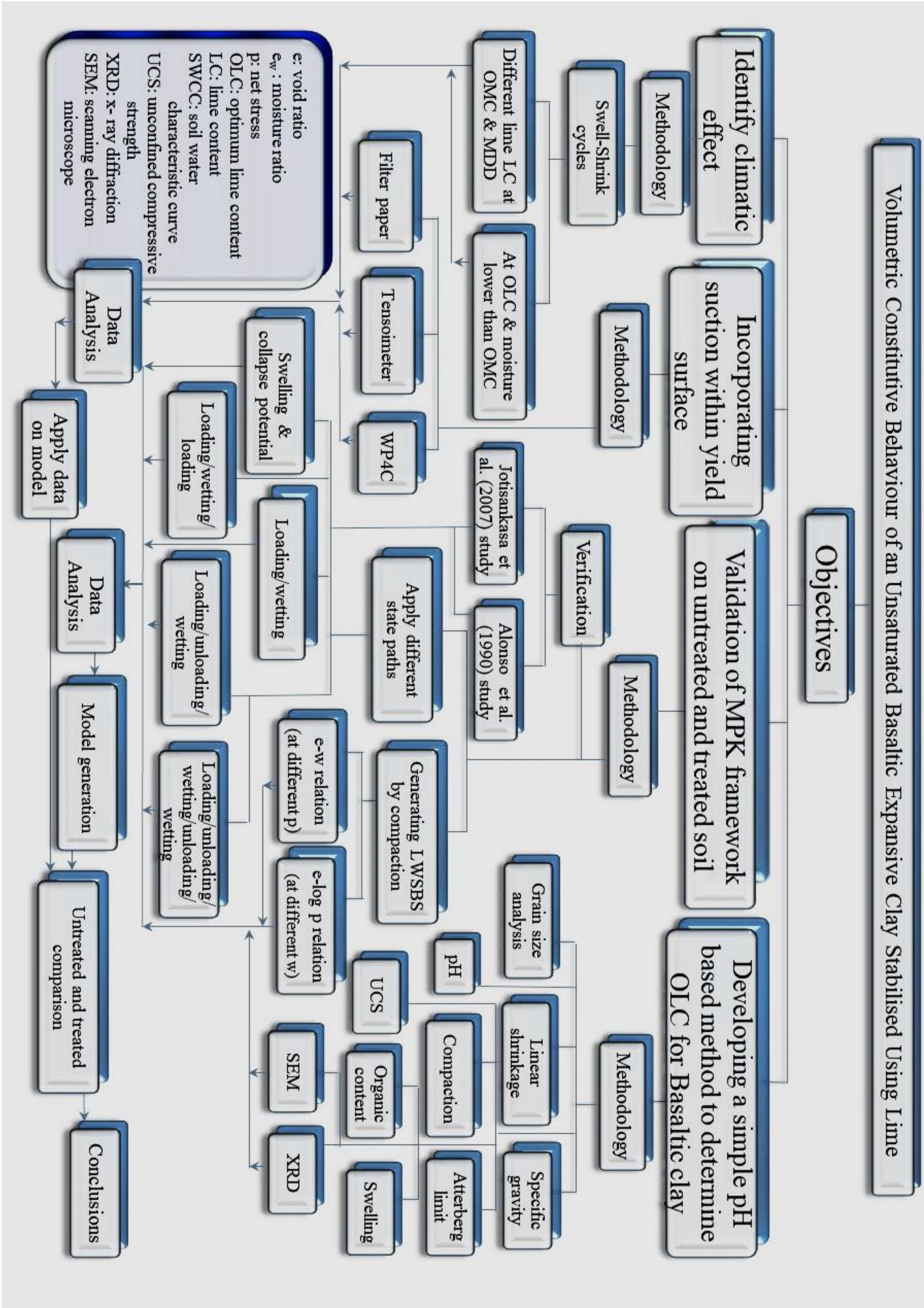

Figure 1.1. Research program

- Different state path tests, such as loading-wetting, loading-wetting-loading, loading-unloading-wetting, loading-unloading-wetting-unloading-wetting, collapse potential and swelling potential were conducted.
- Results from studies, such as Jotisankasa et al. (2007), were applied to the MPK framework. Furthermore, the theory of swelling and collapse according to Kodikara's model (2012) was applied to the study achieved by Alonso et al. (1990).

- The third objective included incorporating suction within the proposed model by investigation of the Soil Water Characteristic Curve (SWCC) at and below the LWSBS for both untreated and treated expansive clay. To achieve this objective, tensiometers (Hyprop), filter paper and a chilled mirror hygrometer (WP4C) were used.
- The fourth objective included identification of the behaviour of compacted lime-stabilised expansive soil under cycles of swell-shrink (climatic effect). To achieve this objective, two sets of specimens were prepared based on initial moisture content and dry density. The first set included specimens at different lime contents that were compacted at optimum moisture content and maximum dry density and subjected to cycles of swell and shrink tests. The second set included specimens at optimum lime content that were compacted at moisture content lower than the optimum.

1.4 Overview of the Thesis

This thesis is divided into eight chapters. A brief description of each chapter is described in the next paragraphs:

Chapter One focuses on the problem statement of unsaturated expansive clay, the behaviour of stabilised expansive clays, and progress achieved via the MPK framework by Kodikara (2012), and outlines the aim and objectives of the current research.

Chapter Two is a literature review that focuses on the history of expansive soil problems and previous studies that have used lime to enhance the engineering properties of these type of soils. Furthermore, a brief review on constitutive models describing the volumetric behaviour of unsaturated soils is provided. These constitutive models include constitutive models based on net stress and suction: the Barcelona Basic Model (BBM), the effective stress model, the Sheng Fredlund Gens (SFG) model, and a new framework called Monash Peradeniya Kodikara (MPK) proposed by Kodikara (2012). This framework uses void ratio, moisture ratio, and net stress as main variables, and uses suction as a dependent variable of moisture content. As this thesis adopts the MPK framework to describe the volumetric behaviour of unsaturated stabilised compacted clay using lime, this chapter focuses on an explanation of the concept of the Kodikara (2012) model. Because a suction parameter is considered a dependent variable of moisture content, the Soil Water Characteristic Curve (SWCC) is studied. Furthermore, the behaviour of compacted expansive clay under swell-shrink cycles in the literature has been reviewed.

In Chapter Three, the site description, soil preparation, preliminary soil tests, experimental apparatus and procedures employed to achieve the aim of this research have been described. It includes a series of tests that were conducted to determine the optimum lime content (i.e. specific gravity, organic content, grain size analysis, Atterberg limits, linear shrinkage, pH concentration, standard Proctor compaction, Unconfined Compressive Strength (UCS), swelling potential, X-Ray Diffraction (XRD), and Scanning Electron Microscopy (SEM)). To investigate the volume behaviour of unsaturated compacted expansive clay and stabilised expansive clay with lime, static compaction and different state path tests were conducted. To study the Soil Water Characteristic Curve (SWCC) for the untreated and treated clay, a tensiometer (Hyprop), filter paper and a chilled mirror hygrometer (WP4C) were used. To identify the climatic effect, cycles of swell-shrink tests were conducted. These test methodologies are explained in this chapter.

Chapter Four investigates the effect of curing on determining the Optimum Lime Content (OLC) for the stabilised basaltic expansive clay (i.e. taking curing time and drop in pH content into account). A new method to measure the OLC for basaltic expansive clays is suggested. This new method depends on measuring pH concentration at different lime contents and curing periods. The results contribute to a better understanding of the impact of curing and low levels of organic matters in the stabilisation of expansive clays, which can ultimately lead to a simplified procedure in the determination of the optimum lime content.

Chapter Five presents the volumetric behaviour of the compacted expansive and lime-treated expansive clay. The optimum lime content, according to swelling potential, was selected to investigate the volumetric behaviour of unsaturated treated clay. Initially, the validation of the MPK model on untreated and treated clay was examined by applying different state path tests. Swelling and collapse potential was tested under a wide range of moisture contents and stress levels. Moreover, the effect of stress history and operational stress on swelling and collapse values is presented. The volumetric behaviour of the unsaturated clay between untreated and lime-treated clay was compared. Furthermore, this chapter includes the application of results from studies, such as Jotisankasa et al. (2007), on the MPK framework. The theory of swelling and collapse according to Kodikara's model (2012) was also applied to previous studies, such as the study achieved by Alonso et al. (1990).

In Chapter Six, the influence of lime stabilisation of an expansive clay soil based on volumetric behaviour and the Soil Water Characteristic Curve (SWCC) is studied. The SWCC is investigated at and below the yield surface that was proposed by Kodikara (2012). To obtain the SWCC at the yield surface, suction values were measured under a compression pressure (preconsolidation pressure) at different moisture ratios, while the SWCC below the yield surface was obtained by measuring suction values under a stress level lower than the compression pressure (unloading zone) at different moisture ratios.

Chapter Seven describes the behaviour of lime-stabilised and compacted expansive soils under cycles of swell-shrink (climatic effect). To achieve this objective, two sets of specimens were prepared based on the initial moisture content and dry density. The first set included specimens with different lime content that were compacted at the optimum moisture content and maximum dry density and then subjected to cycles of swell and shrink tests. The second set included specimens, at the optimum lime content, compacted at a moisture content lower than the optimum moisture content.

Chapter Eight presents the outcomes of the current research program and lists recommendations for future work.

CHAPTER 2. **LITERATURE REVIEW**

To interpret the volumetric behaviour of unsaturated basaltic expansive clays stabilised with lime, it is important to review the history of expansive soil problems and previous studies that focus on using lime to reduce their swelling and collapse behaviours. Furthermore, a brief review of constitutive models to describe the volumetric behaviour of unsaturated soils needs to be considered.

2.1 Introduction

This chapter presents a historical review of expansive soil problems that typically lead to extensive damage in road pavements and lightly loaded structures. Subsequently, it has become important to consider and overcome this problem. Therefore, this chapter reviews expansive soil stabilisation techniques that focus specifically on chemical stabilisation using lime and the mechanism of reaction between lime and clay. It also provides a brief review of the constitutive models representing the volumetric behaviour of unsaturated soils. These constitutive models include those based on net stress and suction: the Barcelona Basic Model (BBM), the effective stress model, the Sheng Fredlund Gens (SFG) model, and a new framework called the Monash Peradeniya Kodikara (MPK) proposed by Kodikara (2012). This new framework uses void ratio, moisture ratio, and net stress as main variables, and uses suction as a dependent variable of moisture content. As this thesis has adopted the MPK framework to describe the volumetric behaviour of unsaturated stabilised compacted clay (using lime), the concept of the Kodikara (2012) model has been explained in detail. In addition, this chapter presents the Soil Water Characteristic Curve (SWCC), which represents the relationship between suction and moisture content. Furthermore, the behaviour of compacted expansive clay under swell-shrink cycles has also been addressed.

2.2 Expansive Soil

Expansive clay minerals typically swell (increase in volume) when water is absorbed by the clay mineral, and shrink (decrease in volume) when water is evaporated (Chen 1998; Delaney et al. 2005; Kerrane 2005; Nelson & Miller 1992; Seco et al. 2011). This volume change can lead to widespread foundation and dam problems (Avsar et al. 2009; Chen 2015; Ferber et al. 2009; Langroudi & Yasrobi 2009).

The extent of the expansive soil problem was first noticed in the U.S. in 1938 (Chen 2012), when new typical brick dwellings started to replace older and more flexible framed residential dwellings. Expansive soils are common in countries such as Australia, China, USA, the United Kingdom, Canada, India, South Africa and Mexico (Chen 1998). In the USA alone, the total damage created by these swelling and shrinkage soils is estimated to cost $U15 billion per year, which is more than twice the damage due to floods, hurricanes, tornadoes and earthquakes in the USA combined (Jones & Jefferson 2012; Kerrane 2005). The annual cost of expansive soil destruction in China has also been assessed to be approximately $U15 billion. According to the United Kingdom, the total damage is estimated to be over £400 million per year (Li et al. 2014). In Australia, approximately 20 per cent of its area is covered with reactive soil (Cameron & Walsh 1997; Li et al. 2014; Richards et al. 1983), and six out of eight of Australia’s largest cities are seriously affected by reactive soil (Delaney et al. 2005; Fityus et al. 2004). A map of the distribution of moderately to highly expansive soils in Australia is shown in **Figure 2.1**.

The problem of expansive soils is caused by moisture content fluctuation in the upper few meters. The moisture content in these upper layers is influenced by climatic and environmental conditions. This zone is generally called either the zone of seasonal fluctuation or the active zone. The distribution of moisture content in the active zone is shown in **Figure 2.2** (Nelson & Miller 1992).

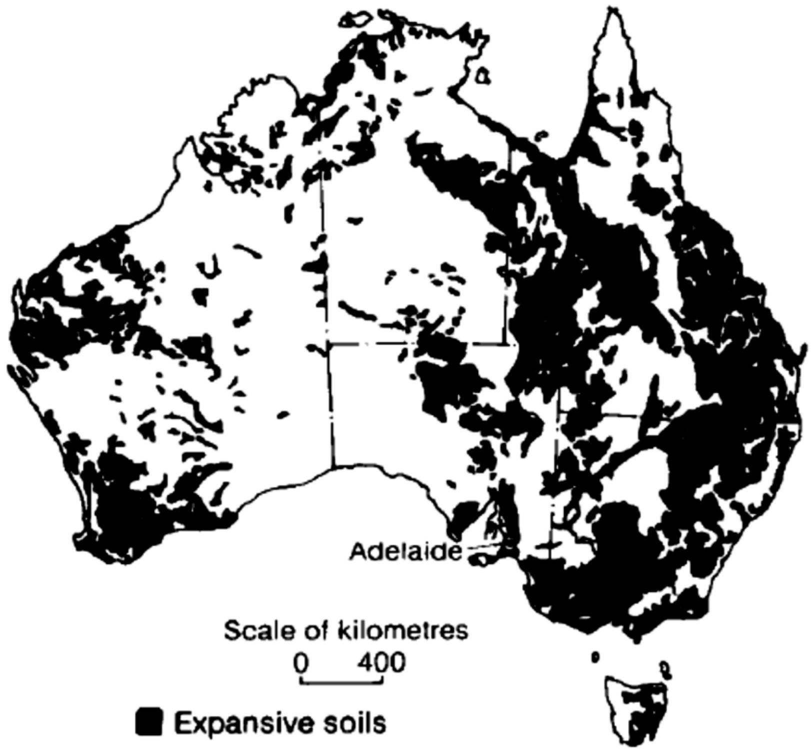

Figure 2.1. Distribution of moderately to highly expansive soils in Australia (Richards et al. 1983)

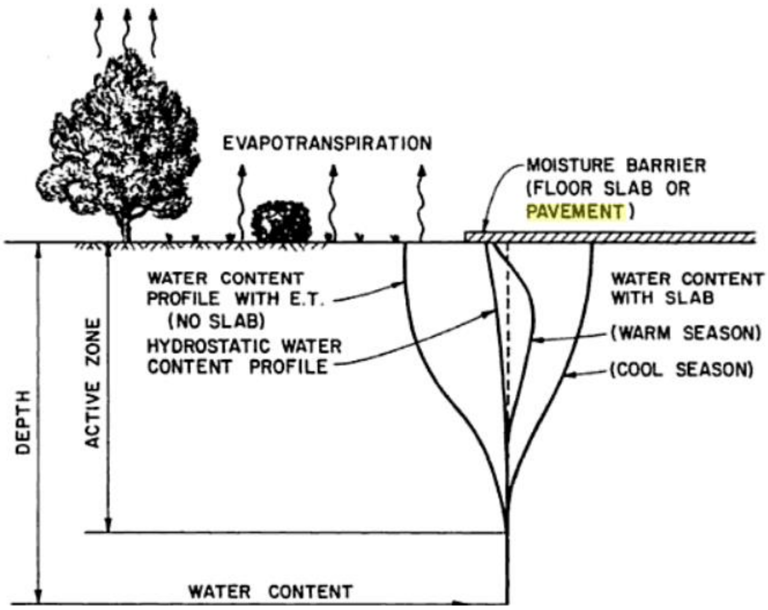

Figure 2.2. Moisture content profile in the active zone (Nelson & Miller 1992)

In this zone, negative pore water pressures exist, but if excess water is added to the surface, moisture contents increase and swelling will occur. Therefore, it is important to identify the depth of the active zone through a site investigation. The depth can change significantly with climate conditions, with depths of 5 to 6m in some countries; however, this depth is reduced in the UK to be 1.5 to 2m (Jones & Jefferson 2012).

Chen (1998) and Chen (2012) claimed that there are three methods to classify the reactivity potential of an expansive soil. These are mineralogical identification, indirect methods and direct measurement. The mineralogical composition of expansive soils has a significant influence on the swelling potential. There are three factors that contribute to the swelling potential. These factors include a negative electric charge on the surface of the clay minerals, the interlayer bond strength, and the cation exchange capacity (CEC). Through the identification of the basic minerals of a soil, the swelling potential can be evaluated. X-ray diffraction, differential thermal analysis, chemical analysis, and electron microscope resolution are techniques that are used to identify the mineralogy of expansive soils.

Indirect methods to classify the reactivity potential of an expansive soil include index properties and activity methods. Nelson and Miller (1992) proposed that index properties include grain size distribution, clay content, and plasticity indices. Atterberg limits can be defined as moisture content boundaries between states of the texture of fine-grained soils.

The most important and reliable method to classify the reactivity potential of an expansive soil is the direct measurement method. This method can be achieved by using the conventional one-dimensional consolidation test.

2.3 Chemical Stabilisation of Expansive Soil

Due to the extensive and continued seasonal damage caused by expansive clays, it has become increasingly important to routinely consider the pressure of expansive soils in the design and construction of road pavements. A range of methods are available (and commonly applied) to reduce the severity of the damage, which includes using chemical additives, prewetting the soil, moisture control techniques, and replacement of soil with compaction control (Muhmed & Wanatowski 2013; Nelson et al. 2015; Nelson & Miller 1992).

Chemical additives can be divided into two groups, including traditional and non-traditional materials. Traditional materials, such as lime, cement, and fly ash, depend mainly on calcium exchange and pozzolanic reactions to effect treatment. Alternatively, non-traditional materials, such as potassium compounds, sulfonated oils, and others, depend on different proprietary and unpublished chemical reactions. Prewetting of expansive soils has been applied with varying levels of success to decrease the expansive potential; recently, it has been used less frequently. This method considers that increasing moisture content in the expansive foundation soils will cause swelling to occur prior to construction. Moisture content control techniques must also be considered, as expansion is due to an increase in moisture content. In order to avoid swelling problems, moisture content would have to be controlled within the soil. However, it is practically impossible to prevent an increase in moisture content of the foundation soils after site development. Nevertheless, it is possible to exercise some control over the rate of increase and the magnitude of seasonal fluctuation. Replacement of soil with compaction control has been used to reduce swelling under a foundation or subgrade. However, there are factors that should be considered when applying this method, including the required depth of removal, and the amount, location, and cost of the fill (Nelson et al. 2015).

Lime and cement are the two most commonly used additives to chemically stabilise an expansive soil (Horpibulsuk et al. 2013; Kampala et al. 2014; Liu et al. 2012; Saride et al. 2013; Seco et al. 2011). Among these two, lime is more widely used for reducing the swelling potential of expansive soils (Al-Rawas et al. 2005), while cement is primarily used when seeking improvement in strength (Liu et al. 2011; Yong & Ouhadi 2007). Fly ash is also used in a wide range of treatment applications to reduce the swelling potential of highly plastic clay soils (Nalbantoğlu 2004; Sharp et al. 1993). Other chemical additives that have been used to stabilise expansive soil are geopolymer-fly ash (Nalbantoğlu 2004; Nalbantoglu & Gucbilmez 2001; Sukmak et al. 2013a; Sukmak et al. 2013b), polypropylene fibre (Cai et al. 2006), rice husk ash (Basha et al. 2005; Seco et al. 2011), burned olive waste (Attom & Al-Sharif 1998), geofiber (Viswanadham et al. 2009), gypsum (Seco et al. 2011; Yilmaz & Civelekoglu 2009) and hay (Mohamed 2013). All of these additives have demonstrated a notable increase in the strength of soils and decrease in swelling potential.

2.3.1 Chemical Stabilisation Using Lime

Lime has been used successfully on many projects throughout history to reduce swelling and enhance soil plasticity and workability. For example, in ancient Mesopotamia, Egypt, Greece, lime was used to stabilise earth roads (McDowell 1959). Clare and Cruchley (1957) mentioned that the first tests including soil stabilisation with lime were performed in the United States in 1904. With the growth of motor traffic in the 1930s, the use of stabilisation of soils started to increase. Currently, lime stabilisation is a technique widely used to improve soil properties throughout the world (Du et al. 1999). It is used in road construction, for rail and airport construction, for embankments, as soil exchange in unstable slopes, and as backfill for bridge abutments and retaining walls (Bell 1996).

Several studies have investigated the importance of using lime as a binder to improve the expansive soil properties, including a reduction in plasticity index, swelling and collapse potential, and an increase in shear strength. However, the majority of these studies that have confirmed the suitability of lime in reducing the swelling potential and increasing the soil strength obtained their results from samples prepared at the Optimum Moisture Content (OMC) and Maximum Dry Density (MDD) (Al-Mukhtar et al. 2012; Bell 1996; Ciancio et al. 2014; de Brito Galvão et al. 2004; Elkady 2015; Gueddouda et al. 2011; Huat et al. 2005; Manasseh & Olufemi 2008; Ramesh et al. 2012; Saride et al. 2013; Schanz & Elsawy 2015; Zhao et al. 2014b). However, at this condition, the behaviour of the dry side of the OMC (unsaturated zone) and behaviour of lime-stabilised soil under different operational stresses have not been considered. Al-Rawas et al. (2005) investigated the effect of lime on the swelling potential of expansive soil from Oman. In the study, the remoulded samples were prepared at natural water content and field dry unit weight to simulate the field condition. However, as these samples were remoulded, the behaviour of these remoulded soils was different to undisturbed soils, even if they had the same initial conditions (Tripathy et al. 2002). Moreover, using one state of unsaturated soil cannot represent the behaviour of unsaturated soil at different moisture contents and operational stresses. de Brito Galvão et al. (2004) measured the collapse potential for two kinds of soils at densities lower than the MDD and at moisture contents lower than OMC. However, the range of moisture contents at the dry side of OMC was not covered in this study. Furthermore, the effect of applied stress at wetting on the collapse values had not been taken into account.

2.3.2 Mechanism of Reaction between Lime and Clay

The reaction between lime and clay is affected by a range of factors, including the solubilities of the minerals, the pH of the environment and temperature (Nwakanma 1979). The chemical stabilisation procedure using lime occurs through two main chemical reactions: short-term and long-term.

For the short-term reaction, the reaction initially starts after adding water to the clay-lime mixture. The hydrated lime dissociates to Ca^{++} and $2(OH)^{-}$ ions. The lime solubility is low and about 0.20 gr/100 ml (Nwakanma 1979) at normal temperature. The study by Nwakanma (1979) showed that the rate of lime consumption was linear with a high gradient up to 7 days, and then the consumption rates deviated during the period between 7 to 28 days. This means that most of the lime consumption occurred during the first 7 days.

As a result of dissociation of hydrated lime and releasing the $(OH)^{-}$ ions, the alkalinity of the mixture is raised. The amount of hydrated lime should be sufficient to raise the pH of the mixture to about 12.4, allowing the second stage of reaction to start. The second stage includes the dissolution of silica and alumina, cation exchange, flocculation and agglomeration (Ouhadi & Yong 2003; Thompson 1968). The solubility of silica and alumina minerals is very high at a pH concentration of 12.4 (Bell 1996). Hansen (1967) studied the quartz mineral dissolution and concluded that this process involved sequent penetration of the electron field of an O^{-2} ion by two protons to form OH^- ions. Two other OH^- ions (from the surrounding medium) enter the electrical domain of the Si^{+4} ion to generate the unstable $Si(OH)_4$ group. Two additional OH^- ions penetrate the $Si(OH)_4$ electrical domain to form a $Si(OH)_6$ ion. The $Si(OH)_6$ cannot form a bond with the other silicon atoms. Finally, the $Si(OH)_6$ combines with two protons to form $H_2Si(OH)_6$, which is free to leave the surface. During this stage, the OH^- ions are consumed, causing a reduction of the environment alkalinity (Dermatas et al. 2005). This means that in spite of the continued lime dissolving during this stage, it might not be sufficient to compensate for the consumption of OH^- ions. Therefore, it is important to maintain sufficient level of OH^- ions during this stage to assure dissolution of silica (Nwakanma 1979) and continuation of the stabilisation process.

Cation exchange, flocculation and agglomeration also occur during this stage under conditions of high alkalinity. Potassium, sodium and hydrogen (monovalent) cations are replaced by calcium ions (divalent), causing a change of electrical charge density around the soil particles. Subsequently, the inter-particle attraction increases, causing flocculation and agglomeration (Cabalar et al. 2014; Ismaiel 2006).

In contrast, a long-term reaction includes pozzolanic reaction. Calcium from the lime interacts with the soluble silica and alumina from the soil to form stable Calcium Silicate Hydrate (CSH) and Calcium Aluminate Hydrate (CAH), which contribute to long-term strength (Chen & Lin 2009; Elkady 2015; Nalbantoğlu 2004; Yong & Ouhadi 2007).

For organic soils, there is an additional decline in pH concentration, as there are two major fractions of organic matter present: humic acid and fulvic acid. Humic acid is the main basis of organic matter affecting the strength improvement of stabilised soil (Onitsuka et al. 2003). The organic matter causes a decline in pH concentration to the limit where dissolution of clay minerals (silica and alumina) no longer occurs (Chen et al. 2009). This is due to some organic components obstructing the hydration process of lime with their tendency to coat the clay particles. In addition, the organic matter has a strong chemical affinity to calcium; therefore, when reacting with hydrated lime ($Ca(OH)_2$), the insoluble reaction products will be formed and precipitated out on the clay particles (Chen & Wang 2006).

2.4 Constitutive Models of Unsaturated Soil Based on Net Stress and Suction

To describe the volumetric behaviour of unsaturated soils, most constitutive models use net stress and suction as constitutive parameters, either independently or in combination (Alonso et al. 1990; Fredlund & Morgenstern 1976; Loret & Khalili 2002; Sheng et al. 2008; Sivakumar & Wheeler 2000; Wheeler & Sivakumar 1995). Past models have demonstrated that the volumetric behaviour of unsaturated soils can be divided into three groups, including the Barcelona Basic Model (BBM), the effective stress model and the Sheng Fredlund Gens (SFG) model. Brief explanations of these models are presented in the following sections

2.4.1 Barcelona Basic Model (BBM)

Alonso et al. (1990), Wheeler and Sivakumar (1995) and Sivakumar and Wheeler (2000) present a constitutive model for illustrating the stress-strain relationship of unsaturated soils. This model, which is called the Barcelona Basic Model (BBM), uses two independent stress variables (the net mean stress and the suction). To evaluate the model's ability to produce the behaviour of unsaturated soils, many laboratory tests were performed under suction control on compacted kaolin and sandy clay (Alonso et al. 1990).

This framework formulated a model for isotropic stress states, including yield. A proper stress space was used to describe the isotropic states (σ, s), where net mean stress $\sigma = \sigma_m - u_a$ is the excess of mean stress σ_m over air pressure (u_a) and s is the suction.

According to an isotropic test, a sample was applied to load increment (σ) along virgin states under a specific suction. Therefore, the virgin normal compression behaviour was produced as:

$$\upsilon = N(s) - \lambda(s)\ \ln\frac{\sigma}{\sigma^{c}} \qquad 2\text{-}1$$

where:

υ : is the specific volume ($\upsilon = 1 + e$),

e: void ratio,

σ^c : is a reference stress state for which $\upsilon = N(s)$ (atmospheric pressure).

$\lambda(s)$: is the slope of compression line (stiffness parameter).

$N(s)$: specific volume at reference net stress.

For unloading and reloading at constant suction, the soil was found to behave as:

$$dv = -k\ \frac{d\sigma}{\sigma} \qquad 2\text{-}2$$

where k is elastic stiffness parameter for changes in net stress.

Figure 2.3 represents Equations 2-1 and 2-2 graphically, and shows the response of two samples loaded, unloaded and reloaded under different suctions (saturation (s=0) and unsaturation (a larger suction s). The pre-consolidation stresses (yields) for the saturated and unsaturated samples are labelled as σ_0^* and σ_0, respectively in Figure 2.3a. It is clear that the saturated sample would yield at a lower isotropic stress (point 3) than the unsaturated sample (point 1).

If points 1 and 3 belong to the same yield curve in a (σ,s) space (Figure 2.3b), a relationship between the saturated yield stress (σ_0^*) and the unsaturated value (σ_0) can be obtained by relating the specific volumes at points 1 and 3 through a path, which includes an initial unloading (at constant suction) from σ_0 to σ_0^*, and a reduction in suction from s to zero (at constant stress σ_0^*). Initially, the sample at point 1 in Figure 2.3a & b follows the path from 1 to 2 to 3. The following identity can be generated:

$$\upsilon_3 = \upsilon_1 + (\upsilon_2 - \upsilon_1) + (\upsilon_3 - \upsilon_2) \qquad 2\text{-}3$$

where υ_2, υ_2, and υ_2 are indicated in Figure 2.3.

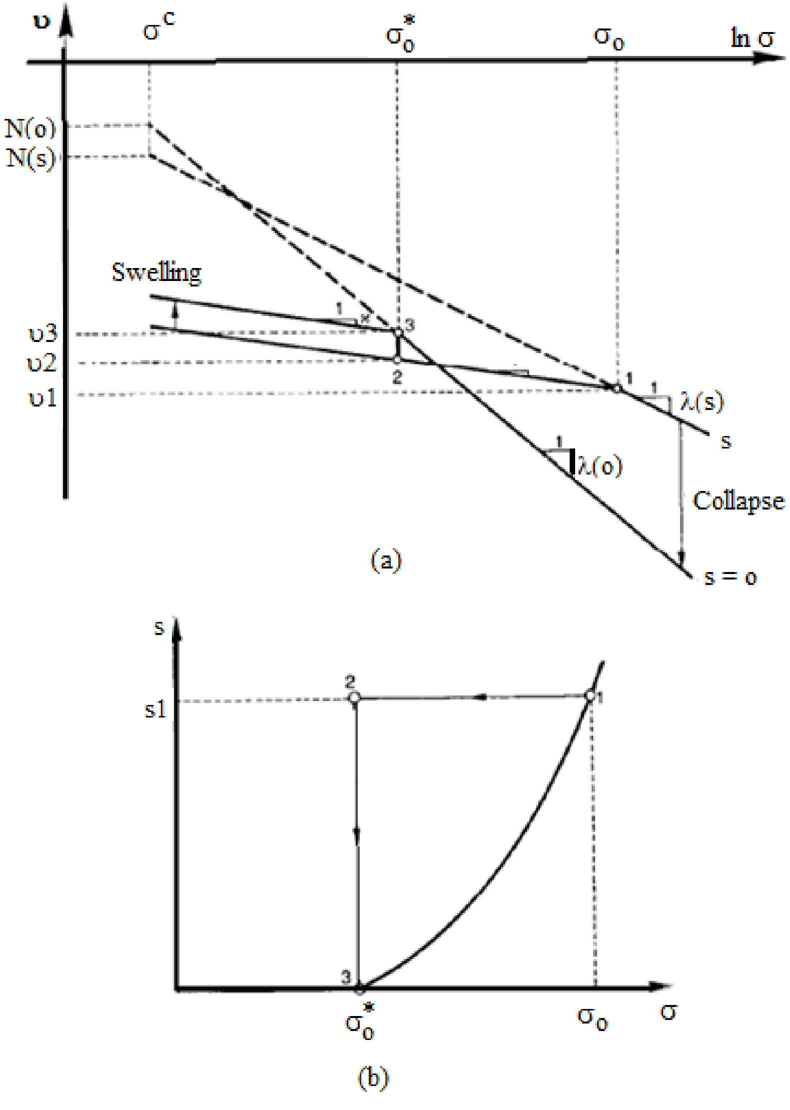

Figure 2.3. Variation of pre-consolidation stresses (a) compression curves for saturated and unsaturated samples, (b) yield curve (after Alonso, Gens & Josa 1990)

The suction unloading from 2 to 3 (after wetting at constant σ_0^*) occurs in elastic domain and under this condition, a reversible swelling $(\upsilon_3 - \upsilon_2)$ can be expressed as a logarithmic function similar to Equation 2-2:

$$d\upsilon = -\kappa_s \frac{ds}{(s+\sigma_{atm})} \qquad \text{2-4}$$

where κ_s is stiffness parameter for changes in suction and $\sigma_{atm}$is atmospheric pressure. σ_{atm} has been added to avoid infinite values when s approaches zero.

By considering Equations 2-1, 2-2, and 2-4, the Equation 2-3 becomes:

$$N(0) - \lambda(0)\ ln\ \frac{\sigma_0^*}{\sigma^c} = N(s) - \lambda(s)\ ln\frac{\sigma_0}{\sigma^c} + k\ ln\ \frac{\sigma_0}{\sigma_0^*} + k_s ln\ \frac{s+\sigma_{atm}}{\sigma_{atm}} \qquad \text{2-5}$$

Equation 2-5 represents the relationship between unsaturated yield stress (σ_0) and suction (s) in terms of some reference values σ_0^*, σ^c, $N(s)$, $\lambda(s)$, k, and k_s. This means that it is possible to draw multiple lines defined by various suction to generate a state boundary surface in υ, σ, s space for normal compression stress (Kodikara 2012; Zhang & Lytton 2009).

The BBM can be considered as the first elasto-plastic model, which is mostly used to describe the volumetric behaviour of unsaturated soil. However, other behaviours of partially saturated soils have not been covered in the BBM model; for example, a moisture content or a degree of saturation parameter has not been incorporated into the constitutive modelling.

2.4.2 Effective stress model

Bolzon et al. (1996) suggested an approach to describe the plastic behaviour of unsaturated soil by modulating an existing model for saturated soils. In this approach, the state of the material was defined in terms of effective stress and suction. Following the Bishop (1959) model, an effective stress was used in this approach as a combination of net stress and suction (Loret & Khalili 2002). This modification is advantageous compared with the BBM when the transition zone between saturated and partially saturated soils is taken into account. The yield surface equation of this model is similar to the BBM, with the net stress replaced by an effective stress. The available experimental work highlights that even with the definition of effective stress, there exists a state boundary surface for virgin compression, since λ and N can still be a function of suction (Kodikara 2012). Thus, this dilutes the efficiency of the effective stress concept. Santagiuliana and Schrefler (2006) considered hydraulic hysteresis in the model; however, this modification did not enhance compaction prediction, as only the wetting path was followed during compaction. Gallipoli et al. (2003a) argued that both λ and N are functions of not only suction, but a degree of saturation, as well. This study suggested Equation 2-6, which displays the acceptable results for volume change, as well as the critical state of the shearing specific database:

$$\upsilon = (N - \lambda \ln\sigma')[1 - a\left(1 - e^{b\xi}\right)] \qquad \text{2-6}$$

where:
$\sigma' = \sigma + S_r\, s$ (effective stress),
N and λ are the normal compression line parameter,
S_r is the degree of saturation,
s is the suction,
a, b are fitting parameter, and
$\xi = f(s)(1 - S_r)$ which is the bonding effect as a result of suction, it is product of the degree of air saturation and function of suction.

With the effective stress model, Loret and Khalili (2002) were able to represent critical state shearing with the effective stress, but not the volume change. Tarantino and Col (2008) interpreted the static soil compaction results by using the average effective stress and modified suction as work conjugates. Furthermore, this study considered the change in suction with loading by incorporating the model developed by Gallipoli et al. (2003b). This model is similar to that proposed by Gallipoli et al. (2003a); however, it uses different stress state variables (Kurucuk 2011).

2.4.3 Sheng Fredlund Gens (SFG) model

The SFG model focused on three issues. These issues included the yield stress change with suction, modelling slurry samples, and the smooth transformation from a saturated to unsaturated state. For unsaturated soils, the volume change due to a suction change may not necessarily be the same as that due to a change in the net stress. The Equation 2-7 represents the state boundary surface as (Sheng et al. 2008):

$$dv = -\lambda_{v\sigma}\frac{d\sigma}{\sigma+s} + \lambda_{vs}\frac{ds}{\sigma+s} \qquad 2\text{-}7$$

where:

$$\lambda_{vs} = \begin{cases} \lambda_{v\sigma} & s < s_{sa} \\ \lambda_{v\sigma}\dfrac{s_{sa}+1}{s+1} & s > s_{sa} \end{cases}$$

$\lambda_{v\sigma}$ is the coefficient of compressibility, function of mean net stress and suction, and s_{sa} is the saturation suction. Sheng et al. (2008) concluded that these coefficients are functions of suction up to the air entry value. This study also stated that λ_{vs} and $\lambda_{v\sigma}$ will have values corresponding to saturated soil, and that they then decrease as suction increases with desaturation.

According to Sheng and Zhou (2011), with the SFG approach, the state boundary surface relies on the state path. This means that if a specimen of soil is dried to a certain suction (s) from the slurry state and then loaded to a certain stress (σ), the specific volume obtained will be different to that obtained when another specimen is loaded to the stress (σ) at saturation and then dried to the same suction (s). Zhang and Lytton (2008) showed that with the SFG model, there can be path dependency even in the elastic space. The major obstruction in its application to compacted soil is that according to Equation 2-7, the void ratio decreases as suction increases (at constant stress) according to the second term of the equation. However, it is well known that in virgin states of compacted soils, the void ratio increases as suction increases, or moisture content decreases due to the introduction of macrostructures during the soil preparation process (Kodikara 2012; Wheeler & Sivakumar 1995).

2.5 Monash-Peradeniya-Kodikara (MPK) for Compacted Unsaturated Soils

Kodikara (2012) suggested a new framework, called Monash-Peradeniya-Kodikara (MPK), to describe the volumetric behaviour of compacted unsaturated soils. This model used net stress (σ), void ratio (e), and moisture ratio (e_w) (e_w = moisture content (w) × specific gravity (G_s)), as main variables in the constitutive model, and suction (s) as a dependent variable. Kodikara adopted the compaction technique to create the Loading Wetting State Boundary Surface (LWSBS), which is the backbone of the MPK framework.

For over a decade, Kodikara and his team at Monash University worked on understanding the behaviour of cracking of unsaturated soils, soil compaction and hydraulic behaviour with atmospheric coupling. In many situations, the effect of moisture content was found to be more important than suction. For example, a hydric coefficient was used ($\alpha = \left(\frac{\partial e}{\partial e_w}\right)_\sigma$) in a soil cracking study to estimate the tensile stresses developed during soil shrinkage (Costa 2010; Kodikara 2012; Kodikara & Choi 2006). This hydric coefficient was also used to investigate soil-structure interaction in soil swelling issues (Rajeev & Kodikara 2011). Gould et al. (2011) used void ratio (e) vs. moisture content (w) vs. stress (σ) space to study the swelling and shrinkage behaviour of soils that environmentally stabilised under loading (soils exposed to wet/dry cycles to reach an equilibrium condition where an equal swelling and shrinkage deformation was achieved). All of these studies suggested that in many field applications, moisture ratio can be used instead of suction.

Fleureau et al. (2002) and Gould et al. (2011) showed that the moisture ratio did not present hydraulic hysteresis with void ratio during wetting and drying cycles (an environmentally stabilised condition) (**Figure 2.4a**). However, this behaviour was clearly observed when suction was used, as shown in **Figure 2.4b.** Figure 2.4b shows that the relationship between void ratio and suction under the wetting path is different to that obtained under the drying path. Tripathy et al. (2002) studied the behaviour of compacted expansive soils under swell-shrink cycles by using moisture content, void ratio, and stress space. It was also discovered that there was no indication of hysteresis. This is because both void ratio and moisture ratio showed a hysteresis with suction; this behaviour did not exist when void ratio and moisture ratio were considered together (Kodikara 2012). Additionally, wetting and drying pores filled with water led to a change in void ratio and subsequently introduced a direct correspondence of the moisture ratio and void ratio. Kodikara (2012) presented a theoretical model for the use of moisture ratio (or specific moisture volume) over suction. However, before reaching the environmental stabilisation, the soil would be exposed to irreversible changes, which reflects the non-unique behaviour in the void ratio and moisture ratio space.

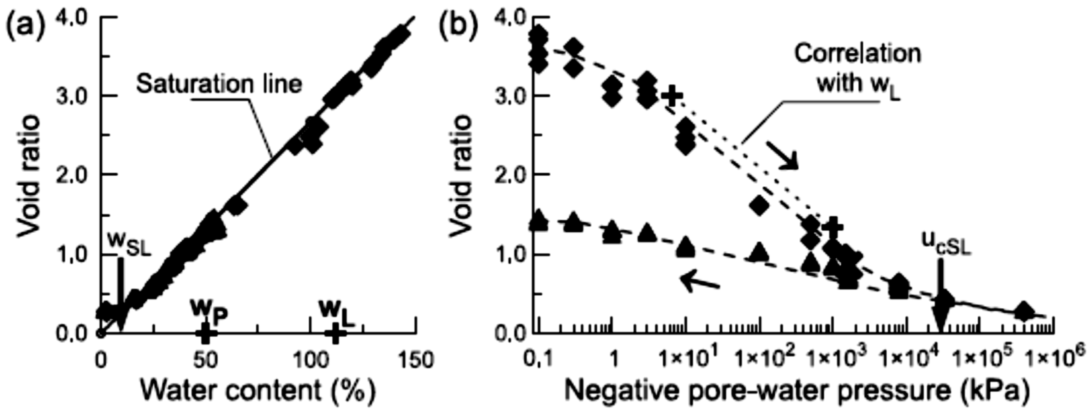

Figure 2.4. Comparison of (a) water content and (b) suction curves (Fleureau et al. 2002)

Neglecting the mechanical dissipation related to fluid flow and air compressibility, and following Houlsby (1997), during volumetric compression, the rate of work input per unit volume of unsaturated soil can be expressed as:

$$\boldsymbol{W = (\sigma + S_r s) d\varepsilon_v - n s S_r} \qquad 2\text{-}8$$

where σ is net vertical stress (for isotropic loading, σ is the mean net stress and for K_0 loading), s is suction, $d\varepsilon_v$ is a volumetric strain, n is porosity. Considering $e_w = S_r e$ gives:

$$nd\boldsymbol{S_r} = -\boldsymbol{S_r}\frac{de}{(1+e)} + \frac{1}{(1+e)}de_w = S_r d\varepsilon_v + \frac{1}{(1+e)}de_w \quad \text{2-9}$$

Substituting Equation 2-9 into 2-8 gives:

$$W = \sigma d\varepsilon_v - \frac{s}{(1+e)}de_w = -\sigma\frac{de}{(1+e)} - \frac{s}{(1+e)}de_w \quad \text{2-10}$$

According to Equation 2-10, under isotropic or K_0 state, the constitutive behaviour can be described by variables e, e_w, σ and suction during volumetric changes. Consequently, Kodikara (2012) suggested the possibility of developing state boundary surfaces using the e-e_w-σ space, where suction is a dependent variable of the moisture ratio using the Soil Water Characteristic Curve (SWCC). Groenevelt and Bolt (1972) pointed out that swelling is affected by void ratio, moisture ratio, net stress, and suction. Thus, there exists a unique value of void ratio and moisture ratio, which completely defines the suction.

2.5.1 Relationship to the compaction curve

Kodikara (2012) studied the direct relationship between traditional compaction curves and the LWSBS. **Figure 2.5b** presents a set of compaction curves in the void ratio (e)-moisture ratio (e_w)-net stress (σ) space. The Line of Optimums (LOO) is also identified. Kodikara (2012) discussed that if the compaction curves are established during the compaction procedure (based on Tarantino and Col (2008) dataset), both elastic and plastic deformations will be included. However, if the compaction curves are established from unloaded soil, then only plastic deformations will be included.

Kodikara (2012) interpreted the importance of the LOO in soil behaviour. When compaction moisture content increases and reaches the LOO, the air is trapped and the air phase becomes discontinuous at the wet side of the LOO (Gilbert 1959; Hilf 1956; Kodikara 2012; Kurucuk 2011). Thus, both air and water pressures will build up when the moisture content becomes higher than optimum. This behaviour can be explained by considering two specimens compacted at loose state (σ =1 kPa) (points $\mathbf{A_0}$ and $\mathbf{B_0}$ in

Figure 2.5c). The specimen $\mathbf{A_0}$ is compressed and reaches the LOO at point **A** when the net stress reaches σ_A. At this point, the air is trapped, but still close to the atmospheric state. Thus, the externally applied stress is equivalent to σ_A. For specimen $\mathbf{B_0}$, the specimen is compressed and reaches the LOO at **B** when the net stress reaches σ_B, which is less than σ_A. If the applied stress (σ_B) is increased to be equivalent to the σ_A, the water and air pressure builds up and the net stress increases, leads to a small reduction in void ratio, and consequently a small increase in dry density and a small increase in saturation (point $\mathbf{B_1}$ in Figure 2.5c). Similarly, for specimen $\mathbf{C_0}$, which was prepared at a higher moisture content and then compressed to the same applied stress (σ_A), the path takes $\mathbf{C_0C_1}$, as shown in Figure 2.5c. If the excess pore water pressure that built up at $\mathbf{B_1}$ and $\mathbf{C_1}$ is permitted to dissipate, the new drained conditions will be obtained ($\mathbf{B_2}$ and $\mathbf{C_2}$ in Figure 2.5c). These drained conditions can be connected as a curve $\mathbf{AB_2C_2}$ that represents the drain path of the e-e_w curve corresponding to the net stress σ_A (Figure 2.5c). The specimen at point $\mathbf{C_2}$ is fully saturated and the pore water pressure is zero. The corresponding effective net stress is σ_A and the void ratio is equal to the moisture ratio. This point will be located on the Normally Consolidated Line (NCL) for fully saturated soil. Figure 2.5 presents the suction contours at the LWSBS. From **A** to $\mathbf{B_2}$ to $\mathbf{C_2}$, the soil suction will decrease.

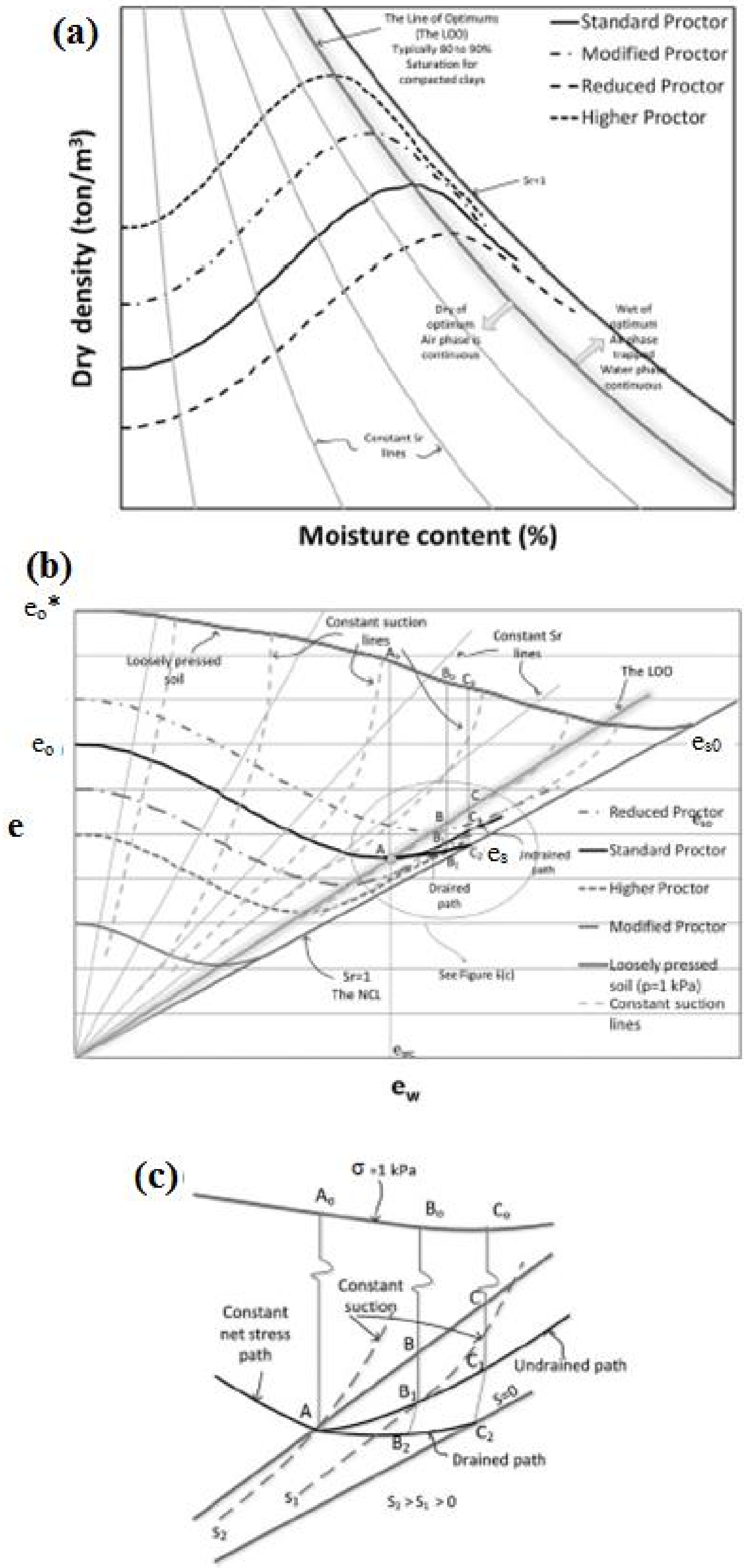

Figure 2.5. (a) Typical compaction curves (b) e-e_w relationship at constant stress (c) the path between LOO and NCL (Kodikara 2012)

2.5.2 The Loading Wetting State Boundary Surface (LWSBS)

The LWSBS in the MPK framework is defined as the surface generated from a set of compaction curves with a drained path between the line of optimums (LOO) and the normally consolidated line (NCL), as shown in Figure 2.5. The drained path phenomena between the LOO and NCL will be explained in detail later. For now, the LWSBS describes the volumetric behaviour of soil, and it is applicable to loading or wetting, or a combination of loading and wetting (Kodikara 2012).

The upper boundary of the LWSBS was the e-e_w curve at σ = 1 kPa (loose soil). Where e_{s0}= e_w for saturated soil (on NCL) and e= e_o* at e_w = 0. In this model, the e-e_w relation was assumed to be a cosine function, as shown in Equation 2-11:

$$\frac{e}{e_s} = \left[\left(\frac{e_0}{e_s} - 1\right)\cos\left(\frac{\varphi\, e_w}{e_s}\right) + (1 - \frac{e_0}{e_s}\cos(\varphi))\right]\frac{1}{(1-\cos(\varphi)} \qquad \text{2-11}$$

where:

φ= π/ (e_{wc}/e_s) ,

e_{wc} : is the optimum moisture ratio for a certain net stress,

the variation of void ratio along NCL and for dry soil are :

$$e_s = e_{s0} - \lambda_1 \ln \sigma \quad \text{(on NCL)} \qquad \text{2-12}$$

$$e_0 = {e_0}^* - \lambda_2 \ln \sigma \quad \text{(for dry soil)} \qquad \text{2-13}$$

where λ_1 and λ_2 are the compression indices for saturated and dry soils, respectively. e_{s0} is the saturated void ratio at σ= 1 kPa and ${e_0}^*$ is the void ratio at e_w= 0 and σ= 1 kPa. Kodikara (2012) showed the general topographic features of the LWSBS in Figure 2.5. In this example, Kodikara (2012) used the following parameters: λ_1 =0.07, λ_2= 0.1, (e_{wc}/e_s)=0.75, e_{s0}=1, and ${e_0}^*$=1.4.

It should be mentioned that the LWSBS describes the upper surface for the volumetric behaviour of soil, and is applicable to loading and wetting paths only. There is another surface that represents the drying state path. This surface is located slightly below the LWSBS (Kodikara 2012).

2.5.3 Loading, unloading and reloading according to the MPK framework

The volumetric behaviour of unsaturated soils due to loading, unloading and reloading behaviour was explained by Kodikara (2012). According to the Kodikara model, when a loose specimen (at a nominal stress) with a certain moisture ratio is compacted to a certain stress level (compaction stress) under constant moisture ratio, the state path will follow the LWSBS from nominal stress to the compaction stress. These moisture ratio paths are shown in **Figure 2.6**. Figure 2.6 shows that each constant moisture ratio path hits the LOO, and with more loading, the path reaches the NCL with a negligible reduction in void ratio. If the specimen is unloaded to a stress lower than the compaction stress, the state path will follow the unloading-reloading line with the slope of κ in the e-log(σ) space. If the specimen is loaded again, it will follow the κ line until it reaches the compaction stress, and then the path will follow the LWSBS.

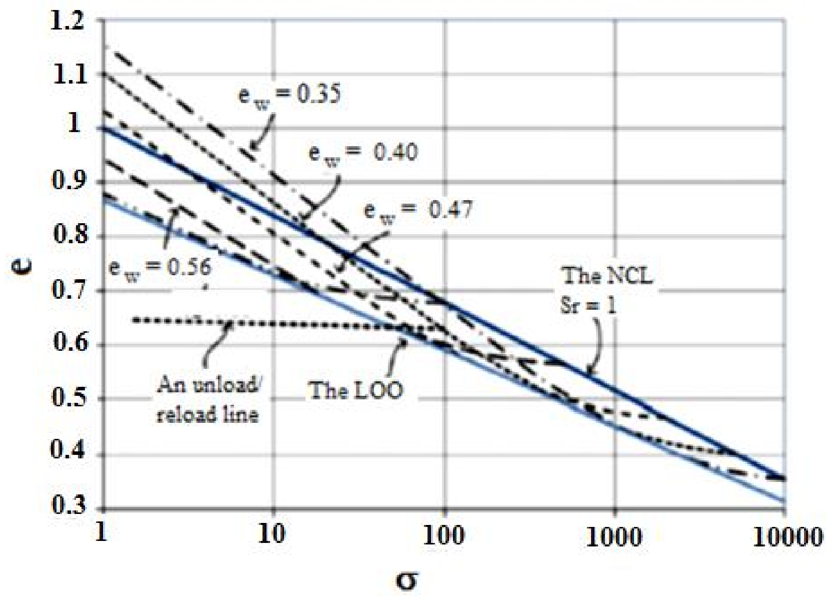

Figure 2.6. Virgin compression lines of constant water content (after Kodikara 2012)

2.5.4 Swelling and collapse

Water is the main factor in many geotechnical issues. It is known that when a compacted soil is wetted (under a certain pressure), it can swell depending on swelling and shrinkage potential, or may collapse, causing a serious settlement (Sivakumar et al. 2010).

Swelling and collapse are the most common problems related to unsaturated soils. The mechanical behaviour of unsaturated soil includes shear strength and volume change (Houston et al. 2001; Jones & Holtz 1973; Qiu & Bian 2013). Heave and collapse may cause the destruction of various kinds of civil engineering structures, such as spread footing or roads constructed on reactive or collapsible soils, or embankment constructed with eroded soil (Al-Homoud et al. 1995; Qiu & Bian 2013).

The value of soil collapsibility commonly relies on porosity, the degree of saturation, silt content and rapid softening in the water. Soils that have a high porosity, a low degree of saturation, or a high silt content can be classified as collapsible soils (Rafie et al. 2008). Geotechnical engineers are confronted with the characteristic of collapse, prediction of degree of wetting and evaluation of collapse settlement (Houston et al. 2001).

Many studies have investigated the behaviour of collapse under different stresses without mentioning the reason for using these stresses. For example, Baghabra Al-Amoudi and Abduljauwad (1995) studied the collapse characteristics of arid saline sabkha soils under a pressure of 233 kPa. Tadepalli and Fredlund (1991) and Fredlund and GAN (1996) investigated the mechanism of collapse of a soil-applied to one-dimensional loading and wetted under a pressure of 50 and 100 kPa. Lim and Miller (2004) investigated the wetting behaviour of compacted Oklahoma soils. The collapse potential was measured under a stress of 200 kPa. Furthermore, Fattah et al. (2012) and Fattah et al. (2014) studied the collapse potential of gypseous soil treated by grouting, under a stress of 200 kPa.

To understand the collapse behaviour, it is important to identify the factors that affected this behaviour. Many researchers have investigated these various factors; however, there was no real reason provided by the authors for this behaviour. Alonso et al. (1987) reported that the collapse potential relies on the initial suction, stress and moisture content. Al-Homoud et al. (1995) studied the control of collapse potential for selected Jordanian fine soils by using different bitumen percentages. The study investigated the collapse potential under pressures of 25, 100 and 400 kPa. The results showed that for some soils, the collapse potential increased, with increasing pressures from 25 to 400 kPa. For other soils, the collapse potential increased, with increasing pressures from 25 to 100 kPa; however, the collapse value decreased by increasing the pressure to 400 kPa. Habibagahi and Taherian (2004) predicted the potential of collapse for compacted soils using artificial networks. This study concluded that the collapse values decreased with an increase in dry density and moisture content. Furthermore, the collapse potential increased with applied stress up to a critical stress, after which the collapse values dropped as the applied stress increased. However, the study did not mention the factors that critical stress depends on, or what that critical stress is. Sun et al. (2004) studied the behaviour of the collapse of unsaturated compacted clay using triaxial tests with controlled suction. The triaxial tests were conducted under various stresses, initial moisture contents, void ratios, confining pressures and controlled suctions. The results showed that the amount of collapse depended on the initial void ratio and net stress. In addition, the collapse value was small at low and high confining pressure, and there was a maximum value of the collapse at yield stress. Qiu and Bian (2013) investigated the collapse potential of remoulded unsaturated soil applied to wetting load under a constant pressure. The results showed that the samples collapsed under high pressure (300 and 400 kPa). de Melo Ferreira and Fucale (2014) evaluated the collapsibility of soils in the semiarid area of Pernambuco, Brazil. The study demonstrated that the maximum collapse occurred under a stress of 640 kPa and that after this stress, the collapse amount decreased. All of the aforementioned studies emphasised that the maximum collapse occurred under high pressures. Nevertheless, these studies did not point out the required stress that leads to maximum collapse or what the high pressure represents.

2.5.5 Swelling and collapse according to the MPK framework

Kodikara examined the swelling and collapse processes within his framework using results from compacted Speswhite kaolin by Sivakumar and Wheeler (2000).

According to Kodikara's model, if a soil is compacted under a constant moisture ratio to a certain stress (**AB** in **Figure 2.7**) and then wetted, the sample will be exposed to a significant collapse (reduction in void ratio). This collapse will continue until reaching the LOO (**BC** in Figure 2.7). After intersecting the LOO, the sample will swell until reaching the normally consolidated line, NCL (**CD** in Figure 2.7). The loading, collapse and swelling paths will follow the LWSBS. That means that every point on the LWSBS (loading zone) will collapse after wetting under a constant compaction stress, and that collapse will continue until reaching the LOO. After reaching the LOO, the soil will swell until reaching the NCL.

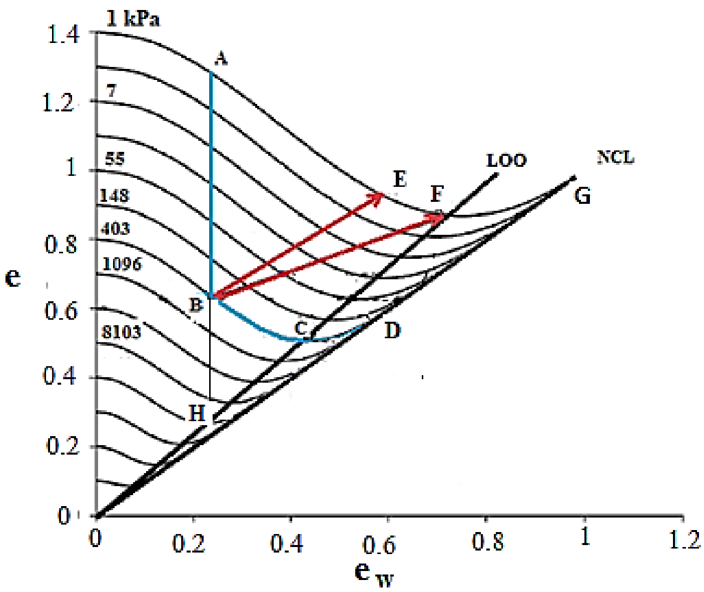

Figure 2.7. Swelling and collapse behaviour according to Kodikara's model (after Kodikara 2012)

However, if a soil is compacted to a certain stress (**AB** in Figure 2.7) and then unloaded (for example, to 1 kPa as shown in Figure 2.7), the specimen will swell (the void ratio increases) after wetting and follow either path **BE** or **BF**. The path of **BE** hits the

LWSBS before the LOO at point **E**, while the path **BF** hits the LWSBS at the LOO at point **F**. If path **BE** is followed, the specimen will collapse with continuous wetting until reaching LOO (**EF**) and then swell to NCL (**FG**). However, if path **BF** is followed, the specimen will swell with continuous wetting until reaching NCL (**FG**). This means that every point located under the LWSBS (unloading zone) will swell after wetting under a constant stress, and the swelling will continue until hitting the LWSBS. If the swelling path hits the LWSBS before the LOO, the specimen will collapse until the LOO is reached and then swell to the NCL. However, if the swelling path hits the LWSBS at the LOO, the specimen will swell until reaching the NCL.

The maximum collapse potential occurs when the specimen is wetted under the compaction stress (i.e. at 403 kPa, as shown in Figure 2.7). The amount of collapse will decrease as the stress increases along **BH**, and reaches zero when the LOO is approached at **H**. **Figure 2.8** shows the calculated collapse potential with the operational stress for different initial positions. It is evident that in all cases, the maximum collapse occurs when the specimens are wetted at the compaction stress, and the collapse value decreases if the operational stress is higher or lower than the compaction stress.

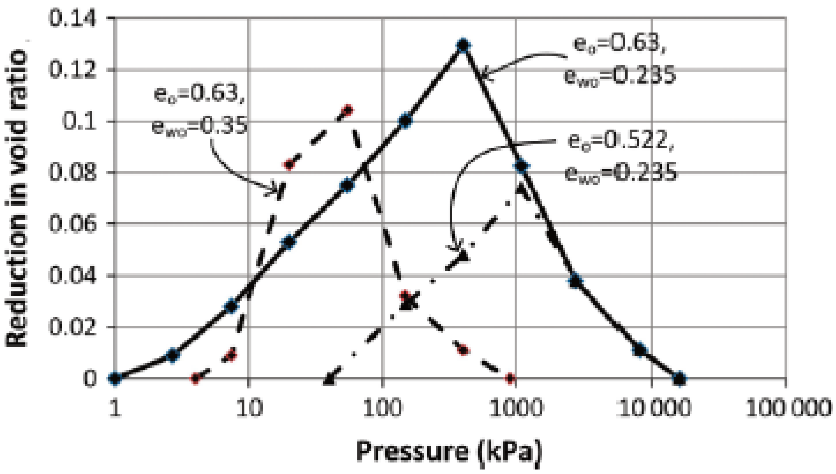

Figure 2.8. The relationship between the collapse potential and the operational stress (Kodikara 2012)

Rajeev and Kodikara (2011) referred to the gradient of **BE** or **BF** as a hydric coefficient (α). According to Sivakumar and Wheeler (2000), using data from compacted kaolin, the value of α can change in a range between 0.14 and 0.25. However, for expansive soils, the experimental data on densely compacted bentonite indicates that α can be higher and reaches approximately 0.61 under a constant net stress of 100 kPa (Lloret et al. 2003; Romero Morales 1999).

2.6 Suction measurement

Soil suction is defined as the potential of soil water in a soil undergoing change. This potential grows due to two major components, which are known as matric and osmotic suction. The summation of these components is referred to as total suction (Mitchell & Avalle 1984).

Matric suction relies on the pore structure that controls the capillary tension (Mitchell & Avalle 1984). A porous medium can absorb and hold water due to its capillarity, surface adsorptive force, and texture. The pores between soil particles (capillaries) absorb and hold water until the maximum amount under gravity force is reached (Shroff 2003). This water is in a negative pressure state, which is referred to as matric suction of the soil corresponding to a certain moisture content. The negative pressure in the capillaries decreases as moisture content increases. At saturation, all of the pores between the particles are completely filled with water; correspondingly, the matric suction will be zero.

The suction change along the depth of the soil above the water table is identified as a suction profile. This profile can be described by using a saturated soil column (**Figure 2.9**). The water level of the container, shown in Figure 2.9b, simulates the water table of a soil profile. Initially, the soil column will be saturated under the water table, after which the water will drain from the bottom, due to gravitational forces. The saturation zone will continue to a certain level, identified as h_d in Figure 2.9a, above the water table with a non-zero matric suction. At this point, air begins to enter and displace the water from the pore space, thereby reducing the water pressure, and causing the water to be in a tension state. The tension in water represents the matric suction of the soil. The air-water interfaces of the pores are curved towards the water phase, as shown in Figure 2.9c. That is an indication that the pore water pressure is in a negative state (Nelson et al. 2015; Nelson et al. 2003). The matric suction is a negative pore water pressure, and is commonly measured in kPa and pF units. The suction in pF is the logarithmic value of the suction in a centimetre of water (Schofield 1935). The relationship between these unit systems can be represented as suction in pF= 1+ $\log_{10}$ (suction in kPa) (Bulut et al. 2001).

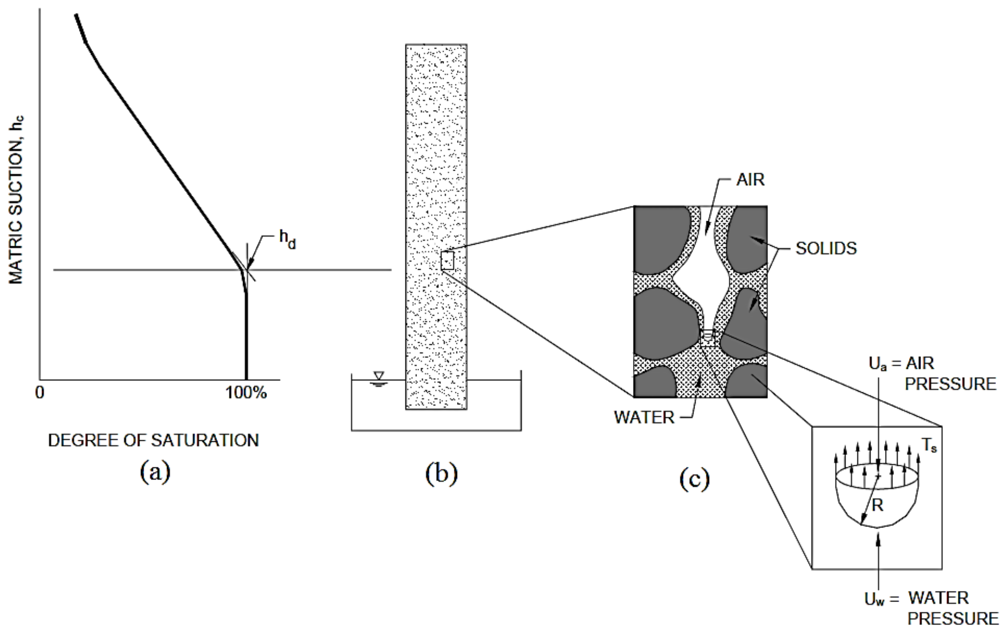

Figure 2.9. Matric suction change along a soil column (Nelson et al. 2003)

The osmotic suction is also a negative pore water pressure, but it is a result of the chemistry of the soil components. **Figure 2.10** shows the mechanism of osmotic suction. This figure presents a chamber of water separated by a semi-permeable membrane. On the left side of the membrane is a salt solution, while the right side is pure water. This membrane permits water molecules to pass, but does not allow any salt molecules to pass. As the salt has an affinity for water, it pulls water molecules to its side. Thus, the pressure that the salt solution applies to the pure water is called the osmotic suction (h_o) (Figure 2.10). This pressure increases as the concentration of the salt increases. The existence of salt in water decreases the soil energy state by decreasing the vapour pressures of the soil and relative humidity, and subsequently, the total suction increases (Nelson et al. 2015; Nelson et al. 2003).

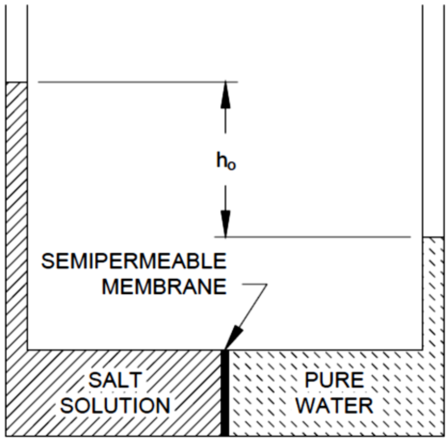

Figure 2.10. Osmotic suction across a semi-permeable membrane (Nelson et al. 2015)

The total suction depends on the amount of water in the soil pores and salt concentration. For some soils, the osmotic suction is relatively constant over a moisture range (Krahn & Fredlund 1972; Nelson et al. 2015). As the soil suction represents the stress state in expansive soils, it is the preferred measurement, rather than the moisture content range (Fredlund & Rahardjo 1993). Therefore, the relationship between soil suction and moisture content can be considered as the major function to describe the behaviour of expansive soil. The soil suction-moisture content relationship is referred to as the Soil Water Characteristic Curve (SWCC).

Various equipment and techniques can be used to measure the suction of a soil. Each technique has a measuring range and requires various equilibration times to produce readings (**Table 2.1**). As no one piece of equipment is able to measure the whole range of suction in a SWCC, the SWCC function needs to be conducted in various stages with different equipment (Murray & Sivakumar 2010; Pan et al. 2010).

Table 2.1. Suction components, typical measurement ranges, and equilibration times for each suction measurement technique (Murray & Sivakumar 2010)

Instrument	Suction component measured	Typical measurement range (kPa)	Equilibration time
Pressure plate	Matric	0-1500	Several hours to days
Tensiometer and suction probes	Matric	0-1500	Several minutes
Thermal conductivity sensors	Matric	0-1500	Several hours to days
Electrical conductivity sensors	Matric	50-1500	Several hours to weeks
Filter paper contact	Matric	0-10000 or greater	2-57 days
Thermocouple psychrometers	Total	100-8000	Several minutes to several hours
Filter paper non-contact	Total	1000-10000 or greater	2-14 days
Electrical conductivity of pore water extracted using pore fluid squeezer	Osmotic	entire range	---------
Suction control			
Negative (or Hanging) water column technique	Matric	0-30 or greater with multiple columns or vacuum control	Several hours to days
Axis translation technique	Matric	0-1500	Several hours to days
Osmotic technique	Matric	0-10000	up to 2 months
Vapour equilibrium technique	Total	4,000-600,000	1-2 months

2.7 Soil Water Characteristic Curve (SWCC)

The Soil Water Characteristic Curve (SWCC) is the suction-moisture content relationship at constant stress and temperature (Fredlund 2006; Fredlund & Vu 2003; Jones et al. 2009). An example is shown in **Figure 2.11**. The moisture content can be expressed in different forms, such as the volumetric moisture content, gravimetric water content or degree of saturation.

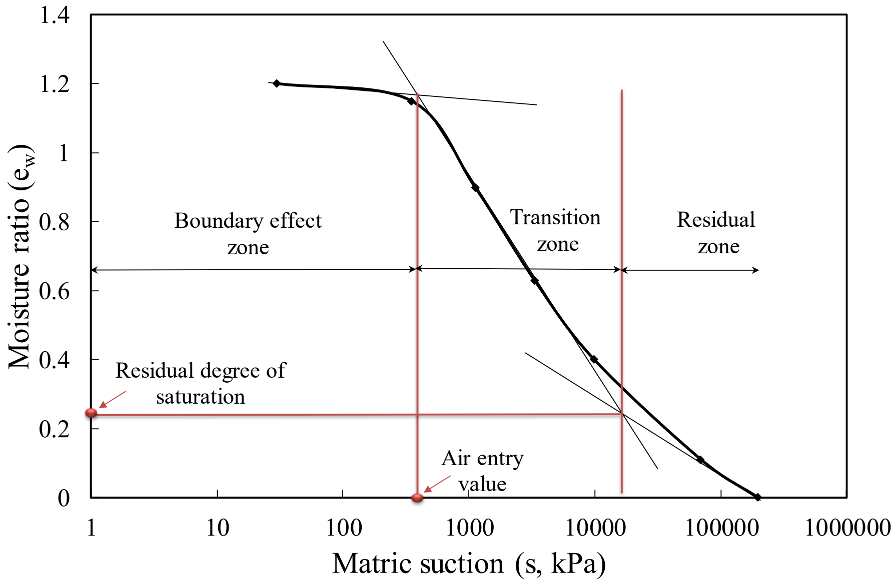

Figure 2.11. General soil water characteristic curve structure (adopted from Colmenares Montanez 2002)

Gould et al. (2011) measured the SWCC in the laboratory, as a set of discrete points. For modelling purposes, these points are represented as a continuous curve by using a mathematical function. According to Fredlund and Xing (1994), the air entry value of the soil represents the suction value where air begins to enter the largest pores of the soil. The residual water content is the water content where a large suction change is required to remove the additional water from the soil. The SWCC can be divided into three zones: (i) boundary effect zone, (ii) transition zone and (iii) residual zone, as shown in Figure 2.11 (Colmenares Montanez 2002; Fredlund 2006). In Figure 2.11, it is noticeable that the slope of the transition zone is greater than the other two zones of the SWCC. Commonly, the value of air entry, which is obtained at the end of the boundary effect zone and at the beginning of the transition zone, occurs close to the LOO. Furthermore, previous research suggests that as the net stress increases, the SWCC moves downward and the residual water content value decreases.

Kodikara (2012) noted that most studies concerning compaction curves have been conducted under stresses lower than the compaction stress (unloaded soil). Subsequently, all reported outcomes achieved from laboratory tests are generally located under the LWSBS (unloading space). However, there is one study by Tarantino and Col (2008) that takes into account load, void ratio and suction during the compaction procedure, in addition to the unloading state. Tarantino and Col (2008) test data present a typical constant net stress and suction contours in e-e_w space, as shown in **Figure 2.12** (Kodikara 2012). This figure shows that the suction contours converge towards the saturation line, as well as intersect constant net stress curves at angles close to a right angle. Dineen et al. (1999) and Romero Morales (1999) conducted tests where the suction was measured on the compaction curves. These studies were conducted on unloaded samples, and subsequently, the achieved constant suction contours were placed under the LWSBS (unloading space). All of the tests that have been presented were conducted on silty or clayey soil. Using a mixture of sand and bentonite, Colmenares Montanez (2002) obtained similar kinds of constant suction contours on compaction curves in the unloading zone. Subsequently, in the unloading zone, the constant suction contours, which are discussed, are popular in the compaction curves for clayey soil.

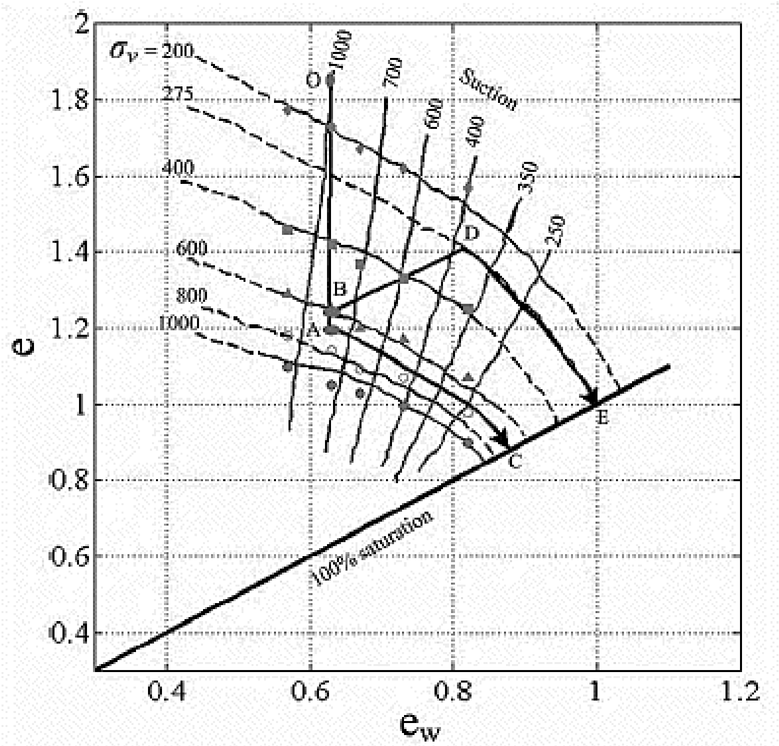

Figure 2.12. Typical constant net stress and suction contours in e-e$_w$ space according to Tarantino and Col (2008) test data (Kodikara 2012)

Many studies have been conducted to obtain empirical correlations to predict the swelling of expansive clays using the Atterberg limit, liquidity index and other properties that can be obtained by simple laboratory tests (Der Merwe 1964; Richards et al. 1984). However, these studies did not interpret the swelling and collapse behaviour of different soils with similar Atterberg limit values that were found to exhibit different volume change behavioural patterns. Fredlund (2000) suggested that the swelling and collapse behaviours for soils in unsaturated condition can be explained by considering the Soil Water Characteristic Curve (SWCC). However, no studies to date have interpreted the swelling and collapse behaviours for lime-stabilised expansive soil, in unsaturated condition, based on the Soil Water Characteristics Curve.

2.8 Swell – Shrinkage Curve

The shrinkage curve presents the change in void ratio due to desiccation. Many studies have been performed to assess the swell-shrink potential or volume change characteristic of undisturbed expansive clays as a function of moisture content (ASTM-D427 1998; Dasog et al. 1988; Ho et al. 1992; Marinho & Stuermer 2000; Mitchell & van Genuchten 1992; Sitharam et al. 1995). In the majority of these studies, clay specimens were dried under no external pressure for one cycle to evaluate shrinkage potential.

Haines (1923) identified different deformation stages that occurred as a result of continuous drying. These stages are now known as (i) structural shrinkage, (ii) normal shrinkage, and (iii) residual shrinkage, as shown in **Figure 2.13**. During the structural shrinkage stage, there is no significant change in a void ratio corresponding to the decrease in water content. However, during the normal stage, the decrease in volume change is equal to the volume of evaporated water. The end of the normal shrinkage slope is the shrinkage limit and the start of the residual shrinkage. At this point, the air enters the voids. Below this point, the degree of saturation is less than 100%. Therefore, as residual shrinkage starts, the volume change can be neglected (Tripathy et al. 2002). Thus, the shrinkage can be considered zero at the last stage (Stirk 1954). Various models have suggested an S-shape curve for shrinkage with the linear relationship in the normal shrinkage zone (Crescimanno & Provenzano 1999).

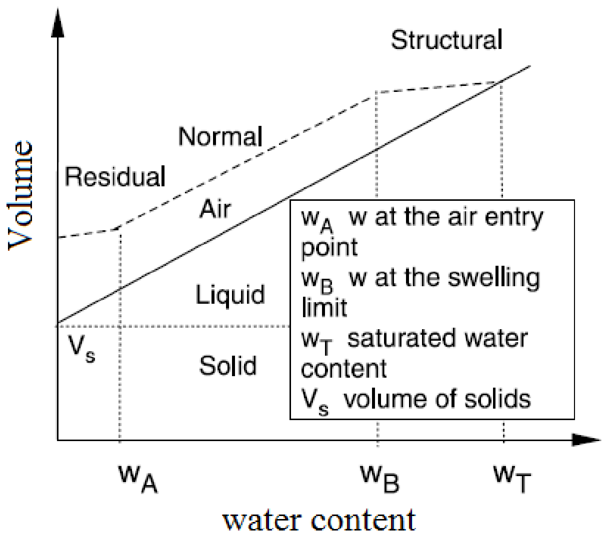

Figure 2.13. Shrinkage curve stages (Tripathy et al. 2002)

The swelling behaviour of dried samples is similar to the shrinkage behaviour of saturated samples. The swelling curve consists of three parts. The first part is the primary swelling, which develops very quickly. The second part is secondary swelling, in which the microcracks close. The third part of the swelling curve shows no further swelling. The typical phases of swelling are presented in **Figure 2.14** (Day & Hager 1999).

Laboratory cyclic swell-shrink tests on reactive clays have shown that swelling deformation may decrease or increase by a factor of two when compared to the initial cycle (Tripathy et al. 2002). Therefore, estimating the behaviour of expansive clay without considering the cyclic fluctuation may underestimate a soil's swelling potential. It is suggested that equilibrium is reached after four or five cycles, indicating that the vertical displacement during swelling and shrinkage are the same after a certain number of cycles (Al-Homoud et al. 1995; Day 1994; Popescu 1980; Songyu et al. 1998; Subba Rao & Satyadas 1987; Warkentin & Bozozuk 1961). Tripathy et al. (2002) studied the effect of the initial dry density and water content condition on the swell-shrink path for different surcharge pressures, and suggested that the effect of the initial condition on the equilibrium swell-shrink path can be neglected. Gould et al. (2011) created a mathematical model to define the shrinkage curve at an equilibrium cycle.

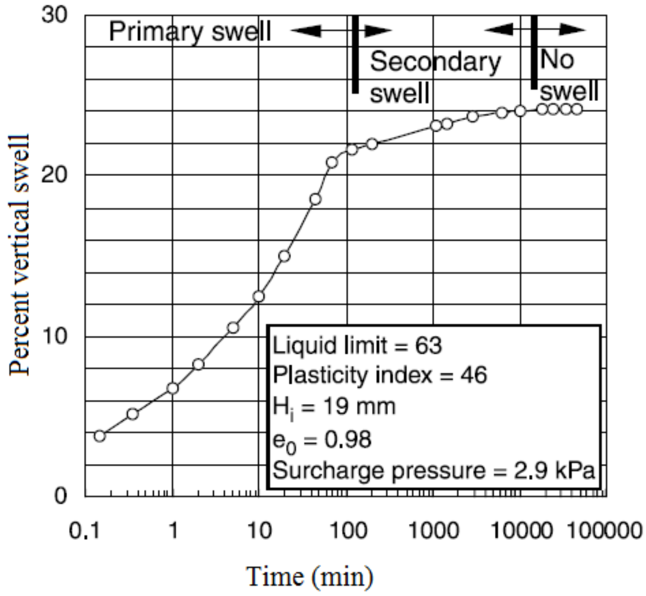

Figure 2.14. Swelling curve stages (Day & Hager 1999)

However, none of these studies showed the effect of lime stabilisation on the swell-shrink path under cyclic conditions. Consequently, the effect of swell-shrink cycles on the structural design was not considered.

2.9 Summary and the Aim of Research

The literature review has investigated the importance of using lime to enhance the expansive clay properties, including the reduction in plasticity index, swelling and collapse, and an increase in shear strength. Most of these studies measured swelling potential for a certain condition where specimens were compacted at OMC and MDD, and did not consider the behaviour on the dry side of OMC (unsaturated zone) and the behaviour of lime-stabilised soil under different operational stresses. Other studies did compact specimens at a moisture content lower than OMC to measure swelling and collapse potential, but the range of moisture contents on the dry side of OMC was not covered, and the effect of applied stress on the collapse values was not considered. In this research, soil behaviour on the dry side of OMC (unsaturated zone) will be considered for stabilised expansive clay at optimum lime content. Furthermore, the effect of applied stress on collapse values will be taken into account. This research will highlight the behaviour of stabilised expansive clay during wetting at the optimum lime content according to the swelling potential (swelling around zero).

Over the past half of a century, numerous studies have focused on modelling the hydromechanical behaviour of unsaturated soil. The constitutive models included constitutive models based on net stress and suction: the Barcelona Basic Model (BBM), the effective stress model, and the Sheng Fredlund Gens (SFG) model. The latest framework, the Monash Peradeniya Kodikara (MPK), was proposed by Kodikara (2012). This framework used void ratio, moisture ratio, and net stress as the main variables, and used suction as a dependent variable on moisture content. As the purpose of this research is to simplify the concept of unsaturated soil by using common variables used for saturated soil, such as net stress, void ratio and moisture content, initially, the model of Kodikara will be adopted. Then, the validity of this model on stabilised compacted clay will be investigated. If required, a new constitutive model will be generated. Kodikara's model depends on the compaction curves to generate this framework; therefore, it is important to choose the most appropriate of the compaction methods.

Sivakumar and Wheeler (2000) studied the effect of static and dynamic compaction on the behaviour of soil during wetting. The study concluded that the influence of static or dynamic compaction on the behaviour of soil during wetting could be neglected. Therefore, the static compaction will be conducted in this study to generate the MPK framework. To cover all parameters of unsaturated soil, the suction parameter will be measured as a dependent variable on moisture content by using the SWCC.

Most of the studies based on compaction curves have been conducted under stresses lower than the compaction stress (unloaded soil). Subsequently, all SWCC achieved from laboratory tests generally are located beneath the LWSBS (unloading space). Therefore, this research will measure the SWCC at and below the LWSBS, with all outcomes above representing the volumetric behaviour of unsaturated clay immediately after compaction (short-term). Therefore, it is important to consider the climate cycles to simulate the field condition for the long-term.

Following the procedure by Tripathy et al. (2002), cycles of swell-shrink tests will be conducted on untreated and treated samples. These tests will be performed to investigate the effect of lime stabilisation on the swell-shrink path after reaching an equilibrium condition.

Finally, a comparison between the volumetric behaviour of untreated and treated unsaturated expansive clay will be identified.

CHAPTER 3. METHODOLOGY

This chapter presents details of how the research was conducted, the research method used and the reason for choosing specific methods.

3.1 Introduction

This chapter presents the site description and descriptions of the soil preparation, preliminary soil tests, experimental apparatus and procedures used to achieve the aim of this research. Braybrook and Whittlesea (western and northern suburbs of Melbourne, Australia) were selected as sites to obtain basaltic expansive clays for testing, and hydrated lime ($Ca(OH)_2$) was selected as a binder. A site description and description of the sample preparation (collection and mixing) were presented. Preliminary soil tests included specific gravity, organic content, grain size analysis, Atterberg limit, linear shrinkage, and standard Proctor compaction. Unconfined Compressive Strength (UCS) and swelling potential were also obtained. As mentioned in Chapter One, four objectives were used to investigate the volumetric constitutive behaviour of the unsaturated basaltic expansive and lime-stabilised clays. Therefore, the experimental tests were divided into four series.

The first series of laboratory tests were conducted to measure the optimum lime content for the basaltic expansive clay according to swelling potential. These included deformation and strength soil tests accompanied by pH concentration, X-ray diffraction (XRD) and Scanning Electron Microscopy tests (SEM). The second series of tests were performed to check the validity of the MPK framework on the untreated and lime-treated basaltic clay. Static compaction tests were performed to generate the virgin compression surface (Loading Wetting State Boundary Surface) proposed by Kodikara (2012) for the untreated and treated basaltic clays. For the third series of tests, different state paths were applied to further check the validity of the MPK framework. To investigate the Soil Water Characteristic Curve (SWCC) at and below the virgin compression surface for both the untreated and treated expansive clay, tensiometers

(Hyprop), chilled mirror hygrometer (WP4C) and filter paper techniques were used. Additionally, this chapter describes the experimental procedure and apparatus used to identify the behaviour of lime-stabilised and compacted expansive soils under cycles of swell-shrink.

3.2 Site and Material

3.2.1 Site selection criteria

The main purpose of site selection was to identify a vacant block of land with reasonably reactive soils. Therefore, the available geology maps were examined to find an appropriate area.

Most of the Melbourne suburbs that have been established on blankets of lava flows rest on an erosion surface of Tertiary and Quaternary sediments, such as Brighton group sediments (Bell et al. 1967). These extensive lava flows belong to newer volcanos (Werribee plane phase), which are comparatively young, in terms of geological time (Bell et al. 1967). The thickness of basalt flows varies from place to place. Deep surface weathering that occurred over millions of years resulted in deposits of residual clay. These newer volcanic soils extend through most parts of western Victoria towards the corner of South Australia (Dahlhaus & O'Rourke 1992). These quaternary volcanic soils are mostly in dark to light grey, and are associated with inter-bedded silty sands and backed soils (Bell et al. 1967). The distribution of Quaternary Basalts soil is shown in pink in **Figure 3.1** (Maps 2015). Mann (2003) provided an expansive soil map of Victoria, as shown in **Figure 3.2**, which suggests that most of the basalt soils shown in Figure 3.1 are expansive. The dark red and orange areas in Figure 3.2 have highly reactive cracking clay soils, whereas the yellowish areas have calcareous clay soils. According to this map, most of the soils in the west and north parts of Melbourne are moderately to highly reactive. Therefore, the investigations were aimed at the western and northern suburbs to find a suitable site to be monitored.

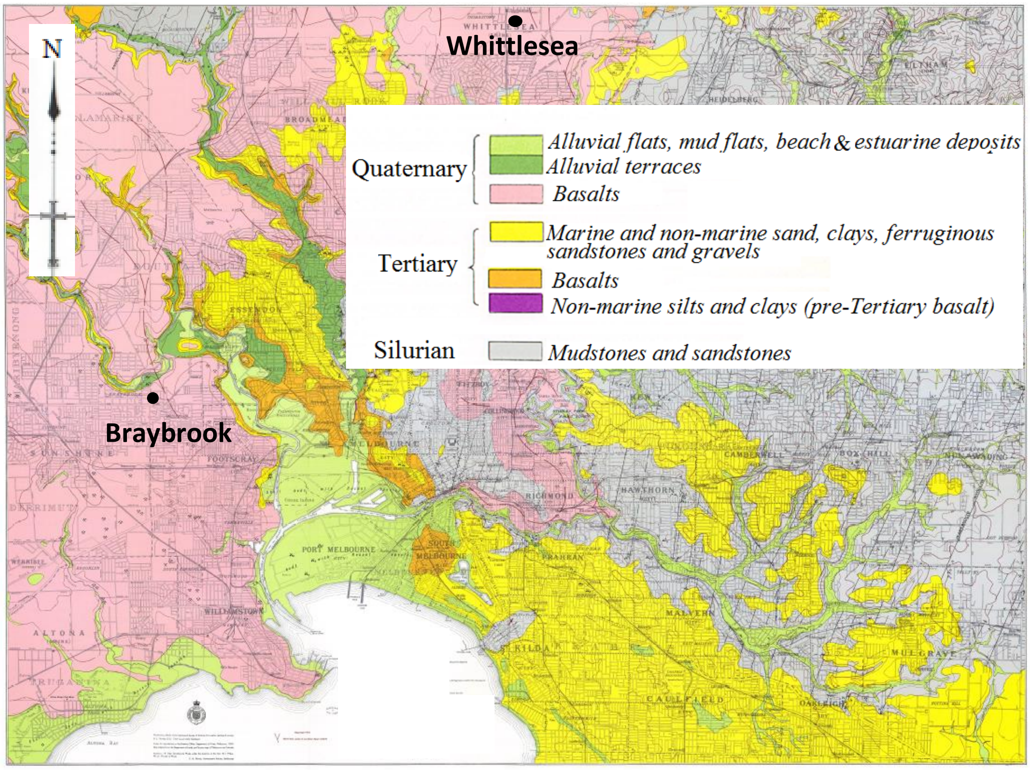

Figure 3.1. Geology of Melbourne-extracted from 1:31680 map of Melbourne (Maps 2015)

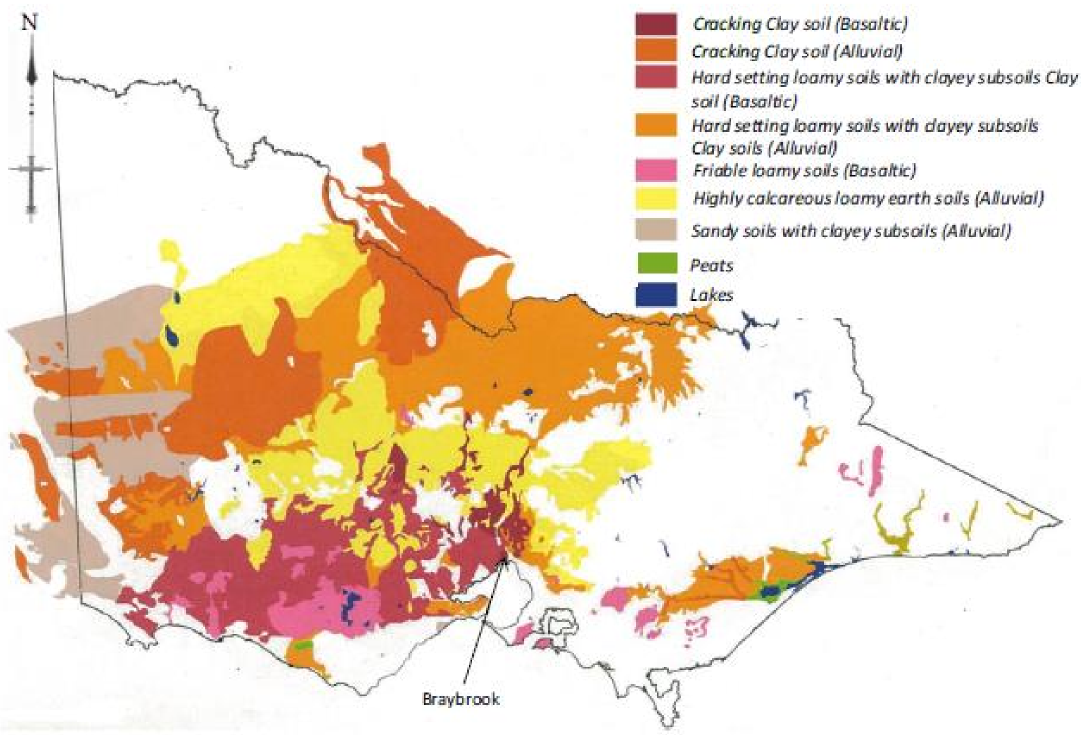

Figure 3.2. Distribution of expansive soils in Victoria (after Mann (2003))

3.2.2 Site description

Braybrook is a western suburb of Melbourne (Victoria, Australia), and its location is shown in Figure 3.1. This suburb was chosen as a source of clay materials for this study. Braybrook samples were taken from a current research site managed by Swinburne University of Technology that was used to study the impact of expansive clay on the structural performance of light residential buildings (Karunarathne et al. 2014b). Results indicate that the index properties are in a narrow band, in that the liquid limit (LL) ranges from 70 to 80 per cent, the plasticity index (PI) ranges from 50 to 55 per cent, and the linear shrinkage (LS) ranges from 17 to 19 per cent (Karunarathne et al. 2014b). Thus, the clay of this site can be categorised as highly reactive (Hazelton & Murphy 2007a). The shrink-swell indices measured according to the Australian standard (AS2870 2011) vary from 4.9 to 5.7 per cent/pF (Karunarathne et al. 2014a). As a result, the characteristic ground surface movement of the site has been calculated at 79 mm (AS2870 2011).

Whittlesea is a northern suburb of Melbourne, and its location is shown in Figure 3.1. This soil was chosen as an additional reactive soil resource to check the validity of a new method proposed in this study to estimate the OLC for basaltic expansive soils (see Chapter 4). As the soil collected from Braybrook is the main soil selected to study the volumetric behaviour of unsaturated basaltic expansive clay stabilised using lime, the sample collection for Braybrook soil has been explained in detail.

3.2.3 Sample collection

Bulk disturbed samples were collected from each site (Braybrook and Whittlesea) at a depth of 1.0-2.0 m. The total mass of collected Braybrook and Whittlesea soils were approximately 300 kg and 50 kg, respectively. For the Braybrook soil, the top layer contained grass, roots and organic materials. The soil up to 0.5 m was dark brown silty clay. The soil between 0.5 and 1.0 m was slightly calcareous brown silty clay, whereas the soil between 1.0 to 2.0 m was found to be dark to light grey silty clay. In general, the soils were found to be stiffer at a lower depth. The soil profile of Braybrook soil is shown in **Table 3.1** (Karunarathne et al. 2014a).

Table 3.1. Soil profile of Braybrook (Karunarathne et al. 2014a)

Depth (m)	Soil description (USCS)
0.0-0.3	Clay (CH), Dark brown, Soft, root fibres present
0.3-0.5	Clay (CH), Dark brown, Stiff, root fibres present
0.5-1.0	Clay (CH), Brown, Stiff, Very slightly calcareous
1.0-1.5	Clay (CH), Brown to dark grey, Stiff, Slightly calcareous
1.5-2.0	Clay (CH), Dark to light grey, Very stiff, Very slightly calcareous
2.0-2.5	Clay (CH), Light grey, Very stiff, Very slightly calcareous
2.5-3.0	Clay (CH), Light grey, Very stiff
3.0-5.0	Clay (CH), Light grey, Very stiff

For Whittlesea soil, the top layer contained grass, roots and organic materials. The soil between 1.0 to 2.0 m was found to be light brown silty clay to clayey silt.

3.2.4 Sample mixing

The total mass of collected Braybrook soil was approximately 300 kg; therefore, it was necessary to follow a robust method to achieve the soil homogeneity. This method can be summarised as the following:

1- The whole sample (300 kg) was transferred to the laboratory and put in ovens in stages under a target temperature of 100-105°C.

2- After drying, the clay sample was put in polythene bags. Each bag contained approximately 12 kg of the soil.

3- To prepare the soil, the soil in each bag was split into three parts. Each part was placed in the Ball and Mill machine to break down the soil into individual grains. The capacity of this machine is approximately 4 kg.

4- After preparing the whole sample, the bags were arranged in a matrix shape (5×5)

5- For the first row, two bags were poured into a big pan and mixed by hand. A sample divider was then used to ensure high division accuracy.

6- The contents of the sample divider were emptied into 5 bags equally (approximately 4.8 kg in each bag).
7- Item 5 was repeated for another two bags, and emptied equally in the same bags mentioned in Item 6.
8- Items 5 and 6 were repeated for the last bag in the first row.
9- The five bags in row 1 then had the same soil, but in different layers. Therefore, to ensure the homogeneity of the soil in each bag, the contents of each bag was divided by using the sample divider.
10- Items 5, 6, 7, 8 and 9 were repeated for the bags in row 2, 3, 4 and 5.
11- Items 5, 6, 7, 8 and 9 were repeated for the bags in column 1, 2, 3, 4 and 5.

Finally, the obtained sample can be considered one homogeneous sample.

3.2.5 Binder

Hydrated lime (calcium hydroxide $Ca(OH)_2$), also known as slaked lime, was used as the binder in this study. It is formed by adding water (hydrating or slaking) to quicklime (CaO), which is produced from limestone burning ($CaCO_3$).

Manufacturing of hydrated lime involves two steps. The first step includes the manufacturing of quicklime by heating limestone in a kiln at temperatures greater than 1000°C. As a result, carbon dioxide is released and calcium oxide is produced. The chemical process can be summarised in Equation 3-1 (AustStab 2002, 2008, 2010):

$$CaCO_3 + \text{heat } (>1000°C) \rightleftharpoons CaO \text{ (quicklime)} + CO_2\uparrow \qquad 3\text{-}1$$

During the second step, the quicklime reacts with water at a temperature of less than 350°C to produce hydrated lime, and releases heat. This chemical process is shown in Equation 3-2 (AustStab 2002, 2008, 2010; Rogers & ROFF 1997):

$$CaO + H_2O \rightleftharpoons Ca(OH)_2 \text{ (hydrated lime)} + \text{heat} \qquad 3\text{-}2$$

Hydrated lime is dry powdered hydrate with a variable density between 450 and 780 kg/m^3 and has an alkaline product of pH> 12 (AustStab 2010). This binder is widely used to reduce the swell-shrink potential of expansive soils and improve strength (Al-Rawas et al. 2005; Hamza 2014; Little & Nair 2009).

Following EN459-2 (2010) and ASTM-25 (2006), the value of available lime as $Ca(OH)_2$ was found to be 76.4 per cent. Subsequently, the type of calcium lime is CL 80, the type of natural hydraulic lime is NHL 2, the type of hydraulic lime is HL 2, and the type of formulated lime is FLA (EN459-1 2010).

3.3 Basic Soil Tests and Results

The physical properties of Braybrook and Whittlesea soils were investigated in this study. These properties included specific gravity, organic content, grain size analysis, Atterberg limit, linear shrinkage, standard Proctor compaction, unconfined compressive strength (UCS) and one-dimensional swell.

3.3.1 Specific gravity and organic content

The specific gravity of Braybrook and Whittlesea clays were found to be 2.71 and 2.69, respectively, according to the ASTM-D854 (2010) procedure. The procedure for oven-dried specimens was adopted. Following the ASTM-D2974 (2000), organic content of Braybrook and Whittlesea clays were found to be 3.1%. and 2%, respectively. According to the organic content specification of AASHTO, ASTM, ISO and Karlsson & Hansbo, these soils can be considered a low organic soil (AASHTO-M145-91 2004; ASTM-D2487 2011; ISO-14688 2002; Karlsson & Hansbo 1989).

3.3.2 Grain size analysis

The grain size distribution curve was obtained following the methodology described in ASTM-D422 (2007). Both soils were washed on sieve No.200 (0.075 mm). The results showed that 96% of Braybrook soil particles passed through the sieve, while approximately 10% of Whittlesea soil particles were retained on it. Hydrometer testing was conducted for both soils, because most of the soil particles were found to be smaller than 0.075 mm. **Figure 3.3** shows the particle size distribution for both soils. For Braybrook soil, the clay and silt contents were found to be 53% and 43%, respectively, while the sand content was only 4%. However, for Whittlesea soil, the clay and silt contents were 46% and 44%, respectively, while the sand content was 10%. **Table 3.2** reports a list of physical properties of Braybrook and Whittlesea expansive soils.

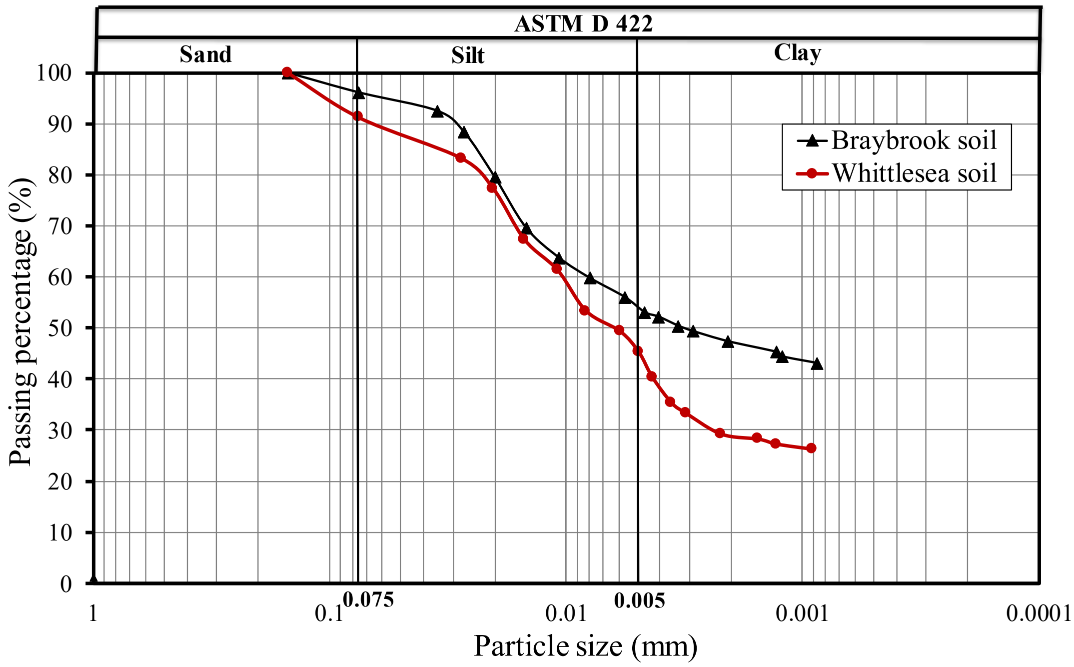

Figure 3.3. Grain size distribution of Braybrook and Whittlesea soils

Table 3.2. Physical properties of Braybrook and Whittlesea soils

Characteristics	Values and descriptions	
	Braybrook	Whittlesea
Colour	Dark grey	Brown
Depth (m)	1-2	1-2
Specific gravity (G_s)	2.71	2.69
Organic content (%)	3.1	2
Grain size analysis Passing No. 200 sieve Sand (4.75 to 0.075 mm) % Silt (0.075 to 0.005 mm) % Clay (< 0.005 mm) %	 96 4 43 53	 90 10 44 46
Atterberg limit Liquid limit (LL) % Plastic limit (PL) % Plasticity index (PI) %	 73.7 23.2 50.5	 50.2 22.6 27.6
Linear shrinkage (LS) %	20.3	9.6
Soil classification (USCS)	CH	CH-MH
Standard Proctor Compaction Maximum Dry Density (MDD) kN/m^3 Optimum Moisture Content (OMC) %	 14.9 25.0	 17.3 18
Modified Proctor Compaction Maximum Dry Density (MDD) kN/m^3 Optimum Moisture Content (OMC) %	 16.71 19.30	 Not available Not available
Unconfined Compressive Strength (UCS) kPa	283	201
Swelling potential (25 kPa) %	6.6	2.1

3.3.3 Atterberg limit

Liquid limit (LL) and plastic limit (PL) tests were conducted according to the ASTM-D4318 (2000) procedure. Before the tests, Braybrook and Whittlesea soils were sieved using sieve No. 40 (0.0425 mm), and the portions of the soils that passed through the sieve were used for the tests. Water was added to the dry soil. The mixture was then left for 24 hrs before starting the tests to allow thorough permeation of the water throughout the soil.

Multipoint (method A) was used to determine the liquid limit of the soils. The liquid limit values for Braybrook and Whittlesea soils were found to be 73.7% and 50.2%, respectively.

For the plastic limit, following the ASTM-D4318 (2000) standard, approximately 10 gm of the soil was rolled to 3.2 mm diameter thread. At this diameter, the soil crumbles under the pressure of rolling. The plastic limits were found to be 23.2% for Braybrook soil and 22.6% for Whittlesea soil. Therefore, the plasticity indices of Braybrook and Whittlesea soil were found to be 50.5% and 27.6%, respectively.

3.3.4 Linear shrinkage (LS)

The linear shrinkage test was performed according to the Australian Standard AS1289.3.4.1 (2008). Dry soil was mixed with water to the liquid limit, and the inside of the mould was lubricated using silicon grease. The mixture was placed in the mould and left to dry at a constant room temperature. Finally, the specimen was dried in an oven at a temperature of 105°C for 24 hrs (**Figure 3.4**). Linear shrinkage values for Braybrook and Whittlesea soils were found to be 20.3% and 9.6%, respectively.

Figure 3.4. Photographic linear shrinkage evidence of Braybrook soil samples

3.3.5 Classification

According to the values of plasticity index (PI) and linear shrinkage (LS), Braybrook soil was categorised as a highly reactive soil, while Whittlesea soil was categorised as a medium reactive soil (Hazelton & Murphy 2007a).

According to the Unified Soil Classification System (USCS), Braybrook was classified as clay with high plasticity (CH); however, Whittlesea was classified as silty clay to clayey silt with high plasticity (CH-MH) (ASTM-D2487 2006).

3.3.6 Proctor compaction test

Proctor compaction tests were performed according to the Australian Standards (AS1289.5.1.1 2017; AS1289.5.2.1 2017). The main objectives of soil compaction are to improve the engineering properties of soil. Soil compaction is commonly evaluated using standard and modified Proctor compaction tests. Water was added to the soil at various moisture contents. The mixtures were then left for 7 days in sealed polythene bags to allow the water to become uniformly distributed throughout the soil before compaction. For the standard Proctor compaction test, a soil at a selected moisture content was placed into a mould of 105 mm diameter and 115.5 mm height in three layers, with each layer compacted by 25 blows of 27 N hammer dropped from a distance of 300 mm, producing a compactive effort of 596 kJ/m^3 (AS1289.5.1.1 2017). For the modified Proctor compaction test, a soil at a selected moisture content was placed into a mould of 105 mm diameter and 115.5 mm height in five layers, with each layer compacted by 25 blows of 49 N hammer dropped from a distance of 450 mm, producing a compactive effort of 2703 kJ/m^3 (AS1289.5.2.1 2017).

The standard and modified compaction curves for Braybrook soil are shown in **Figure 3.5**. Whittlesea soil was used to check the validity of a new method proposed in this study to estimate the OLC for basaltic expansive soils. This method was suggested as a result of traditional tests data, which relied on preparing specimens using the standard compaction test. Therefore, **Figure 3.6** shows only the standard compaction curve for Whittlesea soil. It is obvious that for Braybrook soil, the optimum moisture contents (OMCs) for standard and modified compaction curves were found to be 25% and 19.3%, respectively, while the OMC for Whittlesea soil was 18%. For standard compaction curves, the maximum dry densities (MDDs) were found to be 14.9 kN/m^3 for Braybrook soil and 17.3 kN/m^3 for Whittlesea soil. However, for the modified compaction curve, the MDD for Braybrook soil was 16.71 kN/m^3.

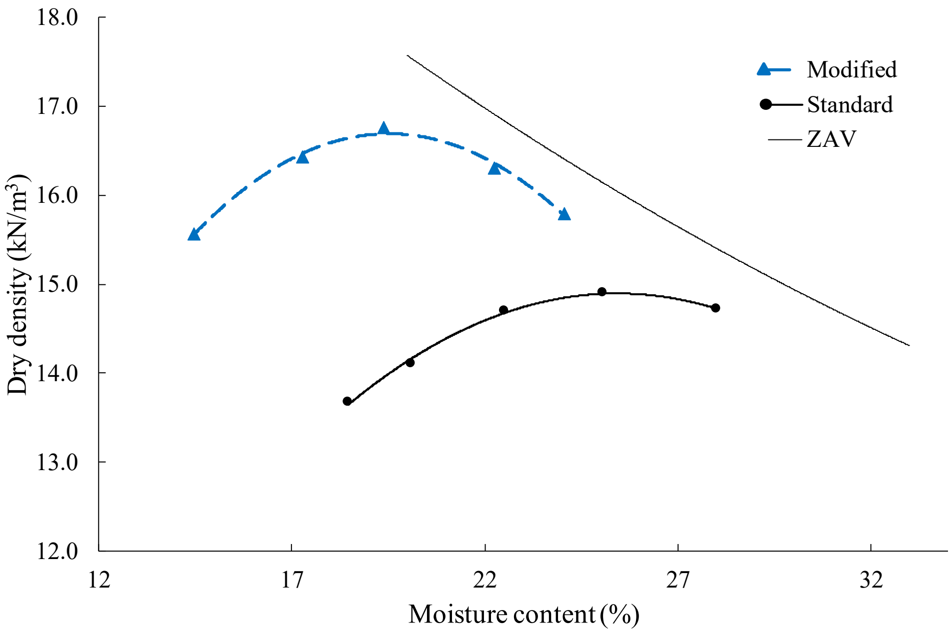

Figure 3.5. Standard and modified Proctor compaction curve of Braybrook soil

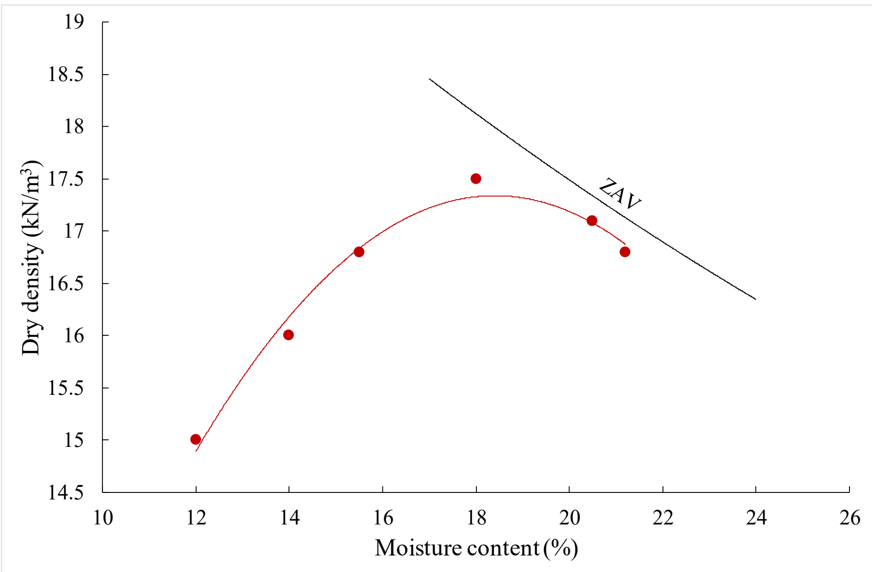

Figure 3.6. Standard Proctor compaction curve of Whittlesea soil

3.3.7 Unconfined compressive strength test

Braybrook and Whittlesea specimens were prepared and compacted using standard Proctor energy at an optimum point (OMC and MDD). The dimensions of these specimens were 102 mm diameter by 115 mm height. Using the Universal Testing Machine (UTM) shown in **Figure 3.7**, the specimens were loaded at a displacement rate of 1 mm/min to ensure the test finished within 15 minutes. This was to ensure that the drying of the specimen was minimal and did not affect the test results. The specimens were loaded until the stress declined after reaching a peak value, or until a strain value of 15% was achieved (AS5101.4 2008). The peak UCS values for Braybrook and Whittlesea soils were found to be 283 kPa and 201 kPa, respectively.

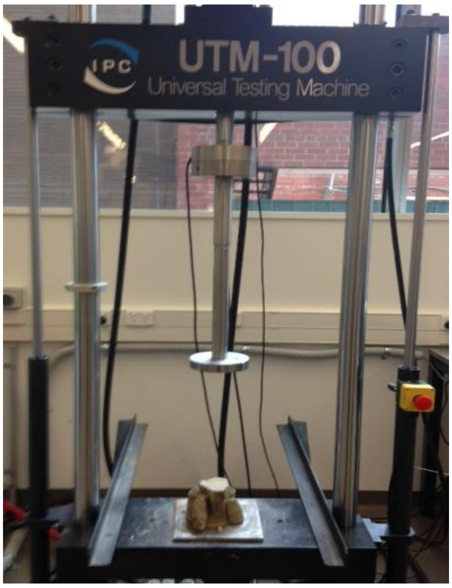

Figure 3.7. Universal Testing Machine (UTM)

3.3.8 One-dimensional swell test

Using the standard Proctor compaction test, both soils were compacted at OMC and MDD. The oedometer samples were then extracted using a ring of 45 mm internal diameter and 20 mm length. The specimens were placed in the consolidation frame and then loaded under a pressure of 25 kPa until no additional movement was recorded. Next, the specimens were inundated with water and allowed to swell under the same applied pressure of 25 kPa. The pressure was chosen to simulate the in-situ stress, similar to that in which the soils are naturally found in. The swelling potential of Braybrook and Whittlesea soil was found to be 6.6% and 2.1%, respectively.

3.4 Experimental Procedure for Determination of the Optimum Lime Content (OLC) for Basaltic Soils

An extensive suite of laboratory tests, including conventional classification, deformation and strength tests, accompanied by pH measurement, X-Ray Diffraction (XRD) and Scanning Electron Microscopy (SEM), were performed on treated and untreated samples (Braybrook and Whittlesea soils) to determine the OLC.

3.4.1 pH measurement

A pH meter is a scientific instrument that measures the hydrogen-ion concentration (pH) in a solution, demonstrating its acidity and alkalinity. This instrument consists of a meter and electrode, as shown in **Figure 3.8**. Firstly, the electrode is calibrated by using at least two calibration standards (buffers) to determine the slope and offset of the electrode. This step compensates for any change in the electrode and determines if it is working properly. Secondly, to measure the pH concentration, the electrode is rinsed in deionised water, then placed in the sample. After recording the value of pH, the electrode is removed from the sample and rinsed with deionised water, then placed in the next sample (Corporation 2006).

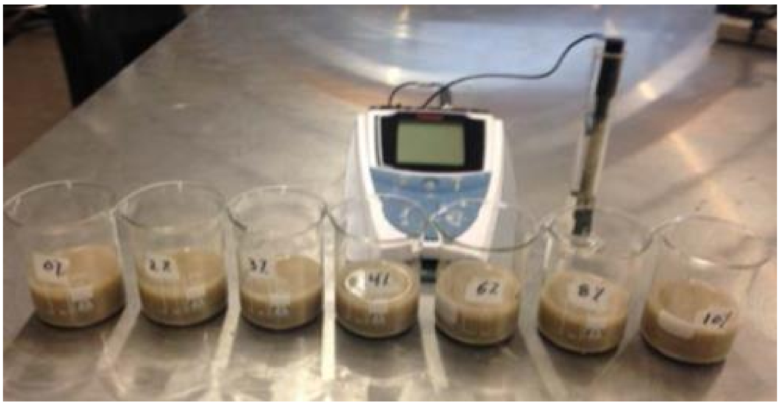

Figure 3.8. pH meter test

3.4.2 X-ray diffraction (XRD)

X-ray diffraction has been performed to study the structural properties of crystalline and amorphous materials on an atomic scale, as well as to investigate the mechanism of soil–lime reaction. One of the important advantages is that X-rays only interact weakly with matter and a single scattering approach is enough to analyse the experimental data (James 1982). Therefore, X-ray diffraction can satisfy many of the requirements of an ideal surface structure probe.

In this study, the D8 ADVANCE device, shown in **Figure 3.9**, was used to investigate the structural properties of crystalline and amorphous materials for Braybrook, lime-stabilised soils at different lime contents and hydrated lime. For the untreated and lime-treated soils, the samples were air dried (at 40°C) and crushed as a powder, then placed in the device container (Yi et al. 2015), as shown in **Figure 3.10**. An individual sample was then fixed inside the vacuum chamber. The entire chamber included the low energy electron diffraction (LEED), Auger spectroscopy and ion-sputter system. LEED was beneficial for describing the surface periodicity of the reconstructed surface. Determination of crystal structure was obtained from the integrated intensities of the reflections. The integrated intensity was measured in a scan, which began away from the reflection at background level, then went through the peak intensity and finished again on the other side of the background level. The detector arrangement was adequately relaxed in angular collimation such that all diffracted photons were detected. In surface X-ray crystallographic work, the integrated intensities were measured by θ (Feidenhans'l 1989). The output data was analysed by using EVA software to identify the main mineral components of these samples.

Figure 3.9. D8 ADVANCE device used in XRD test

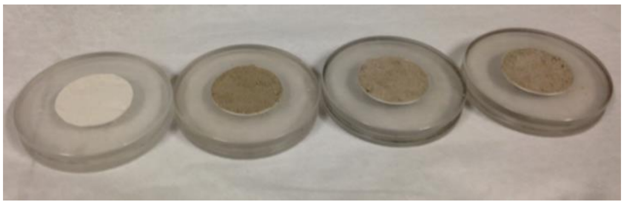

Figure 3.10. Preparation of XRD samples

3.4.3 Scanning electron microscopy (SEM)

The SEM instrument (**Figure 3.11**) uses a beam of a high-energy electron to produce a set of signals at the surface of specimens. The signals that develop from electron-sample interaction detect information about the sample, including texture, chemical composition, and crystalline structure. The principle of the SEM is presented in **Figure 3.12**. Two electronic beams work simultaneously. One hits the specimen and the other hits a cathode ray tube (CRT) viewed by the operator. Due to the impact of the incident beam on the specimen, different electron and photon emissions are released. The selected signal is collected, detected, amplified and used to modulate the brightness of the second electron beam, in which a big collected signal produces a bright spot on the

CRT. However, a small signal produces a dimmer spot. The two electron beams are scanned concurrently so that for each point scanned on the specimen, there is a corresponding point on the CRT. Therefore, a typical SEM instrument consists of two units. The first is the electron column, which includes the electron beam scanning the specimen. The other is the display console, which includes the second electron beam, which impinges on the CRT (Joy 2006).

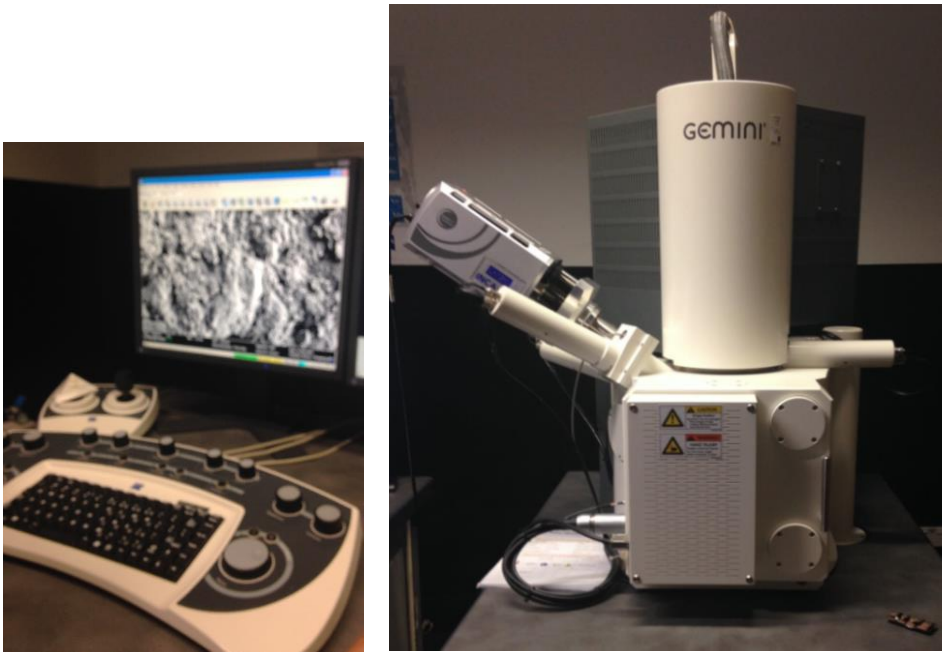

Figure 3.11. SEM instrument

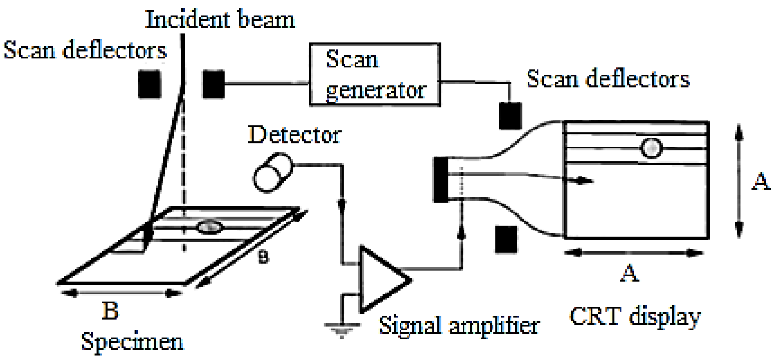

Figure 3.12. Diagram presenting the principles of the SEM (Joy 2006)

In this study, small segments of untreated and treated samples were prepared in irregular shapes and then air-dried at 40°C. The specimens were not good electrical conductors; therefore, it was preferable to provide some conductivity by evaporating a thin gold layer (3 to 10 nm) on the surface of the samples. Thus, the samples can be tested at any desired beam energy (Echlin 2009; Joy 2006). The K975X Turbo-pumped thermal evaporator shown in Figure 3.13 was used to provide a thin gold layer. The samples were then inserted in the sample chamber of the SEM instrument and the crystalline structures of the samples appeared on the display console.

Figure 3.13. K975X Turbo-pumped thermal evaporator used to provide a thin gold layer

3.5 Experimental Procedures for Modification of the MPK Framework

To check the validity of the MPK framework, the LWSBS was first generated for both the untreated and lime-treated specimens by establishing the compaction curves at different net stresses. Each curve was developed by performing static compaction tests at different moisture contents. The different state paths were applied to the clay, and the collapse and swelling potentials were investigated.

3.5.1 Experimental procedure for generation of the LWSBS

The specimens were compacted statically (using a stepper motor closed-loop controlled load frame shown in **Figure 3.14**) into a steel mould of 50 mm internal diameter and 38 mm high. The specimens were compacted from the loosest state after being mixed with various amounts of water. The moisture content varied from 0% to 50%, while the static compaction stress (preconsolidation pressure) varied from 2 kPa to 4000 kPa. The stress of 2 kPa represented the loosest state and resulted from the weight of the loading cap.

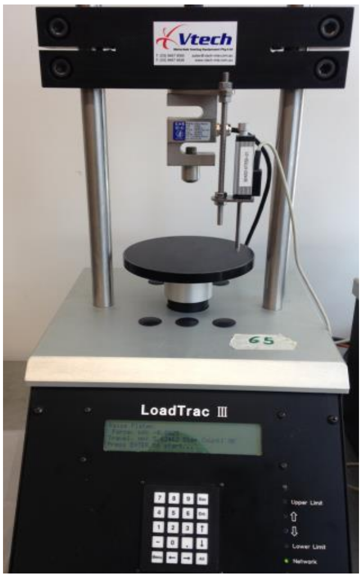

Figure 3.14. Stepper motor closed-loop controlled load frame used to statically compact samples

A custom-built compaction/stress-path chamber was designed and used, as shown in **Figure 3.15**. The static compaction procedure to generate the LWSBS for the untreated sample can be summarised as the following:

1- The dry specimens were mixed with water at different moisture contents and then left in sealed containers for 7 to 10 days to allow the water to become uniformly distributed throughout the soil (AS1289.5.2.1 2017).

2- The inside walls of the mould were lubricated using silicon grease to minimise friction between the wall and the soil.

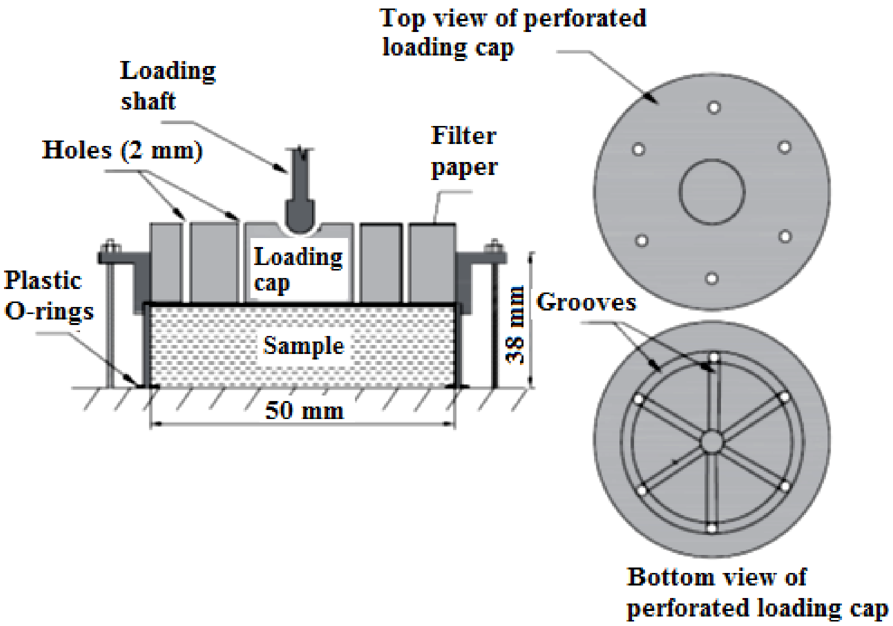

Figure 3.15. Set up of custom-built equipment to statically compact samples and state path tests

3- The soil was then placed into the mould with a sealed bottom, as shown in Figure 3.22. A filter paper was placed at the top of the specimen to capture any water leaving the specimen, which could be measured at a later time.

4- For unsaturated specimens, the net normal stress was the difference between total normal stress and the pore air pressure. To make sure that the air pressure was equivalent to the atmospheric pressure, the rate of stress was controlled. For specimens on the dry side of the line of optimums (LOO) where there was a continuous air phase, the stress rate was high (20 kPa/min for the stress range below 1000 kPa, and 100 kPa/min for the stress range greater than 1000 kPa). However, when the moisture content of the specimen reached the LOO, the air phase was no longer connected and was discontinuous (Hasan & Fredlund 1980). Subsequently, the dry density decreased, and the static compaction curves between the LOO and the normally consolidated line (NCL), where the degree of saturation was equal to 100%, did intersect (Kodikara 2012; Kurucuk 2011). To decrease the reduction in the dry density and subsequently avoid the curves intersecting between the LOO and NCL, the rate of stress was reduced (drained loading). Therefore, when the moisture content of the sample reached the LOO, the stress rate was then lowered to a rate of 0.5 kPa/min for static stresses less than 1000 kPa and 1.5 kPa/min for static stresses greater than 1000 kPa. During compression, the specimen cell was wrapped in plastic wrap and the load frame was contained in a plastic bag to minimise any reduction in water content.

5- At the end of the test, the total weight and specimen volume were measured, which determined the final void ratio. The loss in the water content was calculated to be less than 0.3% of the original measurements. This loss in moisture was to be satisfactory and therefore neglected.
6- The previous steps (1-5) were repeated for other specimens at different moisture contents and net stresses to establish the LWSBS.

The procedure to generate the LWSBS for the lime-treated specimens was slightly different, with the point of differences summarised below:

1- To prepare a compacted stabilised specimen statically, the dry soil was mixed thoroughly with hydrated lime for approximately five minutes. Water was then added and mixed thoroughly in order to allow the cation exchange and flocculation processes to start.
2- For the stabilised specimens with a moisture content beyond LOO, the rate of stress was reduced to 4 kPa/min for static stresses less than 1000 and 8 kPa/min for static stresses greater than 1000 kPa. The reason for increasing the rate of stress was to allow the cation exchange and flocculation process to start once the water was added.
3- The loss in water content was found to be less than 0.5%, slightly higher than the untreated specimen, possibly due to some of the water reacting with the hydrated lime.

3.5.2 Experimental procedure for state paths tests

After generating the LWSBS for untreated and treated samples, a set of state path tests were conducted to investigate the suitability of the MPK framework. For wetting tests, a medical syringe was used to inject a calculated amount of water through the six holes in the top cap (Figure 3.15) in several steps. A series of state path tests for the untreated and lime-treated expansive clay specimens included a combination of Loading and Wetting (LW), Loading-Wetting and Loading (LWL), Loading-Unloading and Wetting (LUW), Loading-Unloading-Wetting-Unloading and Wetting (LUWUW), collapse potential and swelling potential.

The purpose of conducting the combination of Loading and Wetting (LW) and Loading, Wetting and Loading (LWL) tests was to check whether a specimen, loaded to a certain stress level and then wetted at that stress, would follow the LWSBS path or not. To perform the LW path test for untreated clay, the required amount of water was added to the dry clay and then mixed thoroughly. The clay-water mix was then left in a plastic bag in order to achieve equilibrium. Subsequently, the specimen was compacted with static force, from nominal stress (2 kPa) to the planned stress, and then wetted to approximately the LOO in incremental steps. The end of each step was identified when the vertical displacement became insignificant or zero. The time interval for each step ranged from 6 to 24 hrs in duration. For lime-treated specimens, dry clay was mixed thoroughly with hydrated lime. Water was then added and mixed thoroughly, and the specimen was then compressed from a nominal stress of 2 kPa to the target stress. The specimen was cured for 7 days (relative humidity was kept at 95% and the temperature at 20°C) (Al-Taie et al. 2018). After curing, the specimens were loaded from nominal stress (2 kPa) to the target stress, and then wetted to reach saturation. The end of each step was identified when the vertical displacement reached a constant value. The duration of each step ranged from 2 to 4 hrs.

The purpose of conducting the combination of Loading, Unloading and Wetting (LUW) state path was to examine whether a specimen (untreated or lime-treated) loaded to a certain stress (compaction stress) would move inside the LWSBS after unloading to a stress lower than the compaction stress, and then go back to the LWSBS after wetting. In order to allow for direct comparison of the impact of lime treatment on the volumetric behaviour of expansive clays, the untreated and lime-treated samples were tested under similar state paths.

A series of tests were conducted on untreated and lime-treated clay to investigate the variation of collapse and swelling potential with stress levels. Specimens were prepared at a certain moisture content, then compressed to a certain compaction stress. The specimens were then wetted to reach saturation state under various operational stresses. This procedure was repeated for specimens prepared at different moisture contents and then compacted to various compaction stresses.

Finally, a series of tests were also performed to investigate the slope of the unloading-reloading curve (κ) and compression line (λ) for untreated and treated clay soil at various moisture contents. The specimens were loaded to different compaction stresses and then unloaded to different operational stresses. These data were required for modification of the MPK, development of a procedure to predict collapse and swell potential, and SWCC measurement.

3.6 Experimental Procedure for Studying the Soil Water Characteristic Curve (SWCC) at and below the LWSBS

In this study, the SWCC was investigated at and below the yield surface proposed by Kodikara (2012) (LWSBS) for the untreated and lime-treated (4%) expansive clay. The values of suction (water potential) were measured by using Hyprop, filter paper or a chilled mirror hygrometer (WP4C) according to the moisture contents. Hyprop, which relies on the axis translation technique, measures the matric suction of soil within moisture content in low suction ranges (up to 80 kPa) (Ridley & Wray 1996; Tarantino & Tombolato 2005; UMS 2013). This technique takes several minutes to measure the matric suction. However, WP4C, which depends on the chilled mirror dew-point technique, measures the total suction (total suction= matric suction + osmotic suction) of soil within the moisture content in high suction ranges (Decagon 2012). This technique takes several minutes to several hours to measure the total suction (see Table 2-1). The filter paper technique measures both total and matric suction values (ASTM-D5298 1994b). However, this technique takes a considerably longer amount of time to measure the matric and total suction values (2-57 days to measure the matric suction and 2-14 days to measure the total suction), as shown in Table 2-1. Therefore, the filter paper technique was used to measure the osmotic suction, and by subtracting this value from the total suction that was measured from the WP4C, the matric suction could be calculated. Consequently, the SWCC could be obtained in terms of matric suction.

3.6.1 Hyprop measurement

Hyprop, which contains a tensiometer, depends on the axis translation technique to measure matric suction (Tarantino & Mongiovì 2001). Matric suction relies on the adsorptive forces binding water to a matrix and is defined as the difference between pore air pressure and pore water pressure of the soil (u_a-u_w). The Infield7 instrument (UMS 2010) shown in **Figure 3.16** was used in this study. The tensiometer includes a hollow shaft filled with water that is connected to a high air-entry porous ceramic cone at one end and the sensor base (pressure transducer) at the other end, as shown in Figure 3.16. The tensiometer is designed to measure the water potential or tension held in the soil mass. Tension, which relies on the moisture content of the soil, indicates how tightly the water is bound to the soil. It is also a measure of the energy needed to overcome the gravitational and capillary forces required to extract water from the soil mass (Singh & Kuriyan 2003). Once the tensiometer was inserted into the soil specimen (**Figure 3.17**), the ceramic cone transported water (by capillary action) from its interior to the exterior due to the difference between the stress of water inside the tensiometer and the suction of the soil. Subsequently, this movement generated a pressure in the tensiometer shaft; this pressure was referred to as suction. The water flow from the tensiometer shaft into the soil specimen through the cone of the tensiometer continued until an equilibrium was achieved between the water in the tensiometer tube and that in the soil specimen. At equilibrium, the water tension in the tensiometer was equivalent to the suction in the soil, and this value appeared on the instrument monitor. As the soluble salts that create the osmotic suction can transfer through the porous ceramic cone freely, the transducer records only the matric suction (Murray & Sivakumar 2010).

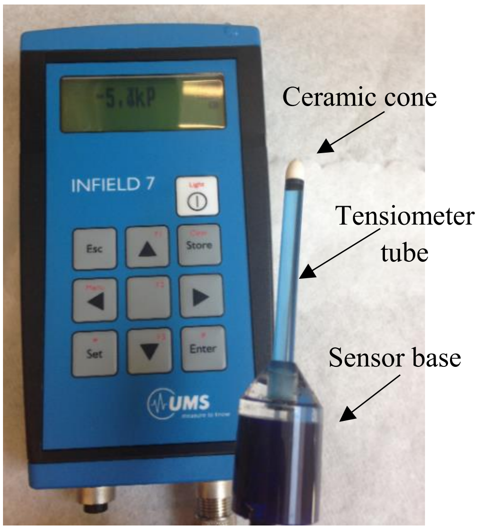

Figure 3.16. Infield 7 instrument used to measure matric suction

Figure 3.17. Matric suction test

As the pressure in the tensiometer shaft represents the matric potential in the soil specimen, it is important to remove any air (dissolved or solved) in the water that is contained in the tensiometer shaft and the sensor base. To achieve this purpose, the tensiometer and the sensor base unit were refilled with degassed water by following the details described in UMS (2015). Degassing was conducted using syringes with spacer snaps. Once the water was degassed, the tensiometer was filled without trapped air bubbles. The tensiometer was kept in an upright position, as shown in **Figure 3.18**. The bottom syringe was filled with degassed water, and the air bubbles were removed before connecting to the ceramic cone. The top syringe was half-filled with degassed water, and suction was applied by locking the spacer snaps (Figure 3.25). Due to this suction, the degassed water from the bottom syringe moved to the top syringe through the ceramic cone and the tensiometer shaft. This procedure removed all trapped air in the tensiometer and took at least 2 hrs. The same procedure was followed to refill the sensor base with degassed water, as shown in Figure 3.25; however, this process needed at least 24 hrs. The refilled tensiometer was then connected to the sensor base.

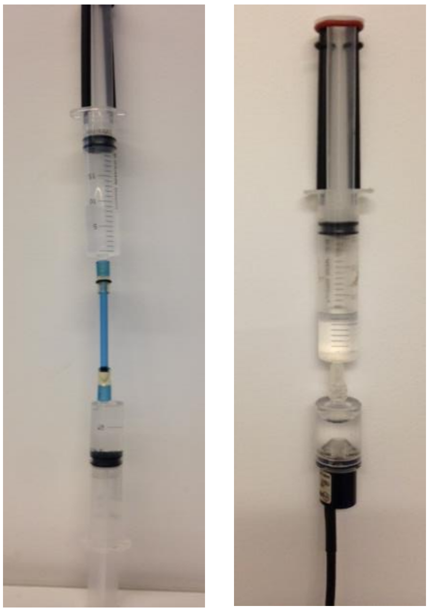

Figure 3.18. Degassing water using the syringe method

3.6.2 WP4C measurement

The WP4C device (Decagon 2012) depends on the chilled mirror dew point technique to measure the total water potential (total suction) of a soil sample. The total suction reading that is observed is in MPa and pF units. The WP4C shown in **Figure 3.19** consists of a temperature sensor, mirror and photodetector cell (Leong et al. 2003).

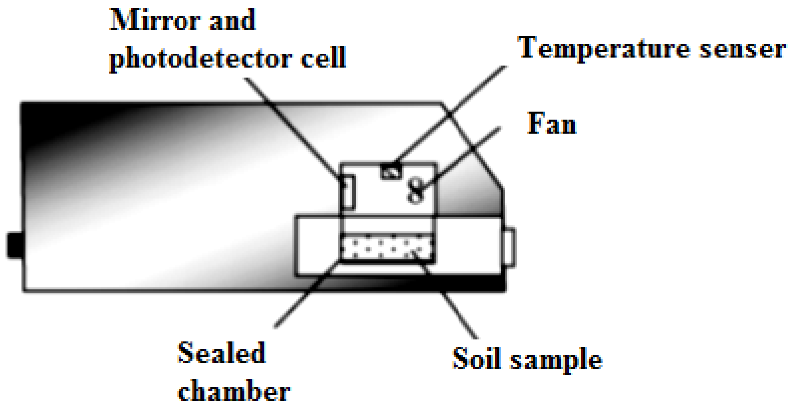

Figure 3.19. Schematic of the chilled mirror dew point device (Leong et al. 2003)

The sample was placed in a standard cup of 37.5 mm diameter and approximately 10 mm height. This cup was made of plastic or stainless steel (ASTM-D6836 2016). The sample was then placed on the drawer, as shown in **Figure 3.20**, and pushed into the chamber. The sample was lifted and the chamber was closed to start the measurement process when the switch was turned to the READ status. Therefore, it was important to prevent filling the standard cup with the sample to avoid the sensor contamination. During READ status, the equilibrium between the relative humidity of the air above the sample and the relative humidity of the air in the pores of the soil sample started (Murray & Sivakumar 2010). This process took approximately 15 minutes. At equilibrium, the mirror temperature was reduced by using temperature control. When the temperature decreased, the vapour began to condense on the mirror at a particular point called the dew point. As the difference of the reflection from the mirror, this point was realised by the photodetector cell (Leong et al. 2003). The temperature at which condensation developed was recorded by a thermocouple attached to the mirror. The relative humidity was measured and then converted in terms of the total section using Equation 3-3 (Bulut et al. 2001; Likos & Lu 2003).

$$\psi = -\frac{R \times T}{\upsilon \times \omega} \ln(RH) \qquad 3\text{-}3$$

where ψ is the total suction (kPa), R is the gas constant (8.3143J/mol.K), T is the absolute temperature (K), υ is the specific volume of water, and ω is the water molecular mass (kg/kmol), and RH is the relative humidity.

Figure 3.20. WP4C device

When the relative humidity is equal to 1 (100%), the total suction is zero, based on Equation 3-3. The total suction value increases as the relative humidity decreases. The WP4C device measures the relative humidity up to ±0.01% accuracy (Leong et al. 2003). This device can record 100% relative humidity if pure water is put in the standard cup, due to the partial pressure of water being equal to the saturated vapour pressure at a certain temperature. That indicated zero matric suction, which is the only suction component of pure water. The saturated vapour pressure of pure water pressure is higher than the unsaturated soil pores, due to the dissolved salts ions and the structure of pores. As a result, the relative humidity of unsaturated soil is less than 100%, and subsequently has higher total suction.

Initially, the WP4C should be calibrated by using any salt solution with known osmotic suction. ASTM-D5298 (1994b) and Decagon (2010) presented the osmotic suction for various salt solutions. In this study, the suction of 0.5 molars KCl was measured and adjusted to the value of 2.2 MPa at 20°C. Decagon (2010) suggests that the calibration should be carried out after every 50 sample measurements.

The WP4C device can measure high suctions (up to 300 MPa). For total suction measurement less than 5 MPa, there is ±0.05 MPa error. However, for the total suction values higher than 5 MPa, there is only a ±1% error (Decagon 2010).

3.6.3 Filter paper

The filter paper technique is the only method that measures both total and matric suction. In this technique, the soil specimen and filter paper are left to reach moisture equilibrium either in contact with each other to measure matric suction, or not in direct contact to measure total suction in a constant temperature (**Figure 3.21**). Direct contact between the soil specimen and the filter paper allows water in the liquid phase and solutes to exchange freely, while the separation between the soil specimen and the filter paper by a vapour barrier allows water exchange in the vapour phase only, and does not allow solute movement (Tarantino et al. 2009). At equilibrium, the suction value of the soil specimen is equivalent to that of the filter paper. After equilibrium, the moisture content of the filter paper is measured. By using a suction versus a filter paper calibration curve, the corresponding suction value is obtained from the curve (ASTM-D5298 2016; Fattah et al. 2013).

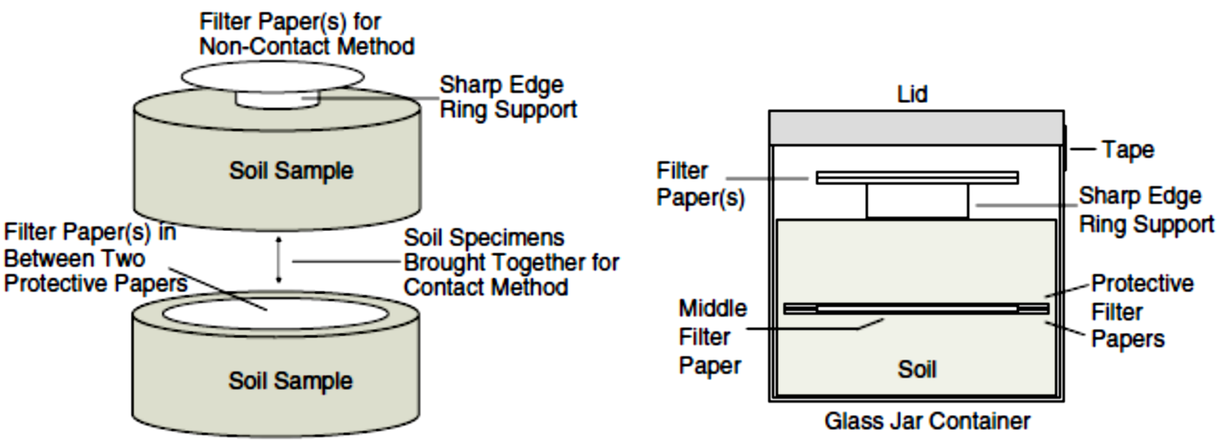

Figure 3.21. Diagram of measuring matric and total suction by using the filter paper technique (Tarantino et al. 2009)

The testing procedure to measure matric suction using filter paper can be summarised as follows:

1- A plastic jar of 250 ml volume was available and could be easily used for suction measurement, as shown in **Figure 3.22a**.
2- To prepare two identical specimens, the dry soil was mixed with a certain amount of water and then compacted statically to a target stress level (Figure 3.22b).
3- A filter paper of 5 cm diameter was placed between two larger protective filter papers. The sandwiched filter papers were placed on top of the soil specimen, as shown in Figure 3.22c & d, and the other soil specimen was then put on the top. Physical contact between the sandwiched filter paper and the soil specimens was very important.
4- The two soil specimens with embedded filter papers were taped together and then placed gently in the jar, as shown in Figure 3.22e.

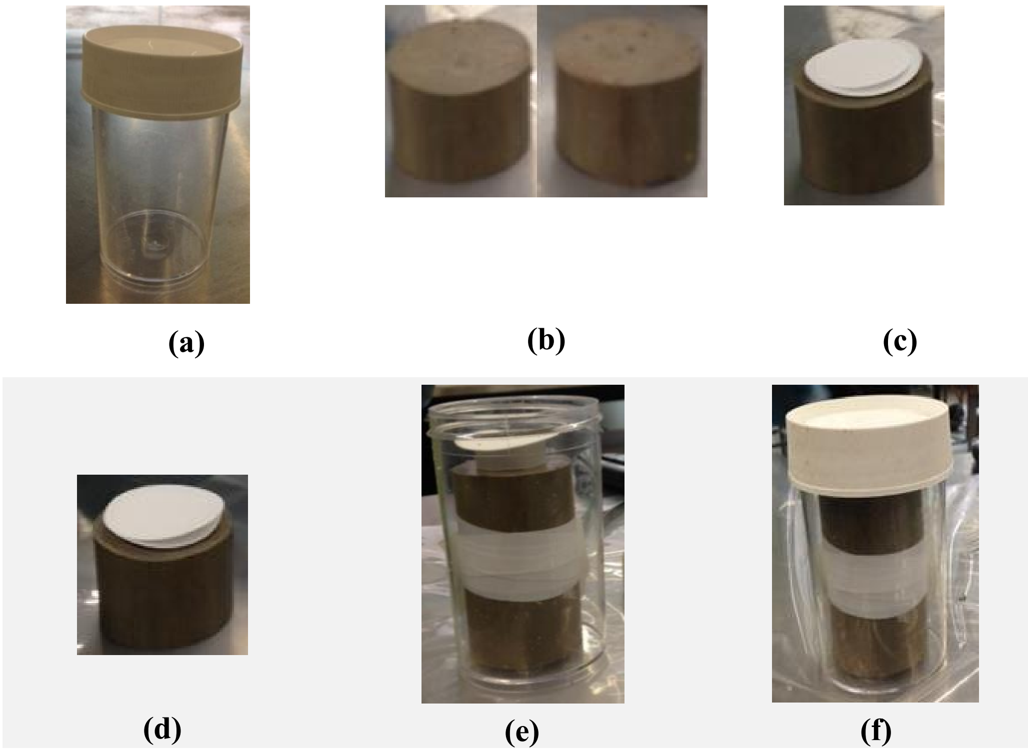

Figure 3.22. Matric suction measurement using the filter paper technique

To measure total suction, the following steps were added:

1- A PVC O-ring, with the sharp edge facing up, was inserted and placed on the top of the soil, as shown in Figure 3.22e.

2- Two filter papers were placed on the top of the ring (Figure 3.22e).
3- The lid was used to close the jar tightly to prevent any moisture exchange between the air inside and outside of the jar (Figure 3.22f).

The jar was kept in an insulated container for suction equilibrium, and left for at least one week. Following that, the moisture contents for the two filter papers on the ring and the filter paper between the protective filter papers were obtained. The corresponded suction values were measured using the calibration curve recommended by ASTM-D5298 (2016).

3.6.4 Experimental procedure for generation of suction distribution at the LWSBS

To identify the suction distribution of the untreated and lime-treated clays at the LWSBS in e-e_w space, firstly, it was important to measure the SWCC at the LWSBS under different net stresses. Specimens were prepared at various moisture ratios and then compacted statically at different net stress levels. The compaction stress varied from 2 to 4000 kPa. The values of suction were then measured by using the Hyprop, filter paper, or chilled mirror hygrometer (WP4C) device based on the respective moisture contents.

The Hyprop, which contains tensiometers, measures the matric suction of a soil within the moisture content over a low range of suction (UMS 2013). However, the WP4C relies on the chilled mirror dew point technique, which measures the total suction (i.e. matric suction and osmotic suction) of the soil within the moisture content varied over high ranges of suction (ASTM-D6836 2016; Decagon 2012). As the filter paper technique can measure total and matric suctions, the osmotic suction was obtained at any moisture content value (ASTM-D5298 1994a). For example, to produce the SWCC for the untreated expansive clay at a planned compaction stress, the steps below were followed:

- Specimens at different moisture contents were prepared and compacted statically to the planned compaction stress, as mentioned previously. The void ratios were then calculated.
- At high moisture contents (i.e. the range of matric suction from 0 to 100 kPa), the Hyprop was used to measure the matric suction.
- The WP4C was used to measure the total suction at low moisture contents.
- The filter paper was used to measure the total and matric suction at different moisture contents; subsequently, the osmotic suction for expansive clay was obtained.
- Steps 1 to 4 were repeated for specimens compacted statically at different net stress levels.

The same procedure was followed for the lime-treated specimens, with the exception being that the specimens were cured for 7 days after compaction, and then the suction values were measured.

Secondly, the relationship between suction and void ratio was obtained at different net stresses. Consequently, the suction distributions of the untreated and lime-treated specimens were plotted.

3.6.5 Experimental procedure for generation of suction distribution below the LWSBS

To obtain the SWCC below the yield surface, specimens were prepared under different moisture ratios and then compressed statically to a certain net stress, then unloaded to an operational stress. The specimens were then wetted with different amounts of water at that operational stress. The suction of each specimen (after wetting) was measured by the Hyprop or WP4C, as mentioned earlier. Consequently, the SWCCs were obtained for each net stress level. For the lime-treated specimens, the same procedure was followed, except that the specimens were cured for 7 days. Furthermore, the volume changes after wetting were recorded and measured when the change in the volume change became negligible. Consequently, the relationship between void ratio and matric suction was obtained. Finally, the suction distribution below the LWSBS was plotted.

In order to measure the suction using the Hyprop or WP4C, it is important to note that after wetting the specimens to a certain amount of water at a certain operational stress and after noticing that the volume change is negligible, the specimens should be removed from the setup and placed in the Hyprop or WP4C. This means that the suction values will be measured under zero operational stress. Therefore, it is important to measure the slope of the unloading-reloading curve (κ) for the untreated and lime-treated clays at different moisture contents.

3.7 Experimental Procedure for Investigating the Behaviour of Soils under Cycles of Swell-Shrink

3.7.1 Swell-shrink cycles

Cycles of swell-shrink tests were conducted on untreated and treated specimens, with 2, 3 and 4 per cent lime content after a curing period of 7 days. These tests were performed to investigate the effect of lime stabilisation on the swell-shrink path after reaching equilibrium, which meant that an equal swelling and shrinkage deformation was achieved for each cycle.

Two sets of specimens were prepared based on initial moisture content and dry density. The first set included specimens with different lime contents that were compacted at optimum moisture content and maximum dry density, then subjected to cycles of swell and shrink tests under low pressures (Al-Taie et al. 2016). The second set included specimens prepared at optimum lime content that were compacted at moisture contents lower than optimum moisture content, then subjected to cycles of swell and shrink tests under low pressures.

The specimens were subjected to cycles of swell and shrink tests according to the procedure developed by Tripathy et al. (2002). The lime-treated specimens were all cured for 7 days and then subjected to cycles of swell-shrink. These tests were performed by using the oedometer device with some modifications (**Figure 3.23**) to allow shrinking of the specimens under controlled pressures of 6.25 kPa and 25 kPa, and a constant temperature of 40 ± 0.5°C. The test device was kept in a temperature controlled environmental chamber during shrinkage to control and maintain the temperature at the desired value. In addition, the top cap was perforated in order to inject water into the samples using a medical syringe during the swelling process (Figure 3.23).

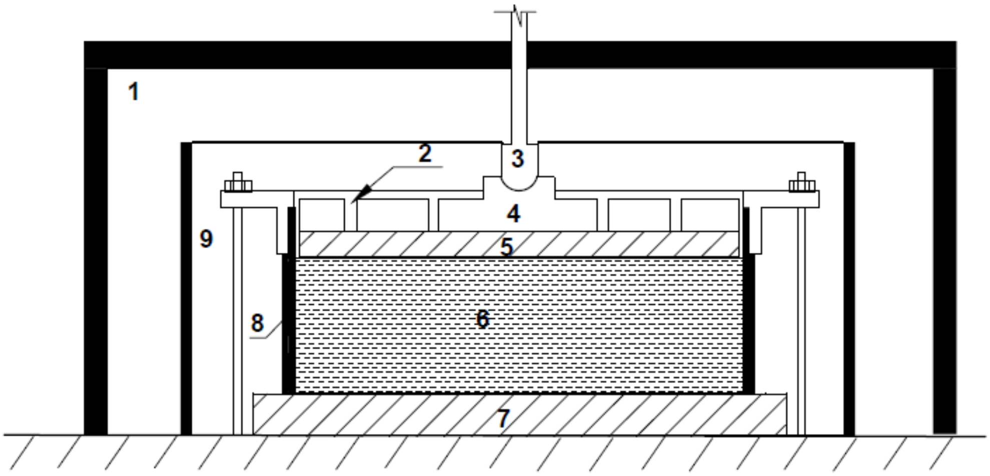

1, Temperature control chamber 2, Injection path 3, Loading shaft 4, Top pressure plate
5, Top porous stone 6, Sample 7, Bottom porous stone 8, Ring 9,Water jacket

Figure 3.23. Modified oedometer cell

A certain pressure was applied to at least six specimens, with dimensions of 45 mm diameter by 20 mm height. The specimens were inundated with water and allowed to swell under room temperature while vertical movements were recorded. When the swelling changes were found to be negligible, the reverse process of shrinkage commenced. Initially, water in the inner cell (around the ring cell) was removed, and the oedometer cells were placed in the chamber at a constant temperature of 40 ± 0.5°C. During this step, a vertical stress (6.25 kPa or 25 kPa) was maintained. The vertical movements were also recorded. The swelling and shrinkage movements were recorded using dial gauges with an accuracy of 0.01 mm and a maximum displacement of 13 mm. At the end of the shrinkage process, the first swell-shrink cycle was achieved. At the end of the shrinkage process, the specimen temperature was returned to room temperature in approximately 2 or 3 hrs. The specimens were again inundated with water to start the second swell-shrink cycle. This procedure was repeated until equilibrium was reached, meaning that the vertical movement of swelling and shrinkage became equal to each other for each cycle.

3.7.2 Paths of void ratio- water content

After five cycles, the change in void ratio with water content was measured for both untreated and lime-treated specimens. The moment that the fifth shrinkage cycle finished, different calculated water amounts were added to each specimen using a medical syringe, through the holes that were provided in the top plate pressure (Figure 3.30). The tests were finished as the height changes became negligible. After measuring the weight, volume and moisture content of the specimens, the void ratios were calculated. To find the void ratio for the oven-dried or partially dried specimens, the volume of the specimens were measured using the kerosene technique, due to the development of cracks, as shown in **Figure 3.24**.

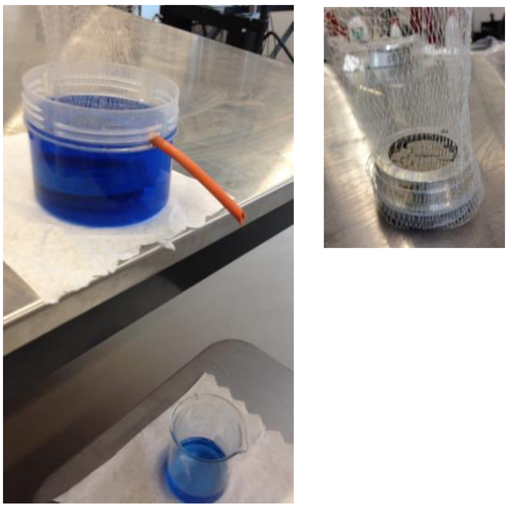

Figure 3.24. Volume measurement of dried samples using kerosene

By using the mathematical model proposed by Gould et al. (2011), the void ratio- water content paths of environmentally stabilised clay were expressed in Equations 3-4 and 3-5:

$$\boldsymbol{e(\omega) = f(\omega, a^*) - f(\omega, b^*) - f(0, a^*) + f(0, b^*) + e_r{}^*} \quad 3\text{-}4$$

$$\boldsymbol{f(x, y) = -\frac{m^*}{\emptyset\, \pi}\left(\emptyset\,(x - y)\, tan^{-1}[\emptyset\,(x - y)] - (0.5) ln\{1 + [\emptyset\,(x - y)]^2\}\right)} \quad 3\text{-}5$$

where: a^*, b^*, $e_r{}^*$, m^*, and $\emptyset$ are fitting parameter.

CHAPTER 4. DEVELOPING A SIMPLE PH BASED METHOD TO DETERMINE OLC

The optimum lime content (OLC) technique is widely used in the lime stabilisation design of soils. Many studies have adopted the Eades and Grim (1966) method to estimate the OLC for expansive soils. However, this method does not consider the effect of curing, which can cause a reduction in pH concentration over time. Therefore, it is important to investigate a method that takes into account the effect of curing on estimating the OLC.

4.1 Introduction

Chapter 4 presents a newly developed method to determine the OLC for basaltic clay. This aim was achieved by investigating the effect of curing on the behaviour of lime-stabilised basaltic expansive clays. The effect of the presence of low levels of organic material in the surface clay on the change in pH of the mixture was also studied. In this study, Braybrook and Whittlesea expansive clays (western and northern suburbs of Melbourne, Australia) were stabilised using different percentages of hydrated lime. Physical properties of untreated samples, and those treated with 2%, 3%, 4%, 6%, and 8% lime, were evaluated. A suite of tests was conducted to investigate the behaviour of the stabilised basaltic expansive clay over the curing period and to find the OLC. These tests included pH concentration at various curing periods (at 1.5 hrs and at 7, 28, and 57 days), Atterberg limit, linear shrinkage (LS) strain (without curing), swelling potential, and unconfined compressive strength (UCS) (under curing periods of 7 and 28 days). Furthermore, X-Ray Diffraction (XRD) and scanning electron microscopy (SEM) were conducted on Braybrook soil to investigate the mechanism of soil–lime reaction. The suitability of the Eades and Grim (1966) (a quick test to determine lime requirements for lime stabilisation) method in determining the OLC was also discussed.

4.2 Principle of the Developed Method

This chapter investigates the effect of curing on determining the optimum lime content for stabilised basaltic expansive clay, taking curing time and drop in pH content into account. This study suggests a modification of the Eades and Grim (1966) method as the preliminary common method to obtain the OLC for basaltic expansive soil. This modified method is based on four pillars. The first pillar includes the test results obtained by investigating two basaltic soils (Braybrook and Whittlesea soils). The second is the theory of the Eades and Grim method (1966). The third base is the study of previous research, such as Yunus et al. (2011) and Saride et al. (2013). The fourth important base is the understanding of the mechanism of reaction between lime and clay.

4.3 Experimental Program

To evaluate the effect of curing on determining the optimum lime content for stabilised basaltic expansive clay, a series of laboratory tests were conducted on Braybrook soil prior to stabilisation. These tests included specific gravity, organic content, grain size analysis, Atterberg limit, linear shrinkage, pH concentration, standard Proctor compaction, Unconfined Compressive Strength (UCS), and swelling potential complemented by XRD and SEM.

The Atterberg limit and linear shrinkage tests were conducted on both untreated and treated samples with no curing period. The tests focused on studying the lime stabilisation process, and included testing pH concentration, swelling potential, UCS, and SEM on both untreated and treated samples with curing periods of 7 and 28 days. The XRD was conducted on hydrated lime, untreated and treated samples that were cured for 28 days. Details of the testing methods are explained in Chapter 3.

4.4 Test Results

4.4.1 Specific gravity, organic content and grain size analysis

As mentioned in Chapter 3, the specific gravity and organic content of Braybrook clay were found to be 2.71 and 3.1%, respectively. According to the grain size distribution curve (Figure 3.8), the fine fraction (< 0.075 mm) of Braybrook soil is approximately 96% (the clay and silt contents are 53% and 43%, respectively), while the sand content is only 4%.

4.4.2 Atterberg Limit and Linear Shrinkage Strain

Liquid and Plastic Limit tests were conducted according to the ASTM-D4318 (2000) procedure. The liquid and plastic limits, and plasticity index, for untreated samples are 73.7%, 23.2%, and 50.5%, respectively. These results are compatible with previous findings of Karunarathne et al. (2014b). The results confirm that Braybrook soil can be classified as clay with high plasticity (CH) according to the Unified Soil Classification System ASTM-D2487 (2011).

The lime-treated samples (**Figure 4.1**) showed a gradual decrease in Liquid Limit (LL) with an incremental addition of lime. The Plastic Limit (PL) increased rapidly with the addition of lime of up to 4%. After this point, there was minimal change in the PL. Figure 4.1 also shows that there was a sharp decrease in the Plasticity Index (PI) with the addition of lime up to 4%. There was a slight decrease in the PI with the addition of lime above 4%. These results are comparable with the results of Kampala et al. (2014) and Kampala and Horpibulsuk (2013), in which they reported the effect of adding lime on the Atterberg limits of expansive clays, and found an increase in the plastic limit and a decrease in both liquid limit and plasticity index.

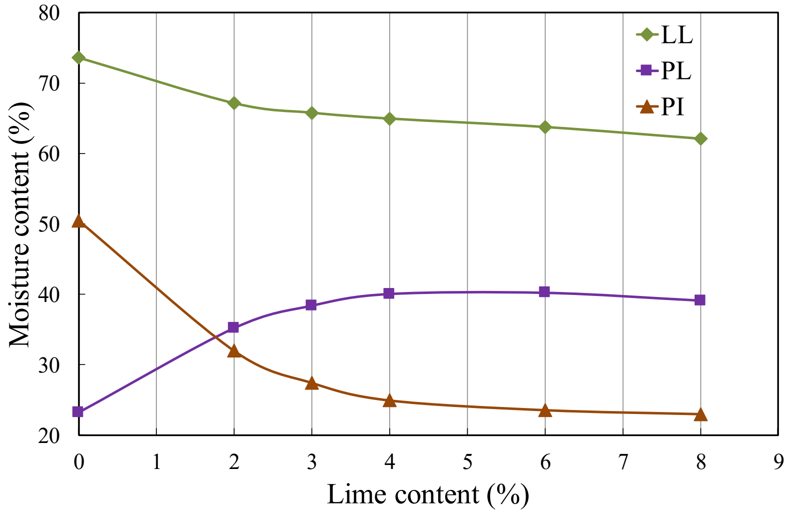

Figure 4.1. Variation in Atterberg limits for Braybrook soil at various lime content

Linear Shrinkage (LS) tests were performed according to the Australian Standard AS1289.3.4.1 (2008), with results presented in **Figure 4.2**. The linear shrinkage of untreated soil was approximately 20% with a plasticity index value of 50.5%. Accordingly, Braybrook clay can be considered highly reactive (Hazelton & Murphy 2007b). After treatment with lime, it was clear that there was a significant decrease in linear shrinkage when adding lime up to 6%. Beyond 6% lime content, there was an only minimal change in linear shrinkage of samples.

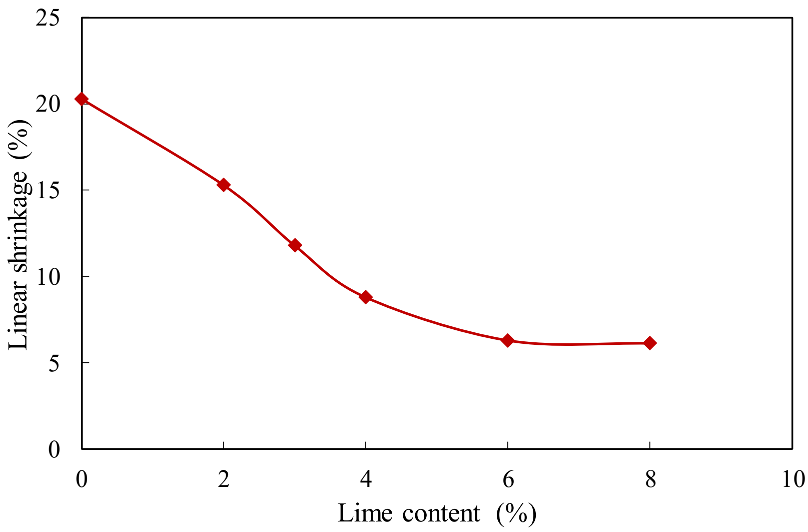

Figure 4.2. Linear shrinkage for Braybrook soil at various lime contents

4.4.3 pH- Concentration

To prepare the samples, the dry soil was passed through sieve No.4 (4.75 mm), and then different lime contents of 0%, 2%, 3%, 4%, 6%, 8% and 10% were added to 20 grams of dried soil. Following this, 100 ml of distilled water was added to these mixtures, which were then shaken for 30 seconds. This procedure was repeated every 10 minutes for at least 1 hr. Then, pH concentration was measured using a calibrated pH meter (Eades & Grim 1966). The results in **Figure 4.3** show increases in the pH concentration with increasing lime content.

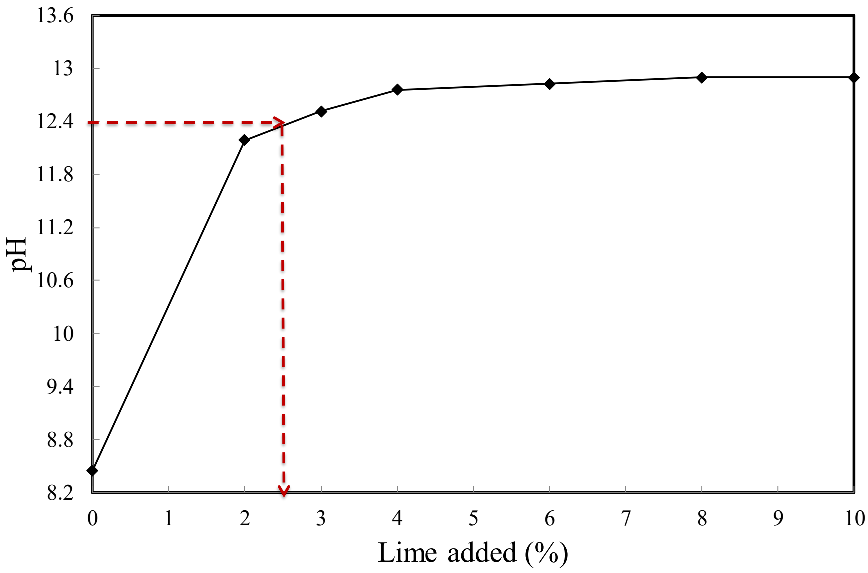

Figure 4.3. Variation in pH concentration with lime content (after 1 hr)

The pH concentrations of stabilised clay were measured after 0, 7, 28 and 56 days of curing, and results are presented in **Figure 4.4**. Figure 4.4 suggests that there was a continuous decline in pH concentration of blends as the curing period increased. These results are compatible with the finding of Saride et al. (2013), who measured the pH concentration for soils of different organic content during curing.

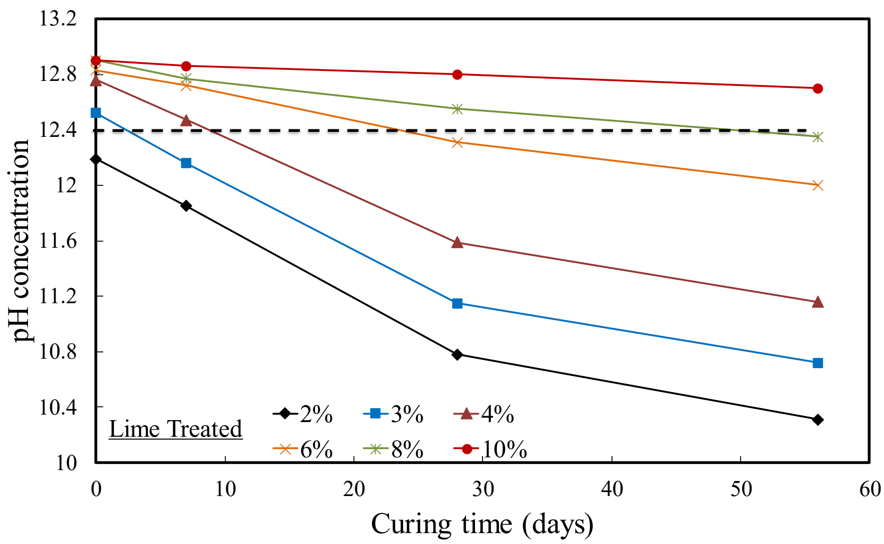

Figure 4.4. Variation in pH concentration of lime-treated clay with curing time

4.4.4 Compaction tests

Standard Proctor compaction tests were performed following the ASTM-D698 (2000) procedures on both untreated and treated soils. The compaction procedure for the untreated sample was described in Section 3.3.6. For the treated samples, the procedure outlined by Ciancio et al. (2014) was followed. Dry soil was mixed thoroughly with hydrated lime for five minutes. Water was then added and mixed, allowing the cation exchange and flocculation processes to start. The whole compaction process was kept under 45 minutes, and the same procedure was repeated for different water contents.

The optimum water content and corresponding maximum dry density were determined for untreated and treated samples at a hydrated lime content of 2%, 3%, 4%, 6% and 8% of dry soil, as shown in **Figure 4.5a**. It is clear that maximum dry density decreases and optimum moisture content increases with increasing lime content (Figure 4.5b). This behaviour can be attributed to physical changes happening during lime stabilisation. The decrease in maximum dry density is due to agglomerated and flocculated stabilised soil particles filling up a larger area, which in turn results in a lower density. On the other hand, the increase in optimum moisture contents with the addition of lime is due to the fact that the cation exchange process requires water to progress.

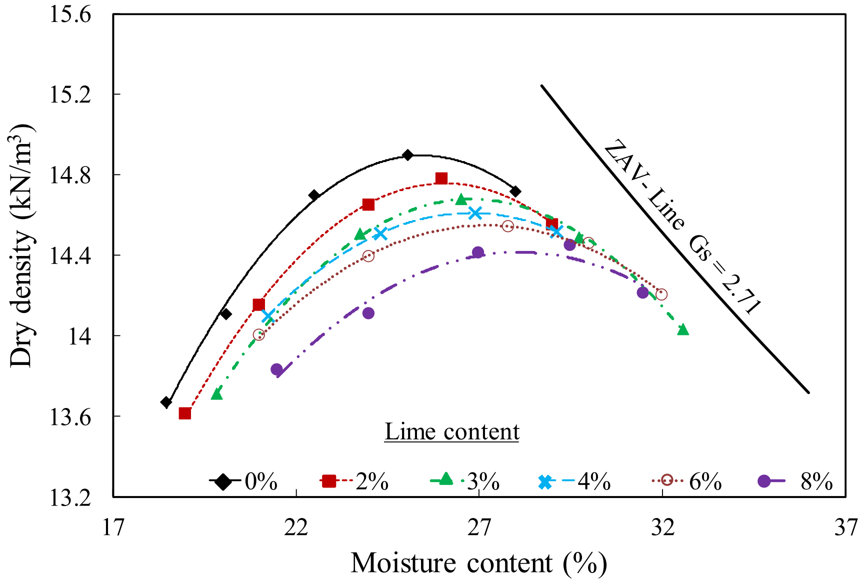

(a)

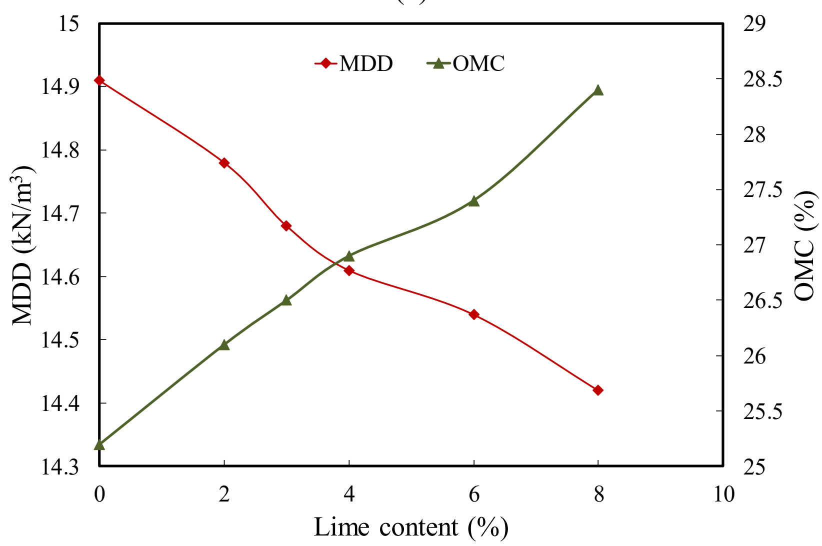

(b)

Figure 4.5. Results of standard compaction tests at different lime contents

4.4.5 Unconfined compressive strength (UCS) test

Several specimens were prepared with different lime contents (0%, 2%, 4%, 6%, and 8%) and compacted using the standard proctor energy at optimum point (optimum moisture content and maximum dry density). Test results are presented in **Figure 4.6**. Figure 4.6 indicates that for samples stabilised with 2 and 4 per cent lime, there was no significant increase in UCS with the curing period increasing from 7 to 28 days.

However, a significant increase was noticed for samples treated with 6% and 8% lime content when curing continued beyond 7 days.

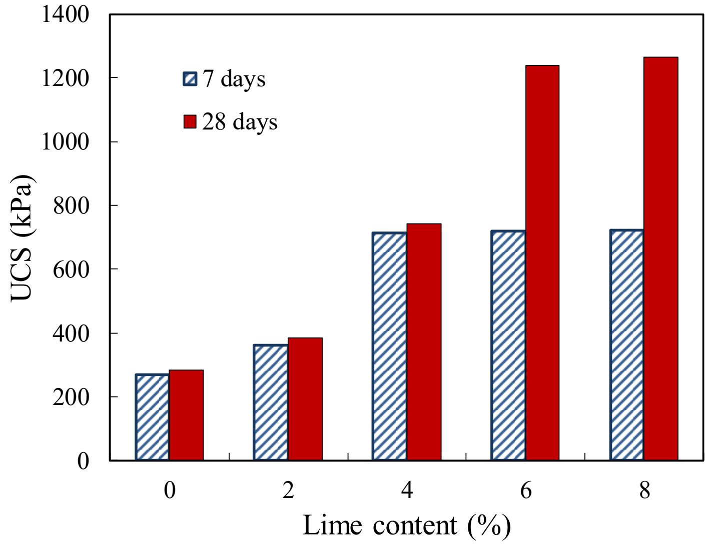

Figure 4.6. Effect of lime content on soil strength with curing time

4.4.6 One dimensional swell test

Untreated and treated samples were compacted with different percentages of lime using the standard Proctor compaction test at OMC and MDD. The untreated specimens' set-up was explained in detail in Section 3.3.8.

For treated samples, in accordance with the process outlined by Zhao et al. (2014b), the specimens were cured for 1, 7 and 28 days, and then the procedure described for untreated samples was used for samples with different lime content. The results of these tests are presented in **Figure 4.7**. Figure 4.7a shows that there was a significant drop in swelling values after adding 2% lime. The swell percentage reached very close to zero after adding 4% lime. Figure 4.7b shows that the greatest reduction in swelling potential occurred within the first 7 days of curing, which is similar to the findings of Zhao et al. (2014b).

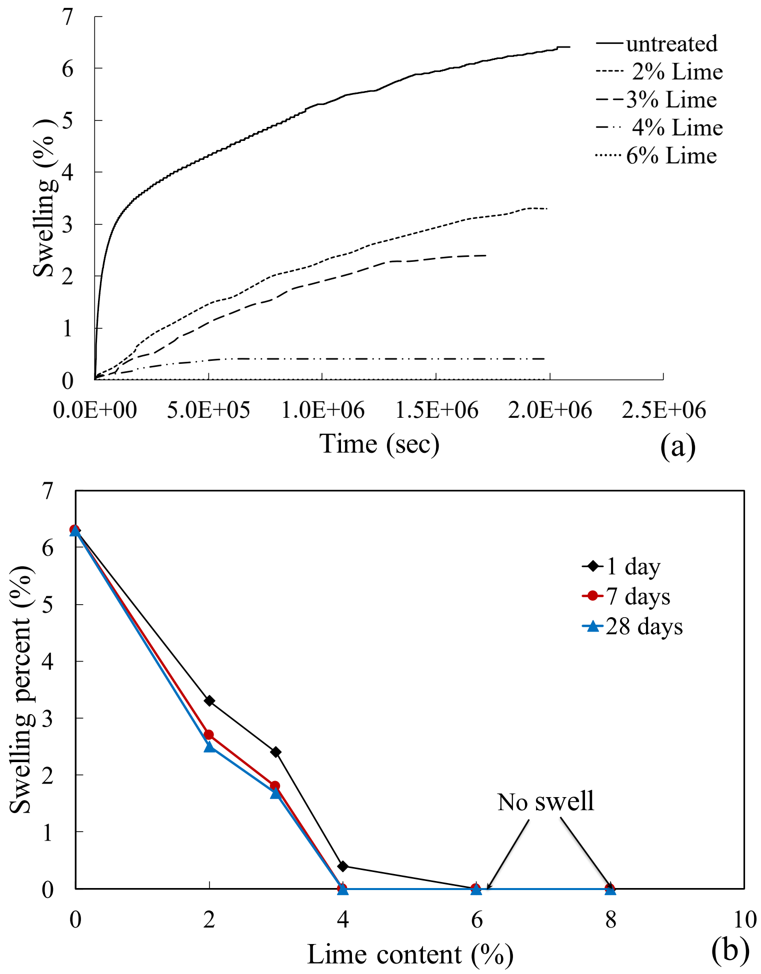

Figure 4.7. Swelling paths of untreated and treated samples (a) after one day of curing and (b) at different curing periods

4.4.7 X-ray diffraction (XRD) test

XRD tests were performed on untreated samples and treated samples with a lime content of 4% and 6% after 28 days of curing in order to understand the crystalline phases within the lime-stabilised matrix.

The lime-treated XRD samples were cut from the centre of the UCS samples (cured for 28 days) and then air dried (at 40°C) and crushed into a powder (Yi et al. 2015). The XRD patterns for untreated and treated samples are presented in **Figures 4.8** and **4.9**.

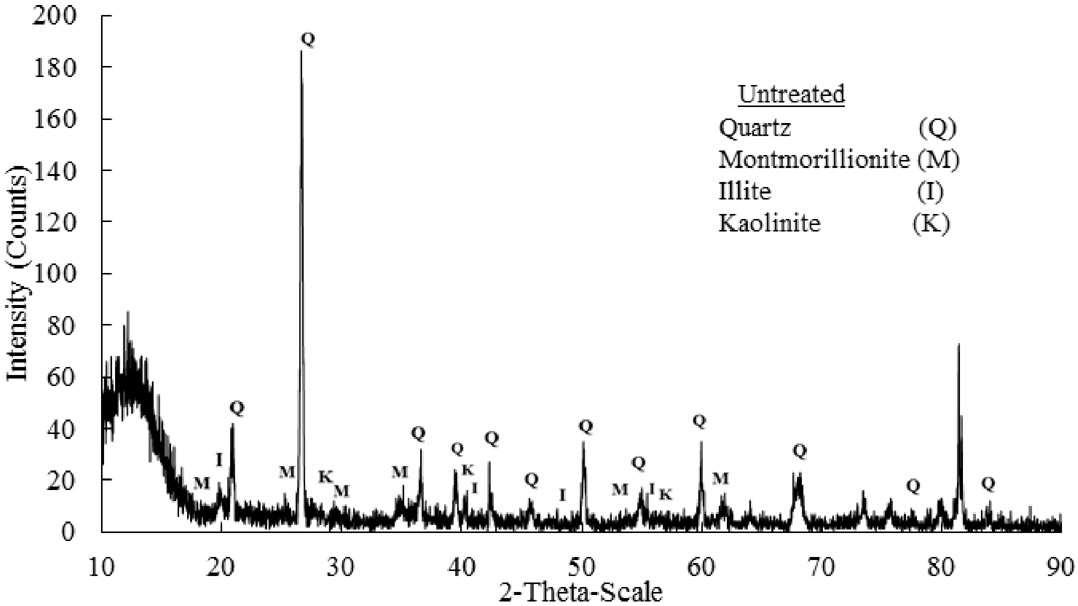

(a)

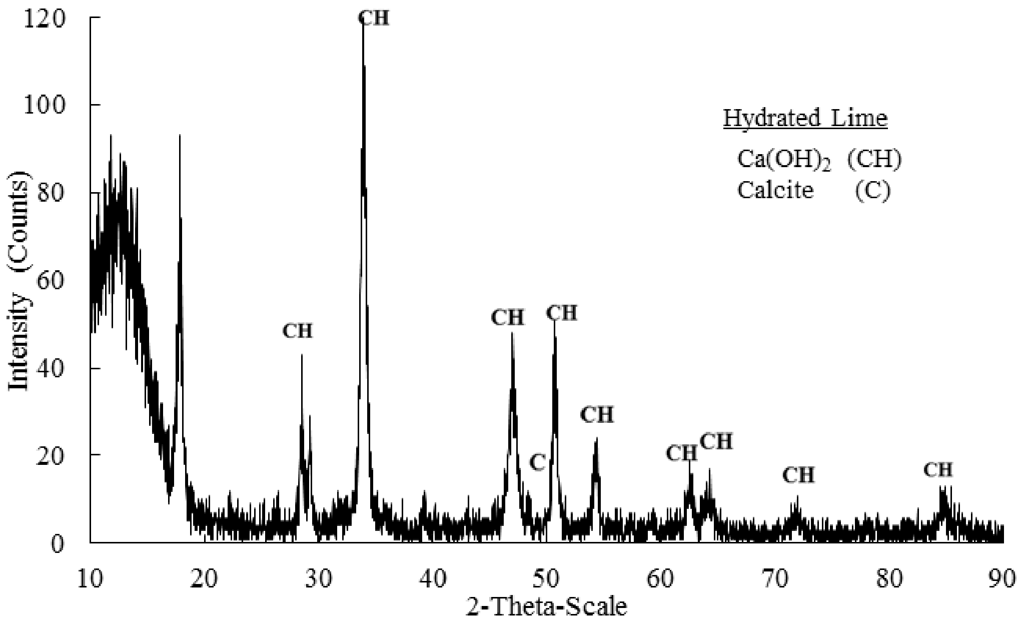

(b)

Figure 4.8. XRD of (a) untreated sample and (b) hydrated lime

The main minerals of Braybrook clay are shown in Figure 4.8, and are a mixture of quartz and montmorillonite, with some illite and kaolinite. The XRD pattern of hydrated lime indicated that the major component is calcium hydroxide ($Ca(OH)_2$), with a small amount of calcite. This suggests that hydrated lime will have the ability to react with the pozzolanic material (in clay) to create cementitious products. Figure 4.9 shows the appearance of Calcium Silicate Hydrate (CSH) and Calcium Aluminate Hydrate (CAH). The XRD patterns detected higher levels of CSH and CAH in 6% lime content samples compared to 4% lime content samples.

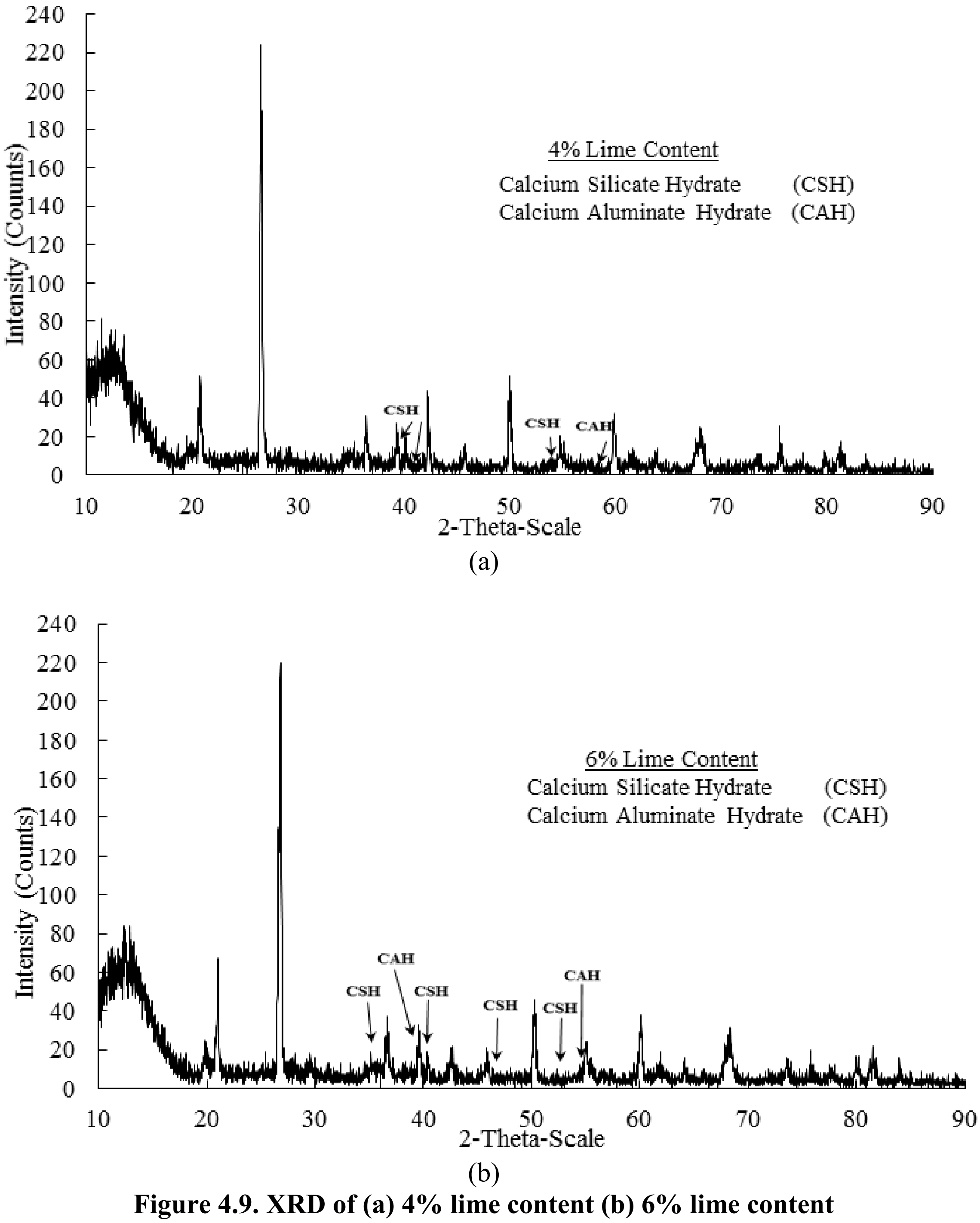

Figure 4.9. XRD of (a) 4% lime content (b) 6% lime content

4.4.8 Scanning electron microscopy (SEM) test

A set of SEM tests were undertaken to study the change in the microstructure of Braybrook clay when it reacts with hydrated lime, and as the curing progresses. The preparation of the samples was similar to that of the XRD, except that after drying, a small segment of the sample was cut (Yi et al. 2015; Zhao et al. 2014b), coated with a thin layer of gold, and placed in a SEM device (Echlin 2009). The SEM micrographs for untreated and treated samples at different lime contents and curing periods are presented in **Figure 4.10**.

Braybrook clay minerals have an irregular shape pattern, as shown in Figure 4.10a. Figure 4.10b displays the microstructure of stabilised clay with 4% lime content after 7 days of curing. It is clear that the original microstructure of the clay is broken into many pieces to form a polygonal sheet ($Ca(OH)_2.nH_2O$ crystals) and then agglomerated and flocculated together to form a large particle.

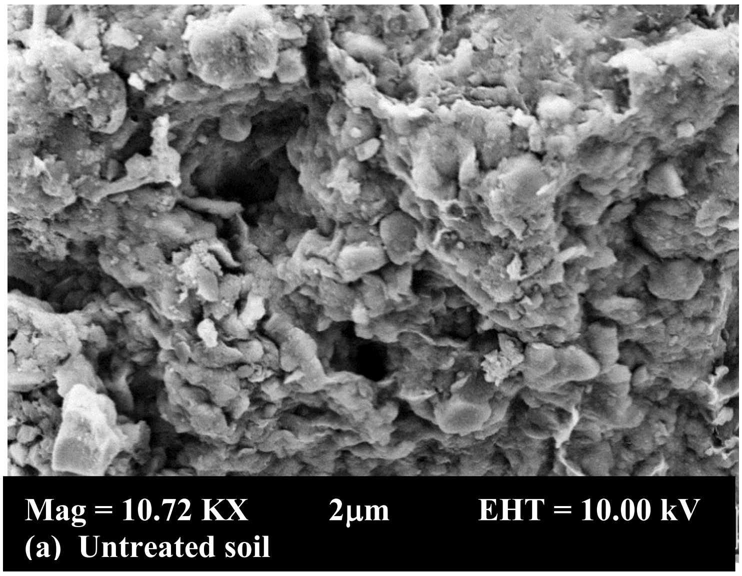

(a) Untreated soil

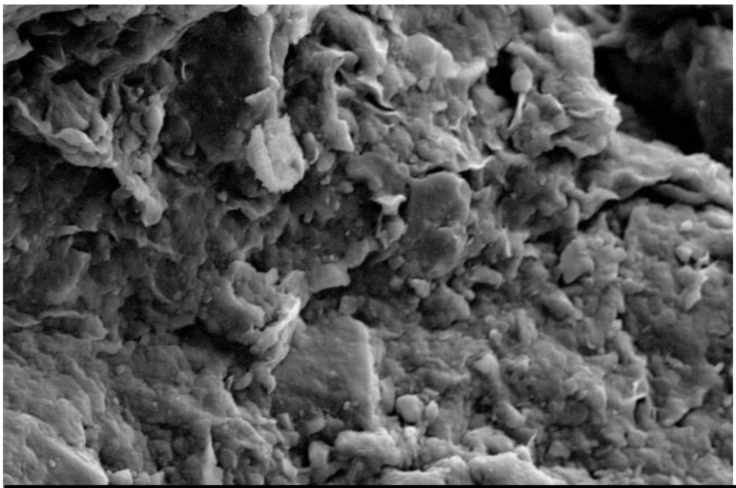

Mag = 10.24 KX 2µm EHT = 10.00 kV
(b) 4% Lime content after 7 days curing

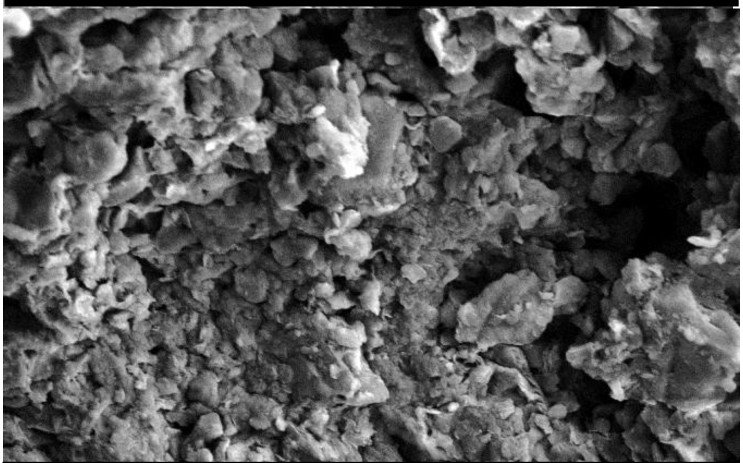

Mag = 10.72 KX 2µm EHT = 10.00 kV
(c) 4% Lime content after 28 days curing

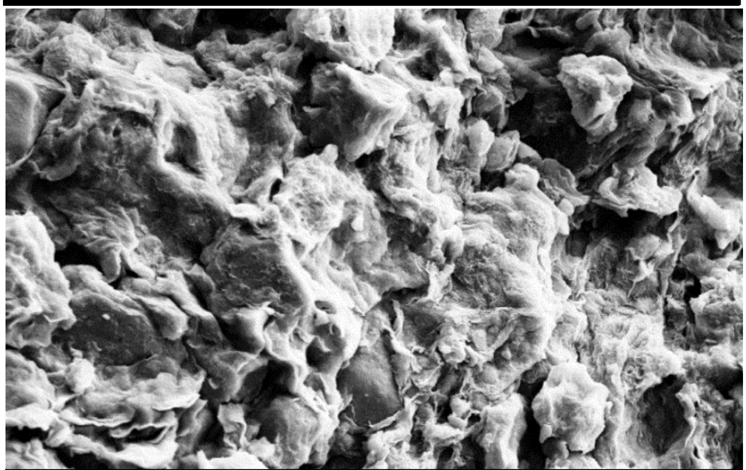

Mag = 10.57 KX 2µm EHT = 10.00 kV
(d) 6% Lime content after 7 days curing

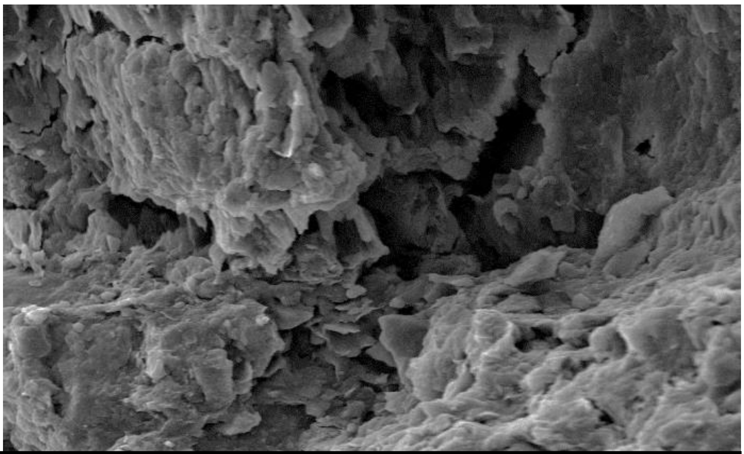

Mag = 10.00 KX 2μm EHT = 10.00 kV
(e) 6% Lime content after 28 days curing

Figure 4.10. SEM images of untreated and treated samples

The microstructure change of stabilised clay with 4% lime content after 28 days of curing is presented in Figure 4.10c. Comparing Figures 4.10b and 4.10c suggests that for samples treated with 4% lime, there is no distinct difference in the particle shape and binding of particles when the curing progresses from 7 to 28 days.

Further destruction in the particles, after adding 6% of lime with 7 days of curing, is shown in Figure 4.10d. Figure 4.10e shows the results of further progress in stabilisation when the curing goes from 7 days to 28 days. In Figure 4.10e, the original particles have been clearly replaced by a fibrous structure, which is an indication of the production of Ca(OH)2.nH2O and pozzolanic materials (CSH and CAH). This is compatible with the XRD results reported in Figure 4.9 suggesting the presence of Calcium Silicate Hydrate (CSH) and Calcium Aluminate Hydrate (CAH) in the mix. SEM results clearly show that the particle size of the stabilised soil is larger than that of the untreated particles due to agglomeration and flocculation. This alternatively reduces the surface area of particles, and decreases their potential for water absorption and swelling or shrinkage.

4.5 Discussions

4.5.1 Optimum lime content (OLC)

The OLC is defined as the lime percentage producing a 12.4 (Ciancio et al. 2014) or a 12.3 pH environment (Saride et al. 2013), which is recognised as a lime-saturated solution. To achieve this, two different methods were followed to determine the OLC for basaltic expansive clay. These methods included the Eades and Grim (1966) method, as well as the traditional method of conducting laboratory tests at different lime dosages and curing durations.

The results of this study on the basaltic Braybrook expansive clay that was tested are presented in Figure 4.3. The work of Eades and Grim (1996), Ciancio et al. (2014) and Saride et al. (2013) suggest that the OLC was approximately 2.64%. To find the OLC using the traditional method, experimental laboratory tests were carried out including the UCS, one-dimensional swell, XRD, and SEM tests.

According to the UCS results (Figure 4.6), there was a small increase in the UCS through the 7 day curing period for lime dosages at 2%. A great increase was noted in the UCS through the same period for lime dosages at 4%. However, no significant increase in the UCS was detected when the curing period was extended from 7 to 28 days for lime dosages of 2% and 4%. Nevertheless, a noticeable increase was observed for the samples treated with 6% and 8% lime content over the same curing period. The reason for this behaviour is believed to be the drop in pH concentration values for samples treated with 2% and 4% lime, which is partially caused by the consumption of the OH^- ions in the silica dissolution process (as mentioned in Section 2.3.2). According to the mechanism of the reaction between lime and clay (Section 2.3.2), there are two opposite processes. The first process is the release of OH^- ions by the dissociation of lime in water contributing to an increase in the pH concentration of the environment. However, the second process requires the consumption of OH^- ions for silica dissolution, which adversely leads to a decline in the pH concentration of the environment. In addition, the rate of lime dissolution is high up to 7 days, but decreases thereafter. Nevertheless, the consumption of OH^- ions (during silica dissolution) is always more than the supply of OH^- ions (during lime dissolution). Therefore, there will be a reduction in the pH concentration. This reduction happens to be higher during the period between 7 and 28 days. It can be concluded that the improvement of soil properties will depend on the value of pH after the reduction. If the value of the pH after the reduction is about equal to or higher than 12.3 or 12.4, the silica dissolution, cation exchange, flocculation, agglomeration, and pozzolanic reaction will continue, and as a result, improvement in soil properties will advance (see **Figure 4.11**).

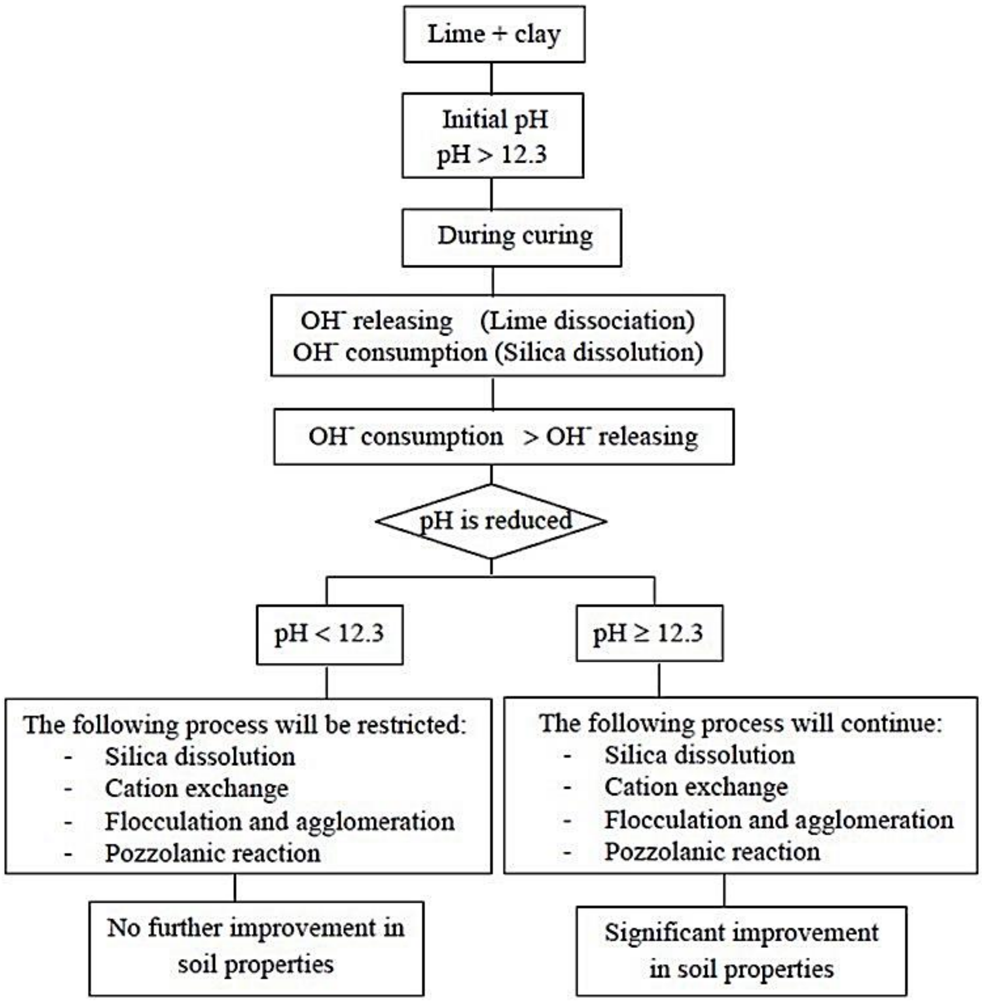

Figure 4.11. Mechanism of lime stabilisation with a variation of pH concentration during curing (Al-Taie et al. 2018)

Since the pH concentration of the 2% blend reduced to 11.85 (which is less than 12.3), it was expected that no real improvement would occur for this sample. This was confirmed by the UCS results presented in Figure 4.6. In contrast, it was expected that improvement in soil strength would occur when the soil was treated with 4% lime content (Figure 4.6), because the pH concentration could be maintained at approximately 12.2 (very close to 12.3) for the first 7 days of curing. For samples treated with 2% and 4% lime, Figure 4.6 suggests that there was no further increase in UCS values during the period between 7 and 28 days, because the alkalinity of the medium was far below 12.3, as shown in Figure 4.4 (10.87 and 11.59, respectively after 28 days of curing). However, for the samples treated with 6% and 8% lime and cured to 28 days, there was a significant increase in UCS values during the period between 7 and 28 days, because the alkalinity of the medium stayed above 12.3 (12.31 and 12.55, respectively) during the 28 days.

Interestingly, the SEM images in Figure 4.10b and 4.10c, samples treated with 4% lime content and cured for 7 and 28 days, showed that there was no significant difference in particles' shape despite an increase in the curing period. This indicates that the silica dissolution, cation exchange, and, subsequently, the flocculation and agglomeration were restricted. As a result, it was expected that the difference in strength would be negligible, which proved accurate, as reflected in the UCS results presented in Figure 4.6.

Samples treated with 6% and 8% lime showed a pH value of 12.34 and 12.55 after 28 days of curing, respectively. In comparing the SEM results presented in Figure 4.10d with 6% lime content and 7 days of curing to the SEM image of Figure 4.10e with the same lime content but a 28 day curing period, a totally different particle structure can be identified. For samples with 28 days of curing (Figure 4.10e), a fibrous structure was dominant, indicating the increase in the inter-particle attraction, which caused further flocculation and agglomeration and the start of a pozzolanic reaction. Consequently, an increase in the strength of samples stabilised with 6% and 8% lime, with curing progressing from 7 to 28 days, was expected and confirmed, as reflected in the UCS results of Figure 4.6.

As shown in Figure 4.4, it is clear that the main reduction in pH concentration occurred during 7 to 28 days of curing. Therefore, to counteract the decline in pH concentration during this curing period for residual basaltic clays, it was important to maintain the alkalinity of the soil at approximately 12.4 for the 28-day curing period. **Figure 4.12** suggests that the minimum lime dosage required for maintaining the pH environment at approximately 12.4 for a period of 28 days was 6%. Any additional lime content showed no additional improvement in the UCS. Therefore, it could be concluded that the OLC was 6% based on UCS results.

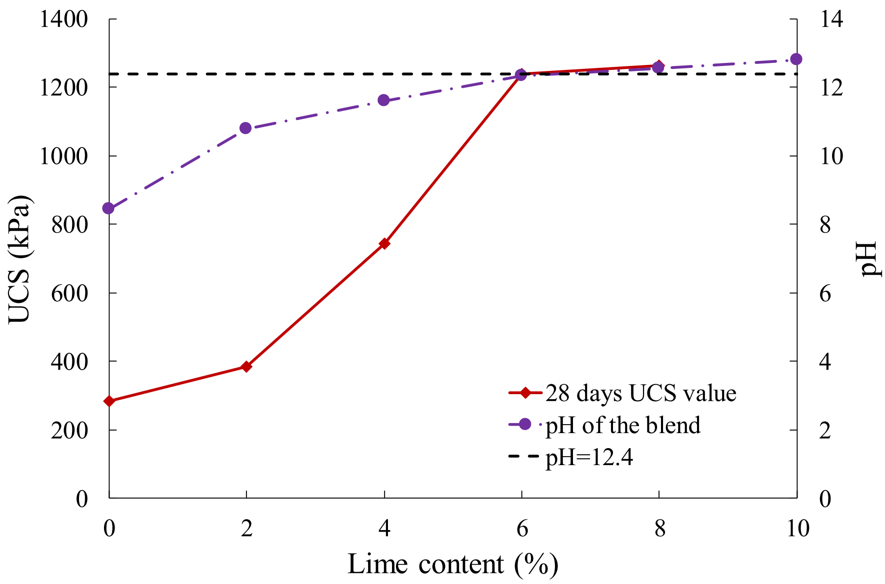

Figure 4.12. Effect of lime content on soil strength after 28 day curing period

However, based on the results of the one-dimensional swell tests, the OLC was determined to be 4% (Figure 4.7b). Zhao et al. (2014b) performed a series of one-dimensional swell tests and SEM to study the change in the microstructure of Nanyang expansive clay when it reacts with lime. Their study pointed out that the greatest reduction in swelling occurs within the first 7 days of curing. Therefore, if the objective of stabilisation is to control the swelling behaviour of the soil, it is important to keep the pH environment at approximately 12.4 for 7 days. From Figure 4.4, it can be observed that the lime content that keeps the environment alkalinity at approximately 12.4 for a 7 day curing period is 4%. Thus, the OLC for swelling reduction was 4% for Braybrook residual expansive clay.

For organic soils, an additional reduction in pH concentration was expected as organic content and the curing period increased (as mentioned in Section 2.3.2). Previous studies that have investigated the effect of humic acid on the shear strength of organic soils suggest that the shear strength values decrease with an increase in humic acid content and a longer curing period (Yunus et al. 2011). For these soils, due to the reduction in pH concentration that consequently results in a decline in the UCS, the Eades and Grim method was not valid to find the OLC for organic soils in this study (Yunus et al. 2011). Harris et al. (2009) followed the Eades and Grim method (1966) to measure the OLC for specimens with varying amounts of humic acid. This study showed that the amount of humic acid did not appear to have an effect on the lime requirements of the soil. As a result, it can be concluded that the pH as measured in the Eades and Grim method (1966) was not affected by increasing humic acid concentration. Therefore, further testing is suggested in order to develop a full understanding of the impact of different organic substances on the stabilisation of different soil types, which is not in the scope of this study.

4.5.2 Proposed modified Eades and Grim method

The Eades and Grim (1966) method can be modified to take into account the effect of curing on the behaviour of stabilised basaltic expansive clay with lime. To measure the OLC, a very simple index of pH concentrations obtained at different curing periods is introduced.

In this modified approach, it is important to know the main soil improvement objective that is sought. If the purpose of improvement is to reduce the deformation (swell-shrinkage potential), then the OLC is the lime percentage that keeps the pH level at approximately 12.4 for 7 days. However, if the purpose of improvement is to increase soil strength (e.g. field CBR is too low for road subgrade), then the lime percentage maintaining the pH level at approximately 12.4 for 28 days should be chosen. The

Eades and Grim (1966) modification to determine the OLC for residual expansive clays is presented in **Figure 4.13**.

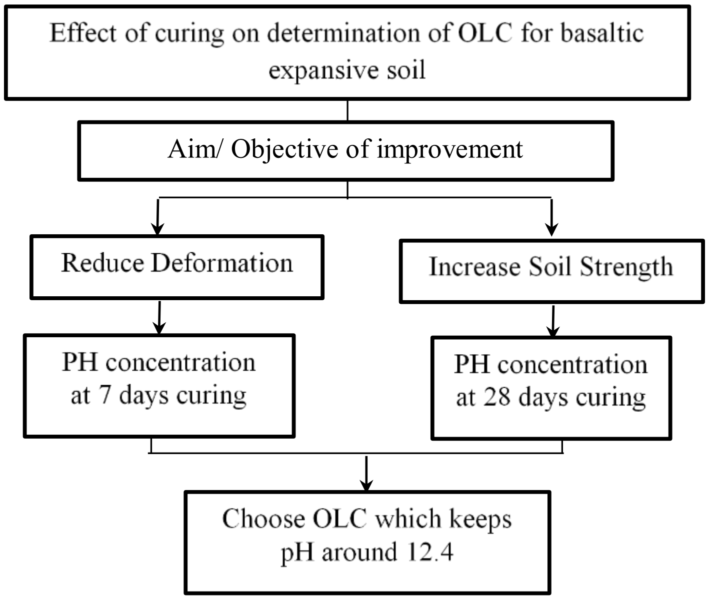

Figure 4.13. Modification of the Eades and Grim method to determine the OLC for basaltic expansive soil (Al-Taie et al. 2018)

4.6 Validation of the Proposed Method

To check the validity of this proposed modified method, another basaltic soil was collected from the Whittlesea site. A series of laboratory tests were conducted on this Whittlesea soil prior to stabilisation. These tests included determining the organic content, grain size analysis, Atterberg limit, linear shrinkage, pH concentration, standard Proctor compaction, Unconfined Compressive Strength (UCS) and the swelling potential. The results of these tests are presented in Table 3.2.

According to this proposed modified Eades and Grim method, developed as part of this research, the first step includes measuring the pH concentrations at different lime contents and curing periods (7 and 28 days), which is shown in **Table 4.1**. The lime contents at which pH concentration of the mixture stays around 12.4 after 7 and 28 days of curing should be highlighted. Table 4.1 shows that the lime content values required to keep the solution pH around 12.4 are 6% and 8% after 7 and 28 days of curing, respectively. That means the OLC is approximately 6% if the purpose of improvement is to control the deformation. However, if the purpose of soil improvement is to improve soil strength, the OLC is approximately 8%. It is important to mention that the OLC is 4% according to the Eades and Grim method (1966).

Table 4.1. Variation of pH concentration vs. curing time for Whittlesea soil

Lime content (%)	Curing periods (days)		
	0	7	28
	pH concentration		
0	7.61		
2	10.23	9.08	8.92
4	12.35	11.36	10.92
6	12.74	12.39	12.01
8	12.80	12.51	12.31
10	12.82	12.70	12.61

To check the validity of these results, traditional tests were conducted to obtain the OLC for the Whittlesea soil, including one-dimensional swell and UCS tests. Standard Proctor compaction tests were performed following the ASTM-D698 (2000) procedures on both untreated and treated soils with 4%, 6% and 8% lime content to obtain the OMC and MDD (**Table 4.2**). One-dimensional swell and UCS tests were conducted for untreated and treated samples at OMC and MDD. Swelling values were measured after 7 days of curing, while the UCS values were obtained after 28 days of curing, as presented in **Table 4.3**. Table 4.3 clearly shows that the OLC according to swelling potential was 6%. However, it is approximately 8% according to the UCS values. This shows that the 4% lime content suggested by the Eades and Grim method (1966) is below the lime content required to improve soil behaviour adequately. In contrast, the new modified method proposed in this thesis can predict the OLC of the clay based on the purpose of soil improvement.

Table 4.2. OMC and MDD results for untreated and treated samples (Whittlesea soil)

Lime percentage (%)	OMC (%)	MDD (kN/m^3)
0	18	17.3
4	20.1	16.1
6	21.2	15.8
8	22	15.1

Table 4.3. Swelling and UCS values at different lime contents (Whittlesea soil)

Lime content (%)	Swelling (%) after 7 days curing	UCS (kPa) after 28 days curing
0	2.1	201
4	0.54	366
6	0	460
8	0	573

4.7 Summary and Conclusions

There are two established methods to determine the OLC. The first method is the Eades and Grim (1966) method that relies on pH concentration to choose the OLC. The second is the traditional method, which consists of conducting a range of laboratory tests to determine the OLC, such as classification tests, strength and deformation tests along with XRD and SEM, and pH concentration measurements carried out on samples with different lime contents and curing periods.

This chapter has presented the properties of Braybrook residual basaltic expansive clay before and after stabilisation with different percentages of hydrated lime. This soil type was used to develop a new method for predicting the OLC for basaltic expansive clay. To check the validity of the newly developed modified method, another basaltic soil collected from another site (Whittlesea) was tested.

Test results conducted for swell, UCS, pH (for Braybrook and Whittlesea soils), SEM and XRD (for Braybrook soil), suggested that due to reductions in pH of the blends during the curing, and according to the mechanism of lime stabilisation, the Eades and Grim method needs to be modified for this kind of soil to take into account the reduction in pH concentration during the curing. The modification developed as part of this research can be summarised as shown in Figure 4.13. Figure 4.13 shows that to control the deformation of this type of clay, the lime dosage that increases the pH environment to approximately 12.4 after 7 days of curing should be selected. If the purpose of soil improvement is to improve clay strength, it is necessary to take into account the lime dosage that contributes to a pH concentration of 12.4 after 28 days of curing.

It is important to mention that the purpose of this study is not to suggest that the Eades and Grim method or the modified version (proposed in this research) should be used in place of traditional tests such as strength or deformation tests. More importantly, this study recommends that for the preliminary determination of the required lime content, taking into account the purpose of soil improvement, different curing periods for pH measurements should be considered. The estimated OLC value obtained from the Eades and Grim method (1966) can be different than the exact value obtained from traditional testing. For example, in this study, the estimated OLC values obtained based on the Eades and Grim method (1966) were approximately 2.64% and 4% for Braybrook and Whittlesea soils, respectively. However, the exact values according to traditional testing (UCS) are 6% and 8%. Furthermore, the study of Yunus et al. (2011) found the OLC according to the Eades and Grim method was 2%, but recommended 5% as the OLC. This is because the Eades and Grim method (1966) does not consider the drop in pH content over time and only relies on the measurement 1 hr after mixing the lime. It should also be noted that for some soils (e.g. Saride et al. (2013)), the drop in pH content during the curing period is not significant; hence, the Eades and Grim method (1966) can still be followed for preliminary determination of the OLC. Despite this, it is recommended to focus on 7 and 28 day pH levels to obtain a more accurate determination of the OLC before moving into expensive characterisation tests, such as swelling, UCS, Atterberg limits etc.

CHAPTER 5. MODIFICATION OF THE MPK FRAMEWORK & ESTIMATION OF COLLAPSE AND SWELLING POTENTIAL

To investigate the volumetric behaviour of unsaturated compacted expansive soil stabilised with lime, a suitable constitutive model was adopted and its validity was assessed. This led to a new constitutive model being developed as a result of this research. The development of this new constitutive model has been discussed in this chapter.

5.1 Introduction

This chapter presents the constitutive volumetric behaviour (in terms of a void ratio (e)-moisture ratio (e_w)-net stress (σ) space) for compacted untreated and lime-treated expansive clay soil. For treated specimens, the optimum lime content was found based on swell potential reduction. Initially, the suitability and validity of the Monash Peradeniya Kodikara (MPK) framework were examined by applying different state path sequences, such as loading-wetting, loading-wetting-loading, loading-unloading-wetting, loading-unloading-wetting-unloading-wetting, collapse and swelling potential. Furthermore, the swelling and collapse potentials were tested under a wide range of moisture contents and stress levels, with special attention given to the effect of stress history and operational stress on the swelling and collapse behaviour. As a result, a new improved model has been suggested. Furthermore, this new method for predicting the swelling and collapse potential was proposed using the virgin compression surface. This chapter also includes the application of the results of studies such as Jotisankasa et al. (2007) on the MPK framework. The theory of swelling and collapse according to Kodikara's model (2012) is also applied to previous studies, such as the study carried out by Alonso et al. (1990).

5.2 Experimental Program

A series of laboratory tests were performed to investigate the volumetric behaviour of the untreated and lime-treated unsaturated compacted expansive clay. The first stage of testing was focused on determining the optimum lime content, which was based on swelling potential, and included standard Proctor compaction and one-dimensional swell tests, as described in Chapters 3 and 4. The optimum lime content was found to be 4%. The second stage of testing was conducted to generate the Loading Wetting State Boundary Surface (LWSBS) for both untreated and lime-treated specimens by establishing the compaction curves at different net stress levels. Each curve was developed using static compaction. The third stage of testing was conducted to identify the volumetric behaviour of the untreated and lime-treated expansive clay specimens by applying different state path tests, such as loading-wetting, loading-wetting-loading, loading-unloading-wetting, loading-unloading-wetting-unloading-wetting, collapse potential and swelling potential.

5.3 Validity of the MPK Framework

To assess the validity of the MPK framework, the Loading Wetting State Boundary Surface (LWSBS) was firstly generated for both the untreated and lime-treated specimens. Secondly, different state paths were applied to the soil, and the collapse and swelling potential were investigated.

5.3.1 LWSBS generation for untreated and lime-treated clay

The LWSBS can be defined as the surface created by a series of compaction curve results beginning from its loosest state at nominal stress. This represents the upper surface for the volumetric behaviour of the soil, which is only applicable to loading and wetting pathways. Any path on this surface can be achieved by compacting a specimen from nominal stress to a certain compaction stress (loading) or wetting, or combination of loading and wetting.

The untreated and lime-treated specimens were compacted statically from the loosest state after being mixed with different amounts of water. The moisture content varied from 0% to 50%, while the static compaction stress varied from 2 kPa to 4000 kPa (50% is a maximum moisture content to present the shape of compaction curve at low-stress level (25 kPa) and 4000 kPa is a maximum static compaction stress, as the maximum capacity of LoadTrac III is 5000 kPa). The procedure mentioned in Section 3.5 was followed to establish the LWSBS for the untreated and lime-treated soils. **Figure 5.1** presents the LWSBS for the untreated expansive soil in e-e_w, e-log(σ) and e-e_w-log(σ) spaces, while **Figure 5.2** shows the LWSBS of the lime-treated expansive soil with 4% lime in e-e_w, e-log(σ) and e-e_w-log(σ) spaces.

In general, Figures 5.1 & 5.2 show that the void ratio decreased as the moisture content increased, with the exception of the soils at the dry end of the moisture content axis. Here, the void ratio increased as the moisture content increased. The variation of the void ratio (at constant stress level) for the untreated clay specimens was higher than that of the lime-treated specimens. In addition, the void ratio variation decreased as the stress increased. This means that the collapse potential of the untreated clay was higher than the lime-treated clay. Furthermore, the treated specimens required more water to achieve maximum collapse. It is clear from Figures 5.1 & 5.2 that the position of the line of optimums (LOO) occurred approximately at the degree of saturation of 86% for both the untreated and lime-treated soils. According to the procedure mentioned in Section 3.5.1, the compaction curve obtained did not intersect between the line of optimums (LOO) and the normally consolidated line (NCL), where the degree of saturation is equal to 100%.

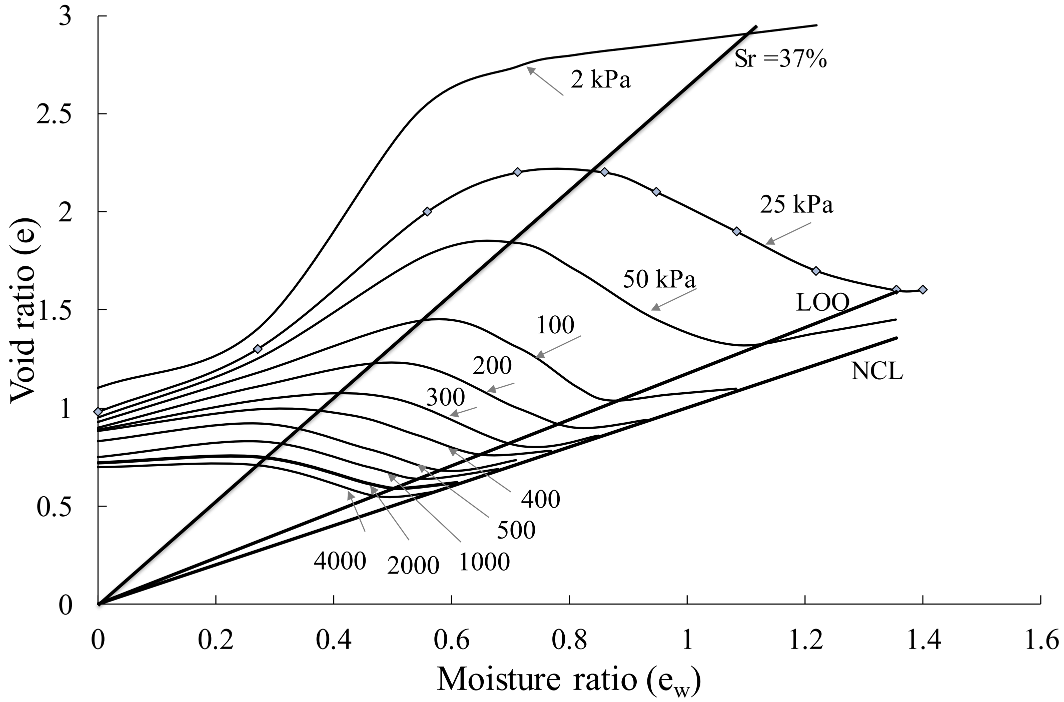
3
2.5
2
1.5
1
0.5
0
Void ratio (e)
0
0.2
0.4
0.6
0.8
1
1.2
1.4
1.6
Moisture ratio (e_w)
Sr =37%
2 kPa
25 kPa
50 kPa
LOO
NCL
100
200
300
400
500
1000
2000
4000

(a)

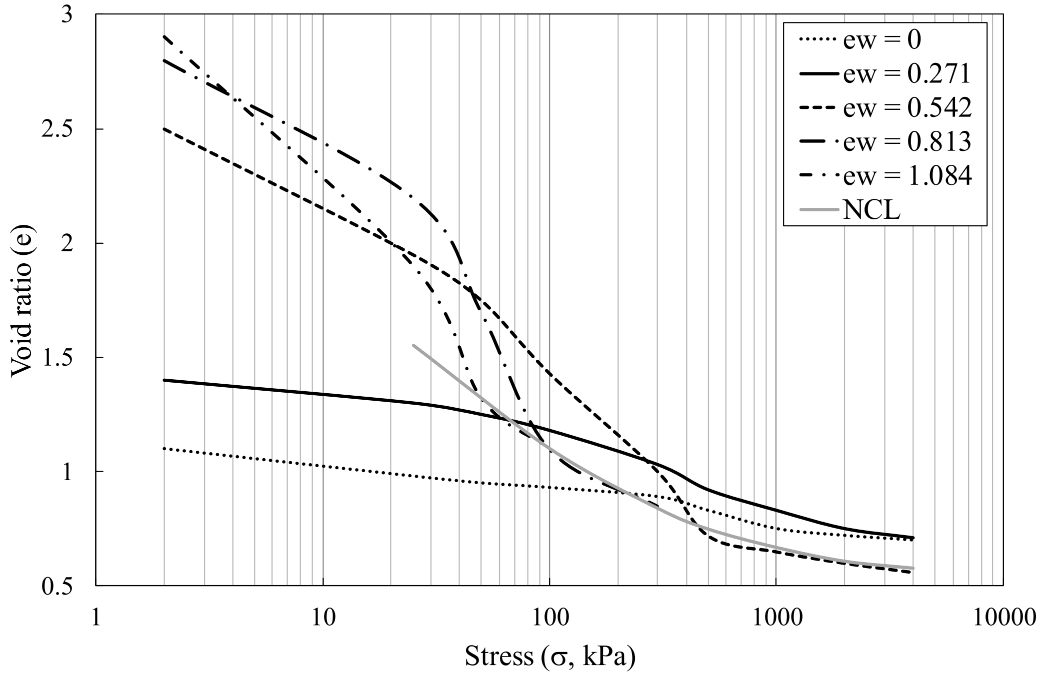
3
2.5
2
1.5
1
0.5
Void ratio (e)
1
10
100
1000
10000
Stress (σ, kPa)
ew = 0
ew = 0.271
ew = 0.542
ew = 0.813
ew = 1.084
NCL

(b)

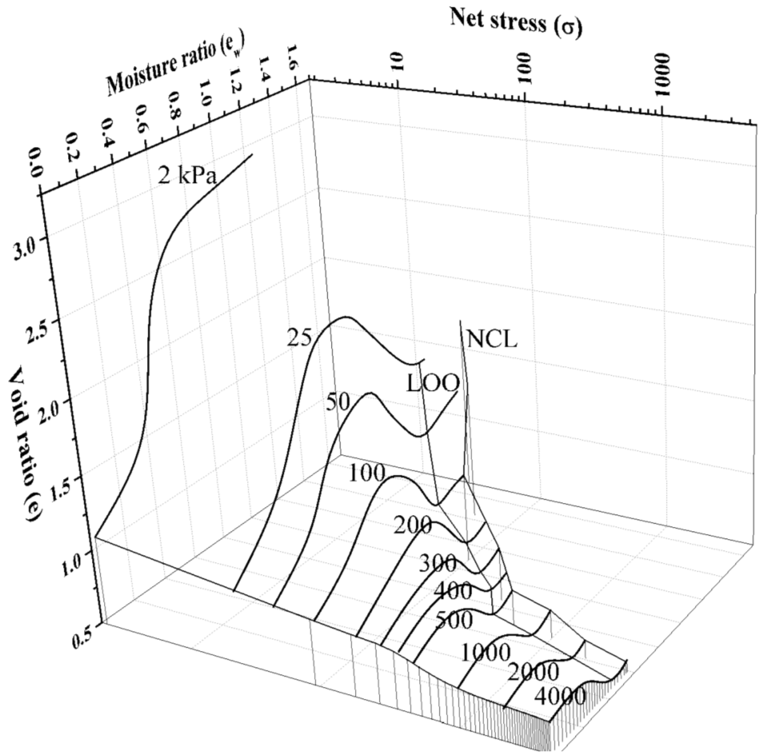

(c)

Figure 5.1. LWSBS for Braybrook expansive soil in (a) e-e_w (b) e-log(σ) (c) e-e_w-log(σ) space

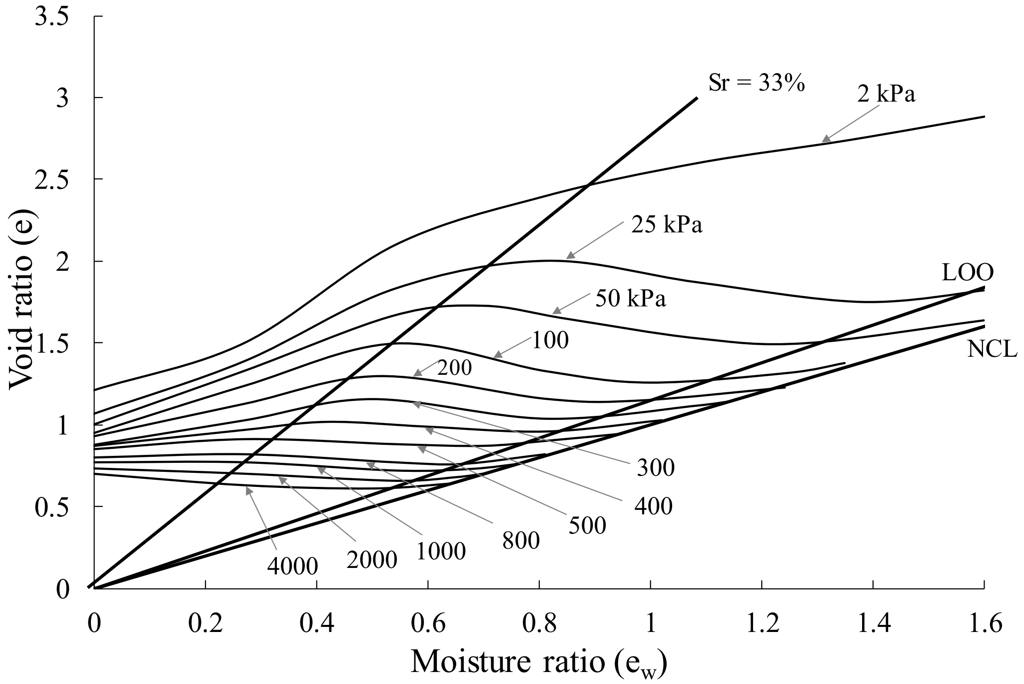

(a)

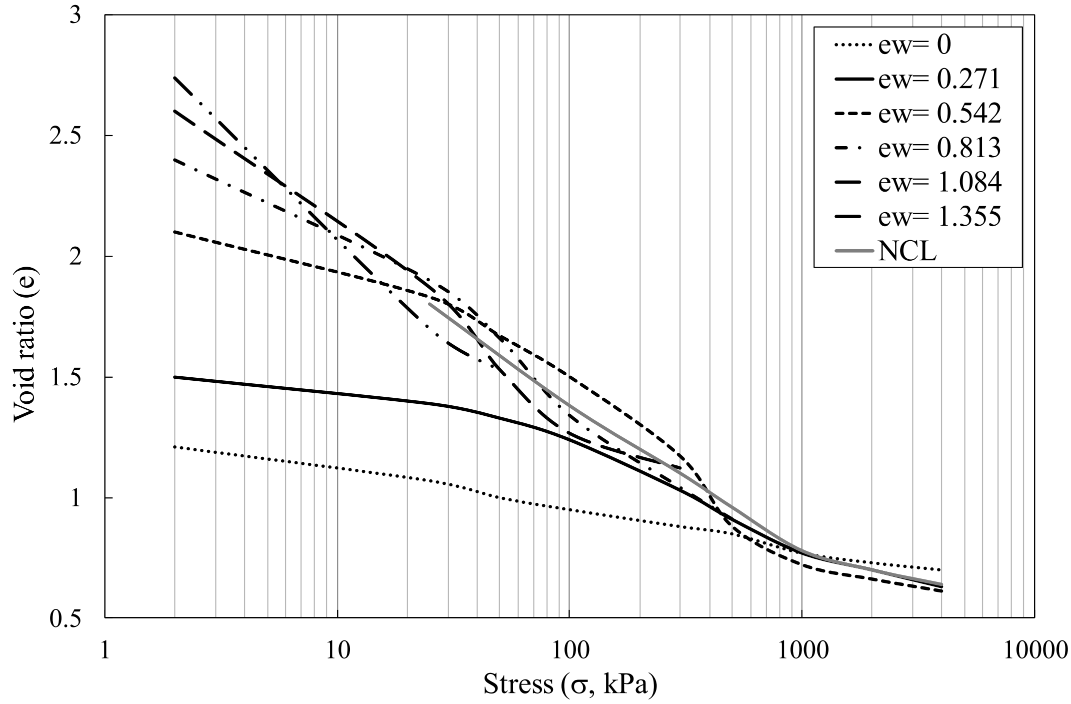

(b)

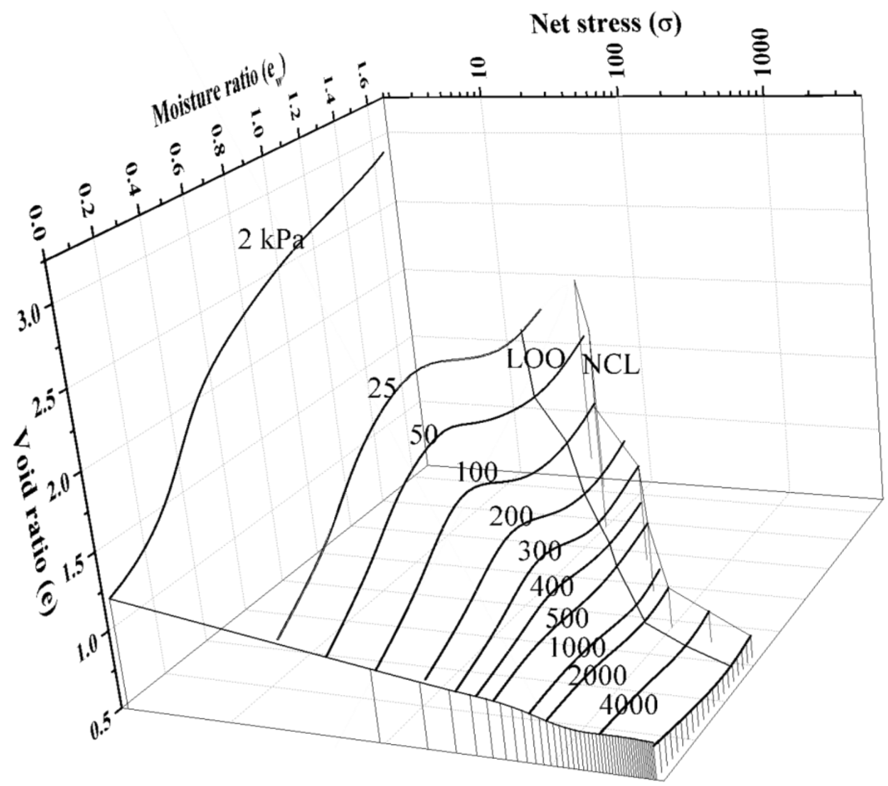

(c)

Figure 5.2. LWSBS for the lime-treated expansive soil with 4% lime in (a) *e*-e_w (b) *e*-log(σ) (c) *e*-e_w-log(σ) space

5.3.2 State paths test series

After generating the LWSBS for the untreated and lime-treated samples, a set of state path tests were conducted to investigate the suitability of the MPK framework for the untreated and lime-treated expansive clay (4% lime). These tests included a combination of Loading and Wetting (LW), Loading-Wetting-Loading (LWL), Loading-Unloading-Wetting (LUW), Loading-Unloading-Wetting-Unloading-Wetting (LUWUW), collapse potential and swelling potential. These state paths are described in more detail in **Tables 5.1, 5.2, 5.3, 5.4** and **5.5**.

Table 5.1. Summary of Loading-Wetting tests conducted on the untreated and lime-treated clay

Soil type	State path test	Description of the test
Loading-Wetting Tests **(L W A B C)** C → wetted to a MC of **C** B → loaded to a stress of **B** A → prepared at a MC of **A** W → wetting L → loading MC: moisture content		
Untreated clay	LW 10 1000 19.5	10% moisture content (e_w=0.271) loaded to 1000 kPa and then wetted to 19.5% moisture content (e_w=0.528)
	LW 20 200 30.3	20% moisture content (e_w=0.542) loaded to 200 kPa and then wetted to 30.3% moisture content (e_w=0.821)
	LW 15 500 21.8	15% moisture content (e_w=0.406) loaded to 500 kPa and then wetted to 21.8% moisture content (e_w=0.590)
	LW 11 100 30.3	11% moisture content (e_w=0.298) loaded to 100 kPa and then wetted to 30.3% moisture content (e_w=0.821)
Lime treated clay	LW 10 500 24	10% moisture content (e_w=0.271) loaded to 500 kPa and then wetted to 24% moisture content (e_w=0.650)
	LW 20 200 35.5	20% moisture content (e_w=0.542) loaded to 200 kPa and then wetted to 35.5% moisture content (e_w=0.962)
	LW 20 300 34	20% moisture content (e_w=0.542) loaded to 300 kPa and then wetted to 34% moisture content (e_w=0.921)
	LW 10 1000 21.7	10% moisture content (e_w=0.271) loaded to 1000 kPa

		and then wetted to 21.7% moisture content (e_w=0.588)
	LW 10 100 36	10% moisture content (e_w=0.271) loaded to 100 kPa and then wetted to 36% moisture content (e_w=0.976)

Table 5.2. Summary of Loading-Wetting-Loading tests conducted on the untreated and lime-treated clay

Soil type	State path test	Description of the test
Loading-Wetting-Loading Tests **(L W L A B C D)** D → loaded to a stress of **D** C → wetted to a MC of **C** B → loaded to a stress of **B** A → prepared at a MC of **A** L → loading W → wetting L → loading		
Untreated and lime treated clays	LWL 15 400 21 500	15% moisture content (e_w=0.406) loaded to 400 kPa then wetted to 21% moisture content (e_w=0.569) and then loaded to 500 kPa

Table 5.3. Summary of Loading-Unloading-Wetting tests conducted on the untreated and lime-treated clay

Soil type	State path test	Description of the test
Loading-Unloading-Wetting Tests **(L U W A B C D)** D → wetted to a MC of **D** C → unloaded to a stress of **C** B → loaded to a stress of **B** A → prepared at a MC of **A** W → wetting U → unloading L → loading		
Untreated clay	LUW 10 1000 25 35.5	10% moisture content (e_w=0.271) loaded to 1000 kPa then unloaded to 25 kPa and then wetted to 35.5% moisture content (e_w=0.962)
	LUW 20 200 25 39.5	20% moisture content (e_w=0.542) loaded to 200 kPa then unloaded to 25 kPa and then wetted to 39.5% moisture content (e_w=1.07)
	LUW 20 300 25 36.5	20% moisture content (e_w=0.542) loaded to 300

		kPa then unloaded to 25 kPa and then wetted to 36.5% moisture content (e_w=0.989)
	LUW 20 200 100 31.7	20% moisture content (e_w=0.542) loaded to 200 kPa then unloaded to 100 kPa and then wetted to 31.7% moisture content (e_w=0.859)
	LUW 20 300 200 30.3	20% moisture content (e_w=0.542) loaded to 300 kPa then unloaded to 200 kPa and then wetted to 30.3% moisture content (e_w=0.821)
	LUW 20 300 100 32.5	20% moisture content (e_w=0.542) loaded to 300 kPa then unloaded to 100 kPa and then wetted to 32.5% moisture content (e_w=0.881)
	LUW 10 1000 300 25.8	10% moisture content (e_w=0.271) loaded to 1000 kPa then unloaded to 300 kPa and then wetted to 25.8% moisture content (e_w=0.699)
Lime-treated clay	LUW 10 1000 25 33.3	10% moisture content (e_w=0.271) loaded to 1000 kPa then unloaded to 25 kPa and then wetted to 33.3% moisture content (e_w=0.902)
	LUW 20 200 25 43	20% moisture content (e_w=0.542) loaded to 200 kPa then unloaded to 25 kPa and then wetted to 43% moisture content (e_w=1.165)
	LUW 20 300 25 39.5	20% moisture content (e_w=0.542) loaded to 300 kPa then unloaded to 25 kPa and then wetted to 39.5% moisture content (e_w=1.07)
	LUW10 1000 300 29	10% moisture content (e_w=0.271) loaded to 1000 kPa then unloaded to 300 kPa and then wetted to 29% moisture content (e_w=0.786)
	LUW 20 300 100 37	20% moisture content (e_w=0.542) loaded to 300 kPa then unloaded to 100 kPa and then wetted to 37% moisture content (e_w=1.003)
	LUW 20 200 100 41.3	20% moisture content (e_w=0.542) loaded to 200 kPa then unloaded to 100 kPa and then wetted to 41.3% moisture content (e_w=1.119)
	LUW 20 300 200 33.5	20% moisture content (e_w=0.542) loaded to 300 kPa then unloaded to 200 kPa and then wetted to 33.5% moisture content (e_w=0.908)

Table 5.4. Summary of Loading-Unloading-Wetting-Unloading-Wetting test conducted on the untreated clay

Soil type	State path test	Description of the test
Loading-Unloading-Wetting-Unloading-Wetting Tests **(L U W U W A B C D E F)** F → wetted to a MC of **F** E → unloaded to a stress of **E** D → wetted to a MC of **D** C → unloaded to a stress of **C** B → loaded to a stress of **B** A → prepared at a MC of **A** W → wetting U → unloading W → wetting U → unloading L → loading		
Untreated clay	LUWUW 15 500 400 20 300 25.5	15% moisture content (e_w=0.406) loaded to 500 kPa then unloaded to 400 kPa then wetted to 20% moisture content (e_w=0.542) then unloaded to 300 kPa and then wetted to 25.5% moisture content (e_w=0.691)

Table 5.5. Summary of collapse and swelling Potential tests conducted on the untreated and lime-treated clays

Soil type	State path test	Description of the test
Collapse and Swelling Potential Tests		
Untreated and lime-treated clays	Compaction stress =200 kPa	20% moisture content (e_w=0.542) loaded to 200 kPa then unloaded to 25 kPa and then wetted to the saturation
		20% moisture content (e_w=0.542) loaded to 200 kPa then unloaded to 50 kPa and then wetted to the saturation
		20% moisture content (e_w=0.542) loaded to 200 kPa then unloaded to 100 kPa and then wetted to the saturation
		20% moisture content (e_w=0.542) loaded to 200 kPa and then wetted to the saturation
		20% moisture content (e_w=0.542) loaded to 300 kPa and then wetted to the saturation
Untreated and lime-treated clays	Compaction stress =300 kPa	20% moisture content (e_w=0.542) loaded to 300 kPa then unloaded to 25 kPa and then wetted to the saturation
		20% moisture content (e_w=0.542) loaded to 300

		kPa then unloaded to 50 kPa and then wetted to the saturation
		20% moisture content (e_w=0.542) loaded to 300 kPa then unloaded to 100 kPa and then wetted to the saturation
		20% moisture content (e_w=0.542) loaded to 300 kPa then unloaded to 200 kPa and then wetted to the saturation
		20% moisture content (e_w=0.542) loaded to 300 kPa and then wetted to the saturation
		20% moisture content (e_w=0.542) loaded to 500 kPa and then wetted to the saturation
Untreated and lime-treated clays	Compaction stress =1000 kPa	10% moisture content (e_w=0.271) loaded to 1000 kPa then unloaded to 25 kPa and then wetted to the saturation
Untreated clay		10% moisture content (e_w=0.271) loaded to 1000 kPa then unloaded to 50 kPa and then wetted to the saturation
Untreated and lime-treated clays		10% moisture content (e_w=0.271) loaded to 1000 kPa then unloaded to 100 kPa and then wetted to the saturation
Untreated clay		10% moisture content (e_w=0.271) loaded to 1000 kPa then unloaded to 200 kPa and then wetted to the saturation
Untreated and lime-treated clays		10% moisture content (e_w=0.271) loaded to 1000 kPa then unloaded to 300 kPa and then wetted to the saturation
		10% moisture content (e_w=0.271) loaded to 1000 kPa then unloaded to 500 kPa and then wetted to the saturation
Lime-treated clay		10% moisture content (e_w=0.271) loaded to 1000 kPa then unloaded to 650 kPa and then wetted to the saturation
Lime-treated clay		10% moisture content (e_w=0.271) loaded to 1000 kPa then unloaded to 800 kPa and then wetted to the saturation
Untreated and lime-treated clays		10% moisture content (e_w=0.271) loaded to 1000 kPa and then wetted to the saturation
		10% moisture content (e_w=0.271) loaded to 2000 kPa and then wetted to the saturation

5.3.2.1 Loading and Wetting (LW) and Loading, Wetting and Loading (LWL) State Paths for Untreated Clay

The state path for the untreated specimen at 10% moisture content (e_w = 0.271) was loaded from a nominal stress of 2 kPa to 1000 kPa, as shown in **Figure 5.3** (from point 1 to 2), and then wetted to reach a moisture content close to the LOO (w =19.5%, e_w =0.528) (from point 2 to 3) in steps. This specimen is labelled as LW10 1000 19.5 in Figure 5.3. It is clear that the void ratio decreased during loading (under a constant moisture ratio of 0.271) and that the path did follow the LWSBS. During wetting, the void ratio continued to decrease and followed the 1000 kPa contour of the LWSBS until it reached the LOO. Several LW tests were performed on the untreated specimens, and similar results were observed for tests starting at different moisture ratios and then undergoing different loading and wetting paths. These tests included (LW20 200 30.3), (LW20 300 26.2) and (LW15 500 21.8). The results of LW20 200 30.3 and LW15 500 21.8 are also presented in Figure 5.3 as examples.

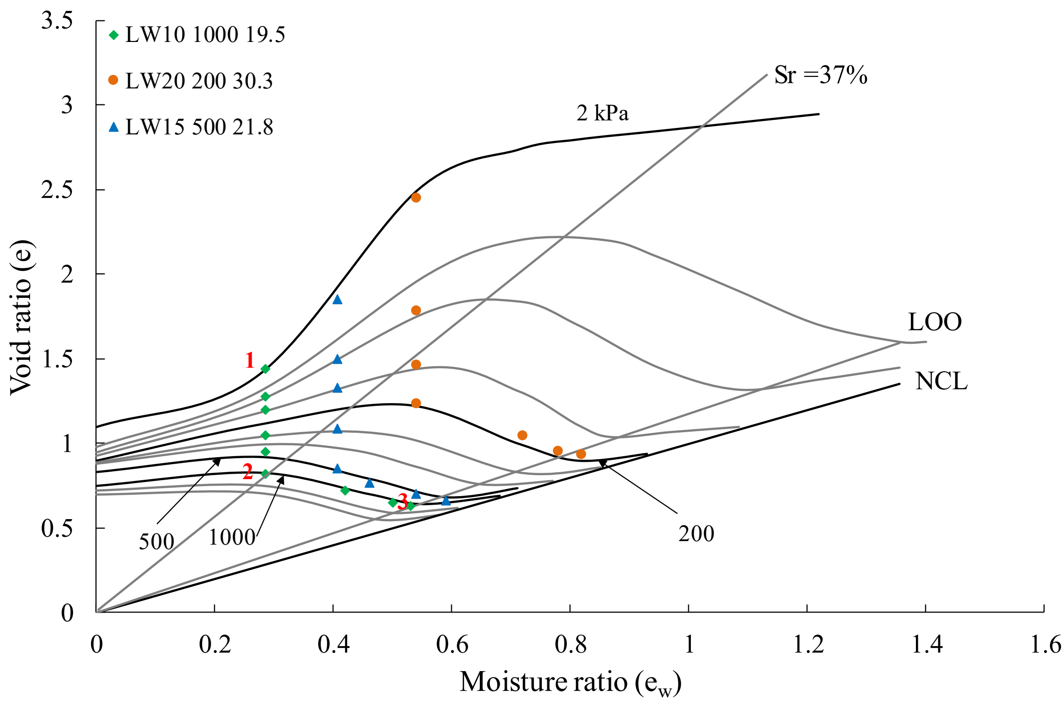

(a)

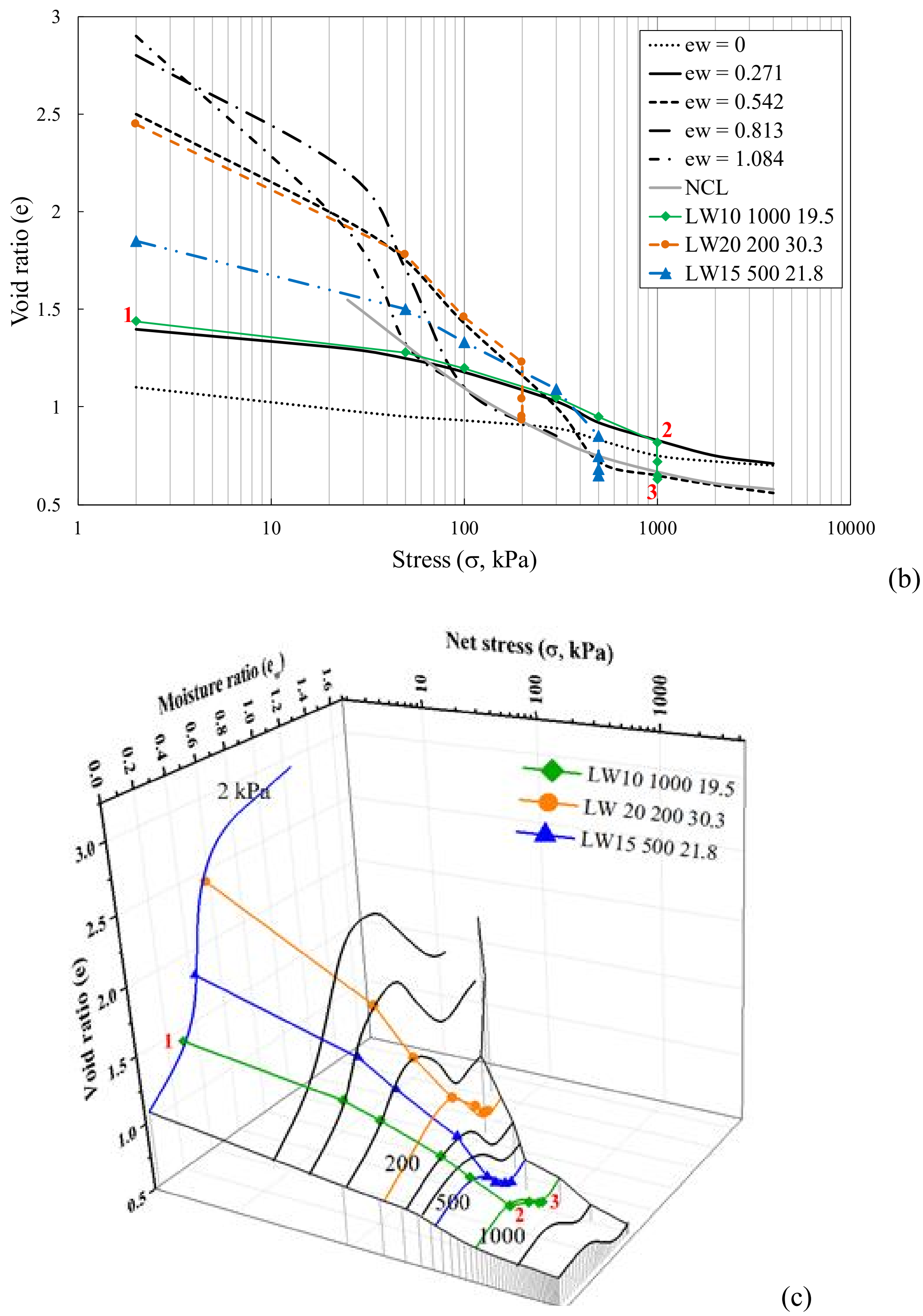

Figure 5.3. State path of loading to 1000, 200 and 500 kPa at constant moisture of 10% (e_w=0.271), 20% (e_w=0.542) and 15% (e_w=0.406), respectively, then wetting to the LOO in (a) e-e_w (b) e-log(σ) (c) e-e_w-log(σ) space (untreated clay)

However, as shown in **Figure 5.4**, when the loading path for untreated specimen LW11 100 30.3 at 11% moisture content (e_w = 0.298) did follow the LWSBS (from point 4 to 5 during loading), the wetting path then shifted to the inside of the LWSBS after wetting. This path remained below the LWSBS (from point 5 to 6) with continuous wetting. Thus, the loading path followed the LWSBS, but the wetting path did not. This is an important finding and its significance will be discussed later in Sections 5.4, 5.5 & 5.6.

The same procedure was followed to examine the behaviour of the LWL state path, except that after wetting, the specimen was loaded to check if the loading path was still following the LWSBS. **Figure 5.5** presents specimen LWL15 400 21 500, which was prepared at 15% moisture content (e_w = 0.406) and loaded to 400 kPa (from point 1 to 2), and then wetted to a moisture content of 21% (e_w = 0.569) (from point 2 to 3) and loaded to 500 kPa (from point 3 to 4). It is apparent that all three segments of this path (loading, wetting, loading) followed the LWSBS.

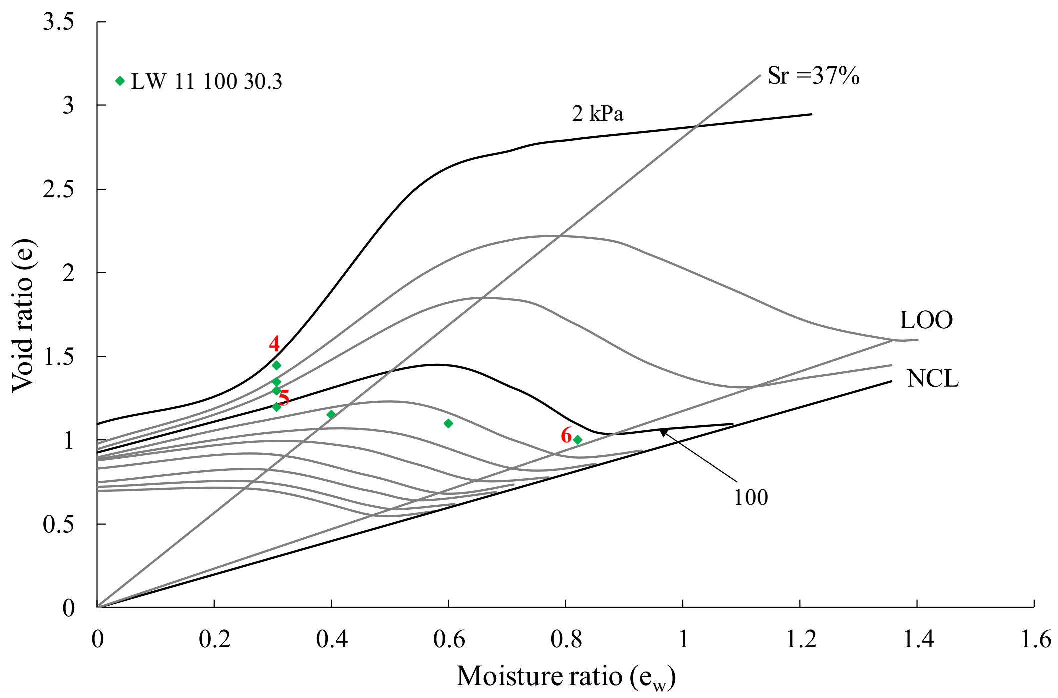

(a)

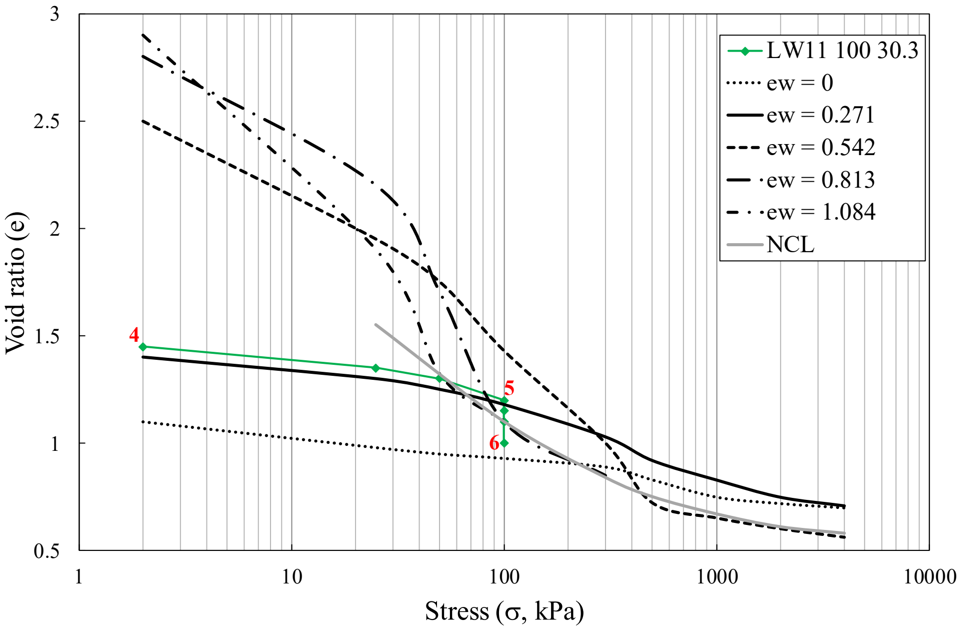

(b)

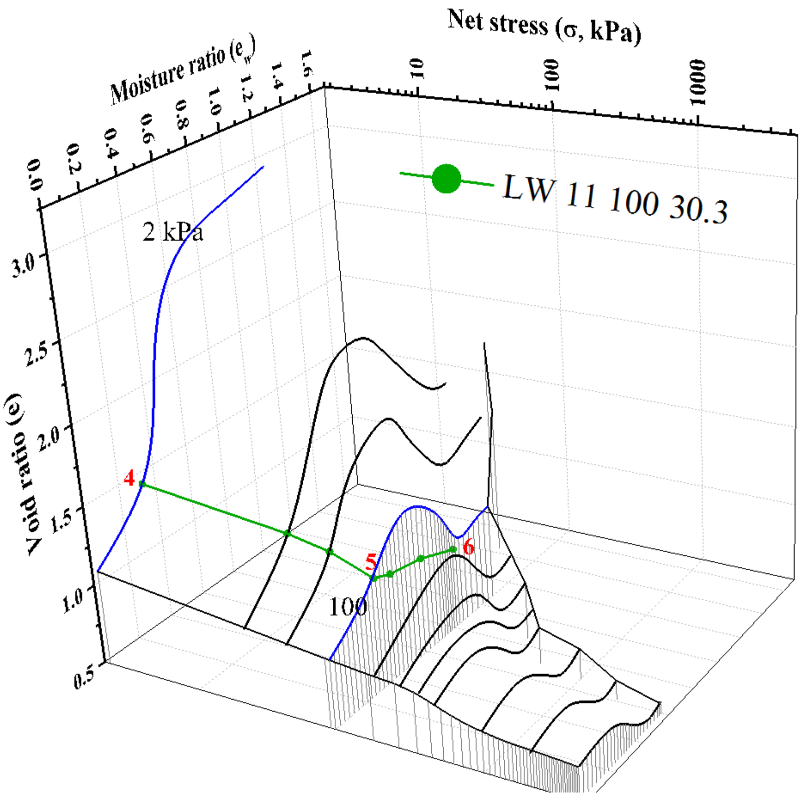

(c)

Figure 5.4. State path of loading to 100 kPa at constant moisture of 11% (e_w=0.298) and then wetting to the LOO in (a) e-e_w (b) e-log(σ) (c) e-e_w-log(σ) space (untreated clay)

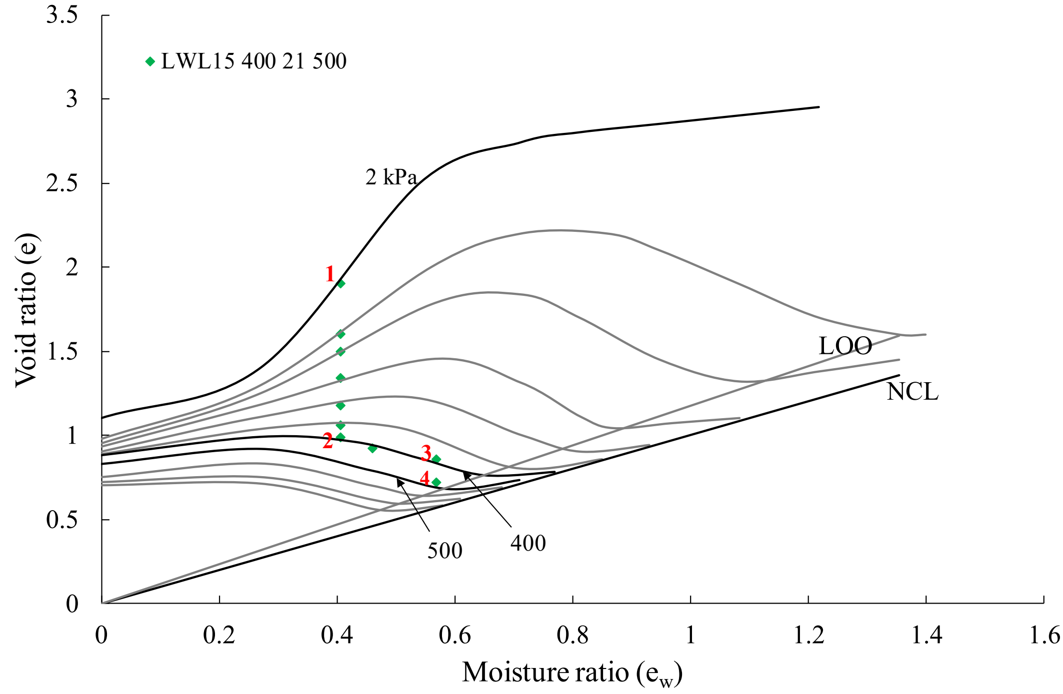
LWL15 400 21 500
2 kPa
1
2
3
4
500
400
LOO
NCL
Void ratio (e)
Moisture ratio (e_w)
3.5
3
2.5
2
1.5
1
0.5
0
0
0.2
0.4
0.6
0.8
1
1.2
1.4
1.6

(a)

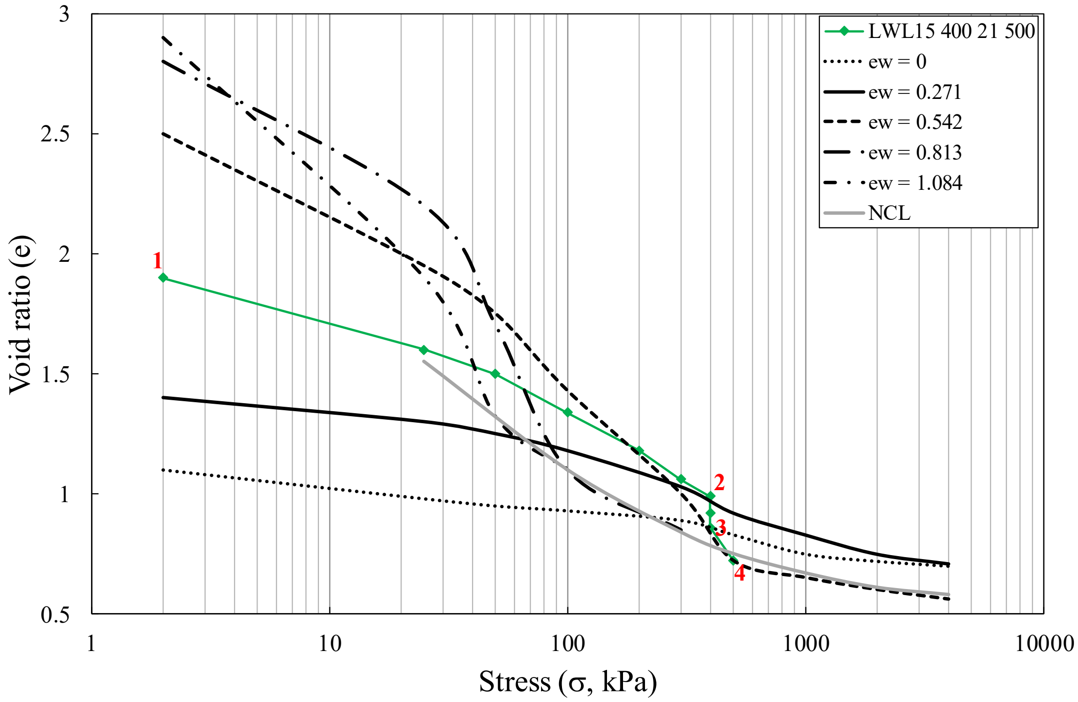
LWL15 400 21 500
ew = 0
ew = 0.271
ew = 0.542
ew = 0.813
ew = 1.084
NCL
1
2
3
4
Void ratio (e)
Stress (σ, kPa)
3
2.5
2
1.5
1
0.5
1
10
100
1000
10000

(b)

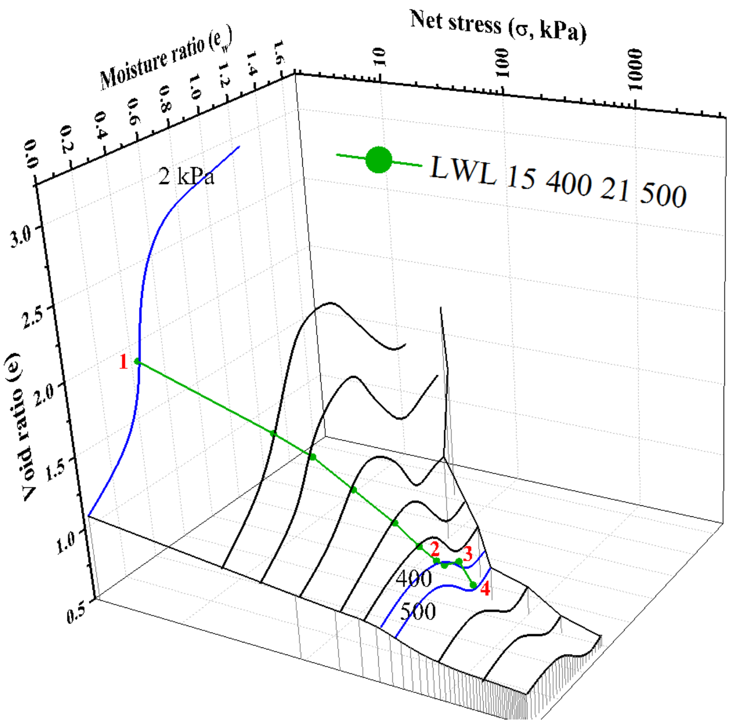

(c)

Figure 5.5. State path of loading to 400 kPa at constant moisture of 15% (e_w=0.406) then wetting to 21% (e_w=0.569) then loading to 500 kPa in (a) e-e_w (b) e-log(σ) (c) e-e_w-log(σ) space (untreated clay)

After examining the validation of the MPK framework for the untreated specimens selected for this study, it was noted that the wetting paths, including LW and LWL, did follow the MPK framework. However, the MPK could not be shown to extend to specimens prepared at a degree of saturation (S_r) less than approximately 37% and then wetted under stress levels to less than 1000 kPa, as presented in Figure 5.4.

5.3.2.2 Combination of Loading, Unloading and Wetting (LUW) State Paths for Untreated Clay

The state path for the untreated specimen LUW 10 1000 25 35.5 is shown in **Figure 5.6**. This specimen was prepared at a moisture content of 10% (e_w = 0.271) and loaded to a stress of 1000 kPa (from point 1 to 2 in Figure 5.6), then unloaded to 25 kPa (from point 2 to 3), and then wetted to the NCL (w = 35.5%, e_w = 0.962) (from point 3 to 4). From Figure 5.6, it is clear that the loading path did follow the LWSBS, and then moved inside the LWSBS during the unloading. The specimen then swelled toward the stress contour for 25 kPa of the LWSBS. At the end of the swelling, the position of the swelling path remained inside the LWSBS.

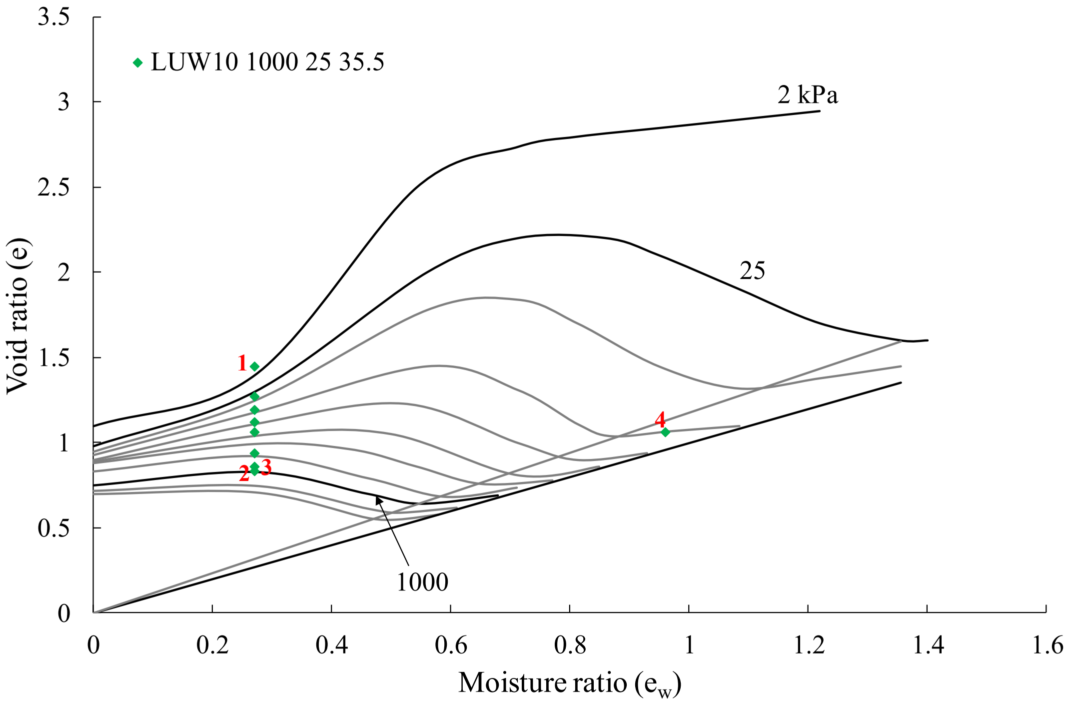

(a)

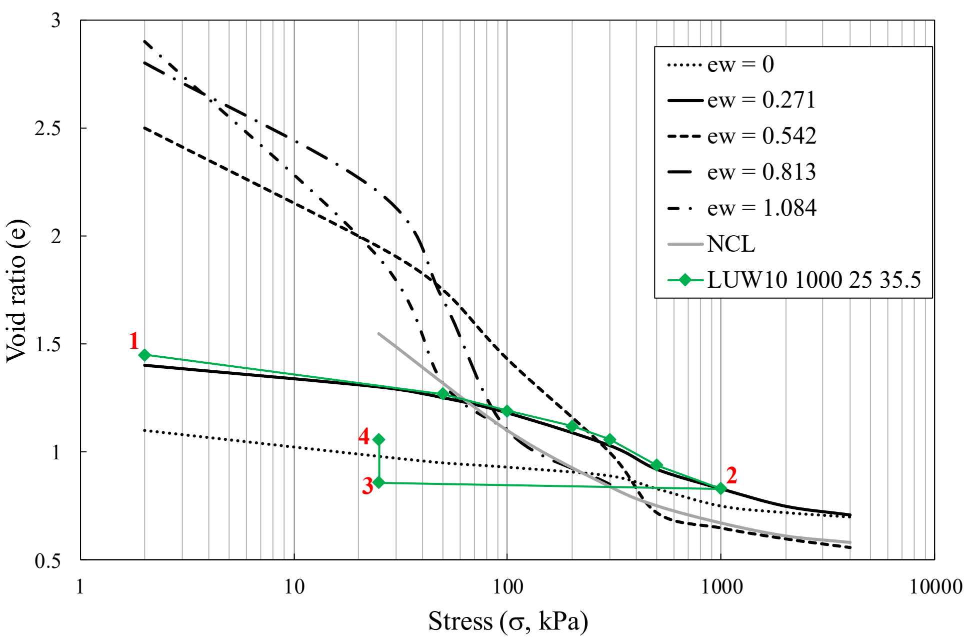

(b)

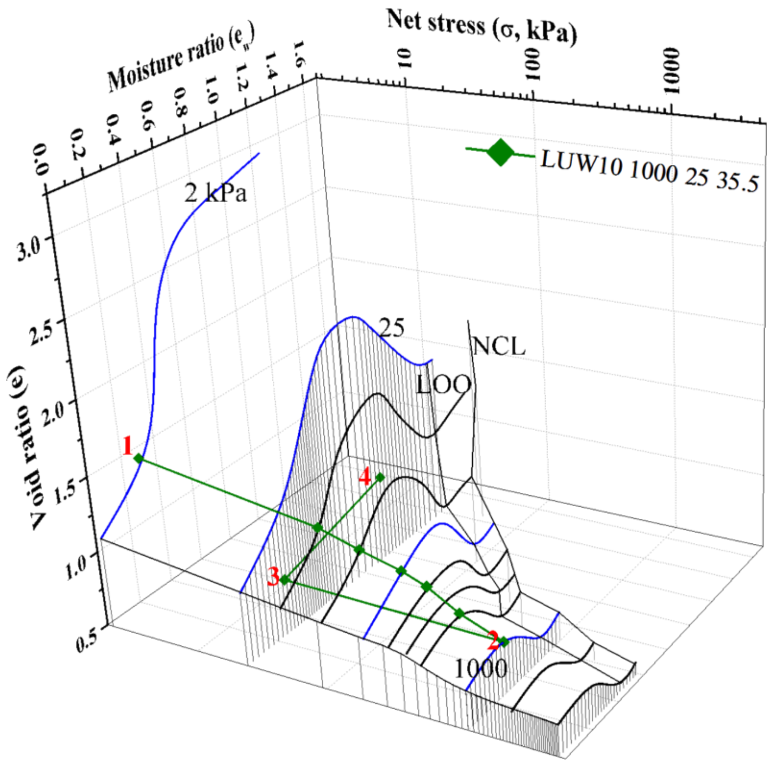

(c)

Figure 5.6. State path of loading to 1000 kPa at constant moisture of 10% (e_w=0.271) then unloading to 25 kPa and then wetting to the NCL in (a) e-e_w (b) e-log(σ) (c) e-e_w-log(σ) space (untreated clay)

This pattern was observed for two specimens with a moisture content of 20% (e_w = 0.542) loaded to different stresses. One specimen was loaded to a stress of 200 kPa (from point 5 to 6 in **Figure 5.7**), while the other was loaded to 300 kPa (from point 9 to 10 in Figure 5.8). Both of them were unloaded to 25 kPa (from point 6 to 7 in Figure 5.7 and from point 10 to 11 in **Figure 5.8**) and then wetted to the NCL (w= 39.5%, e_w= 1.07 & w = 36.5%, e_w= 0.989) (from point 7 to 8 in Figure 5.7 and from point 11 to 12 in Figure 5.8).

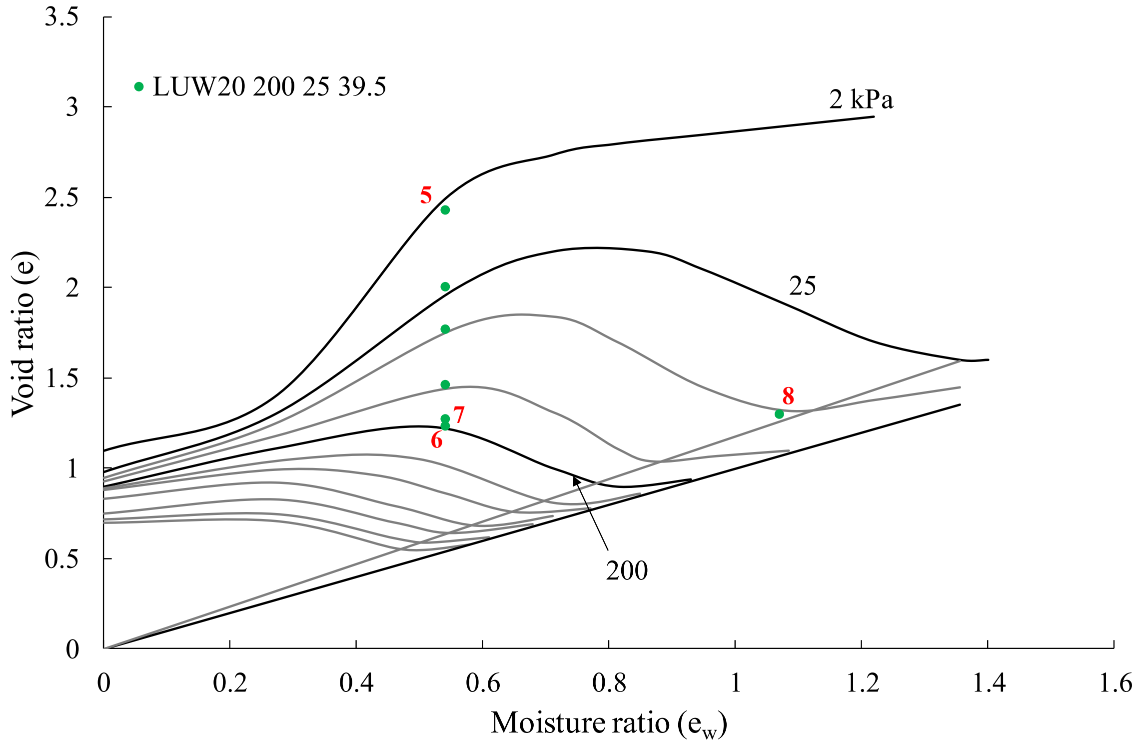

LUW20 200 25 39.5
2 kPa
25
200
5
6
7
8
Void ratio (e)
Moisture ratio (e_w)

(a)

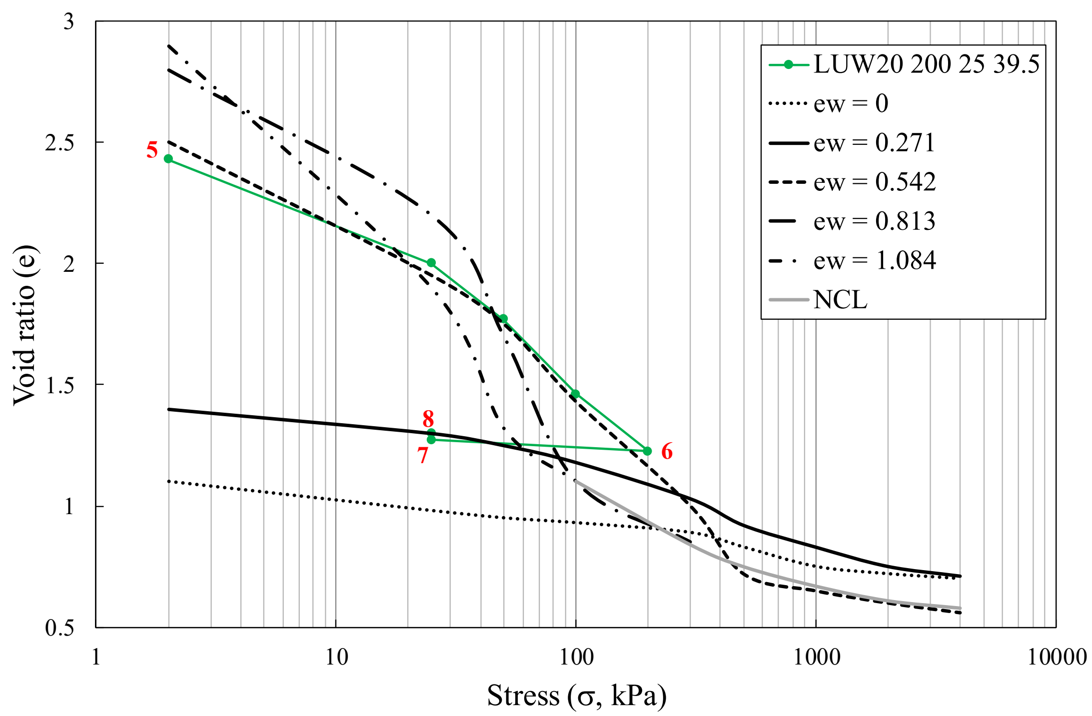

LUW20 200 25 39.5
ew = 0
ew = 0.271
ew = 0.542
ew = 0.813
ew = 1.084
NCL
5
6
7
8
Void ratio (e)
Stress (σ, kPa)

(b)

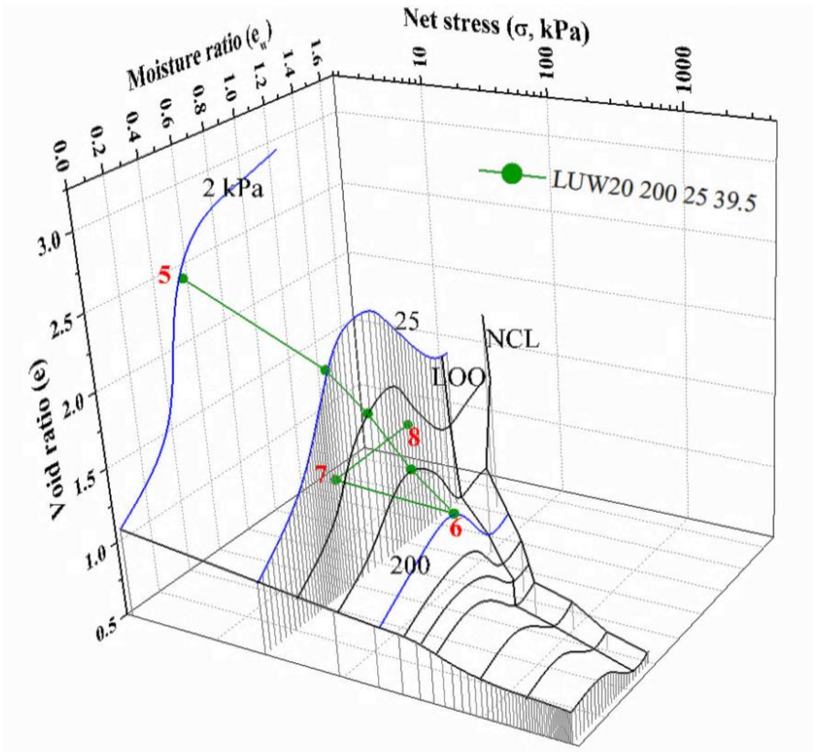

(c)

Figure 5.7. State path of loading to 200 kPa at constant moisture of 20% (e_w=0.542) then unloading to 25 kPa and then wetting to the NCL in (a) e-e_w (b) e-log(σ) (c) e-e_w-log(σ) space (untreated clay)

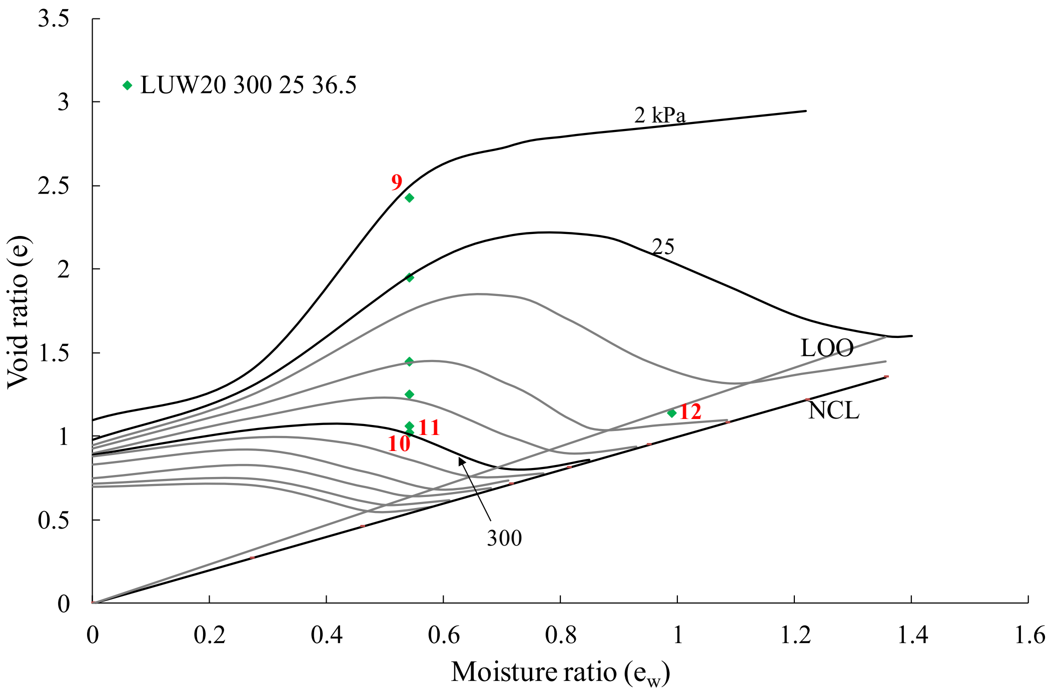

(a)

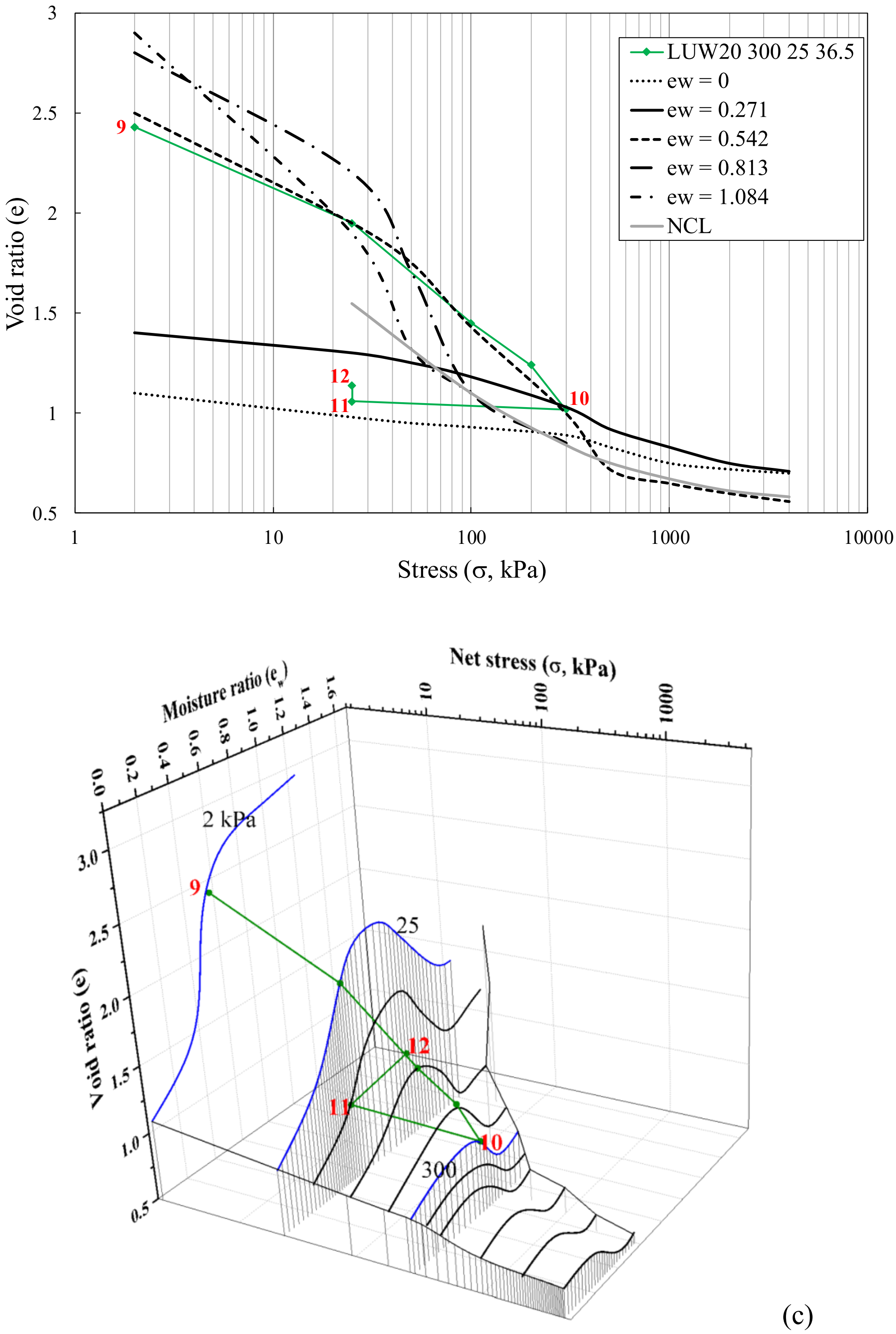

(b)

(c)

Figure 5.8. State path of loading to 300 kPa at constant moisture of 20% (e_w=0.542) then unloading to 25 kPa and then wetting to the NCL in (a) e-e_w (b) e-log(σ) (c) e-e_w-log(σ) space (untreated clay)

Specimens LUW20 200 100 31.7 & LUW20 300 200 30.3 prepared at a moisture content of 20% (e_w = 0.542) and loaded to different stresses are presented in **Figures 5.9** & **5.10**. The first specimen was loaded to a stress of 200 kPa (from point 1 to 2 in Figure 5.9), and then unloaded to 100 kPa (from point 2 to 3). The second was loaded to 300 kPa (from point 6 to 7 in Figure 5.10), and then unloaded to 200 kPa (from point 7 to 8). Both specimens were then wetted to a moisture content close to LOO (wetted to point 5 in Figure 5.9 & to point 10 in Figure 5.10, respectively) and both swelled during wetting. The amount of swelling was very small and can be neglected, and the path of swelling hit the LWSBS at a position before the LOO (at point 4 for the first specimen and at point 9 for the second specimen). Therefore, by adding water beyond this point, the specimen collapsed (i.e. a reduction in void ratio) and followed the LWSBS (from point 4 to 5 for the first specimen and from point 9 to 10 for the second specimen). This collapse continued up to the LOO.

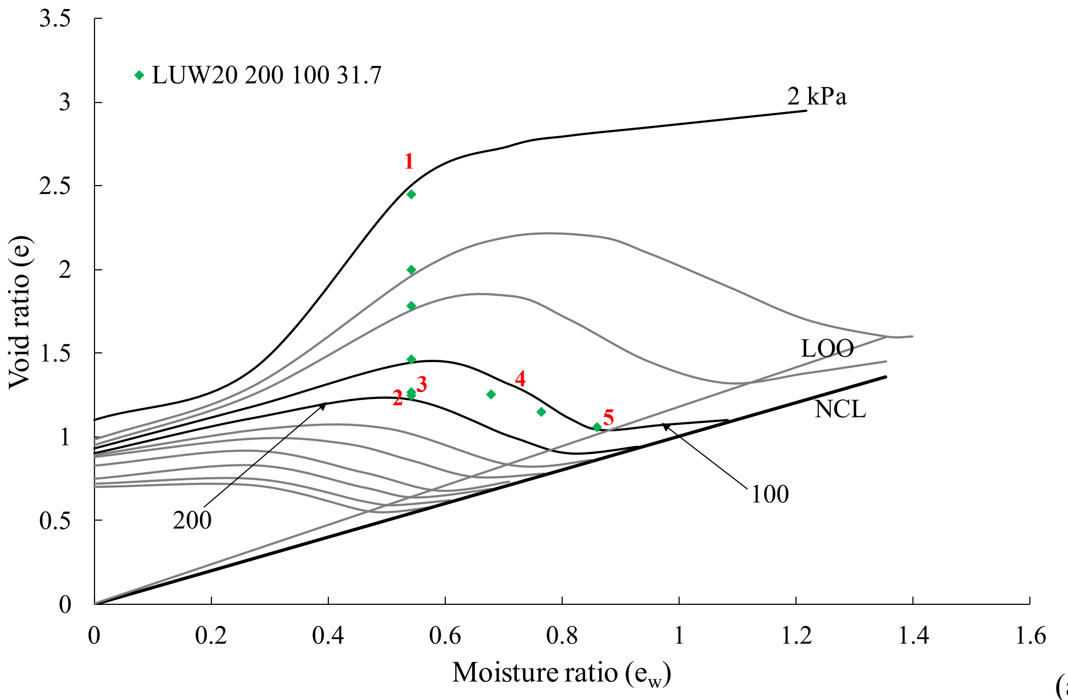

(a)

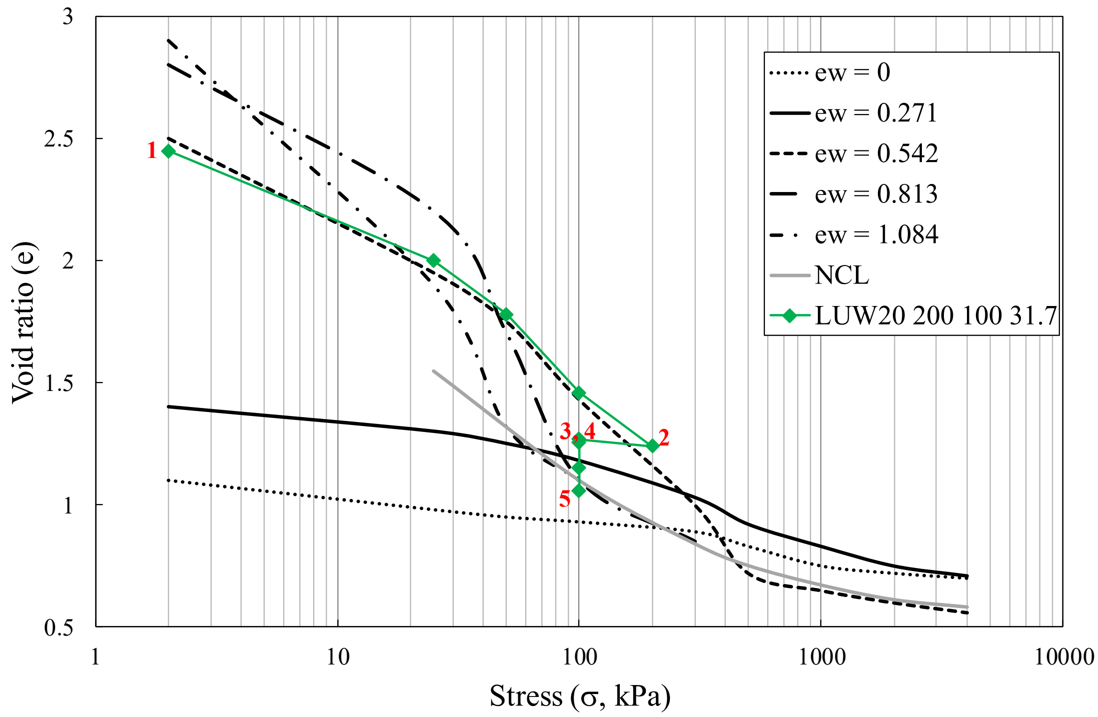

(b)

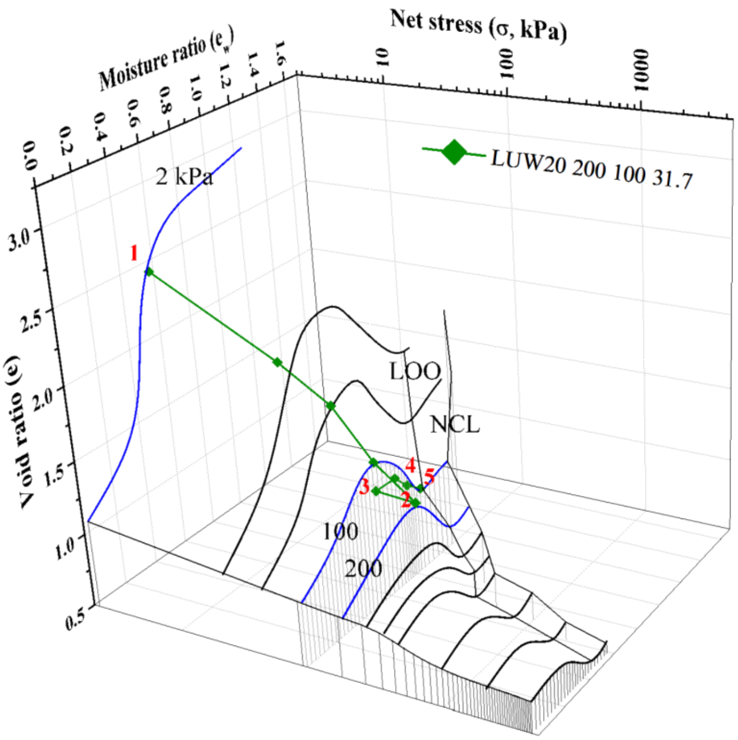

(c)

Figure 5.9. State path of loading to 200 kPa at constant moisture of 20% (e_w=0.542) then unloading to 100 kPa and then wetting to the NCL in (a) e-e_w (b) e-log(σ) (c) e-e_w-log(σ) space (untreated clay)

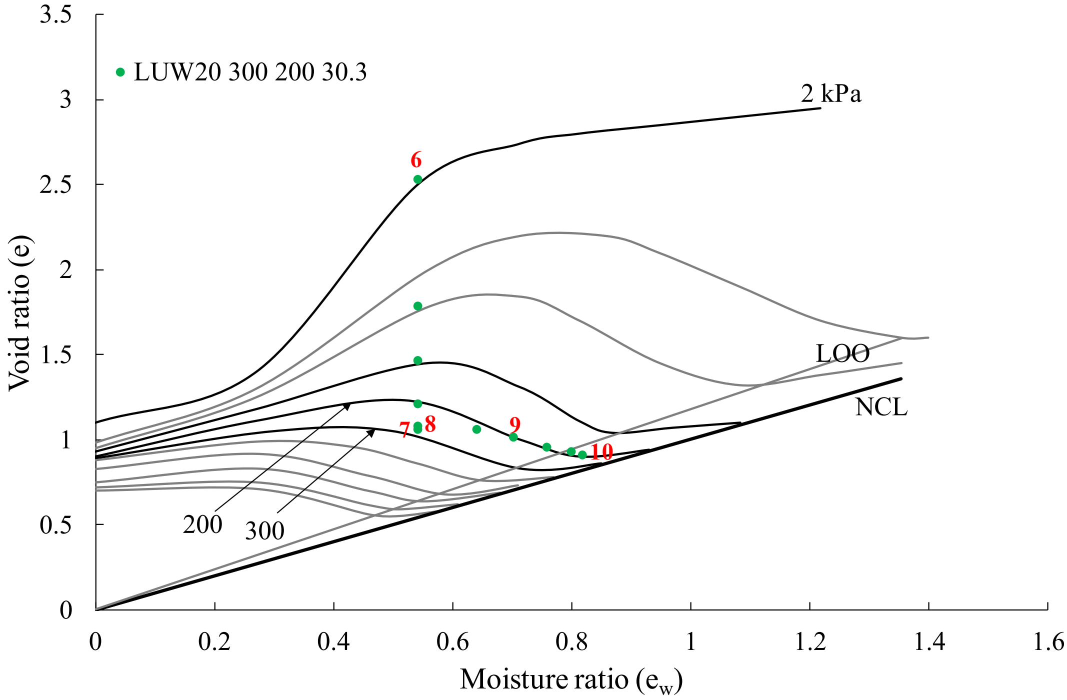
LUW20 300 200 30.3
2 kPa
6
7
8
9
10
LOO
NCL
200
300
Void ratio (e)
Moisture ratio (e_w)

(a)

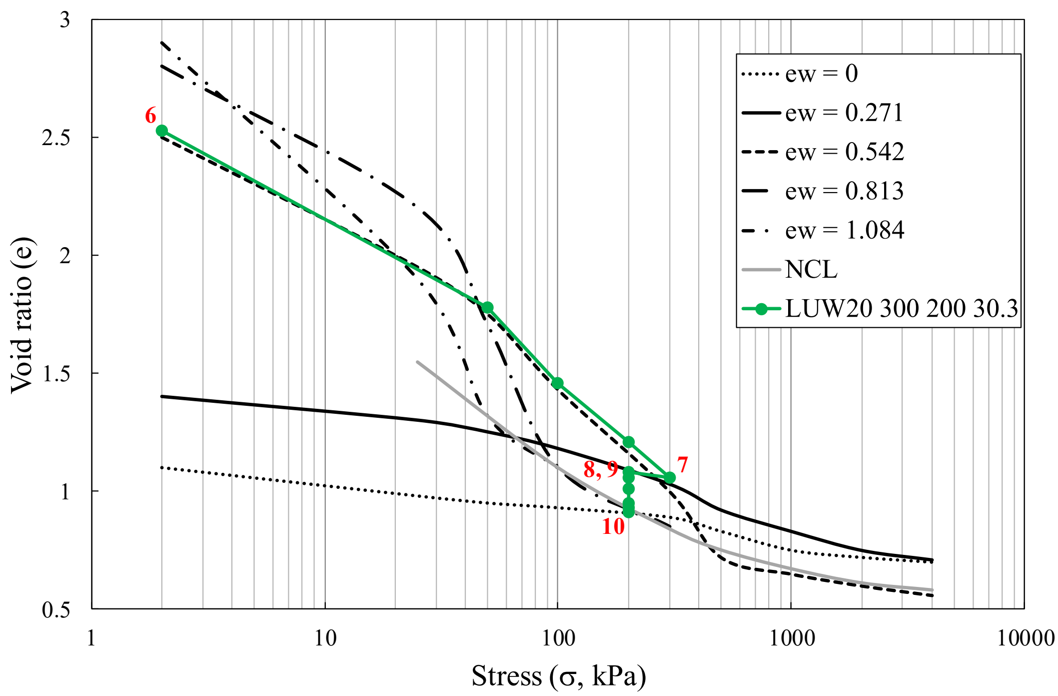
ew = 0
ew = 0.271
ew = 0.542
ew = 0.813
ew = 1.084
NCL
LUW20 300 200 30.3
6
7
8, 9
10
Void ratio (e)
Stress (σ, kPa)

(b)

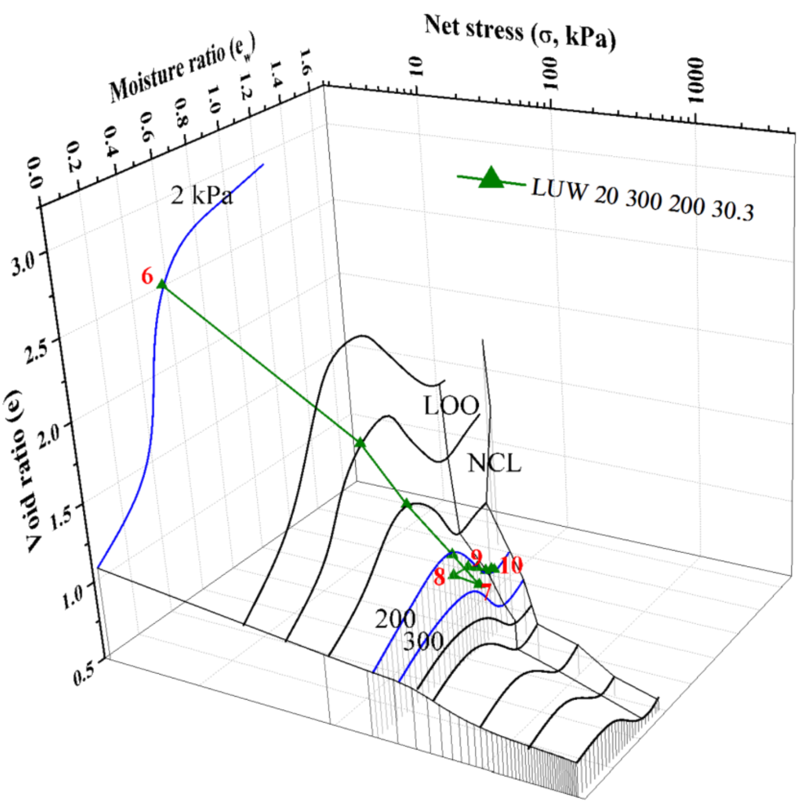

(c)

Figure 5.10. State path of loading to 300 kPa at constant moisture of 20% (e_w=0.542) then unloading to 200 kPa and then wetting to the NCL in (a) e-e_w (b) e-log(σ) (c) e-e_w-log(σ) space (untreated clay)

This same path was followed for a specimen with the moisture content of 20% (e_w = 0.542), loaded to a stress of 300 kPa (from point 11 to 12 in **Figure 5.11**), unloaded to 100 kPa (from point 12 to 13), and then wetted to the NCL (w= 32.5%, e_w= 0.881) (from point 13 to 14 to 15), as shown in Figure 5.11 (LUW20 300 100 32.5). A similar behaviour was observed when a specimen with the moisture content of 10% (e_w = 0.271) was loaded to 1000 kPa (from point 16 to 17 in **Figure 5.12**), then unloaded to 300 kPa (from point 17 to 18), and then wetted to about the NCL (w = 25.8%, e_w= 0.699) (from point 18 to 19 to 20 in Figure 5.12). It is apparent that the specimen collapsed (to a lesser extent) after the wetting path hit the LWSBS, as shown in Figure 5.12 (LUW10 1000 300 25.8).

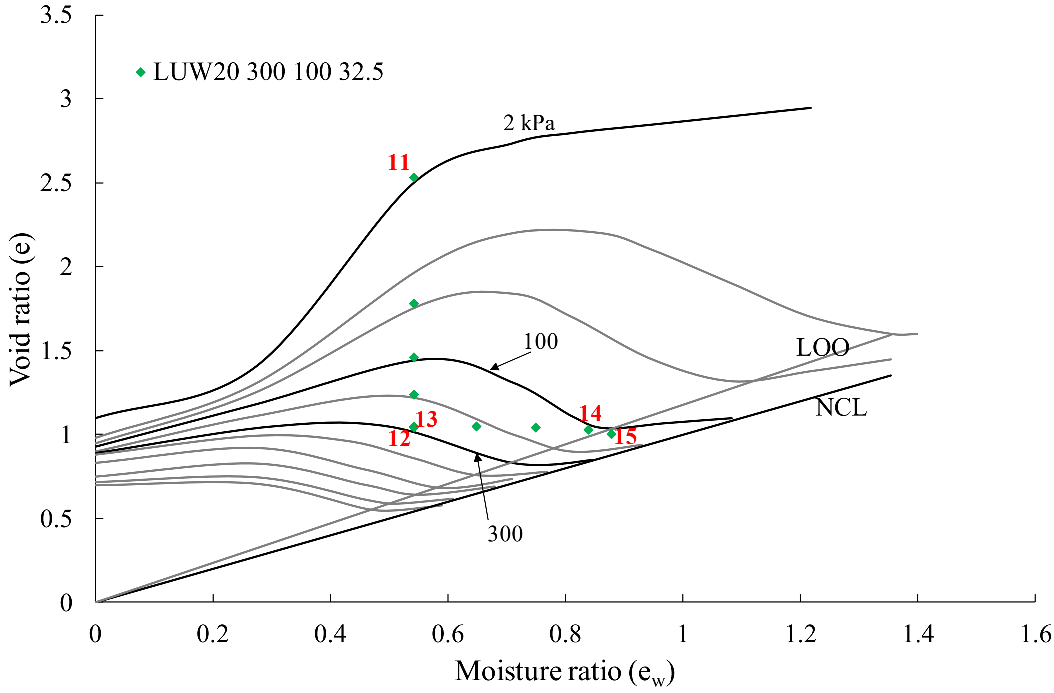
LUW20 300 100 32.5
2 kPa
100
300
LOO
NCL
11
12
13
14
15
Void ratio (e)
Moisture ratio (e_w)
3.5
3
2.5
2
1.5
1
0.5
0
0
0.2
0.4
0.6
0.8
1
1.2
1.4
1.6

(a)

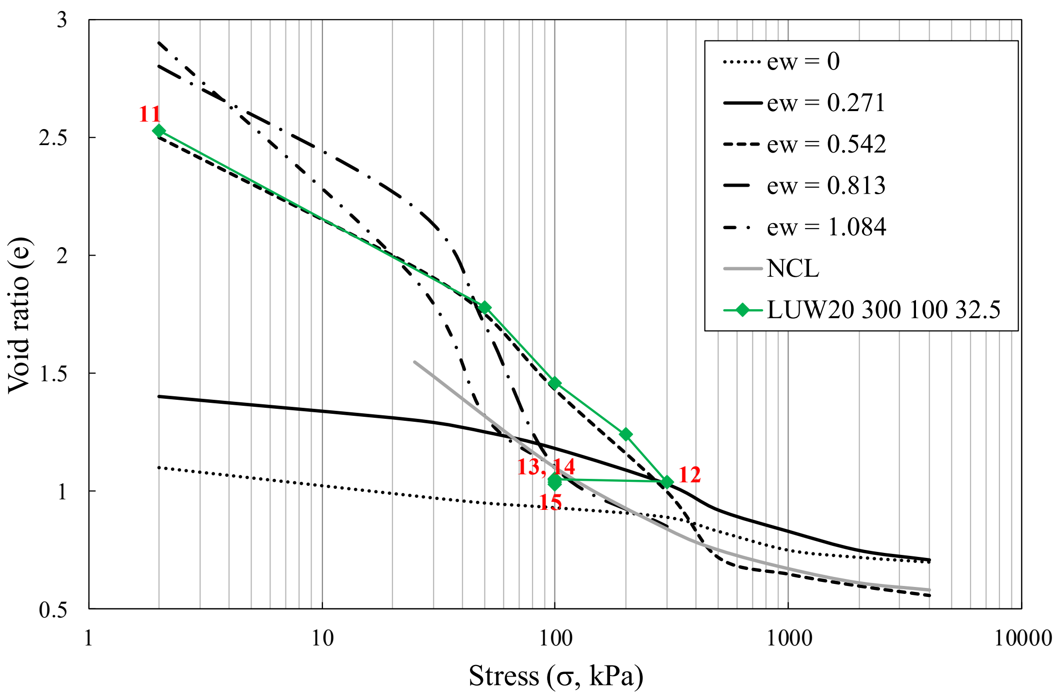
ew = 0
ew = 0.271
ew = 0.542
ew = 0.813
ew = 1.084
NCL
LUW20 300 100 32.5
11
12
13, 14
15
Void ratio (e)
Stress (σ, kPa)
3
2.5
2
1.5
1
0.5
1
10
100
1000
10000

(b)

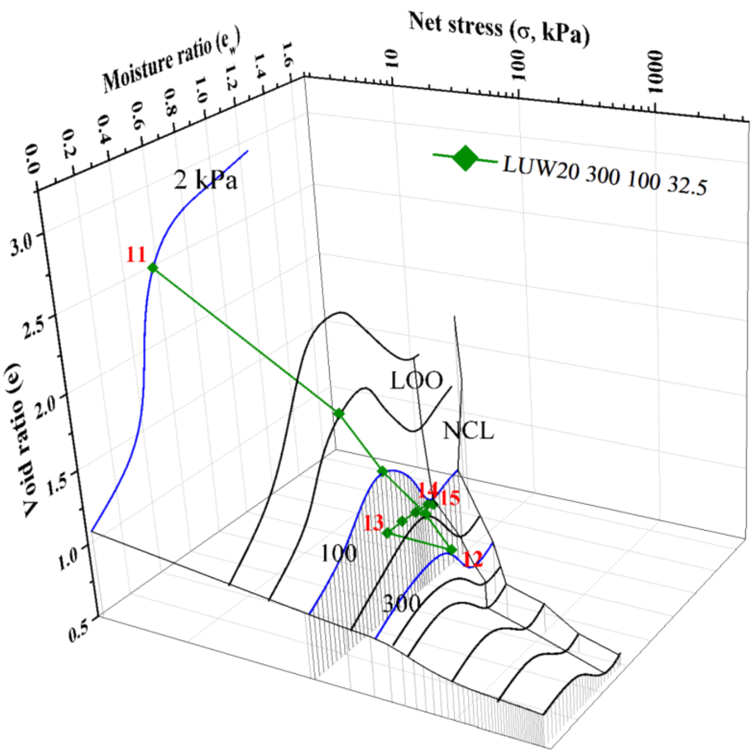

(c)

Figure 5.11. State path of loading to 300 kPa at constant moisture of 20% (e_w=0.542) then unloading to 100 kPa and then wetting to the NCL in (a) *e-e$_w$* (b) *e-*log(σ) (c) *e-e$_w$*-log(σ) space (untreated clay)

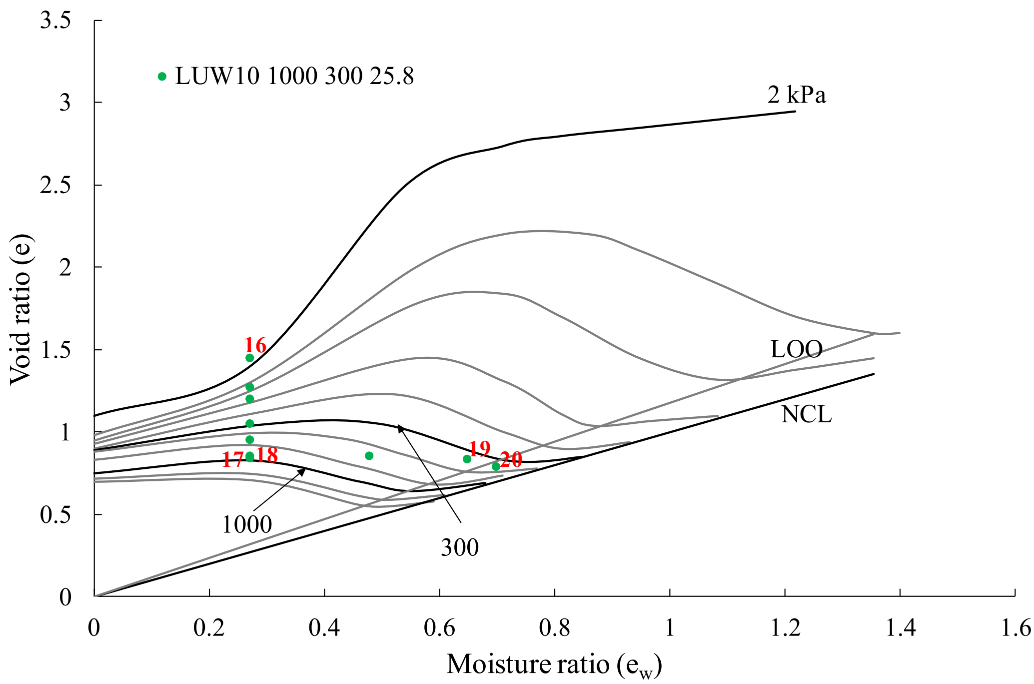

(a)

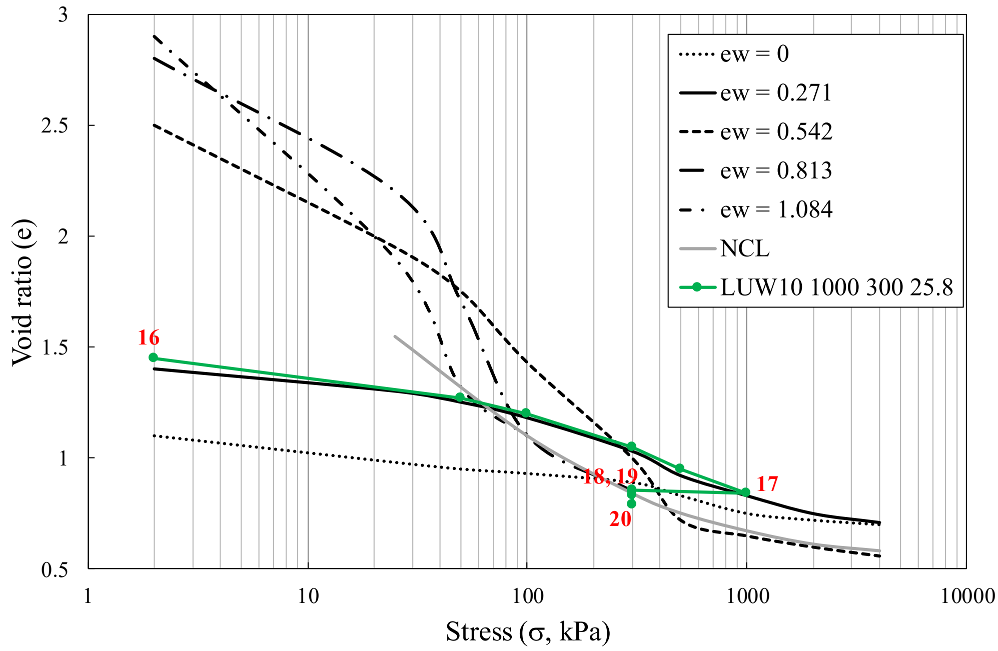

(b)

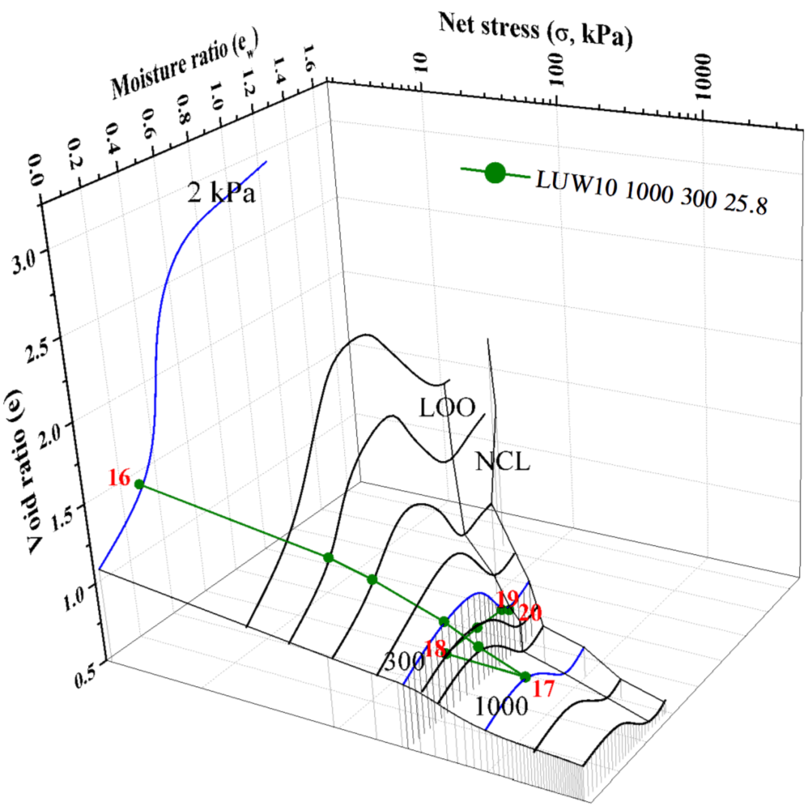

(c)

Figure 5.12. State path of loading to 1000 kPa at constant moisture of 10% (e_w=0.271) then unloading to 300 kPa and then wetting to the NCL in (a) *e*-e_w (b) *e*-log(σ) (c) *e*-e_w-log(σ) space (untreated clay)

This behaviour was repeated for a specimen with the moisture content of 15% (e_w = 0.406) and loaded to a stress of 500 kPa, then unloaded to 400 kPa, then wetted to 20% (e_w = 0.542), then unloaded to 300 kPa, and then finally wetted to the NCL (w = 25.5%, e_w = 0.691), as shown in **Figure 5.13** (LUWUW15 500 400 20 300 25.5). This specimen followed the LWSBS when loaded to 500 kPa. After unloading to 400 kPa, the specimen reached the 400 kPa stress contour of the LWSBS, and when wetted, the collapse was observed. The same behaviour was observed when the specimen was unloaded to 300 kPa and then wetted.

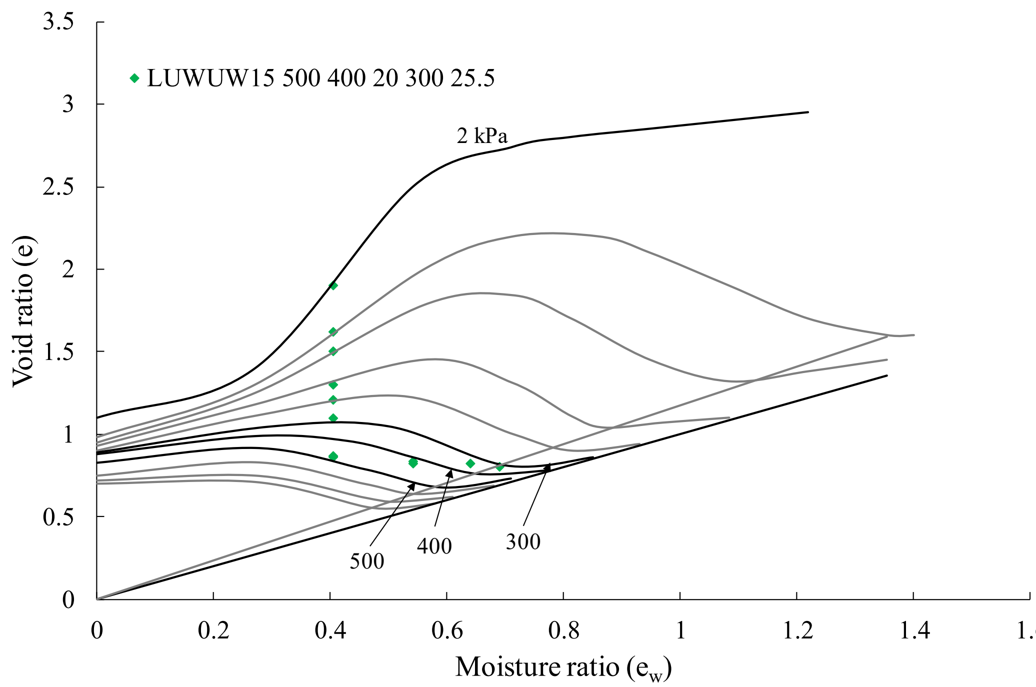

(a)

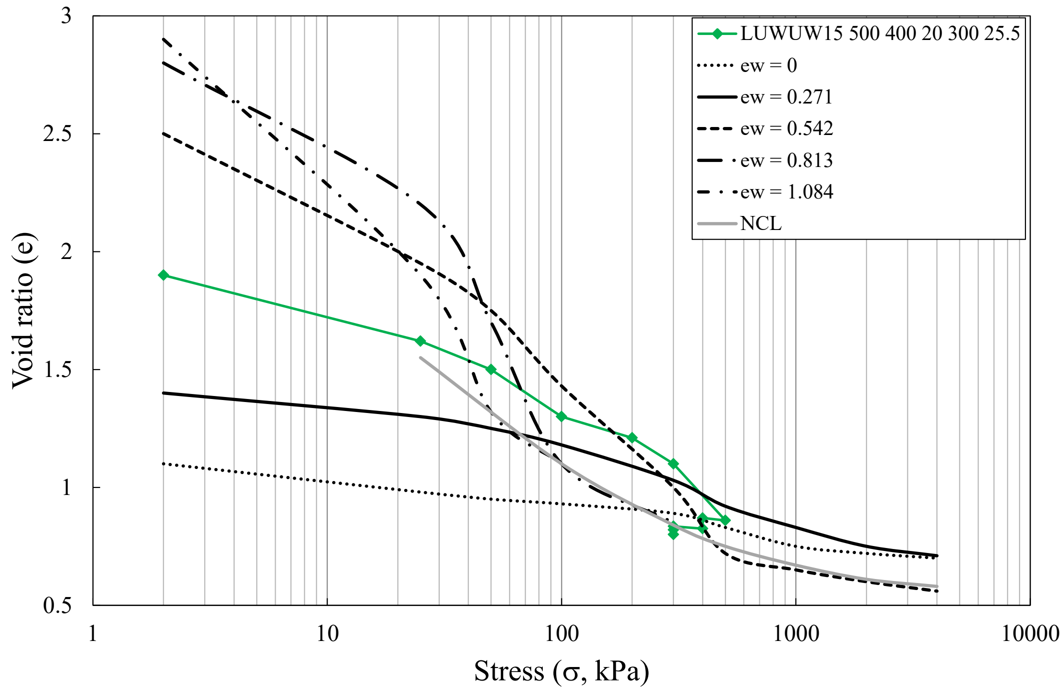

(b)

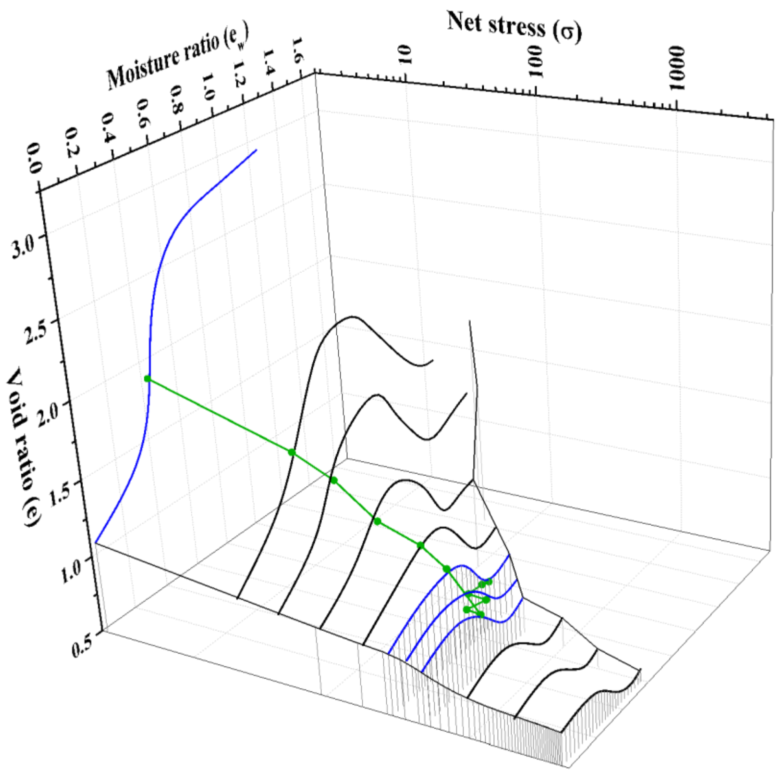

(c)

Figure 5.13. State path of loading to 500 kPa at constant moisture of 15% (e_w=0.406) then unloading to 400 kPa then wetting to the moisture content of 20% then unloading to 300 kPa and then wetting to the moisture content of 25.5% (e_w=0.691) in (a) e-e_w (b) e-log(σ) (c) e-e_w-log(σ) space (untreated clay)

5.3.2.3 Collapse and Swelling Tests for Untreated Clay

Three sets of tests were conducted on untreated clay to investigate the variation of collapse and swelling potential at various stress levels. For the first set of tests, specimens with a moisture content of 20% (e_w =0.542) were prepared and compressed to 200 kPa. The specimens were then wetted to reach saturation state under stress levels of 25, 50, 100, 200 and 300 kPa. The collapse and swelling behaviours for these specimens are plotted in **Figure 5.14** as points 1 to 4. In this figure, the specimen was shown to swell when wetted under a stress of 25 kPa (point 1). This is due to the specimen moving inside the LWSBS after unloading to 25 kPa, with its location well below the LWSBS. Therefore, after wetting, the amount of swelling was insufficient to get the specimen back to the LWSBS. However, at 100 kPa, the specimen did swell after adding a small amount of water, which was sufficient enough for it to reach the LWSBS. With continued wetting, the specimen then collapsed and followed the 100 kPa contour on the LWSBS (point 2 in Figure 5.14). At 200 kPa, the specimen collapsed after wetting and followed the 200 kPa contour on the LWSBS (point 3). The collapse potential recorded due to loading to 200 kPa, unloading to 100 kPa and then wetting was less than the collapse caused by loading to 200 kPa and then wetting. This may initially indicate that the collapse potential increased as the stress increased. However, when the same specimen was wetted under 300 kPa, the collapse potential decreased (point 4). Therefore, for this reason, it can be concluded that the collapse potential increases as the stress increases up to the compaction stress. Beyond this stress, the collapse potential decreases with an increase in stress.

In the second set of tests, the same behaviour was observed when specimens at a moisture content of 20% (e_w =0.542) were prepared and then compressed to 300 kPa (see Figure 5.14). The specimens were then wetted close to saturation under different stress levels. The specimen swelled after unloading to 25 kPa and then wetting (point 5), while the specimens wetted under the stresses of 100 kPa and 200 kPa collapsed (points 6 & 7). The specimen loaded to 300 kPa (compaction stress) also collapsed after wetting (point 8). The maximum collapse was recorded for the specimen wetted under the stress of 300 kPa; beyond this stress level, the collapse value decreased with an increase in stress (point 9).

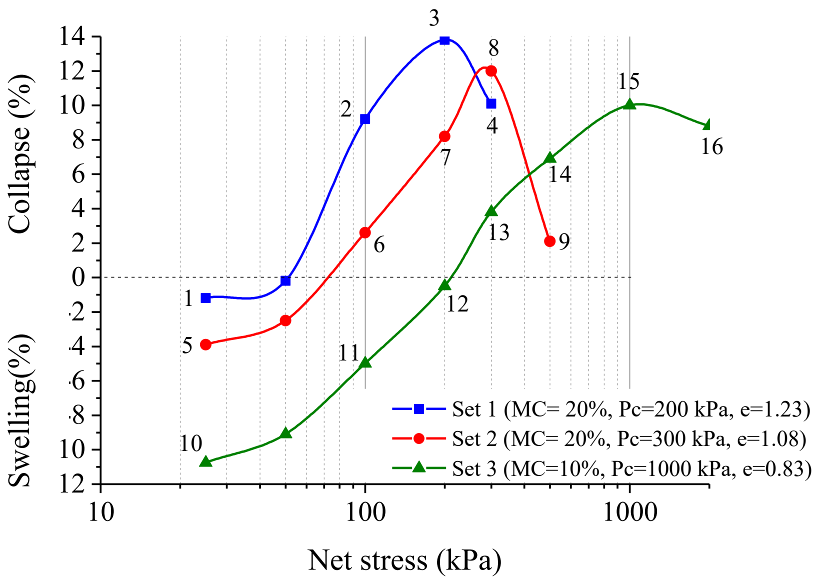

Figure 5.14. Collapse and swelling results for untreated specimens (compressed under different compaction stresses and then wetted under different operational stresses)

Another set of tests was performed on specimens at a moisture content of 10% (e_w = 0.271) and compressed to 1000 kPa. The specimens were subsequently wetted close to saturation under different stress levels (see Figure 5.14). The specimen swelled after unloading to 25 kPa, 100 kPa and 200 kPa and then wetting (points 10, 11 and 12). The specimens unloaded to 300 kPa and 500 kPa collapsed after they experienced wetting (points 13 & 14). The maximum collapse was recorded for the specimen wetted under the stress of 1000 kPa (point 15), and then the collapse value decreased with an increase in stress (point 16).

5.3.2.4 Loading and Wetting (LW) and Loading, Wetting and Loading (LWL) State Paths for Lime-Treated Clay

To carry out the Loading Wetting (LW) tests, the dry soil was mixed thoroughly with hydrated lime for five minutes. Water was added and mixed thoroughly, and then compressed from a nominal stress of 2 kPa to the planned stress. The specimen was then cured for 7 days based on the method outlined in Chapter 4. After curing, the specimens were loaded to the compaction stress and then wetted to reach saturation.

It is important to mention that the effect of curing could be neglected if a specimen was taken from the dry side of the optimum moisture content; however, the effect of curing duration appeared when a specimen moved toward the optimum moisture content, as shown in **Figure 5.15**. This behaviour can be attributed to the mechanism of the reaction between lime and clay. The first reaction begins after adding water to the clay-lime mixture. The hydrated lime dissociates to Ca^{+2} and $2(OH)^{-1}$ ions, and consequently, the cation exchange, flocculation, and agglomeration start. That means that enough water must be provided to start the stabilisation process. As a result, the effect of curing appeared when a specimen moved toward the optimum moisture content. Figure 5.15 presents the effect of moisture ratio and curing duration on swelling and collapse potential. However, for the next stage of research, all specimens in this study were cured for 7 days.

The results of these loading-wetting path tests are shown in **Figure 5.16**. The results highlighted the behaviour of specimen LW10 500 24 at a 10% moisture content (e_w = 0.271), loaded from the nominal stress of 2 kPa to 500 kPa (from point 1 to 2 in Figure 5.16), and then wetted in steps to reach a moisture content close to the LOO (w = 24%, e_w = 0.650) (from point 2 to 3). It is evident that the void ratio decreased during the loading (under a constant moisture ratio of 0.271) and that the path did follow the LWSBS. After wetting, the void ratio continued decreasing, following the 500 kPa contour of the LWSBS until reaching the LOO. Several LW tests were conducted on lime-treated expansive clay and the same behaviour was observed. These tests included a specimen (LW20 200 35.5) with 20% moisture content (e_w = 0.542) loaded (under constant moisture) to 200 kPa and then wetted (under a constant stress) to reach the LOO (w = 35.5%, e_w = 0.962), as shown in Figure 5.16. Results of two other state paths, (LW20 300 34) and (LW10 1000 21.7), are also presented in **Figure 5.17**.

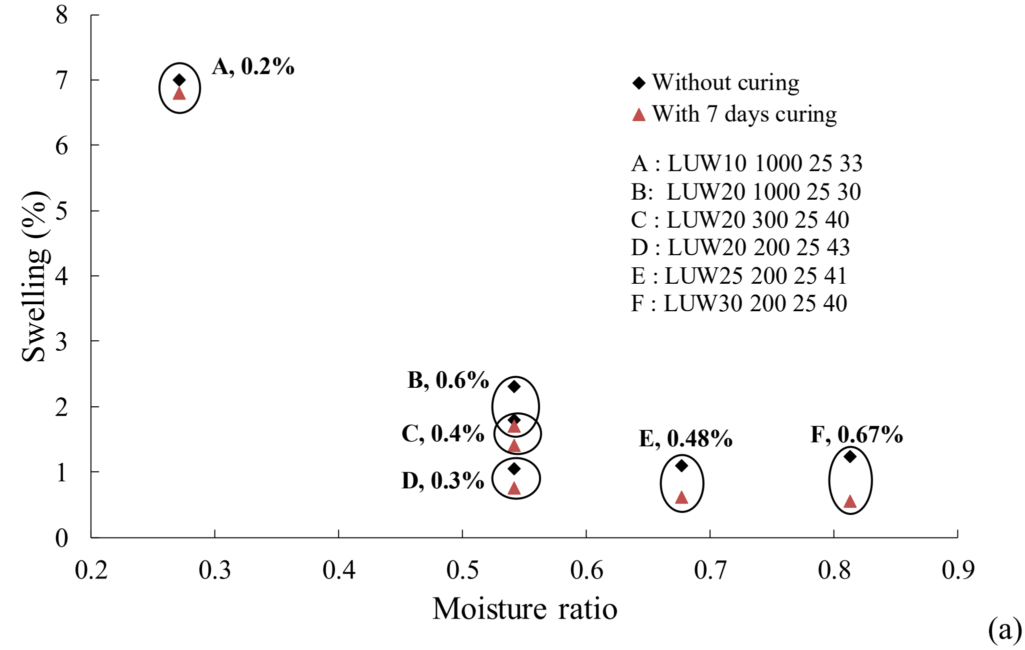

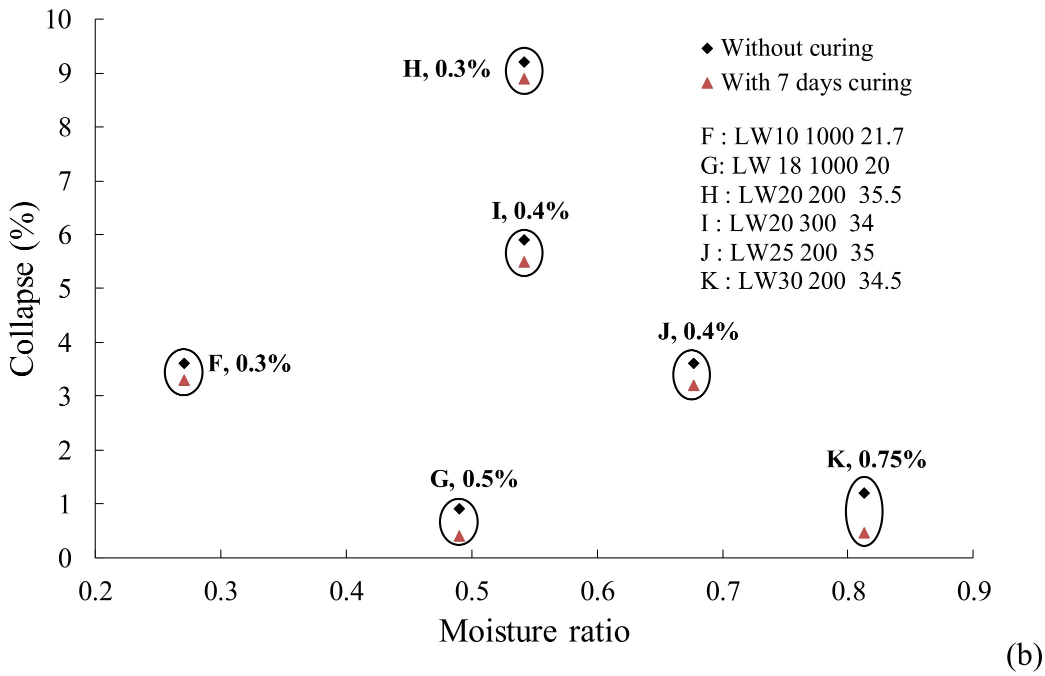

Figure 5.15. Effect of the moisture ratio and curing for 7 days on (a) swelling (b) collapse for lime-treated clay

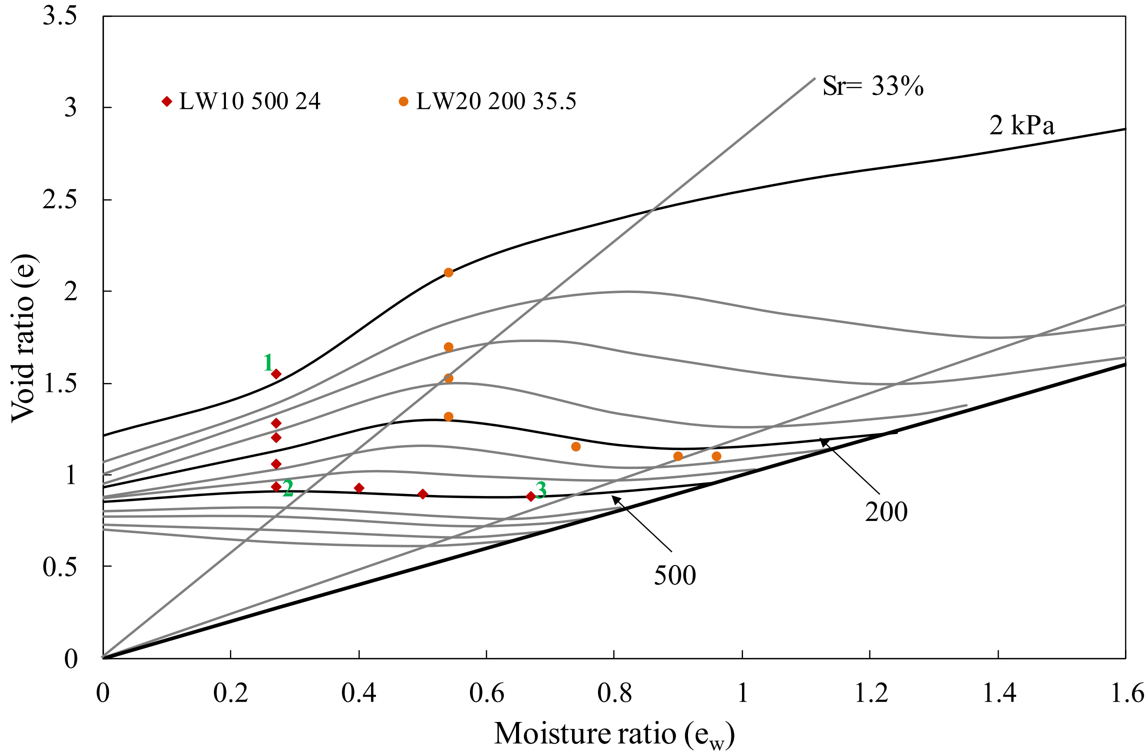
LW10 500 24
LW20 200 35.5
Sr= 33%
2 kPa
200
500
1
2
3
Void ratio (e)
Moisture ratio (e_w)

(a)

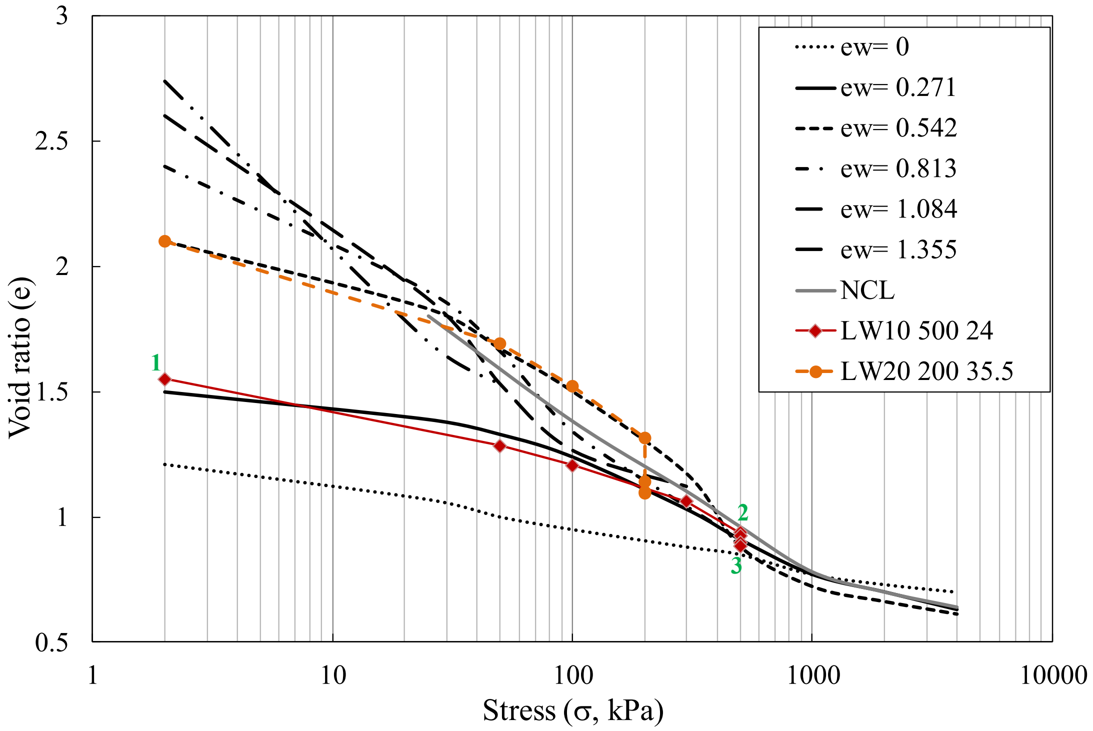
ew= 0
ew= 0.271
ew= 0.542
ew= 0.813
ew= 1.084
ew= 1.355
NCL
LW10 500 24
LW20 200 35.5
1
2
3
Void ratio (e)
Stress (σ, kPa)

(b)

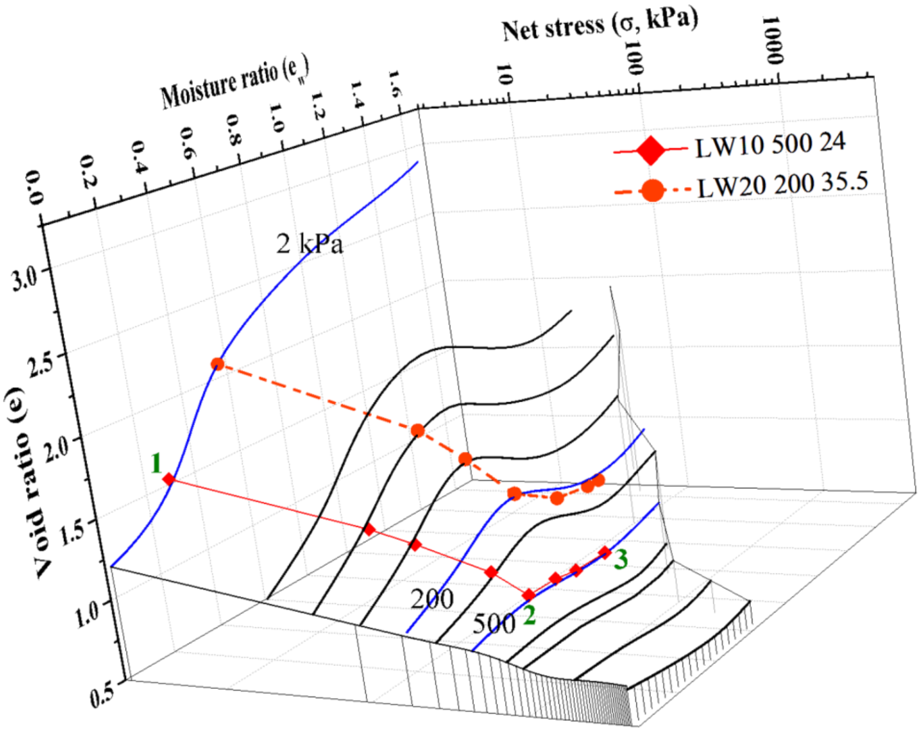

Figure 5.16. State path of loading to 500 and 200 kPa at constant moisture of 10% (e_w=0.271) and 20% (e_w=0.542), respectively, then wetting to the LOO in (a) e-e_w (b) e-log(σ) (c) e-e_w-log(σ) space (lime-treated clay)

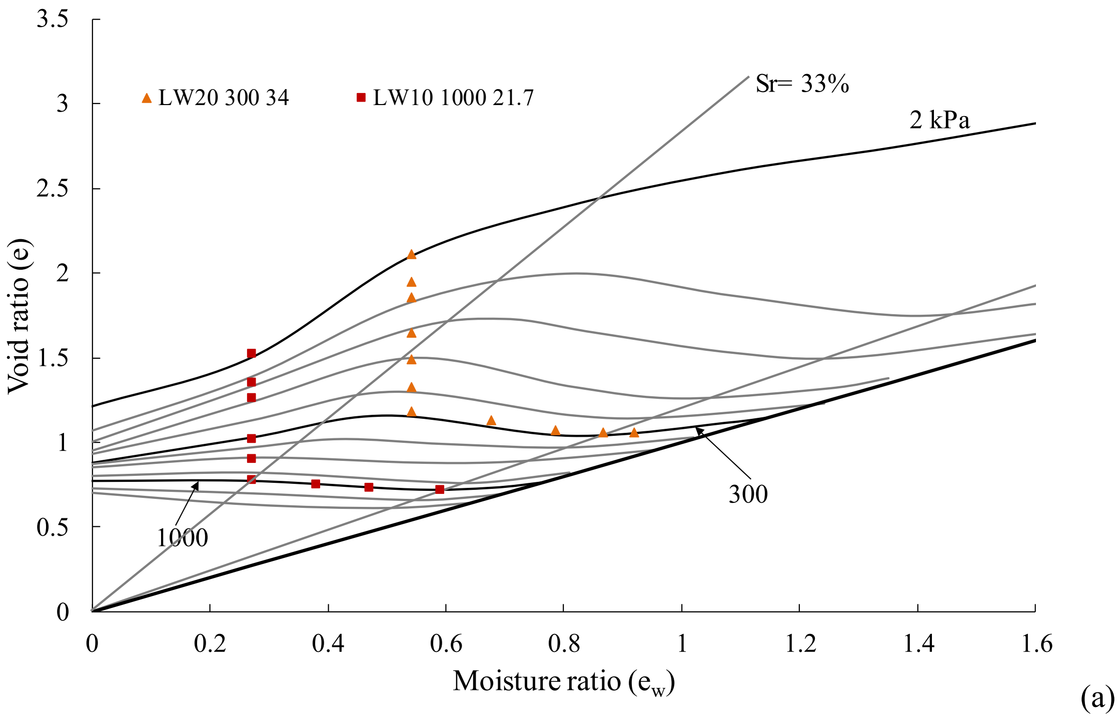

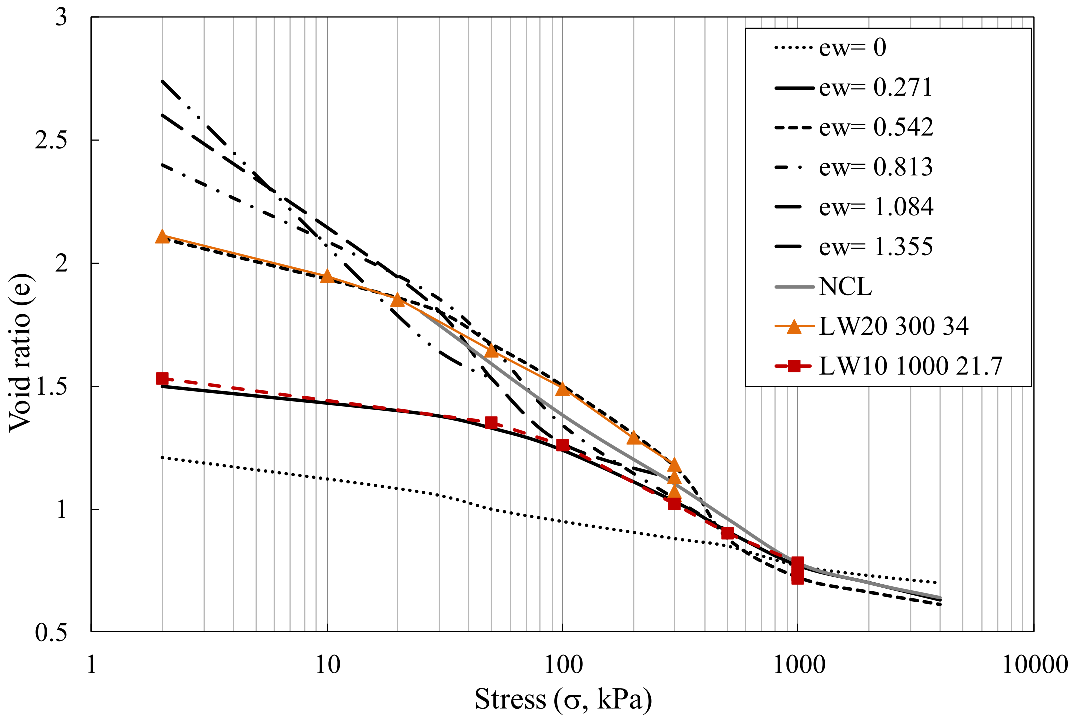

(b)

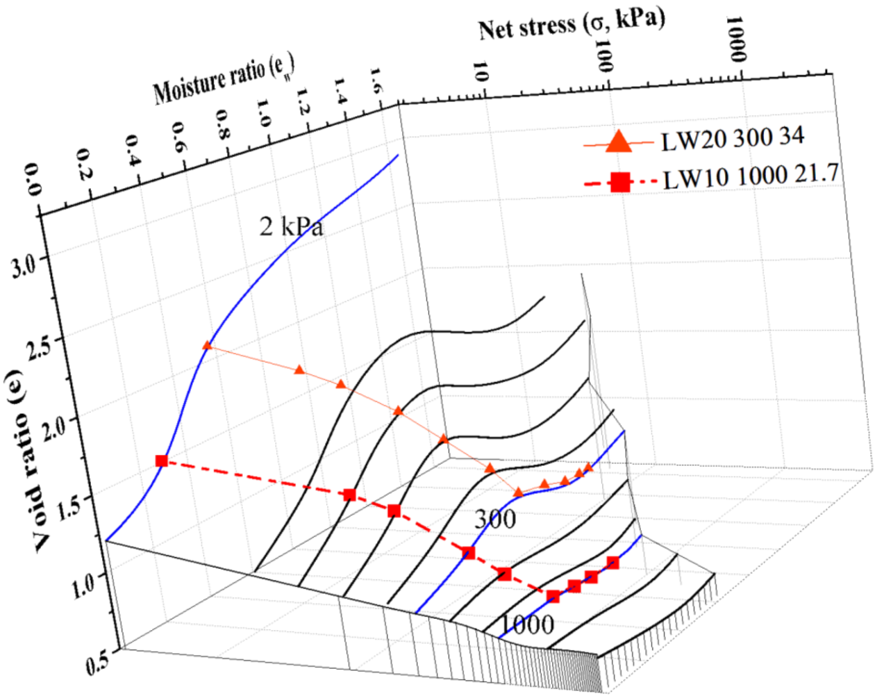

(c)

Figure 5.17. State path of loading to 300 and 1000 kPa at a constant moisture of 20% (e_w=0.542) and 10% (e_w=0.271), respectively, then wetting to the LOO in (a) e-e_w (b) e-log(σ) (c) e-e_w-log(σ) space (lime-treated clay)

The state path shown in **Figure 5.18** suggests that for the lime-treated specimen LW 10 100 36 at 10% moisture contents (e_w = 0.271), loaded to 100 kPa (from point 1 to 2 during loading), and then wetted to reach a moisture content close to the LOO (w = 36%, e_w = 0.976) (from point 2 to 3), the wetting path moved to the inside of the LWSBS, and with continuous wetting, the paths remained below the LWSBS.

The same procedure was followed to examine the behaviour of the LWL state path, except after wetting, the specimen was loaded to check whether the loading path after wetting was still following the LWSBS. **Figure 5.19** presents specimen LWL15 400 21 500, which was prepared at 15% moisture content (e_w = 0.406) and loaded to 400 kPa, then wetted to a moisture content of 21% (e_w = 0.569) and then loaded to 500 kPa, suggesting that all steps followed the LWSBS.

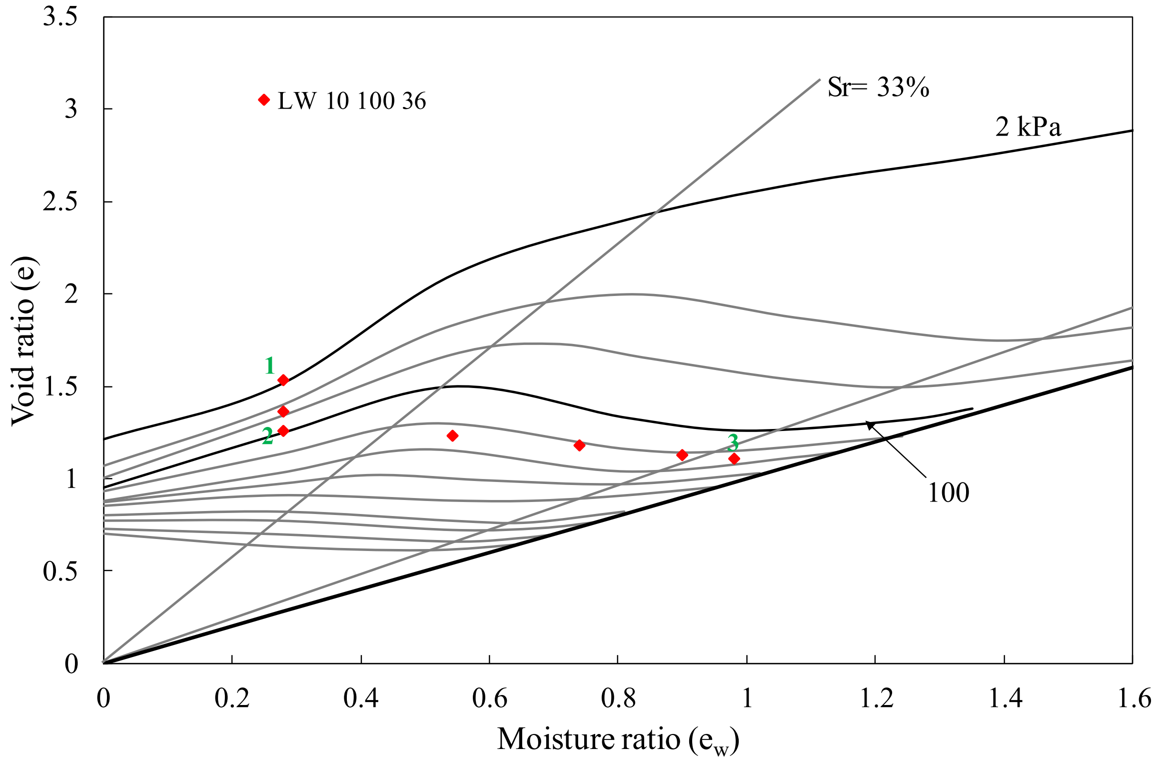

(a)

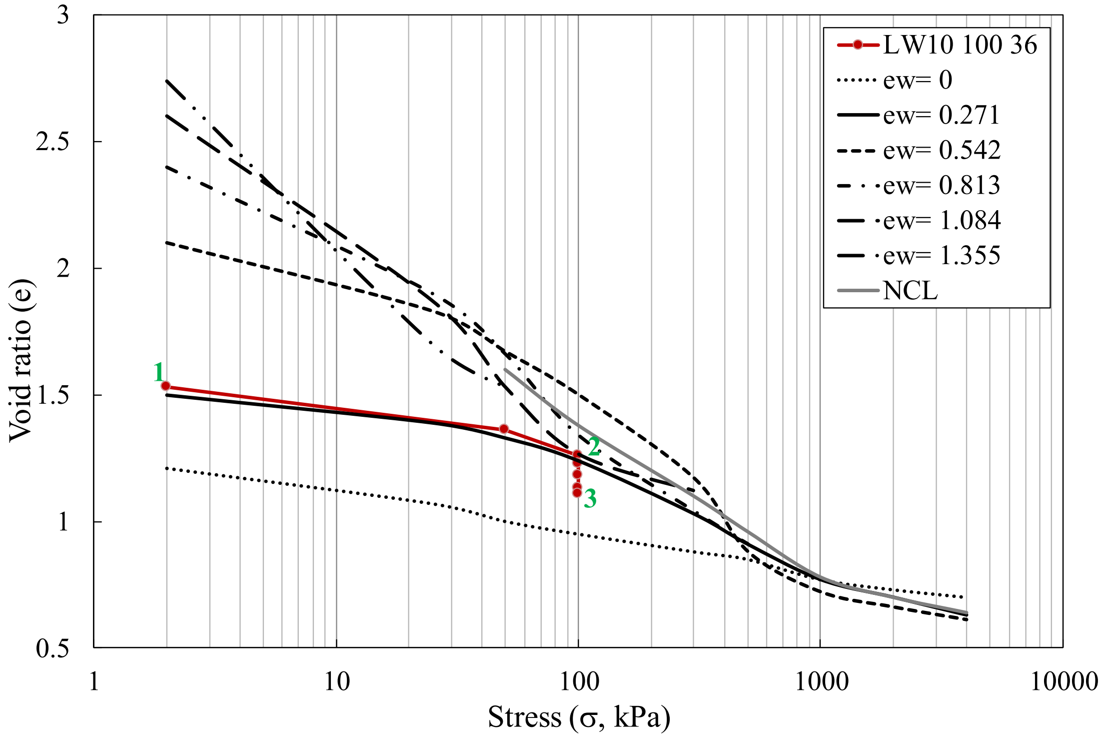

(b)

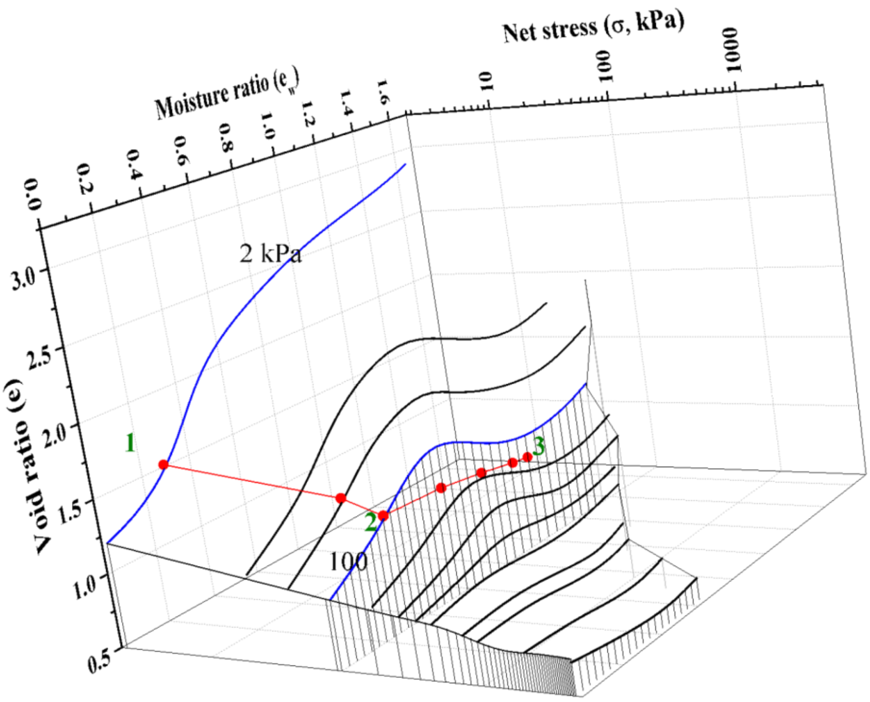

(c)

Figure 5.18. State path of loading to 100 kPa at constant moisture of 10% (e_w=271) then wetting to the LOO in (a) e-e_w (b) e-log(σ) (c) e-e_w-log(σ) space (lime-treated clay)

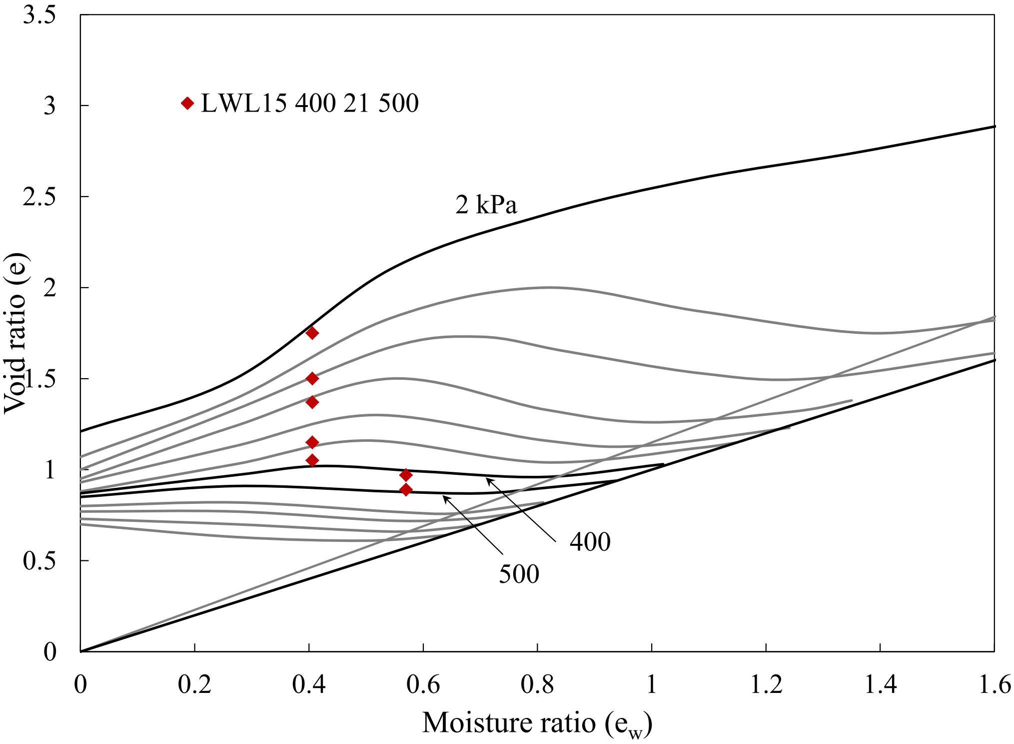
LWL15 400 21 500
2 kPa
400
500
Void ratio (e)
Moisture ratio (e_w)
0
0.5
1
1.5
2
2.5
3
3.5
0.2
0.4
0.6
0.8
1.2
1.4
1.6

(a)

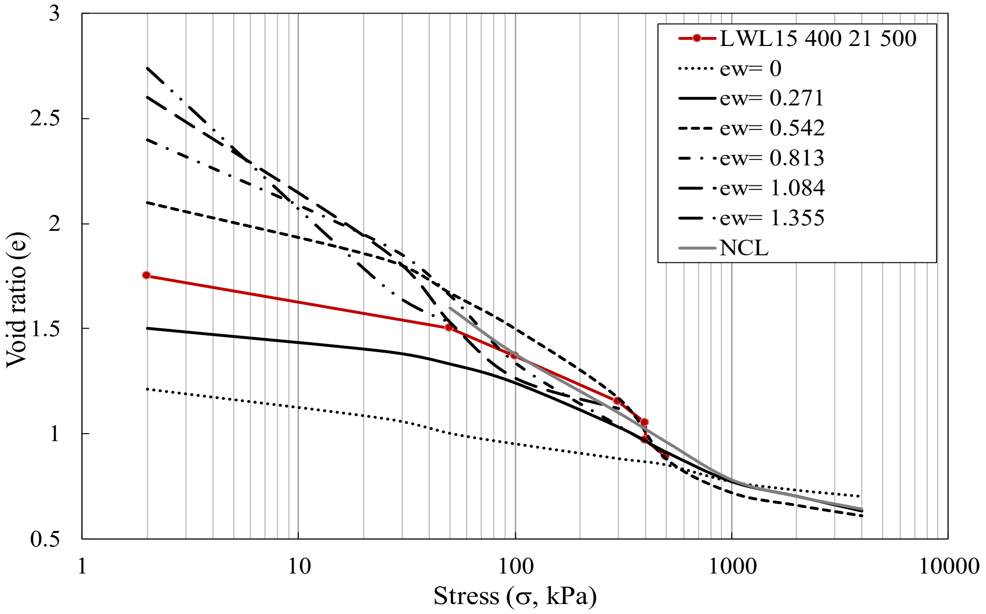
LWL15 400 21 500
ew= 0
ew= 0.271
ew= 0.542
ew= 0.813
ew= 1.084
ew= 1.355
NCL
Void ratio (e)
Stress (σ, kPa)
0.5
1
1.5
2
2.5
3
10
100
1000
10000

(b)

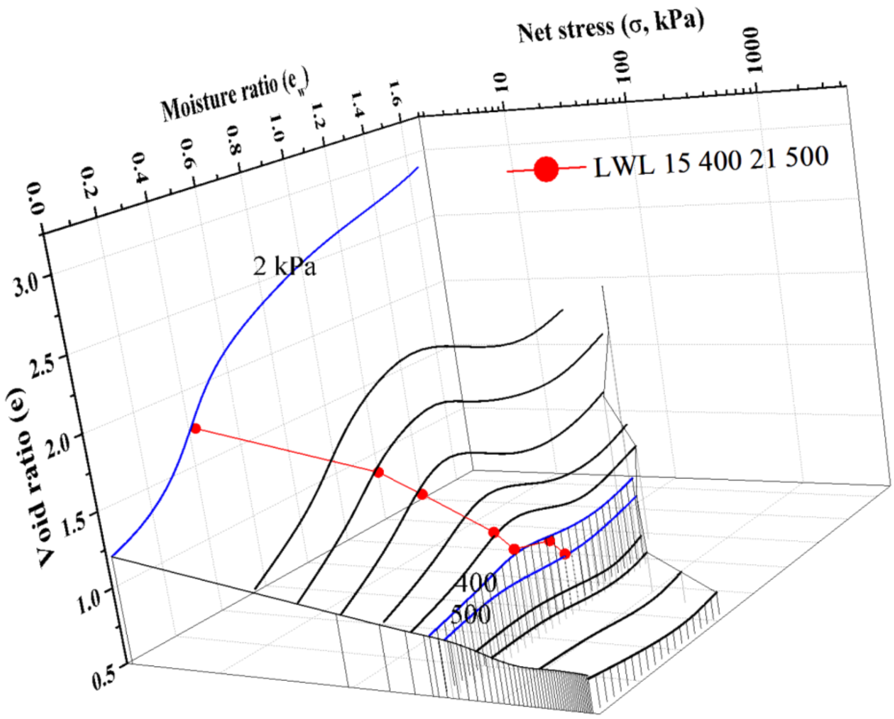

(c)

Figure 5.19. State path of loading to 400 kPa at constant moisture of 15% (e_w=0.406), then wetting to 21% (e_w=0.569), then loading to 500 kPa in (a) e-e_w (b) e-log(σ) (c) e-e_w-log(σ) space (lime-treated clay)

Consequently, it is evident that wetting paths including LW and LWL did follow the MPK framework, but the MPK framework could not be shown to extend to specimens prepared at a degree of saturation (S_r) less than approximately 33% and then wetted under stress levels to less than 500 kPa, as presented in Figure 5.18.

5.3.2.5 Combination of Loading, Unloading and Wetting (LUW) State Paths for Lime-Treated Clay

In order to allow for direct comparison of the impact of lime treatment on the volumetric behaviour of expansive clays, the untreated and lime-treated samples were tested under the same conditions (moisture content and net stress). **Figure 5.20** shows a specimen LUW10 1000 25 33.3 prepared at a moisture content of 10% (e_w = 0.271) and loaded to 1000 kPa (from point 1 to 2 in Figure 5.20), then unloaded to 25 kPa (from point 2 to 3), and then wetted to moisture content close to the NCL (w = 33.3%, e_w = 0.902) (point 3 to 4).

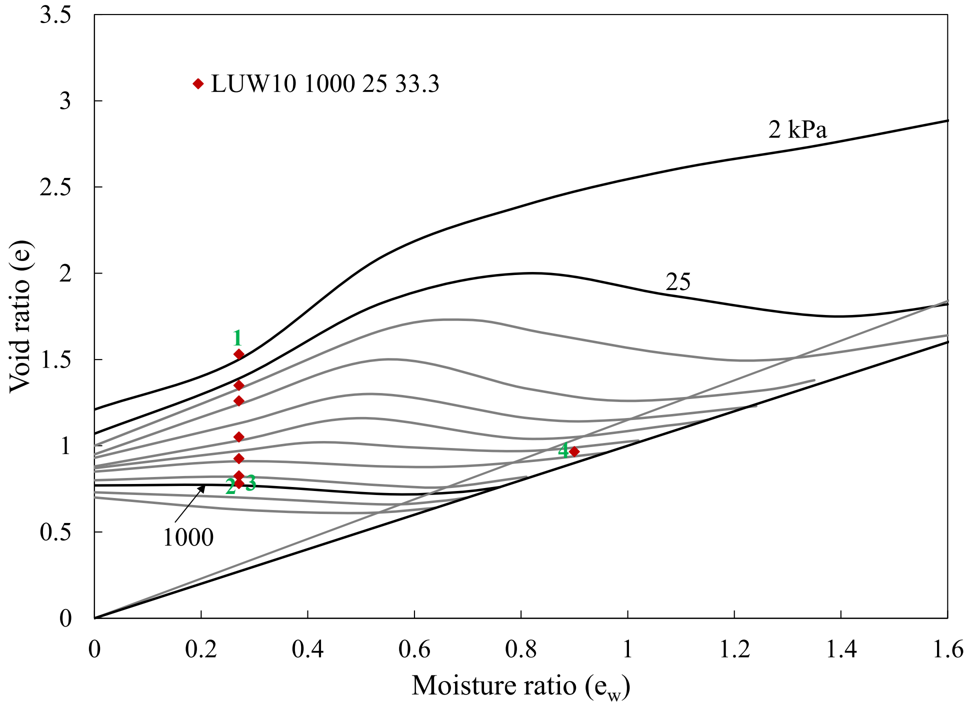
LUW10 1000 25 33.3
2 kPa
25
1000
1
2
3
4
Void ratio (e)
Moisture ratio (e_w)
3.5
3
2.5
2
1.5
1
0.5
0
0
0.2
0.4
0.6
0.8
1
1.2
1.4
1.6

(a)

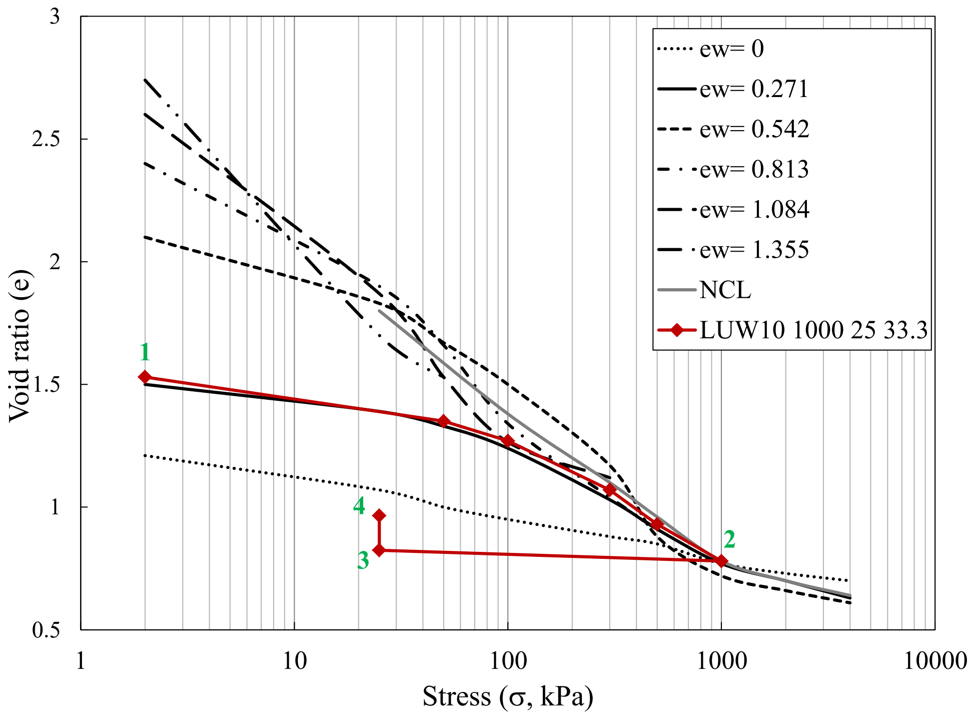
ew= 0
ew= 0.271
ew= 0.542
ew= 0.813
ew= 1.084
ew= 1.355
NCL
LUW10 1000 25 33.3
1
2
3
4
Void ratio (e)
Stress (σ, kPa)
3
2.5
2
1.5
1
0.5
1
10
100
1000
10000

(b)

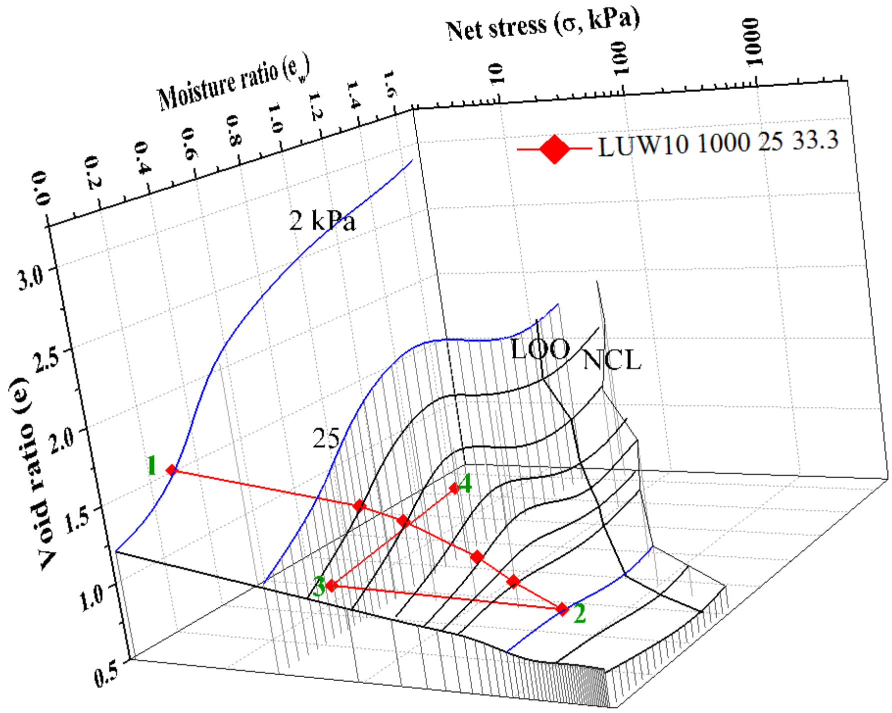

(c)

Figure 5.20. State path of loading to 1000 kPa at constant moisture of 10% (e_w=0.271), then unloading to 25 kPa, and then wetting to the NCL in (a) e-e_w (b) e-log(σ) (c) e-e_w-log(σ) space (lime-treated clay)

From Figure 5.20, it is evident that the loading path did follow the LWSBS, and then moved inside the LWSBS during the unloading. The specimen then swelled toward the stress contour for 25 kPa of the LWSBS. At the end of the swelling, the position of the swelling path remained inside the LWSBS.

This path was observed for two specimens (LUW20 200 25 43 in **Figure 5.21** and LUW20 300 25 39.5 in **Figure 5.22**) with a moisture content of 20% (e_w = 0.542) loaded to different state paths. The first specimen was loaded to 200 kPa (from point 5 to 6 in Figure 5.21), and the other specimen to 300 kPa (from point 9 to 10 in Figure 5.22). They were both then unloaded to 25 kPa (from point 6 to 7 in Figure 5.21 and from point 10 to 11 in Figure 5.22) and consequently wetted to the NCL (w = 43%, e_w = 1.17 & w = 39.5%, e_w = 1.07, respectively) (from point 7 to 8 in Figure 5.21 and from point 11 to 12 in Figure 5.22). The same behaviour was observed for the untreated specimens (LUW10 1000 25 35.5, LUW20 200 25 39.5 & LUW20 300 25 36.5), except that the swelling potential of the lime-treated specimens was less than that of the untreated specimens.

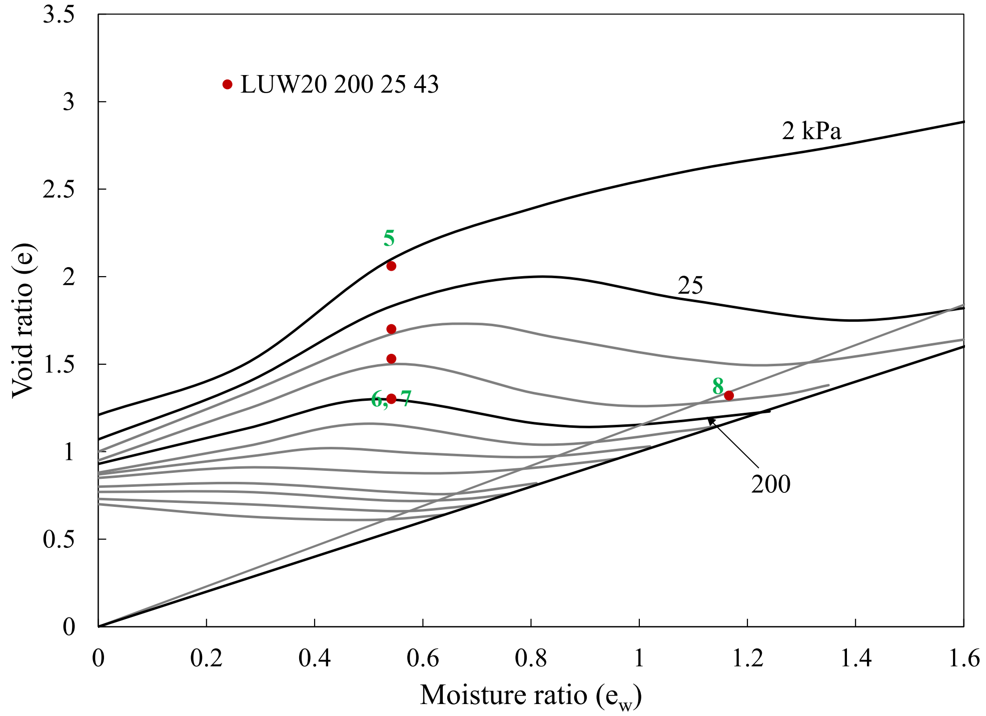

(a)

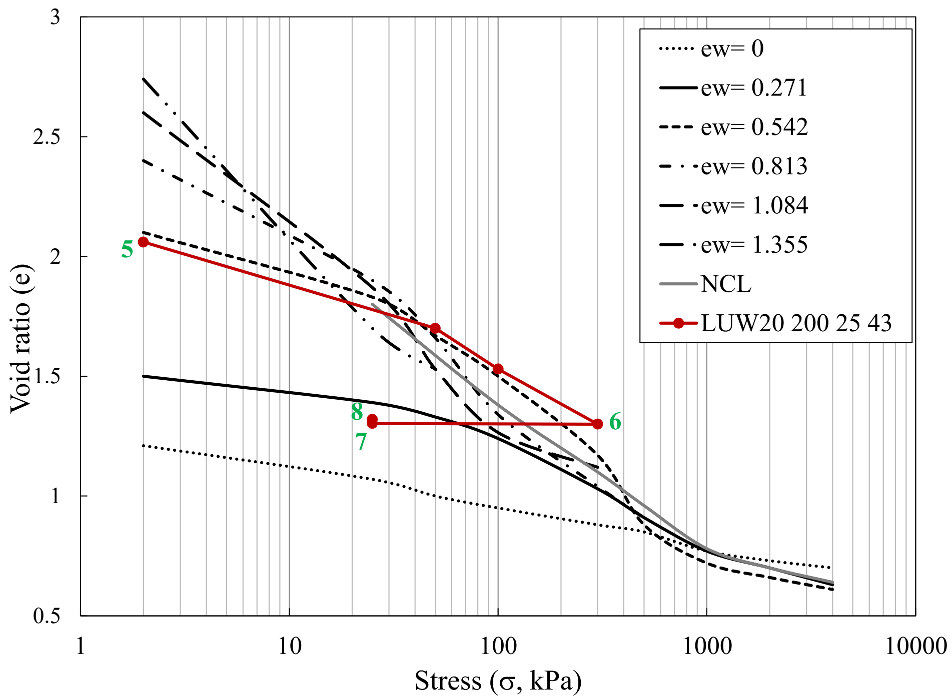

(b)

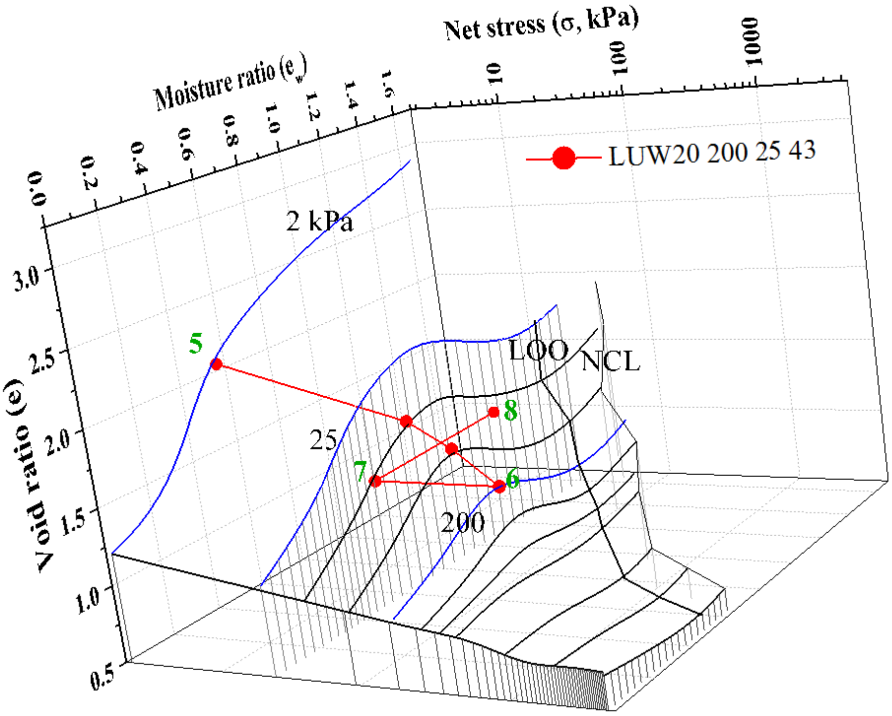

(c)

Figure 5.21. State path of loading to 200 kPa at constant moisture of 20% (e_w=0.542), then unloading to 25 kPa, and then wetting to the NCL in (a) e-e_w (b) e-log(σ) (c) e-e_w-log(σ) space (lime-treated clay)

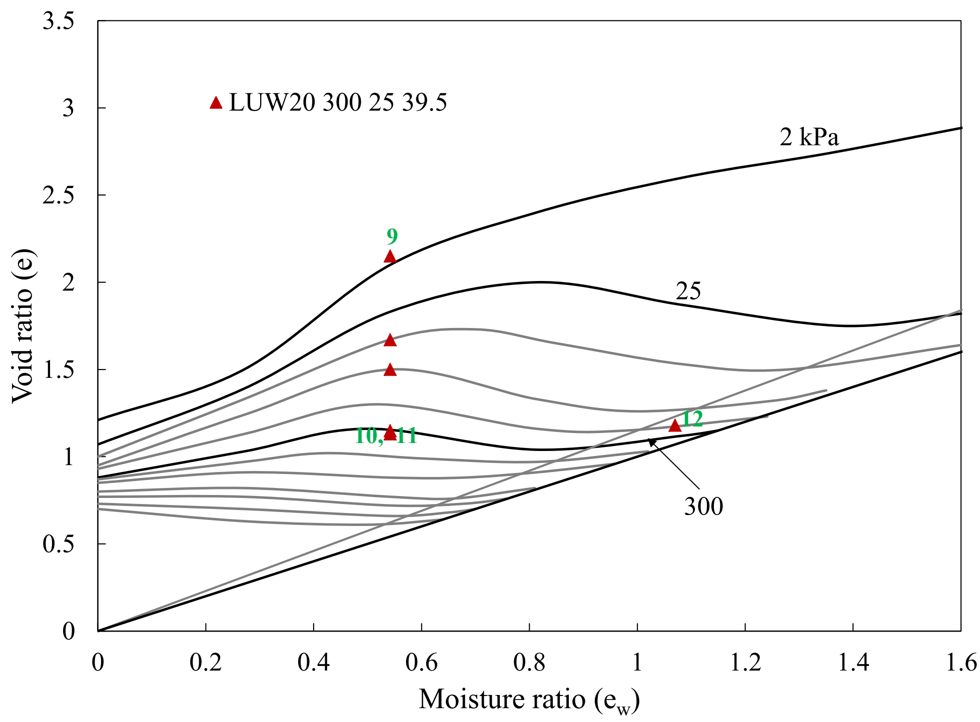

(a)

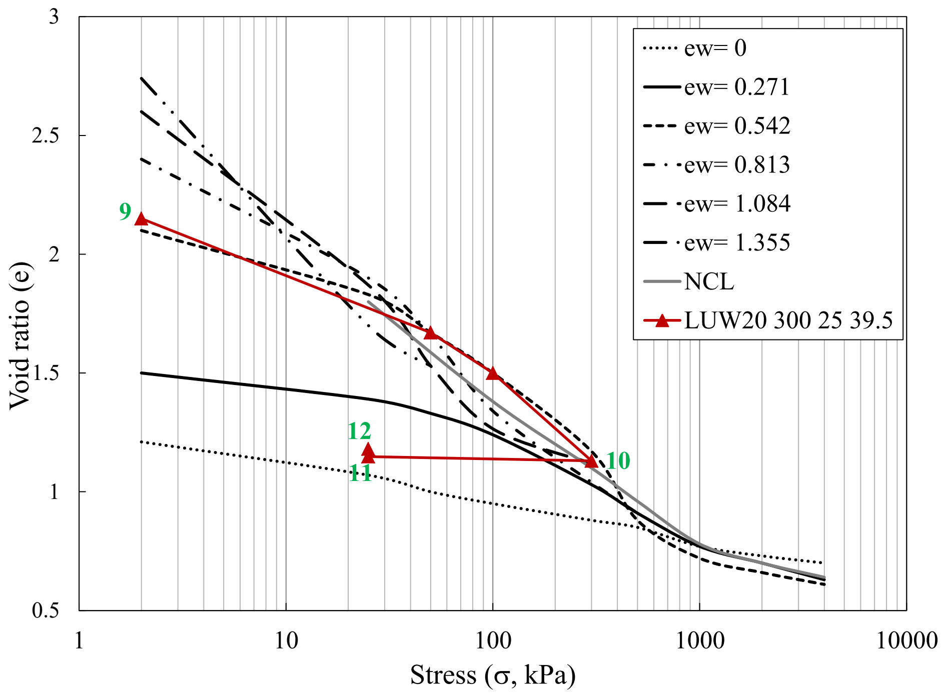

(b)

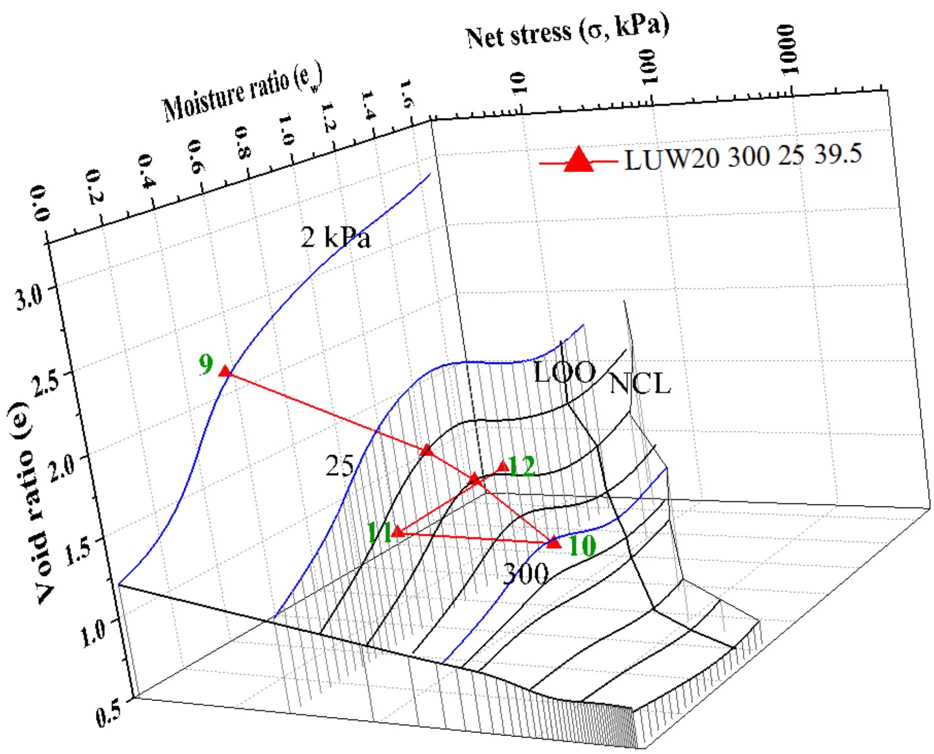

(c)

Figure 5.22. State path of loading to 300 kPa at constant moisture of 20% (e_w=0.542), then unloading to 25 kPa, and then wetting to the NCL in (a) e-e_w (b) e-log(σ) (c) e-e_w-log(σ) space (lime-treated clay)

The same path was applied to specimens prepared at 10% and 20% moisture contents and loaded to 1000 kPa (from point 1 to 2 in **Figure 5.23**) and 300 kPa (from point 5 to 6 in **Figure 5.24**), unloaded to 300 kPa (from point 2 to 3 in Figure 5.23) and 100 kPa (from point 6 to 7 in Figure 5.24), respectively, and subsequently wetted to the moisture contents of 29% (e_w= 0.786) (from point 3 to 4 in Figure 5.23) and 37% (e_w = 1.003) (from point 7 to 8 in Figure 5.24). After wetting, the specimen swelled toward the contours for 300 kPa and 100 kPa of the LWSBS, as shown in Figures 5.23 & 5.24 (LUW10 1000 300 29 & LUW20 300 100 37). The same state path was followed for the untreated specimens (LUW10 1000 300 25.8 & LUW 20 300 100 32.5); however, the specimens collapsed after wetting. The reason for this behaviour will be discussed in Section 5.7.

The specimens LUW20 200 100 41.3 & LUW20 300 200 33.5 at a moisture content of 20% (e_w = 0.542) and loaded to different stresses are presented in **Figures 5.25** & **5.26**. The first specimen was loaded to 200 kPa (from point 1 to 2 in Figure 5.25), and then unloaded to 100 kPa (from point 2 to 3 in Figure 5.25). The other specimen was loaded to 300 kPa (from point 6 to 7 in Figure 5.26), and then unloaded to 200 kPa (from point 7 to 8 in Figure 5.26). Both specimens were then wetted to the moisture content of 41.3% (e_w = 1.119) (from point 3 to 5 in Figure 5.25) and 33.5% (e_w = 0.908) (from point 8 to 10 in Figure 5.26), respectively, and experienced swelling as a result. The amount of swelling was very small and can be neglected, and the path of swelling hit the LWSBS at a position before the LOO (at point 4 in Figure 5.25 for the first specimen and at point 9 in Figure 5.26 for the second specimen). Therefore, by adding water beyond this point, the specimen collapsed and followed the LWSBS. This collapse continued up to the LOO. These results collectively suggest that the MPK framework was valid for the LUW paths of lime-treated expansive clay. The same behaviour was observed for the untreated specimens (LUW20 200 100 31.7 & LUW20 300 200 30.3), except that the collapse potential of the lime-treated specimens was less than that of the untreated specimens.

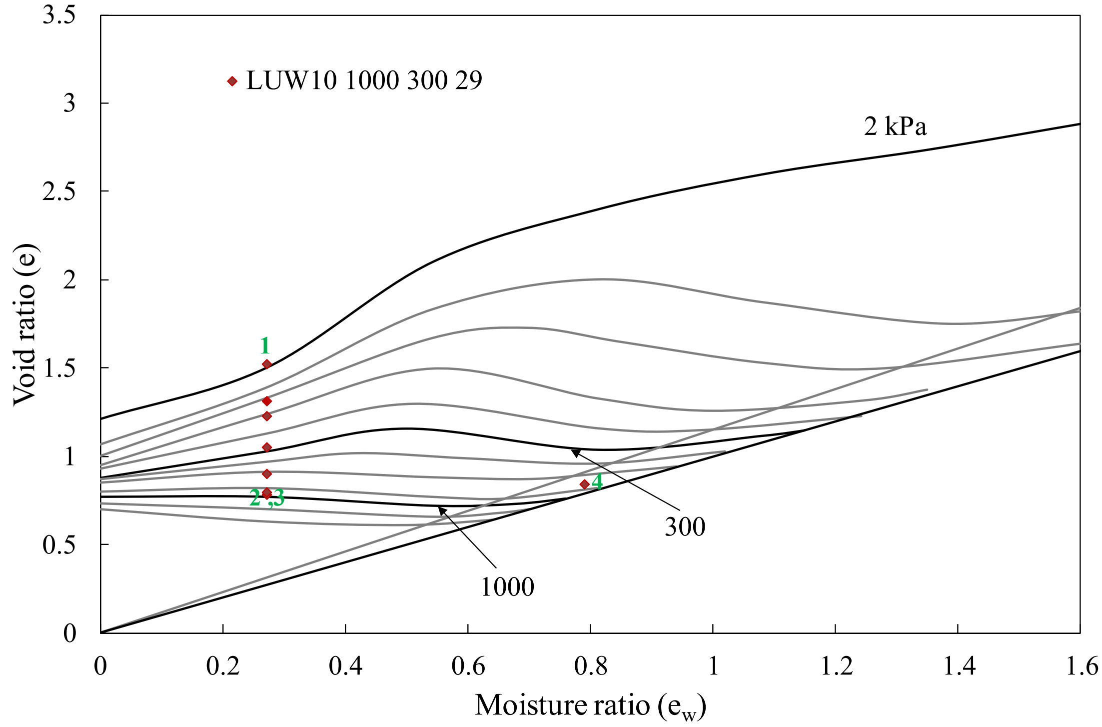
LUW10 1000 300 29
2 kPa
300
1000
1
2,3
4
Void ratio (e)
Moisture ratio (e_w)
0
0.5
1
1.5
2
2.5
3
3.5
0
0.2
0.4
0.6
0.8
1
1.2
1.4
1.6

(a)

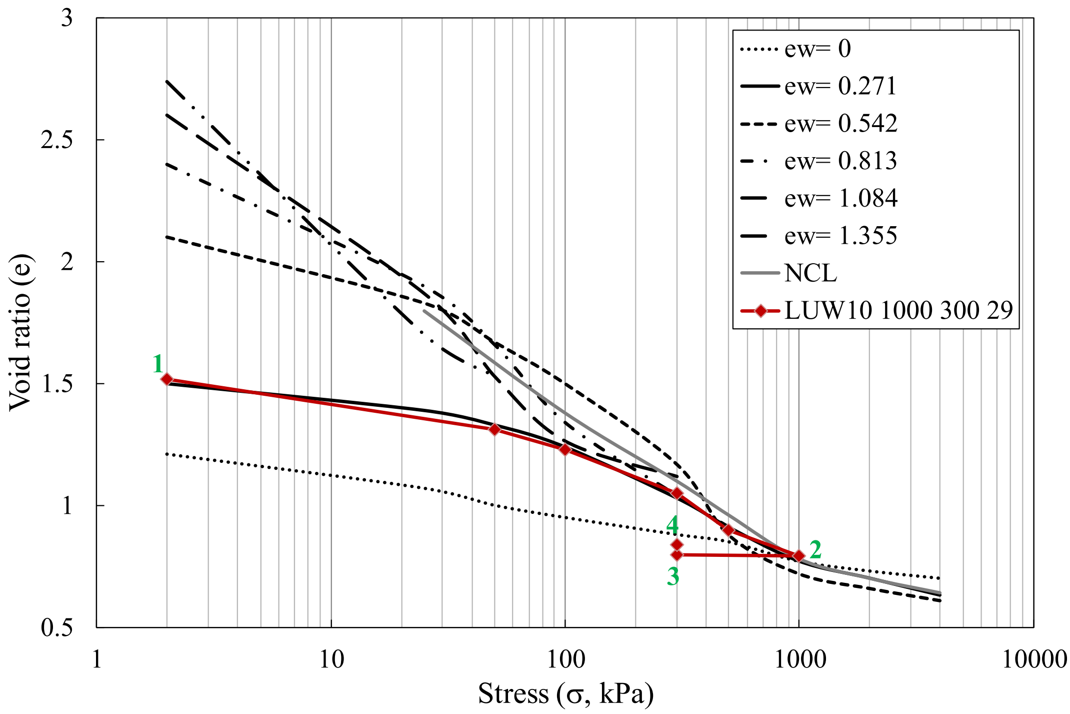
ew= 0
ew= 0.271
ew= 0.542
ew= 0.813
ew= 1.084
ew= 1.355
NCL
LUW10 1000 300 29
1
2
3
4
Void ratio (e)
Stress (σ, kPa)
0.5
1
1.5
2
2.5
3
1
10
100
1000
10000

(b)

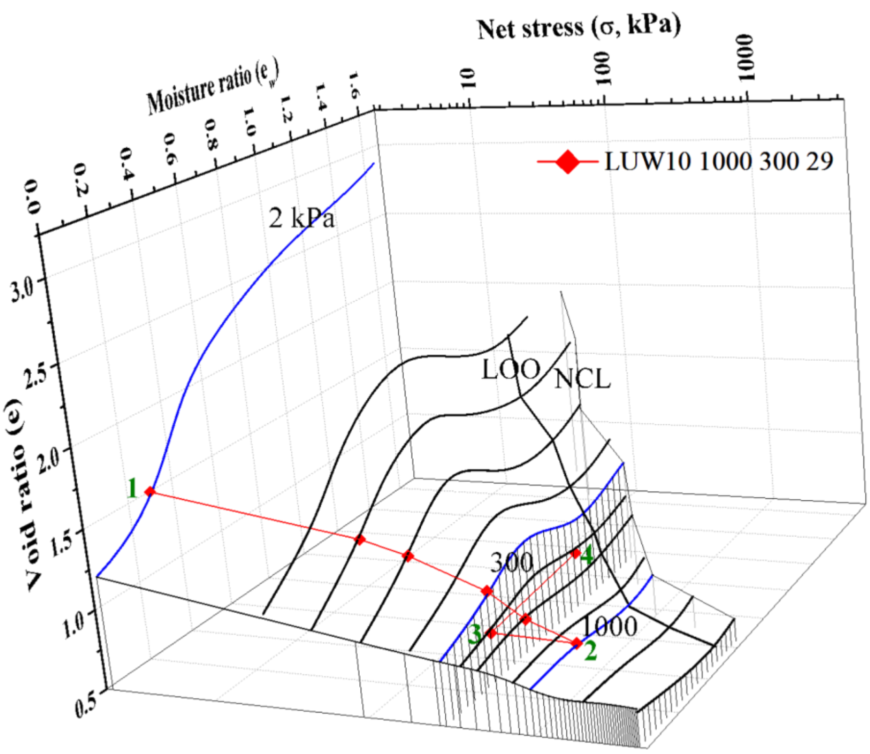

(c)

Figure 5.23. State paths of loading to 1000 kPa at constant moisture of 10% (e_w=0.271), then unloading to 300 kPa, and then wetting to the NCL in (a) e-e_w (b) e-log(σ) (c) e-e_w-log(σ) space (lime-treated clay)

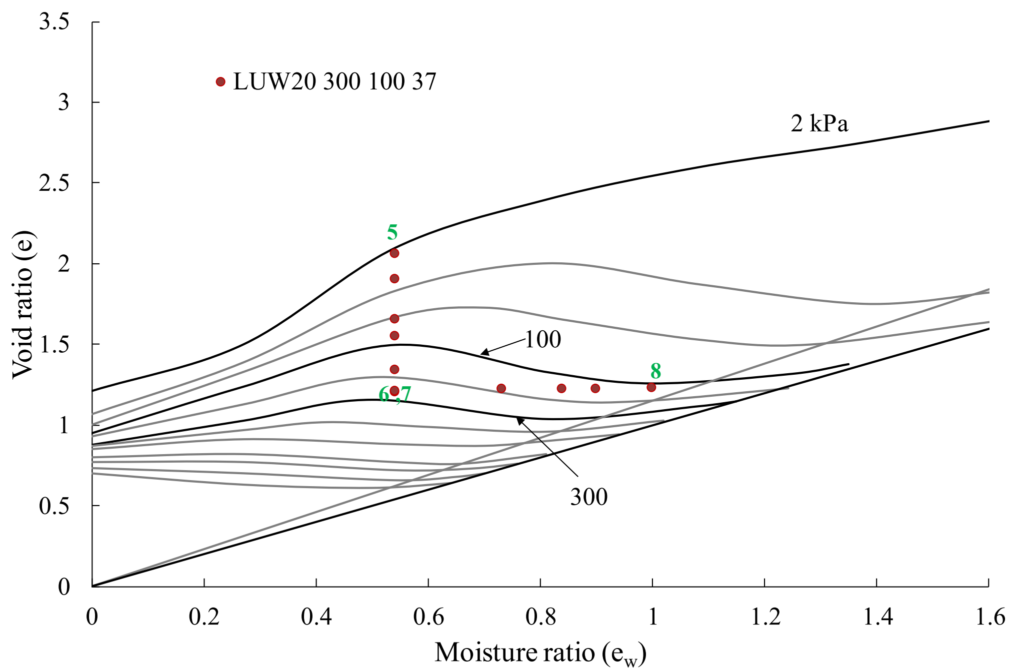

(a)

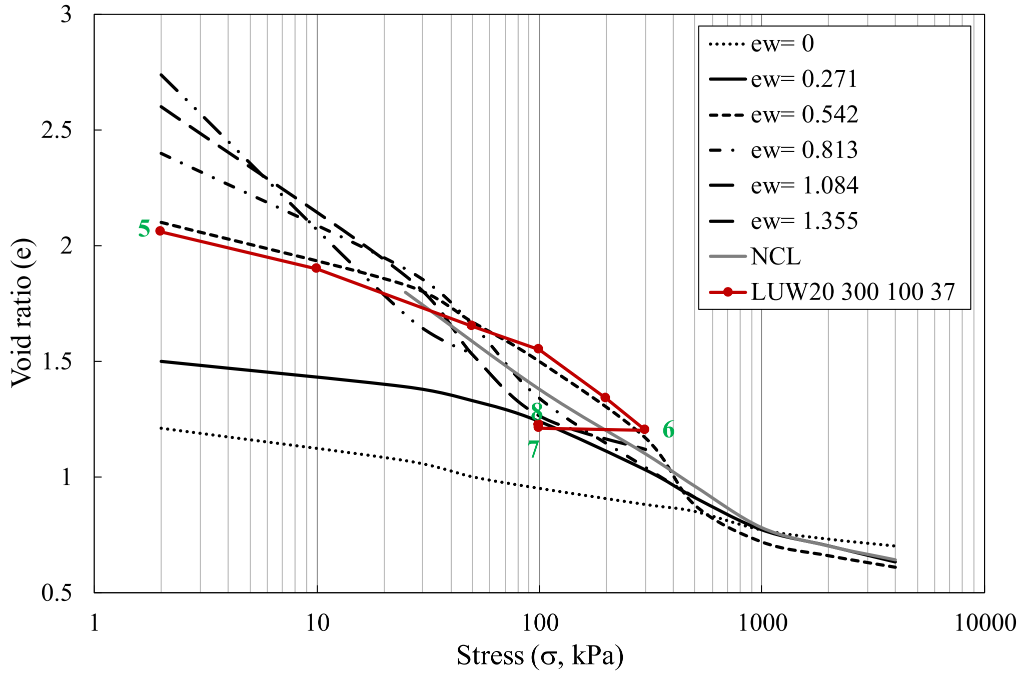

(b)

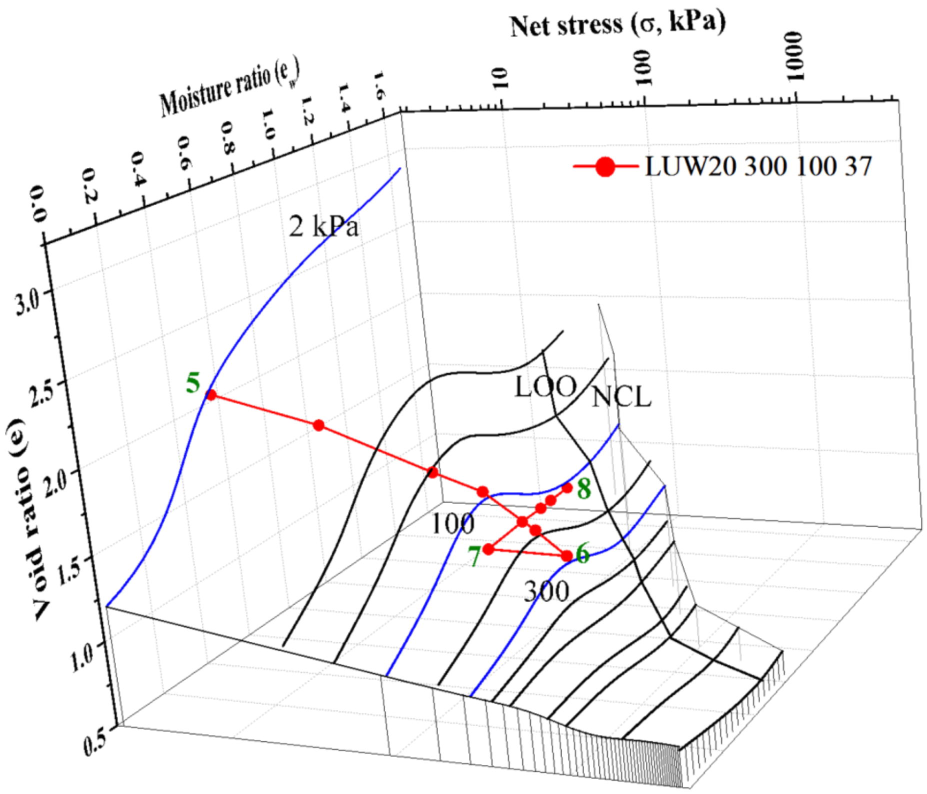

(c)

Figure 5.24. State paths of loading to 300 kPa at constant moisture of 20% (e_w=0.542), then unloading to100 kPa, and then wetting to the NCL in (a) e-e_w (b) e-log(σ) (c) e-e_w-log(σ) space (lime-treated clay)

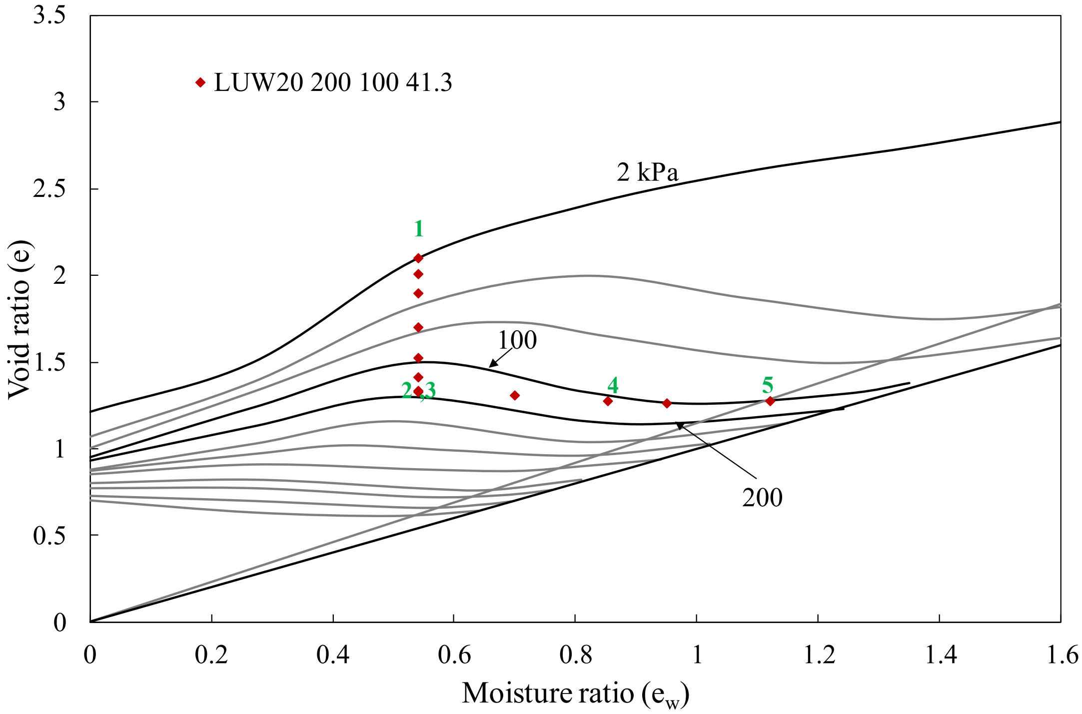
LUW20 200 100 41.3
2 kPa
100
200
1
2, 3
4
5
Void ratio (e)
Moisture ratio (e_w)
0
0.5
1
1.5
2
2.5
3
3.5
0.2
0.4
0.6
0.8
1.2
1.4
1.6

(a)

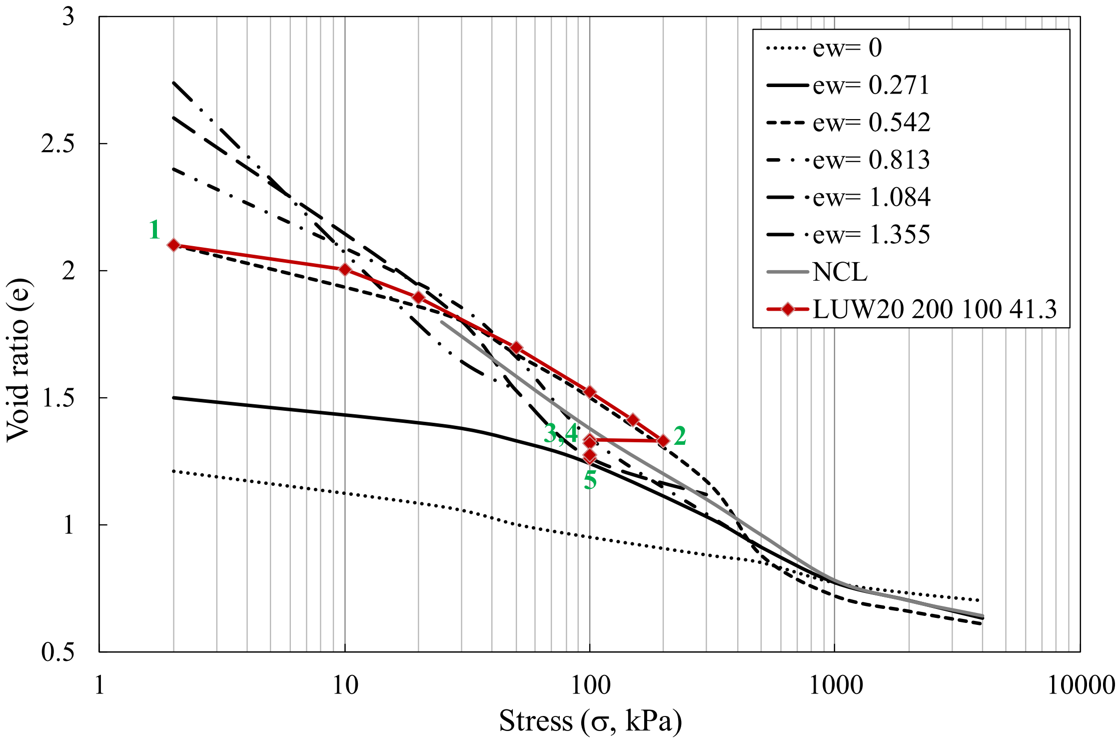
ew= 0
ew= 0.271
ew= 0.542
ew= 0.813
ew= 1.084
ew= 1.355
NCL
LUW20 200 100 41.3
1
2
3, 4
5
Void ratio (e)
Stress (σ, kPa)
0.5
1
1.5
2
2.5
3
10
100
1000
10000

(b)

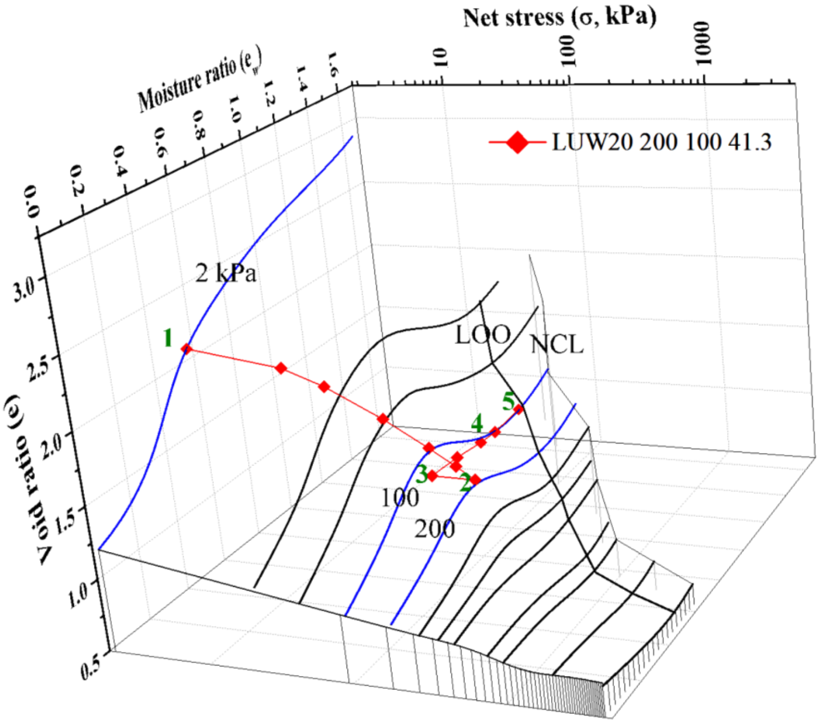

(c)

Figure 5.25. State paths of loading to 200 kPa at constant moisture of 20% (e_w=0.542), then unloading to 100 kPa, and then wetting to the NCL in (a) e-e_w (b) e-log(σ) (c) e-e_w-log(σ) space (lime-treated clay)

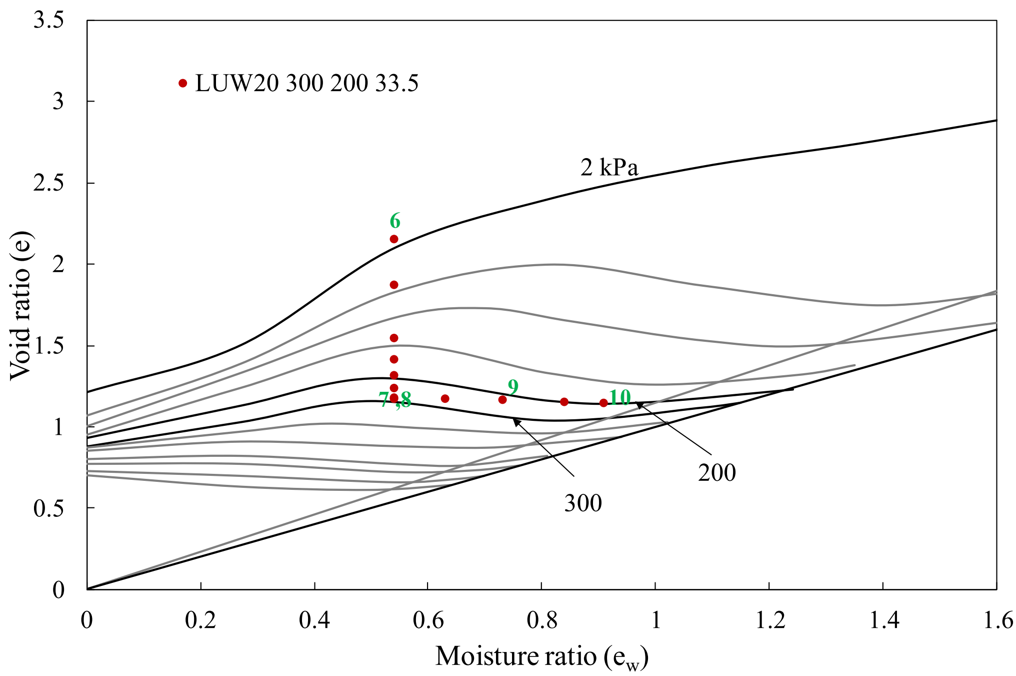

(a)

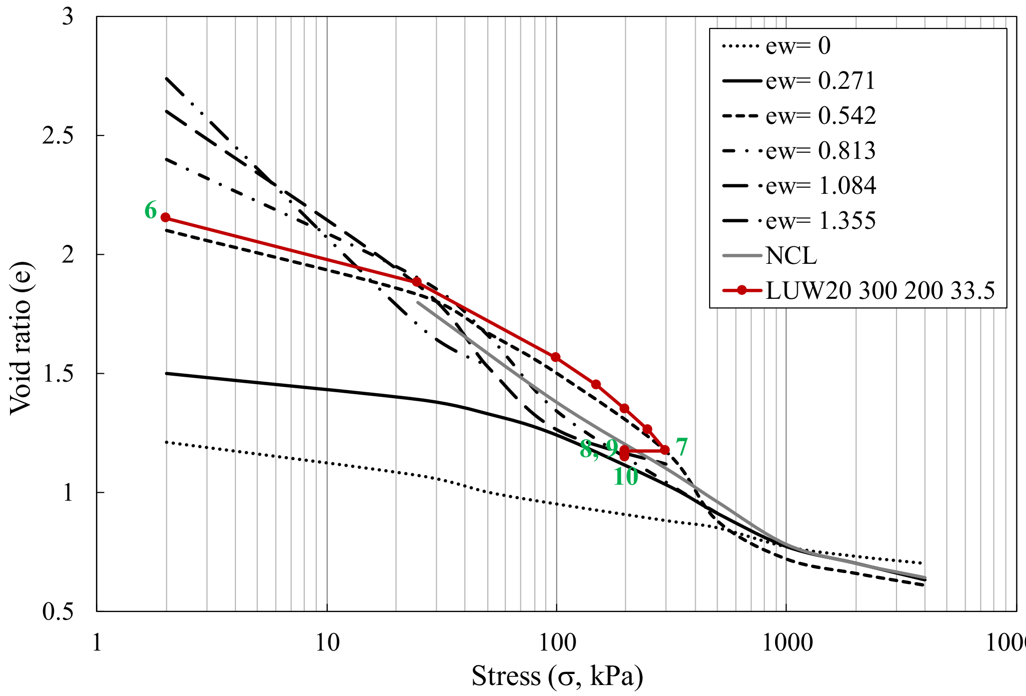

(b)

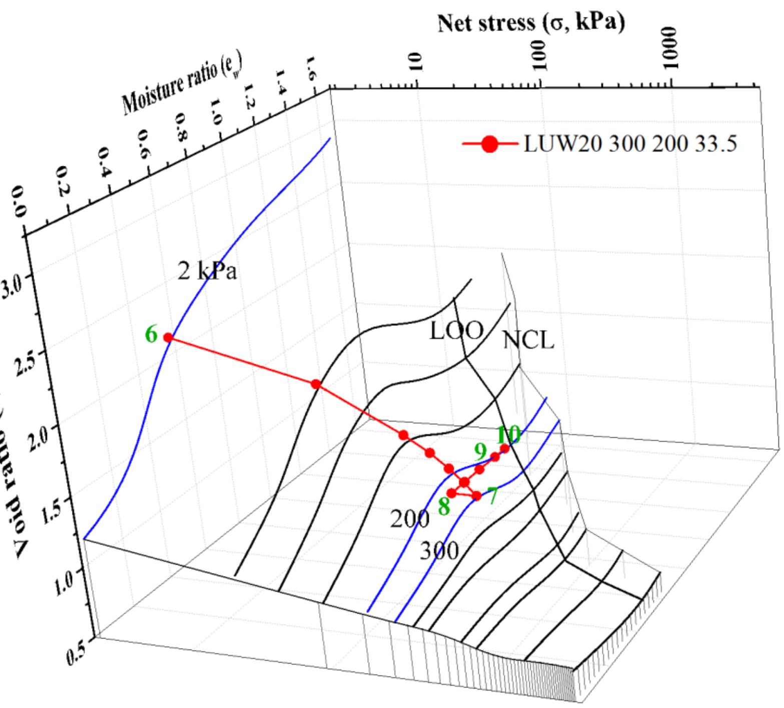

(c)

Figure 5.26. State paths of loading to 300 kPa at constant moisture of 20% (e_w=0.542), then unloading to 200 kPa, and then wetting to the NCL in (a) e-e_w (b) e-log(σ) (c) e-e_w-log(σ) space (lime-treated)

5.3.2.6 Collapse and Swelling Tests for Lime-Treated Clay

Three sets of tests were performed on lime-treated expansive clays to investigate the variation of collapse and swelling potential at various stress levels. The first set included specimens with a moisture content of 20% (e_w =0.542) that were prepared and then compressed to 200 kPa. The specimens were then wetted to reach saturation state under stress levels of 25, 50, 100, 200 and 300 kPa.

The collapse and swelling behaviours for these specimens are plotted in **Figure 5.27** as points 1 to 5. As shown in the figure, the specimens were swelled when wetted under a stress of 25 kPa and 50 kPa (points 1 & 2). The specimens moved inside the LWSBS after unloading to 25 kPa and 50 kPa, and their locations were far under the LWSBS. Therefore, after wetting, the swelling amount was not enough to get the swelling path to reach the LWSBS. However, at 100 kPa, the specimen did swell after adding a small amount of water. This amount of swelling was very small and sufficient to reach the LWSBS. With continued wetting, the specimen collapsed and followed the contour for 100 kPa of the LWSBS (point 3). The specimen wetted under a stress of 200 kPa collapsed after wetting, and followed the contour of 200 kPa of the LWSBS (point 4). The collapse potential, which was recorded due to loading to 200 kPa, unloading to 100 kPa and then wetting was less than that of specimen loaded to 200 kPa then wetted. This may indicate that the collapse potential increased as the stress increased, while, when the specimen was wetted under 300, the collapse potential decreased (point 5). This suggests that the collapse potential increased as the stress increased up to the compaction stress, and that after reaching this stress threshold, the collapse potential decreased with an increase in stress.

The same behaviour was observed when specimens at a moisture content of 20% (e_w =0.542) were prepared and then compressed to 300 kPa (Figure 5.27). The specimens were then wetted to reach saturation state under different stress levels of 25, 50, 100, 200, 300 and 500 kPa. The specimens swelled after wetting under stress levels of 25, 50, 100 kPa (points 6, 7 and 8), while the specimens wetted under 200 and 300 kPa stress levels collapsed (points 9 & 10). The maximum collapse was recorded for the specimen wetted under the stress of 300 kPa (compaction stress); beyond this stress level, the collapse value decreased as the stress increased (point 11).

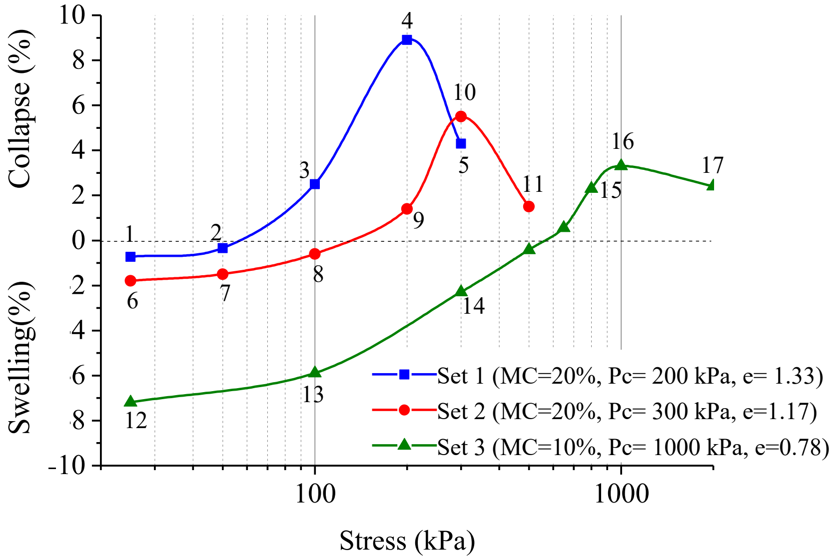

Figure 5.27. Collapse and swelling results for lime-treated specimens (compressed under different compaction stresses and then wetted under different operational stresses)

Another set of tests was performed in which specimens at a moisture content of 10% (e_w =0.271) were prepared and then compacted under a stress level of 1000 kPa. The specimens were wetted to reach saturation state under stress levels of 25, 100, 300, 800, 1000 and 2000 kPa (Figure 5.27). The specimens did swell after unloading to 25, 100 and 300 kPa and then wetting (points 12, 13, and 14). The specimens wetted under stresses of 800 and 1000 kPa collapsed (points 15 & 16). The maximum collapse was recorded for the specimen wetted under the stress of 1000 kPa (compaction stress); then, the collapse value decreased as the stress decreased (point 17). However, when the specimen was wetted under 2000 kPa, the collapse potential decreased.

5.3.3 Slope of the unloading-reloading curve (κ) and compression line (λ) for untreated and lime-treated clay

As mentioned in Chapter 3, a series of tests were performed to investigate the behaviour of unloading-reloading of an unsaturated expansive clay soil (untreated and treated with lime) at various moisture contents (0-20%) (e_w = 0-0.542). The specimens were unloaded to 25, 100, 300, 500, 1000, 2000 and 4000 kPa. For the untreated clay specimens, the average value of the unloading-reloading slope (κ) for a range of moisture ratios indicated that the values of κ were very small and ranged between 0.006 and 0.045, as shown in **Figure 5.28**. Therefore, κ can be considered to be constant over this range of moisture content and stress levels. For the lime-treated clay specimens, the values of κ were also found to be consistent and ranged between 0.016 to 0.028, as shown in Figure 5.28.

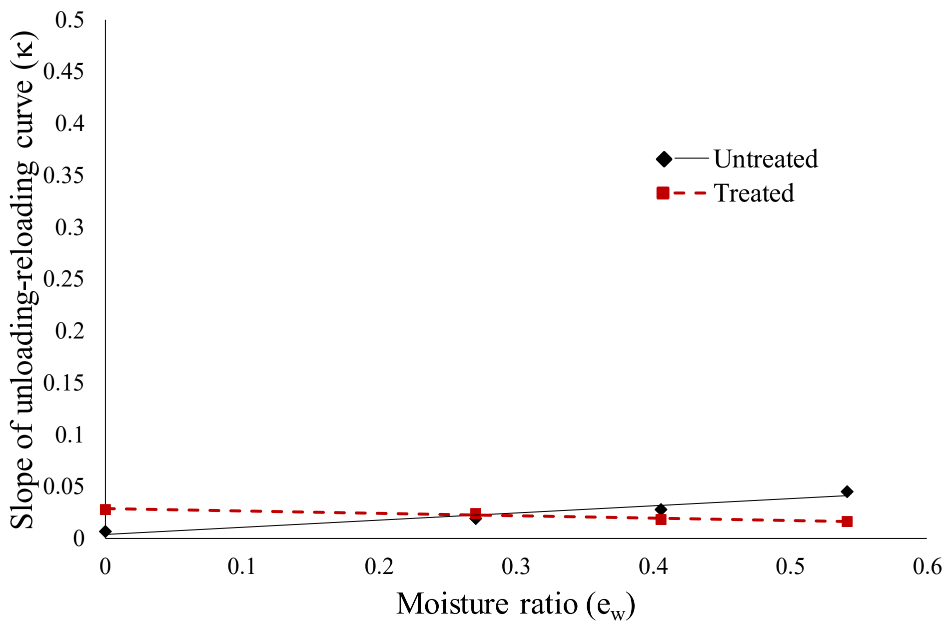

Figure 5.28. Average value of the unloading-reloading slope at different moisture ratios (0-0.542) (untreated and lime-treated soils)

Using the data in Figures 5.1 & 5.2, for untreated and lime-treated clay, the gradients of the compression lines (λ) at various moisture ratios were measured, and are shown in **Figure 5.29**. Figure 5.29 shows the value of λ increased as moisture ratio increased.

This behaviour indicated that the compressibility of dry expansive and lime-treated clay was less than that of wet clay. Figure 5.29 also shows that the variation of λ for the treated clay was less than that for the untreated clay, and the evidence of improvement. The relationship between the gradient of the compression line (λ) (for untreated and lime-treated clay) and moisture ratio (e_w) can be represented in a linear format (Equation 5-1).

$$\lambda = ae_w + b \qquad 5\text{-}1$$

where *a* and *b* are fitting parameters. For the untreated clay specimens, the values for *a* and *b* were shown to be 0.4494 and 0.0609, respectively. For the lime-treated clay specimens, the values for *a* and *b* were shown to be 0.174 and 0.1027, respectively.

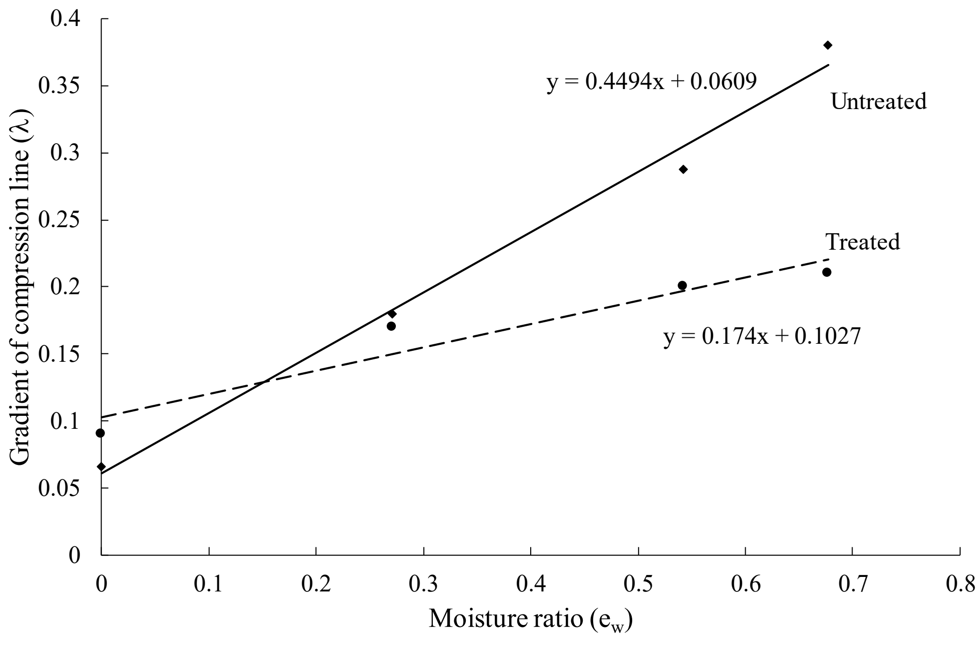

Figure 5.29. Variation of the gradient of compression line with moisture ratio

5.4 Loading-Collapse Curve in terms of Moisture Ratio and Net Stress

Establishing the LWSBS means establishing the yield positions at which plastic collapse occurs during loading and wetting or reloading and wetting. Loading-Collapse (LC) is one of these yield loci. The LC can be defined as the relationship between suction (s) and net stress (σ) at the constant void ratio. This relationship describes the hardening, yielding and collapse of compacted soil (Alonso et al. 1990). As the MPK framework considers moisture ratio as the main parameter and suction as the secondary parameter, it is important to establish a relationship between e_w and σ at the constant void ratio.

To achieve this relationship using the LWSBS for the untreated clay, the LWSBS in the e-e_w space was divided into many horizontal lines (constant void ratio lines, LV), as shown in **Figure 5.30**. The results presented in this research clearly suggest that the wetting paths follow the MPK framework. However, the MPK framework does not extend to specimens prepared at a degree of saturation less than 37% and then compressed under stress levels less than 1000 kPa. Figure 5.30 shows that the maximum decrease in void ratio occurred when the wetting path reached the LOO. Therefore, the constant void ratio lines (LVs) were drawn from the highest void ratio value of each stress contour to the LOO. At a certain LV in Figure 5.30, the moisture ratio-net stress relationship could be obtained, as shown in **Figure 5.31**. The variation of moisture ratio (e_w) with net stress (σ) can be represented as an exponential function (Equation 5-2):

$$\boldsymbol{e_w = e_{wi} + d\left(e^{(-\sigma/0.82f)} + e^{(-\sigma/f)}\right)} \qquad 5\text{-}2$$

where e_{wi} is the initial moisture ratio, and d & f are fitting parameters.

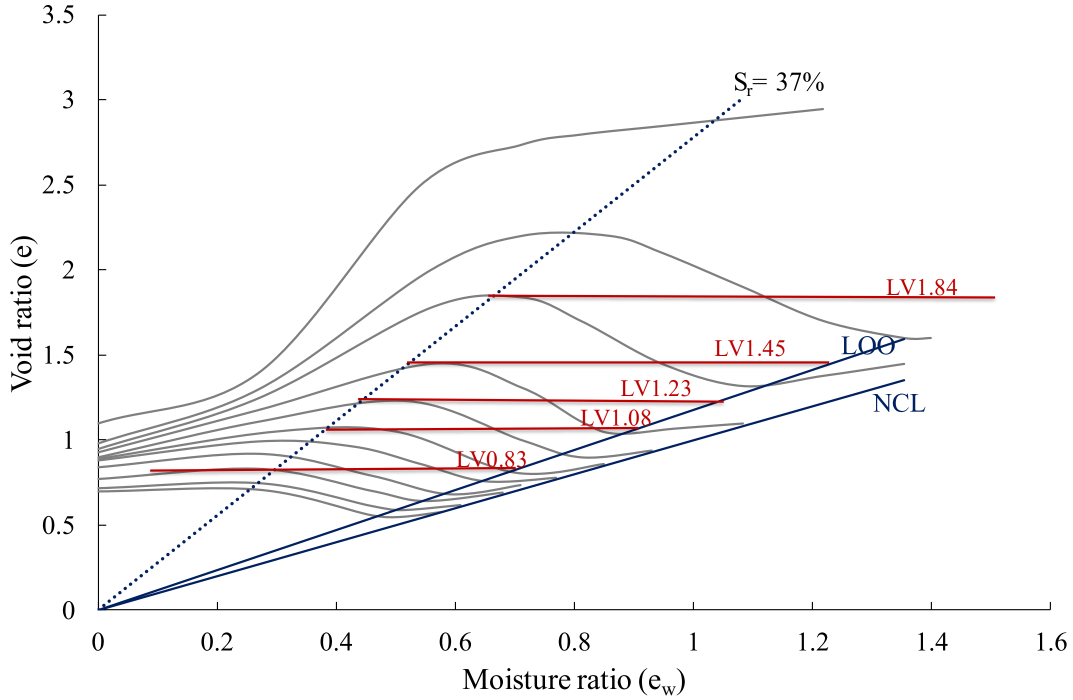

Figure 5.30. Constant void ratio lines on the LWSBS (untreated clay)

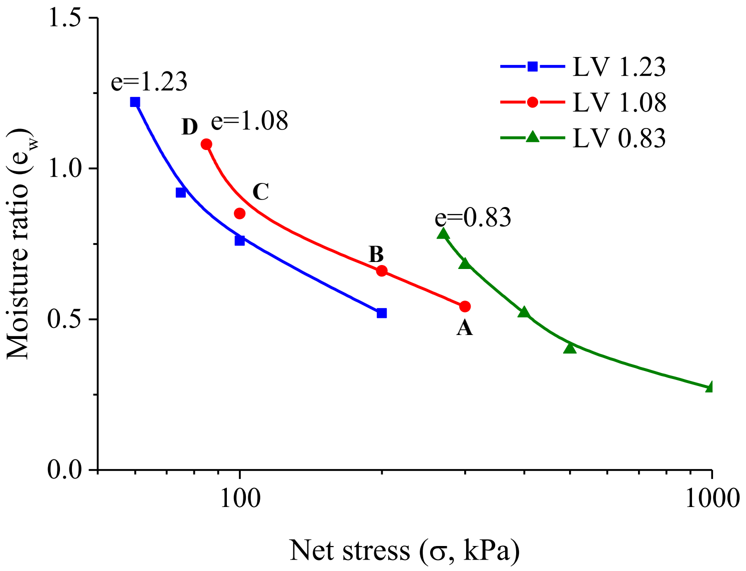

Figure 5.31. Loading-Collapse curves in e_w-σ space (untreated clay)

Similarly, for the lime-treated expansive clay, the LWSBS in the e-e_w space was divided into several LVs, as shown in **Figure 5.32**. The results presented in this research clearly show that the wetting paths followed the MPK framework. However, the MPK framework does not extend to the behaviour of specimens prepared at a degree of saturation less than 33% and then compressed under stress levels less than 500 kPa. Using the data in Figure 5.32, the e_w-σ relationship was plotted and has been presented in **Figure 5.33**. The variation of moisture ratio (e_w) with net stress (σ) can be expressed as shown in Equation 5-3:

$$\boldsymbol{e_w = e_{wi} + g e^{(-\sigma/h)}} \quad \text{5-3}$$

where g & h are fitting parameters.

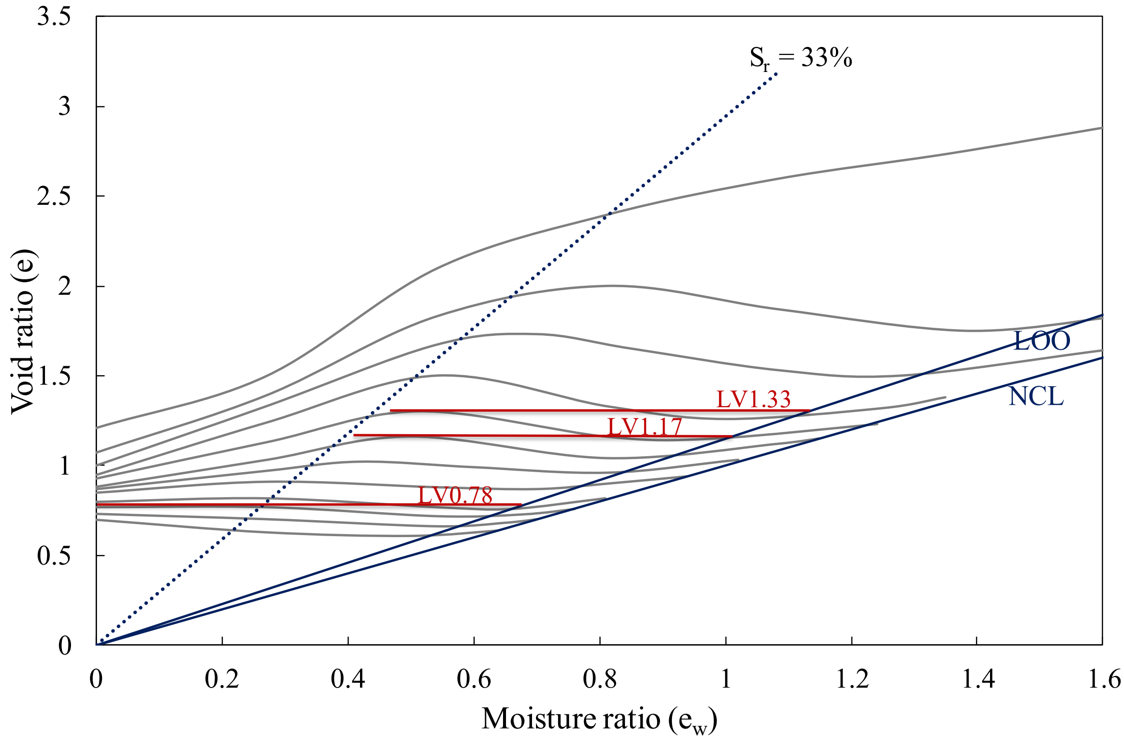

Figure 5.32. Constant void ratio lines on the LWSBS (lime-treated clay)

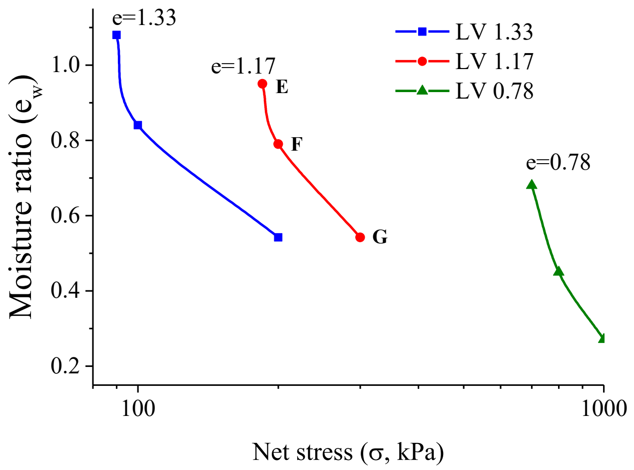

Figure 5.33. Loading-Collapse curves in e_w-σ space (untreated clay)

5.5 Modified Loading Wetting State Boundary Surface (LWSBS)

Kodikara (2012) established the LWSBS by developing representative curves. These curves represented the typical compaction curves with a drained section between the LOO and NCL. Details of the MPK and governing equations are provided in Chapter 2, but some appear here again for direct comparison with the new modified model developed in this research. Kodikara (2012) assumed that the variation of e with e_w can be expressed as a cosine function given in Equation 5-4.

$$\frac{e}{e_s} = \left[\left(\frac{e_0}{e_s} - 1\right) \cos\left(\frac{\varphi\, e_w}{e_s}\right) + \left(1 - \frac{e_0}{e_s}\cos(\varphi)\right)\right] \frac{1}{1-\cos(\varphi)} \qquad 5\text{-}4$$

$$e_s = e_{s0} - \lambda_1 ln\sigma \qquad 5\text{-}5$$

$$e_0 = e_0^* - \lambda_2 ln\sigma \qquad 5\text{-}6$$

where $\varphi=\pi/(e_{wc}/e_s)$ and e_{wc} is the optimum moisture ratio for net stress σ, e_0 and e_s are the void ratios at e_w=0 (S_r=0) and on NCL (S_r=1), respectively, for net stress σ. The compaction curve corresponding to σ=1 kPa (the loosest state) represents the upper boundary condition where e_0^* and e_{s0} represent the void ratios at e_w=0 and on NCL (saturated soil), respectively. λ_1 and λ_2 are the gradient of the compression line at dry and saturated conditions. According to Equations 5-4, 5-5 & 5-6, the cosine function starts from e_w=0 (S_r=0) (Kodikara 2012).

However, according to the compaction curves obtained for the untreated and lime-treated clay in this research, the cosine function starts from a specific degree of saturation represented as S_r. Therefore, the LWSBS can be divided into two parts (**A** and **B**). Part **A** represents the LWSBS where the Kodikara (2012) model is valid. This part includes each specimen prepared at a degree of saturation higher than S_r or compacted under high stress. In this study, Part **A** is defined when $S_r \geq$ 37% & 33% for the untreated and lime-treated clay specimens, respectively. The high-stress range was found to be equivalent to a net stress ≥ 1000 kPa and ≥ 500 kPa for the untreated and lime-treated clay specimens, respectively. Furthermore, Kodikara (2012) considered that the compaction curve corresponding to σ=1 kPa (the loosest state) represented the upper boundary condition. However, this curve is not accurate, especially when a specimen is prepared at a high degree of saturation (the cosine shape does not appear clearly for σ=2 kPa curves shown in **Figure 5.34**). Thus, it is recommended to choose another compaction curve at $\sigma = \sigma_i$ where the cosine function appears clearly. This curve can be considered as the upper boundary condition where e^*_{0i} and e^*_{so} represent the void ratios at e_w=e^*_{w0i} (at degree of saturation S_r) and on NCL (saturated clay), respectively. Consequently, Equation 5-4 has now been modified to take into account the degree of saturation S_r and the upper boundary condition as follows:

$$\frac{e}{e'_s} = \left[\left(\frac{e'_0}{e'_s} - \mathbf{1}\right) \boldsymbol{cos}\left(\frac{\varphi(e_w - e_{w0})}{e'_s - e_{w0}}\right) + \left(\mathbf{1} - \frac{e'_0}{e'_s}\mathbf{cos}(\boldsymbol{\varphi})\right)\right]\frac{\mathbf{1}}{\mathbf{1}-\mathbf{cos}(\boldsymbol{\varphi})} \quad \text{5-7}$$

$$\boldsymbol{e'_0} = \frac{e_{w0}}{S_r} \quad \text{5-8}$$

$$\boldsymbol{\sigma} = \left(\boldsymbol{e}^{(e^{*\prime}_0 - e'_0)/\lambda_0}\right) \times \boldsymbol{\sigma_i} \quad \text{5-9}$$

$$\boldsymbol{e'_s} = \boldsymbol{e^*_{so}} - \lambda_1 \boldsymbol{ln}\left(\frac{\sigma}{\sigma_i}\right) \quad \text{5-10}$$

where:

e_{w0}: the initial moisture ratio at stress σ and degree of saturation S_r,

e_0': the initial void ratio at stress σ, moisture ratio e_{w0} and degree of saturation S_r,

e_{w0i}^* = moisture ratio at S_r and $\sigma = \sigma_i$

$e_0^{*\prime}$: the initial void ratio at stress $\sigma = \sigma_i$, moisture ratio e_{w0} ($e_{w0} < e_{w0i}^*$),

λ_0: the gradient of compression line at $e_w = e_{w0}$ (Equation 5-1),

e_s': the void ratio on NCL and at stress σ,

e_{so}^*: the void ratio on NCL and at stress σ_i,

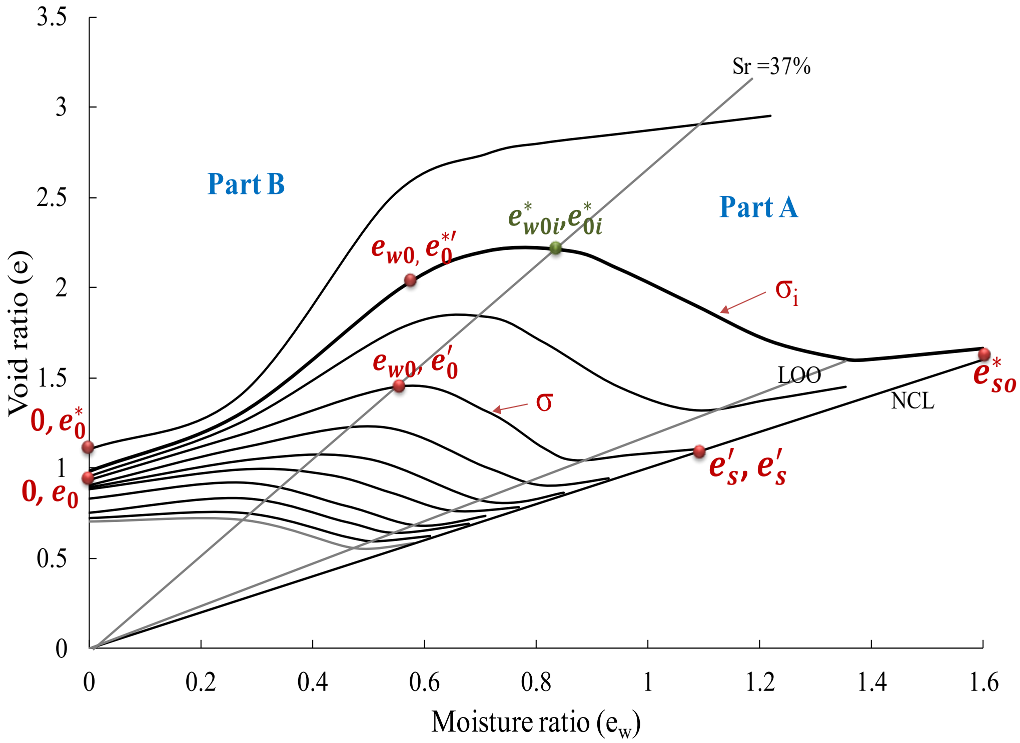

Figure 5.34. Modified MPK framework

The domain of the cosine function starts from $e_w = e_{wo}$ to $e_w = e_s$ (on NCL). For part **B** (Figure 5.34), where the MPK framework by Kodikara (2012) does not extend, the variation of e with e_w can be expressed as an exponential function (Equation 5-11). This function is valid from $e_w = 0$ to $e_w = e_{w0}$.

$$\boldsymbol{e = e_0\, e^{ce_w}} \qquad 5\text{-}11$$

where c is a fitting parameter, and by using Equations 5-6, 5-8 & 5-9, the parameter c can be determined as:

$$\boldsymbol{c = \frac{1}{e_{w0}} ln \frac{e_0'}{e_0}} \qquad 5\text{-}12$$

5.6 Estimation of Collapse and Swelling Potential

Results of laboratory tests conducted to investigate the volumetric behaviour of untreated and lime-treated clays showed that it is easy to estimate the collapse and swelling potential after wetting. This estimation can be achieved by identifying the void ratio at a certain compaction stress.

By identifying the void ratio at a certain compaction stress, a constant void ratio line (LV) can be drawn on the LWSBS. All points (specimens) generated by the intersection between the LV and stress contours will collapse after wetting. For example, the LV1.08 (**Figure 5.35**) includes the stress contours of 300, 200, 100 and 85 kPa. All points generated by the intersection between the LV1.08 and the stress contours of 300, 200, 100 and 85 kPa (estimated between 100 kPa and 50 kPa stress contours) will collapse after wetting. The intersection points **A**, **B**, **C** and **D** are shown in Figures 5.31 & 5.35. As an example, specimen **A**, prepared with 18.5% moisture content (e_w= 0.501) and compressed to 300 kPa, collapsed after wetting to reach the LOO by following the **AA′** line (Figure 5.35). Specimen **B** was prepared with 18.5% moisture content (e_w = 0.501) and compressed to 300 kPa, then unloaded to 200 kPa, and then wetted to a moisture content of 25% (e_w = 0.68). This specimen collapsed after continuous wetting to reach the LOO by following the **BB′** line in Figure 5.35. Note that **BB′** is smaller than **AA′**. As the difference in void ratio during the **AA′** path is higher than that for the **BB′** path, it is expected that the collapse obtained during the **AA′** path is higher than that for the **BB′** path. Thus, at a constant LV, the collapse value increased as the operational stress increased (**AA′** > **BB′** > **CC′** > **DD′**, as shown in Figure 5.35). To calculate the collapse value for the specimen **A** (with a void ratio of e_A), for example, after wetting, the void ratio value at the LOO ($e_{A'}$) should be found. By identifying the value of the $\varphi=\pi/(e_{wc}/e_s')$ in Equation 5 and measuring the e_s' from Equation 8, the value of e_{wc} can be obtained. By substituting the e_{wc} (e_w= e_{wc}) in Equation 5-7, the value of $e_{A'}$ will be obtained. Finally, the collapse value can be calculated (collapse%=$\frac{e_A - e_{A'}}{1+e_A} \times 100\%$).

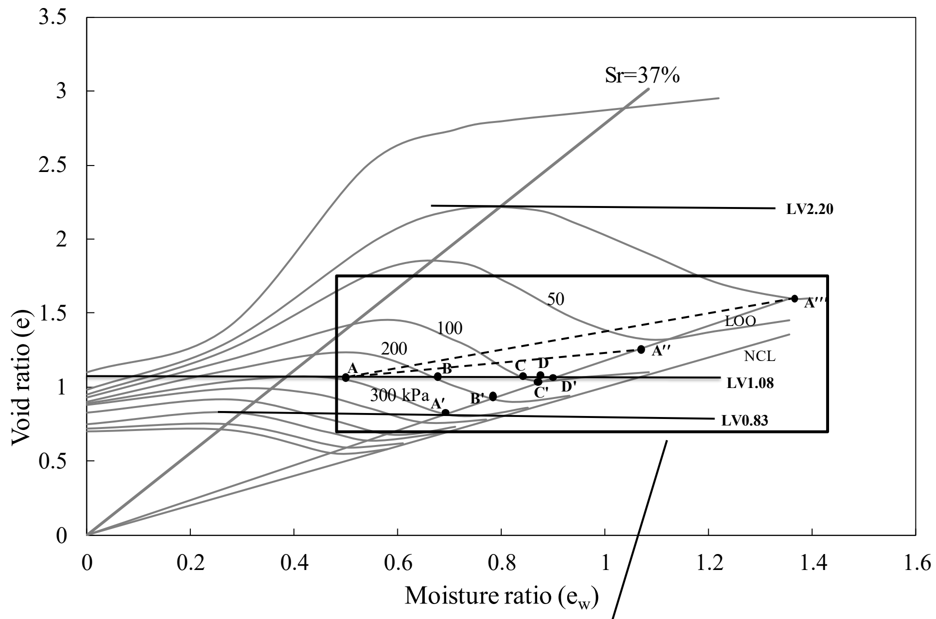

(a)

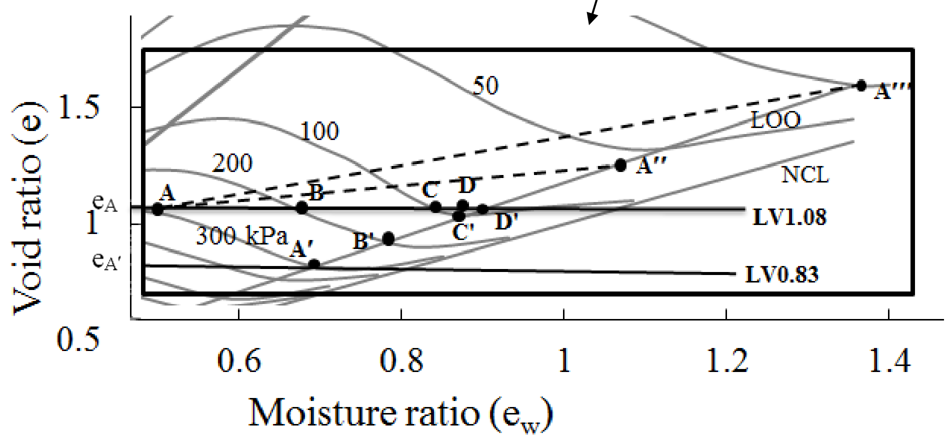

(b)

Figure 5.35. Collapse and swelling estimation by identifying the void ratio of a specimen compacted at a certain stress (untreated clay)

For the lime-treated expansive clay, the LV1.17 in **Figure 5.36**, for example, includes the stress contours of 300, 200 and 185 kPa (estimated between 200 kPa and 100 kPa stress contours). All points generated by the intersection between the LV1.17 and the stress contours of 300, 200 and 185 kPa will collapse after wetting. The intersection points **E**, **F**, and **G** are also shown in Figures 5.33 & 5.36. For reference, the lime-treated specimen **E**, prepared at 20% moisture content (e_w = 0.542) and compressed to 300 kPa, collapsed after wetting to the LOO by following the **EE′** line (Figure 5.36).

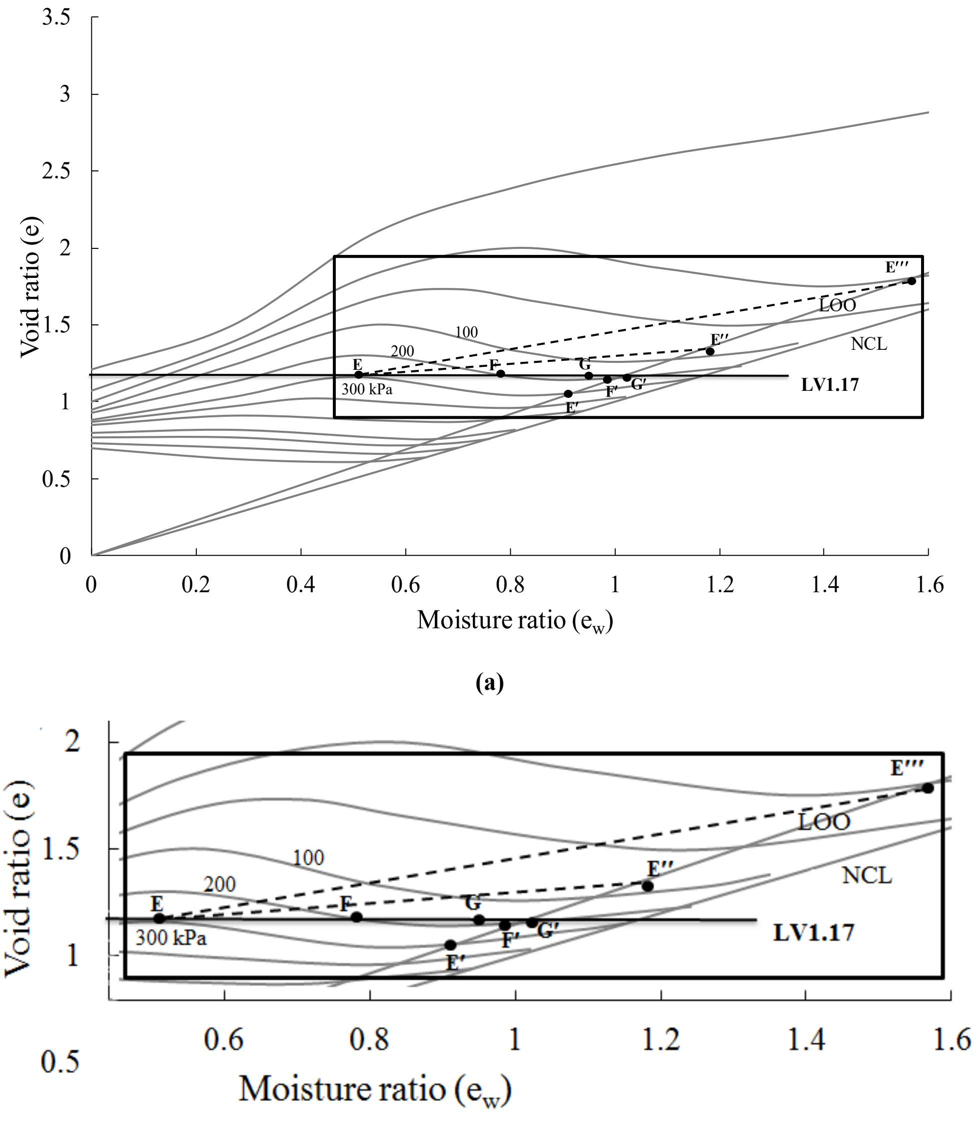

(b)

Figure 5.36. Collapse and swelling estimation by identifying the void ratio of a specimen compacted at a certain stress (lime-treated clay)

The verification of this method with the 1-D experimental work for the untreated and lime-treated clays is presented in **Figure 5.37**. Specimens were compacted to 300 kPa at 20% moisture content and then wetted under different operational stresses (untreated specimens LUW 20 300 100 32.5, LUW 20 300 200 30.3 LW 20 300 26.2 and treated specimens LUW 20 300 185 32, LUW 20 300 200 33.5 and LW 20 300 34). It is clear that the collapse values obtained according to this method are close to those obtained using an oedometer.

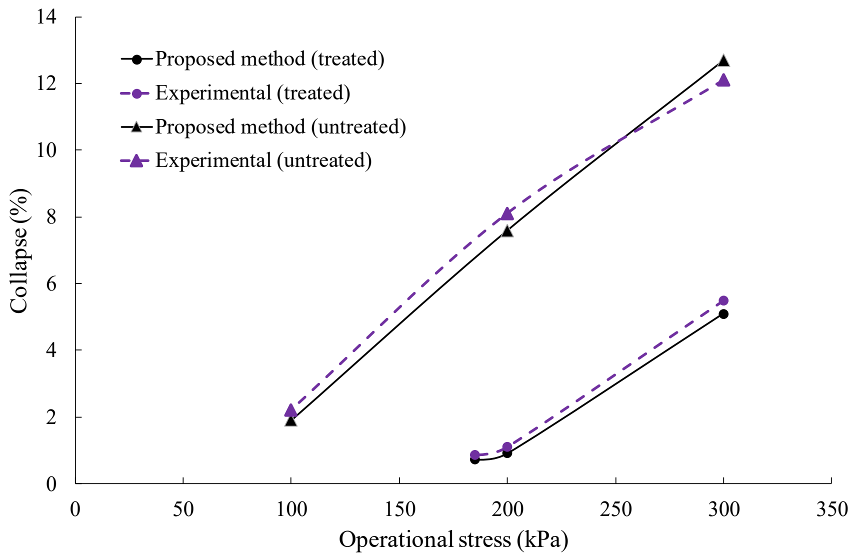

Figure 5.37. Verification of collapse estimation method with experimental work (specimens compacted to 300 kPa at 20% moisture content and then wetted under different operational stresses)

Since the unloading-reloading slope (κ) values of untreated and lime-treated clays are very small, it can be assumed that the change in void ratio after unloading can be neglected. Furthermore, as mentioned before, the specimen after unloading moved inside the LWSBS, then swelled to hit the LWBSB, and then collapsed up to the LOO. Because the location of the specimen after unloading was close to the LWSBS, the value of the swelling was very small (negligible). Therefore, it can be assumed that the wetting path will intersect the LWSBS at the same LV. As a result, the swelling value can be neglected for each point located on the LV, and therefore the important behaviour that should be measured is collapse.

For the untreated and lime-treated clays, if a specimen was unloaded to a stress above the LV, the specimen only swelled. As an example, untreated specimen **A** (Figure 5.35) was prepared at 18.5% moisture content and compressed to 300 kPa, then unloaded to 25 kPa. As the stress contour of 25 kPa is above the LV1.08, it was expected that the specimen would swell following the **AA″** line (under the LWSBS) path or the **AA‴** line (to reach the LWSBS), as shown in Figure 5.35. The path of swelling depended on the gradient of the swelling path (α) for untreated clay. For the lime-treated clay, specimen **E** (Figure 5.36) was prepared at 20% moisture content and compressed to 300 kPa, and then unloaded to 25 kPa. The stress contour of 25 kPa is above the LV1.17; therefore, it was expected that the specimen would swell following the **EE″** path (under the LWSBS) or **EE‴** path (to reach the LWSBS), as shown in Figure 5.36. The path of swelling was also dependent on the gradient of the swelling path (α') for the lime-treated clay.

For simplicity, each operational stress located above a certain LV can be considered as low operational stress and the specimen will swell after wetting at that stress. Alternatively, each operational stress located on the LV can be considered as high operational stress, and the specimen will collapse after wetting at that stress.

5.7 Discussion

To understand the volumetric behaviour of a residual expansive clay soil under different stress and wetting paths, a large number of tests were conducted on untreated and lime-treated specimens. Static compaction tests were performed to generate the MPK framework proposed by Kodikara (2012). The behaviour of all clay specimens tested during loading, unloading and wetting closely followed the MPK framework proposed by Kodikara (2012). However, this research suggests that the MPK framework does not extend to untreated and lime-treated specimens prepared at a degree of saturation (S_r) less than 37% for untreated basaltic clay and 33% for lime treated basaltic clay, which is then wetted under stress levels less than 1000 kPa & 500 kPa, respectively, as shown in Figures 5.1 & 5.2.

Although the optimum lime content was initially obtained based on swelling tests (for the selected clay), it was important to investigate the full volumetric behaviour of the lime-treated clay during wetting. This is because the optimum lime content is mostly determined on specimens that have been compacted at MDD and OMC, as commonly done in the majority of previous research works. The degree of saturation of the specimens in this condition is approximately 86% and very close to being fully saturated. The second reason is that collapse is considered to be a major issue in unsaturated soil behaviour, and while specimens located on the LOO never experience collapse under any stress level (Sivakumar & Wheeler 2000), it is important to investigate collapse on the dry side of the LOO for lime-treated expansive clay.

To compare the behaviour of untreated and lime-treated specimens during LW and LUW state paths, the data presented in this study were evaluated. For all untreated and lime-treated specimens, the void ratio value decreased as the moisture content increased at all stress levels tested, due to the macroscopic structure build-up. However, this relation reversed when a specimen with very low moisture content (S_r < 37% for untreated clay and S_r < 33% for lime-treated clay) was wetted under low-stress conditions (i.e. σ < 1000 kPa for untreated clay and < 500 kPa for lime-treated clay). The occurrence of this feature is similar to having compaction curves with multiple peaks, and appears to be related to the weakening of the effect of suction, which enables stronger contacts to be formed among aggregates that give larger macro void space. Figure 5.1 shows that under a constant stress level, the void ratio varied within a narrow range of moisture content for untreated expansive clay. On the contrary, as shown in Figure 5.2, for lime-treated expansive clay, under constant stress level, the void ratio varied within a wider range of moisture content. Furthermore, the variation in the void ratio (at a constant stress level) for the untreated expansive clay was higher than that of the lime-treated expansive clay, as expected. In addition, the void ratio variation decreased as the stress increased. This meant that the collapse potential of the untreated clay was higher than that of the lime-treated clay. Furthermore, the lime-treated specimens required more water to reach maximum collapse. This behaviour is evident in Figures 5.1 & 5.2.

A series of tests were conducted to measure swelling and collapse values for different conditions (moisture content, dry density, loading and unloading stresses) for the untreated and lime-treated clays to understand the behaviour during wetting. These results are as presented in Figures 5.14 & 5.27. The results showed that at a constant compaction stress, all specimens swelled after wetting under low operational stress and collapsed after wetting under high operational stress. Furthermore, the swelling magnitude decreased as the operational stress increased. However, the collapse potential increased as the operational stress increased, up to the compaction stress. Beyond this point, the collapse value decreased as the operational stress increased. In addition, Figures 5.14 & 5.27 showed that the swelling potential increased as the compaction stress increased, while the collapse potential decreased as the compaction stress increased.

Reviewing the results in Figures 5.14 & 5.27, and focusing on the behaviour of untreated and lime-treated expansive clay specimens prepared with 20% and 10% moisture contents and subsequently compressed to 300 and 1000 kPa, and then unloaded to 100 and 300 kPa, respectively (points 6 & 13 in Figure 5.14 and points 8 & 14 in Figure 5.27), it is clear that the untreated specimen compressed at 20% moisture content to 300 kPa and then unloaded to 100 kPa collapsed after wetting (point 6 in Figure 5.14). The same conditions were followed for the lime-treated specimen, but the specimen swelled after wetting (point 8 in Figure 5.27). The same behaviour was found to be repeated when the untreated 10% moisture specimen was compressed to 1000 kPa and then unloaded to 300 kPa, and collapsed after wetting (point 13 in Figure 5.14). However, when the same state path was followed for the lime-treated specimen, the specimen swelled after wetting (point 14 in Figure 5.27). These results can be explained by establishing the LV. For the untreated specimen compressed to 300 kPa (point 2 in **Figure 5.38**) and upon reaching the LV1.08 on the LWSBS, the LV1.08 intersected the 300, 200, 100 and 85 kPa stress contours. This means that all specimens after unloading to 200, 100 and 85 kPa and then wetted to the LOO will collapse. Thus, after unloading to 100 kPa (from point 2 to 3 in Figure 5.38) and wetting, the specimen collapsed and followed the path from point 4 to 5 in Figure 5.38.

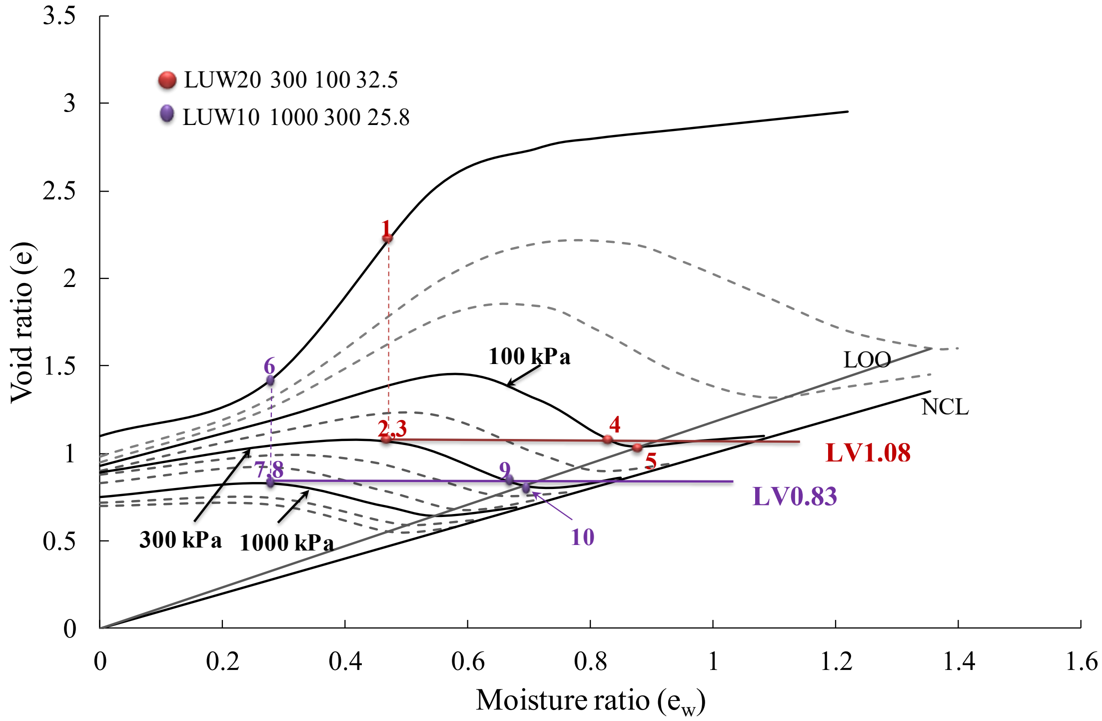

Figure 5.38. Paths followed when two untreated specimens at moisture contents of 20% & 10% were compacted to 300 kPa & 1000 kPa, then unloaded to 100 kPa & 300 kPa, and finally wetted to the LOO

However, given the same conditions for the lime-treated specimen, the specimen reached the LV1.17 after being compressed to 300 kPa (point 2′ in **Figure 5.39**). Here, the LV1.17 intersected the stress contours of 300, 200 and 185 kPa, which means that all specimens after unloading to the stresses of 200 and 185 kPa and wetted to the LOO will collapse. Therefore, the stress of 100 kPa was above the LV1.17, and as such, the specimen followed the path from point 2′ to point 3′ after unloading, and then swelled to follow the path from point 3′ to point 4′ after wetting. The same pattern was observed for the other untreated and lime-treated specimens, as shown in Figures 5.38 & 5.39.

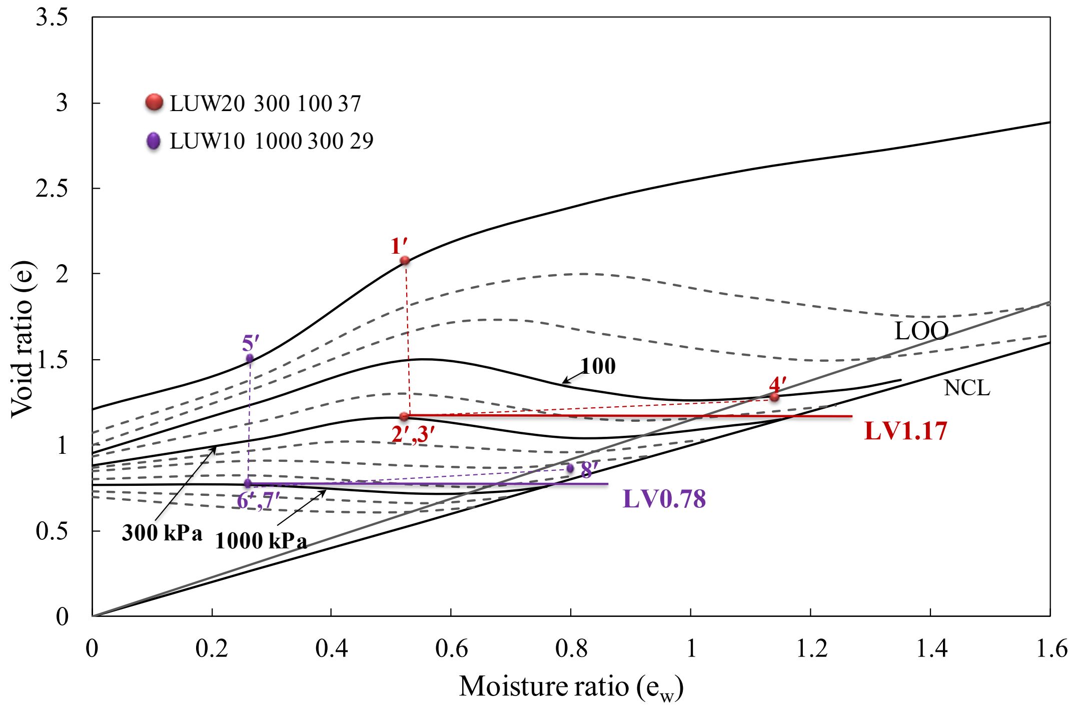

Figure 5.39. Paths followed when two lime-treated specimens at moisture contents of 20% & 10% were compacted to 300 kPa & 1000 kPa, then unloaded to 100 kPa & 300 kPa, and finally wetted to the LOO.

Figures 5.14 & 5.27 also revealed an improvement from adding lime to the clay, in terms of reducing the collapse potential. For example, the untreated specimen, prepared at 20% moisture content and compressed to 200 kPa, collapsed after wetting to the LOO with a collapse potential of 13.8% (point 3 in Figure 5.14). According to the specifications of Lin and Wang (1988) and ASTM-D5333 (2003), the specimen can be classified as a very highly collapsible soil. However, the improvement in behaviour appeared when the specimen was treated with lime and prepared under the same conditions (initial moisture content = 20% and compressed to 200 kPa), and then wetted to approximately the LOO. The collapse potential was reduced to 8.9% (point 4 in Figure 5.27). According to this reduction in collapse potential, the stabilised specimen was considered to fall into the category of being just a "high collapsible" soil (ASTM-D5333 2003; Lin & Wang 1988). For the untreated specimen, prepared at 20% moisture content, compressed to 200 kPa and then unloaded to 100 kPa, the collapse occurred after wetting to the LOO, with the amount of collapse being 9.2% (point 2 in Figure

5.14). According to collapse specifications (Baghabra Al-Amoudi & Abduljauwad 1995; Rafie et al. 2008), the specimen can be classified as “high collapsible” soil. Alternatively, the stabilised specimen, prepared under similar conditions (initial moisture content = 20% and compressed to 200 kPa and unloaded to 100 kPa), collapsed after wetting to the LOO, but the collapse potential was reduced to 2.5% (point 3 in Figure 5.27) and accordingly, the collapse was categorised as a “medium collapsible” soil. This data proves that hydrated lime at the percentage found based on the OLC can contribute to improving the collapsibility of clays from “high collapsibility” to “medium collapsibility”. The results presented in Figures 5.14 & 5.27 show that the collapse potentials were reduced after stabilisation and the values of collapse after improvement should be considered.

It is also important to mention that Figure 5.27 shows significant swelling had occurred when the specimen was prepared at a very low moisture content (i.e. dry side of the LOO) (10%), then compacted to 1000 kPa, and then wetted under an operational stress of 25 kPa. To check these results, two identical lime-treated specimens were prepared at a moisture content of 10% and then loaded to 1000 kPa. One of the specimens was unloaded to 25 kPa, and then wetted to the saturation state. The swelling value was then obtained. The other specimen was cured for 7 days, and the same procedure was then followed to obtain the swelling value. It was observed that the difference in swelling values was small and could be neglected. This behaviour can be attributed to the mechanism of the reaction between lime and clay. The first reaction begins after adding water to the clay-lime mixture. The hydrated lime dissociates to Ca^{+2} and $2(OH)^{-1}$ ions; consequently, the cation exchange, flocculation, and agglomeration start. That means that enough water should be provided to start the stabilisation process. As a result, adding a small amount of water to the clay (the clay is still dry) will not affect the stabilisation process during curing. However, the OLC was obtained at the OMC, meaning that there was enough water to start the stabilisation process during curing.

5.8 Verification

To verify the suitability of the theory of swelling and collapse according to the MPK framework, it is important to see if the MPK framework stays valid when results of previous studies are applied to it. Previous studies that were examined for this purpose were performed based on one-dimensional consolidation tests under controlled suction conditions. Therefore, this section presents the application of the results of previous studies, such as the work by Jotisankasa et al. (2007), on the MPK framework. Furthermore, the theory of the MPK framework is applied to experimental results obtained in previous studies, such as the study conducted by Alonso et al. (1990).

5.8.1 Application of Jotisankasa et al. (2007) results on the MPK framework

Jotisankasa et al. (2007) investigated the collapse behaviour of an unsaturated soil using a suction-monitored oedometer test. The soil used in the study was a mixture of 70% silt, 20% kaolin and 10% London clay. A modified oedometer was used to monitor the changes in suction during loading and wetting. Suction was measured by using suction probes (Ridley & Burland 1993).

Three series of specimens were selected for the experimental studies, and were referred to as "1", "2," and "3". The series of specimens were compacted using a static method inside the oedometer cell. The initial properties of the series are given in **Table 5.6**. The testing program for the specimens of series 1 is presented in **Table 5.7**.

Table 5.6. Initial properties of the test series studied by Jotisankasa et al. (2007)

Series	Specific volume (1+*e*)	Moisture content (%)	Degree of saturation (%)	Initial suction (kPa)
1	1.7	10.2	38	475±15
2	1.71	13.6	51	150±15
3	1.5	10.0	53	475±15

Table 5.7. Testing program for test series 1 (Jotisankasa et al. 2007)

Group	Test	State paths followed after compaction
1	1-SL	Soaked at 11kPa/ loading to 7336 kPa/ unloading to 11 kPa
2	1-D 1-G 1-H 1-K 1-T	W (10.6%)/ L (3220)/ U (54) W (14.8%)/ L (3220)/ U (54) W (13.5%)/ L (3220)/ U (54) L (3220)/ U (54) D (9.2%)/ L (3220)/ U (54)
3	1-P 1-U 1-V 1-W	D (0.81%)/ L (7523)/ U (125) D (3.9%)/ L (7526)/ U (125) D (4.3%)/ L (7523)/ U (125) D (2.0%)/ L (7523)/ U (125)
4	1-I 1-J 1-N 1-Q	L (430)/ W (130 kPa)/ L (3220)/ U (54) L (215)/ W (50 kPa)/ L (861)/ U (54) L (108)/ W (10 kPa)/ U (54) L (594)/ W (40 kPa)/ U (54)
5	1-L	L (215)/ W (140 kPa)/ L (3220)/ U (54)
W= wetting L= loading U= unloading		

In this study, the series 1 was selected to investigate the concept of LV using the MPK framework, and involved five groups. Group 1 involved a specimen, saturated under a vertical stress of 11 kPa, compressed in a fully saturated condition to the stress of 7336 kPa, and then unloaded to 11 kPa. Groups 2 and 3 involved loading specimens under a constant moisture content to a particular compaction stress, and then unloading to a certain stress. Group 4 involved wetting specimens at a constant stress level to achieve collapse. Group 5 involved the 1-L test, in which a specimen was wetted under the stress level of 215 kPa without causing collapse, and then the loading path was followed at a constant moisture content.

The results of Groups 1 and 2 are presented in terms of specific volume (1+*e*), the degree of saturation, suction, and net stress. However, to serve our study, the specific volume was converted to void ratio (**Figure 5.40a**). Figure 5.40 presents the values of yield points (preconsolidation pressures) for specimens compressed under a various degree of saturation. It is clear that the yield points of all specimens occurred at about the same void ratio value. To apply this state to the MPK framework, an average line connecting the yield points (LV0.67) was plotted as shown in Figure 5.40a. This line can be obtained from two methods. The first method is through loading specimens, prepared at various initial moisture contents, to different net stresses. The obtained void ratio values are approximately the same after loading. The second method is through wetting. In this case, the line connects all preconsolidation pressure (yield points) values of specimens that are compressed to the same stress level under a constant moisture content, and then wetted to different moisture contents. This line can be referred to as the yield line or constant void ratio line (LV).

According to the experimental tests of Jotisankasa et al. (2007), the LV was drawn according to the second described method. From Figure 5.40a, it is clear that the average line that connected the yield points was located at a constant void ratio of 0.67 (LV0.67). This line can be represented on the MPK framework as shown in **Figure 5.41**.

To explain the data of Jotisankasa et al. (2007) on the MPK framework, firstly, the initial properties of the specimens (after compaction) were identified. These properties included moisture content, preconsolidation pressure (yield point), and corresponding void ratio. As shown in Table 5.6, the moisture content of the series 1 specimens was 10.2% (e_w = 0.266, where G_s=2.61). The 1-K test given in Table 5.7 (Group 2) and shown in Figure 5.40a represented the e-log(σ) relationship for a specimen immediately after compaction (initial condition). As shown in Figure 5.40a, the preconsolidation pressure was determined to be approximately 750 kPa, with a corresponding void ratio of 0.66. At this stage, the first point on the MPK framework (e, e_w, σ) was identified (0.66, 0.266, 750) (Figure 5.41). That means that all specimens in each of the five groups presented in Table 5.7 were compressed at a moisture content of 10.2% to the stress level of 750 kPa, and then different state paths were performed to achieve a specific target.

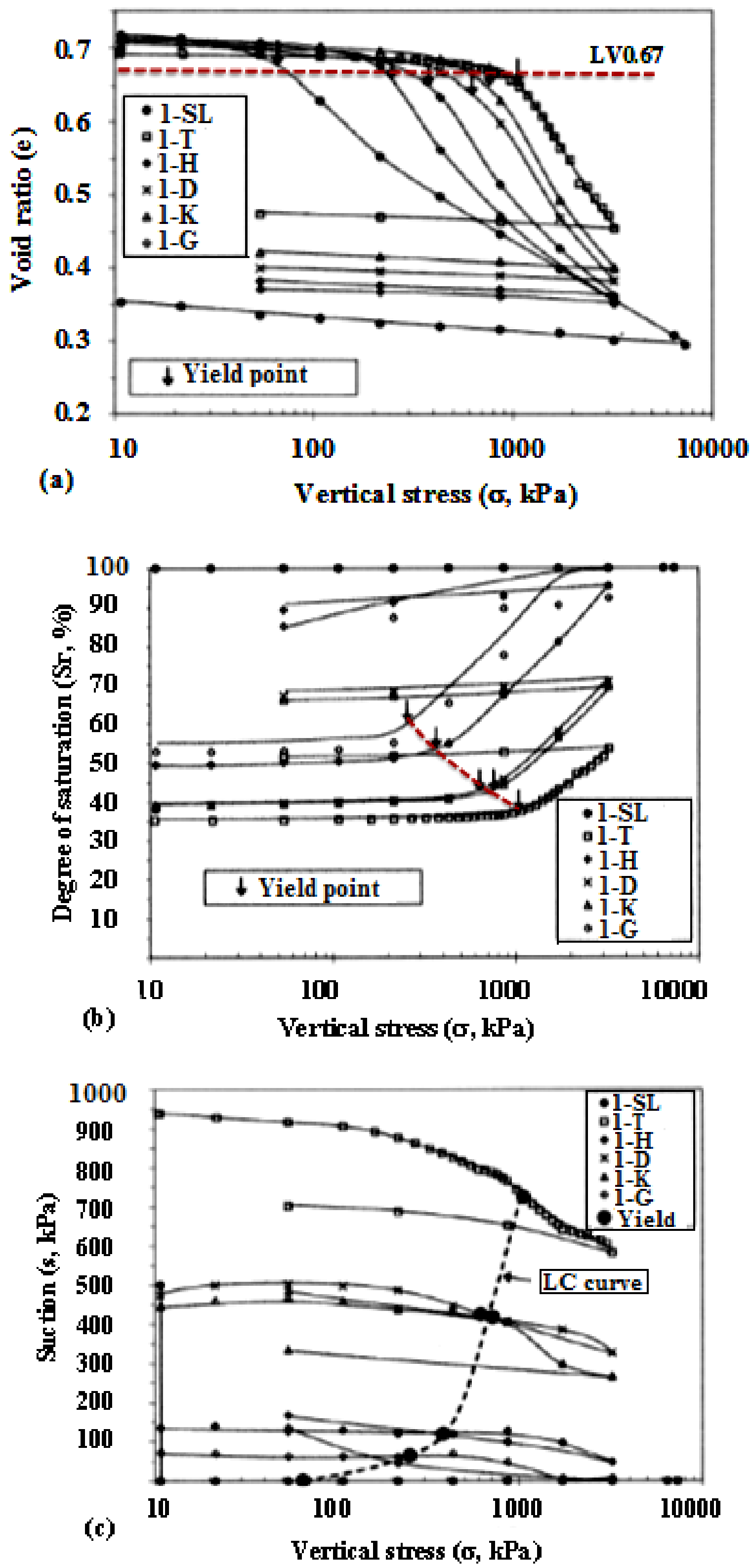

Figure 5.40. Results of loading tests under constant moisture content for series 1 (after Jotisankasa et al. (2007))

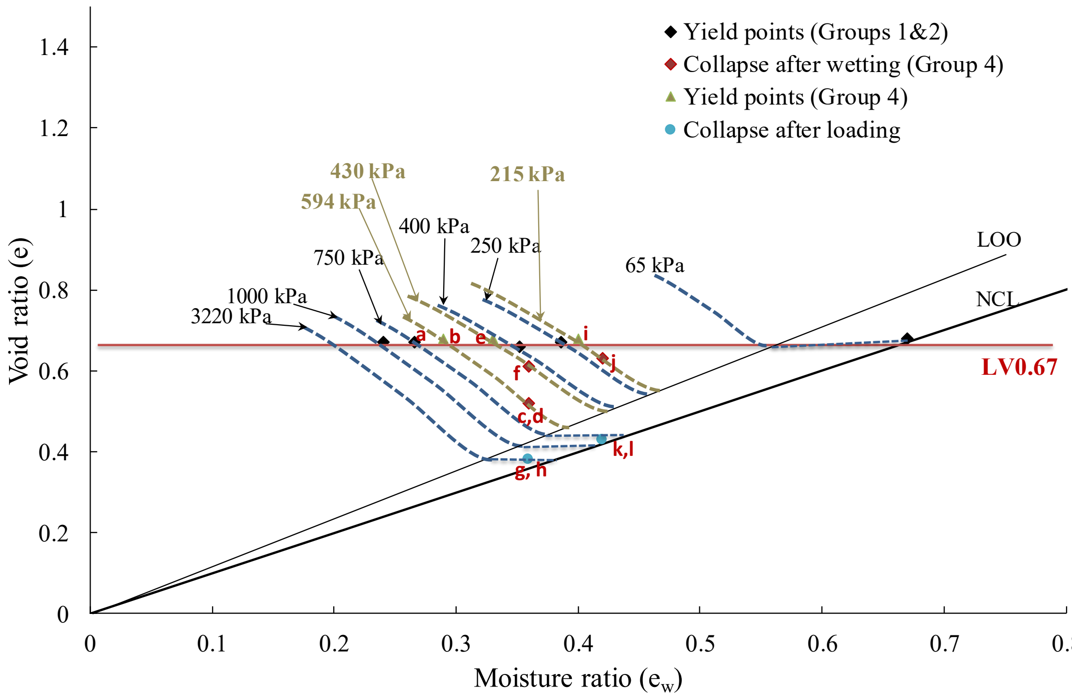

Figure 5.41. Results of Groups 1 and 2 in terms of void ratio and net stress

From Group 2, the preconsolidation pressures at various moisture contents were obtained. For example, for the specimen prepared at a moisture content of 10.2% and compressed to the stress level of 750 kPa, then wetted to the moisture content of 13.5% ($e_w = 0.352$) (1-H), the preconsolidation pressure was 400 kPa, with a void ratio of 0.66. Consequently, the second point on the MPK framework was found to be (0.66, 0.352, 400) (Figure 5.41). For the specimen with 10.2% moisture content compressed to the stress level of 750 kPa, then wetted to the moisture content of 14.8% ($e_w = 0.386$) (1-G), the preconsolidation pressure was 250 kPa, with a void ratio of 0.66. Therefore, the third point was found to be (0.66, 0.386, 250) (Figure 5.41). For the specimen with 10.2% moisture content compressed to the stress level of 750 kPa and then dried to the moisture content of 9.2% ($e_w = 0.240$) (1-T), the preconsolidation pressure was 1000 kPa, with a void ratio of 0.67. Therefore, the fourth point was found to be (0.67, 0.240, 1000). However, the specimen in Group 1 (1-SL) was compacted to the stress of 750 kPa and then saturated. The preconsolidation pressure was found to be 65 kPa, with a void ratio of 0.68. Therefore, the last point was found to be (0.68, 0.68, 65), as shown in Figure 5.41.

After plotting these points, an average horizontal line was drawn to pass through them. This line intersected the void ratio axis at a value of 0.67 (LV0.67). Therefore, the LV0.67 intersected the stress contours of 65, 250, 400, 750, and 1000 kPa at points of (e_w =0.68, e =0.67), (e_w =0.386, e =0.67), (e_w =0.352, e =0.67), (e_w =0.266, e =0.67), and (e_w =0.24, e =0.67), respectively (Figure 5.41). According to the studies of Tripathy et al. (2002) and Islam (2015), the LOO line was assumed to occur at a degree of saturation of 85%.

Figure 5.40b shows the relationship between the degree of saturation and net vertical stress. If the yield points are connected using a curved line, as shown in Figure 5.40b, a relationship between the degree of saturation and net stress can be obtained. To find the Loading–Collapse curve in terms of moisture ratio and net stress, the equivalent moisture ratio values (at yield points) were measured according to the data presented in Figure 5.40b. **Figure 5.42** presents the Loading-Collapse curve in terms of moisture ratio and net stress, and is compatible with the results obtained from this research. Figure 5.40c presents the Loading-Collapse in terms of suction and net stress, which will be discussed later.

The results of Group 4 tests induced collapse potential due to wetting as shown in **Figure 5.43**. To represent these results within the MPK framework, three tests were selected. These tests involved 1-Q, 1-I, and 1-J. The state paths of these tests involved loading to the stresses of 594, 430, and 215 kPa, respectively. Therefore, it was important to find the intersection points (yield points) between the LV0.67 and the stress contours of 594, 430, and 215 kPa. The yield points (point **b**, **e** and **i** in Figure 5.41) were allocated according to the data presented in Figure 5.40b. For the 1-Q test, the specimen with 10.2% moisture content was compressed to the stress of 750 kPa (point **a** in Figure 5.41), then unloaded to the stress of 594 kPa. In this case, the unloaded path moved inside the LWSBS. As mentioned previously, as the stress contours of 750 and 594 kPa are located on the same LV, a very small amount of swelling due to wetting was enough to hit the LWSBS (point **b** in Figure 5.41), meaning that the amount of swelling can be neglected. Therefore, the specimen collapsed after wetting, and followed the path from point **b** to **c**. The specimen was then unloaded to the stress of 54 kPa, and followed the path from point **c** to **d** (the path moved inside the LWSBS), as shown in Figure 5.41.

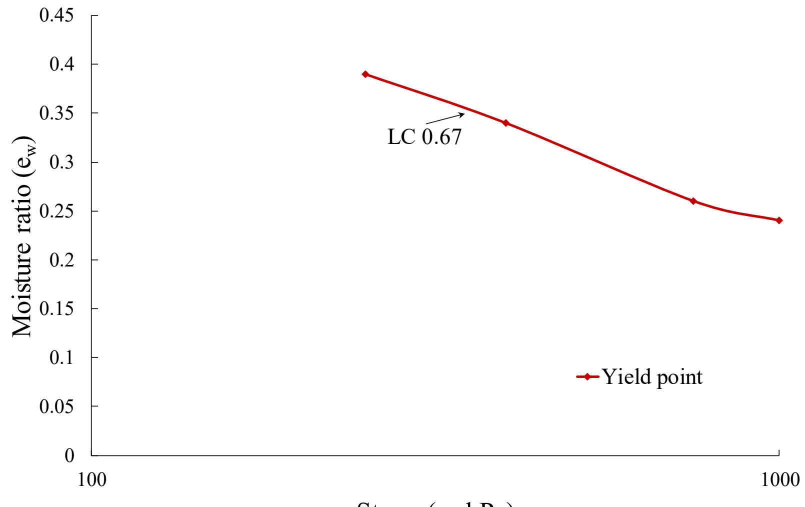

Figure 5.42. Relationship of moisture ratio and net stress based on Jotisankasa et al. (2007) results

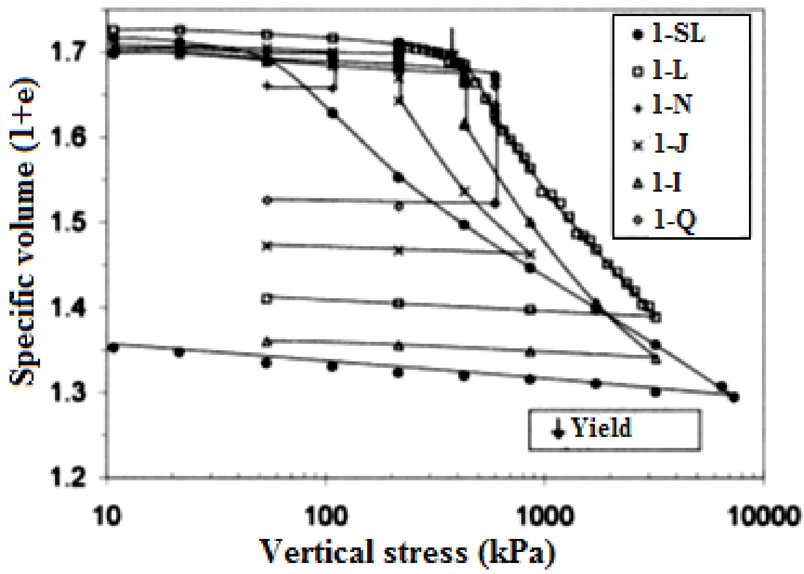

Figure 5.43. Results of Group 4 tests induced collapse due to wetting (Jotisankasa et al. 2007)

For specimen test 1-I, the specimen with 10.2% moisture content was compressed to 750 kPa (point **a** in Figure 5.41), then unloaded to 430 kPa. For the same reason, in the test of specimen 1-Q (the stress contours of 750 and 430 kPa located on the same LV), the wetting path hit the LWSBS at point **e** (see Figure 5.41). With continuous wetting, the specimen collapsed and followed the path from point **e** to **f**. After that, the specimen was loaded to 3220 kPa and followed the path from **f** to **g** as shown in Figure 5.41. Finally, the specimen was unloaded to 54 kPa and it followed the path from point **g** to **h** (the path moved inside the LWSBS).

For specimen test 1-J, the specimen with 10.2% moisture content was compressed to 750 kPa (point 1 in Figure 5.41), then unloaded to 215 kPa. As the stress contours of 750 and 215 kPa were located on the same LV, the wetting path hit the LWSBS at point **i** (Figure 5.41). Then the specimen collapsed and followed the path from **i** to **j**. After that, the specimen was loaded to 861 kPa and it followed the path from **j** to **k** as shown in Figure 5.41. Finally, the specimen was unloaded to54 kPa and it followed the path from point **k** to **l** (the path moved inside the LWSBS).

5.8.2 Application of collapse and swelling mechanism according to the MPK framework based on the study of Alonso et al. (1990).

The model of Alonso et al. (1990) derived the location of yield points in the stress-suction space, as mentioned in Chapter 2. To allocate the yield points, Alonso et al. (1990) identified the preconsolidation stresses for two specimens loaded, unloaded, and loaded at different suction values. To apply the mechanism of collapse and swelling according to the MPK framework on the study of Alonso et al. (1990), two untreated and two lime-treated specimens were compacted statically 300 kPa under a constant moisture content of 20% (e_w=0.542).

For the first untreated specimen, the preconsolidation pressure (yield) was identified by subjecting it to a constant load and recording a settlement. Once the settlement was completed, the next constant load was applied. The oedometer cell was covered with plastic wrap to avoid moisture loss. The load varied from 2 to 3600 kPa. After plotting the data in the *e*-log(σ) space, the preconsolidation pressure was obtained. It was approximately 280 kPa (point 1 in **Figure 5.44**), which was close to the compaction stress value of 300 kPa. Meanwhile, the second untreated specimen, compacted to the stress of 300 kPa under a constant moisture content of 20%, was inundated with distilled water under a stress of 2 kPa. Following that, the specimen was subjected to different constant vertical stresses every 24 hrs (ASTM-D2435 1996). By plotting the data in the *e*-log(σ) space, the preconsolidation pressure for saturated soil was approximately 63 kPa (point 4 in Figure 5.44).

In Figure 5.44, it is seen that if a specimen was compacted statically to 300 kPa under a constant moisture content of 20% (point 1), then wetted to saturation condition (under the stress of 280 kPa), it collapsed and followed the path from point 1 to point 2. However, if the specimen at point 1 in Figure 5.44 was unloaded to an equivalent stress to the preconsolidation pressure of saturated soil (63 kPa), there was no additional collapse; the specimen started to swell and followed the path from point 3 to point 4, as shown in Figure 5.44.

Following the model of Alonso et al. (1990), the preconsolidation pressures (yield) were obtained in the σ-*e* space, as shown in Figure 5.44 (points 1 & 4). The values of suction were measured using tensiometers (Hyprop) or a chilled mirror hygrometer (WP4C), and will be explained in the next chapter. As the relationship between net stress and suction was represented as a curve, a third point needed to be obtained. The third specimen was initially compacted to 300 kPa at a moisture content of 20%, then wetted to a moisture content of 24% under a stress of 2 kPa. The specimen was covered with plastic wrap and left for 24 hrs to equilibrate. The same procedure conducted on the first specimen was followed again in order to measure the preconsolidation pressure, which was found to be 190 kPa. **Figure 5.45** presents the behaviour of the untreated soil (Loading-Collapse) in the σ-*s* space as a curve, which matches the finding of Alonso et al. (1990) (Figure 2.4b).

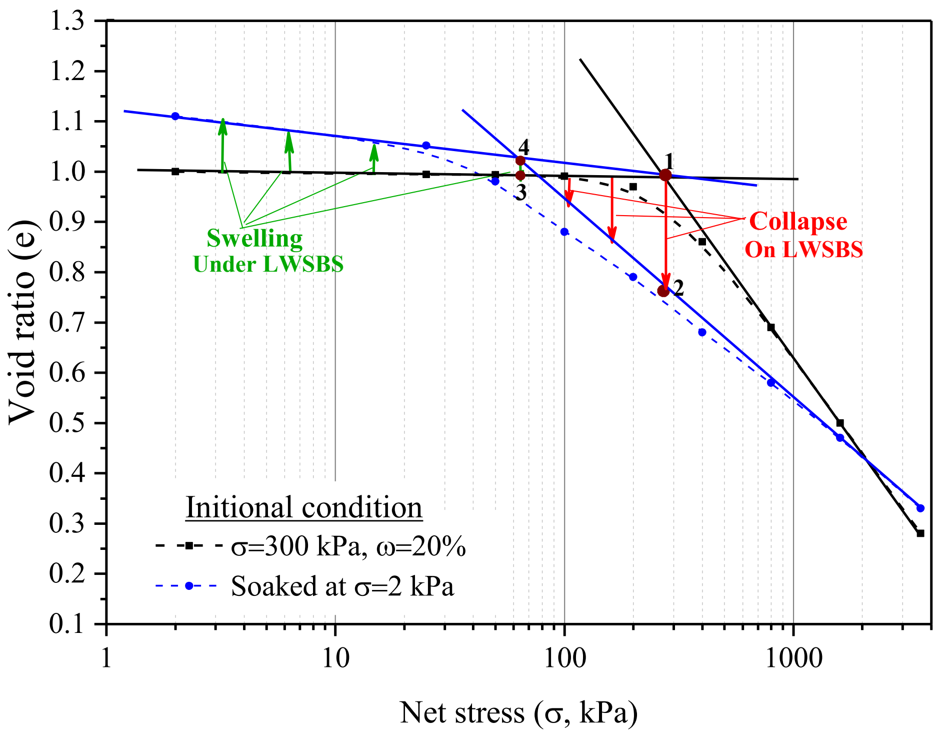

Figure 5.44. Preconsolidation stresses for saturated and unsaturated specimens and mechanism of collapse and swelling according to Alonso et al. (1990) model (untreated soil)

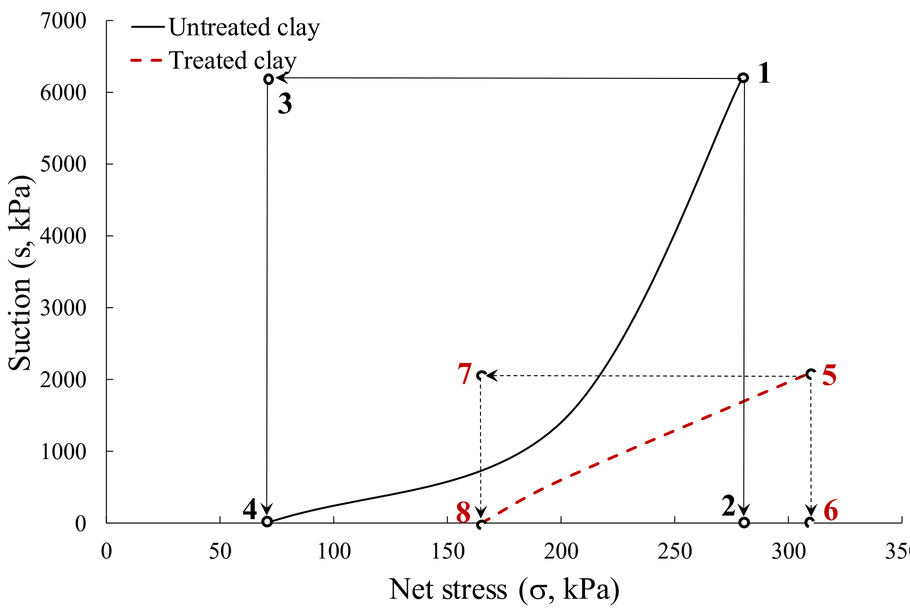

Figure 5.45. Yield curves for untreated and lime-treated soils in *σ-s* space

For the lime-treated specimens, the same procedure was followed to measure the preconsolidation pressure. The first specimen was compacted statically to 300 kPa under a constant moisture content of 20%. The preconsolidation pressure was found to be 310 (point 5 in **Figure 5.46**), which was close to 300 kPa (compaction stress). However, the second specimen was compacted statically to 300 kPa under a constant moisture content of 20% and then soaked with distilled water under a stress of 2 kPa. The preconsolidation pressure was found to be 165 kPa (point 8 in Figure 5.46). Figure 5.46 shows that if specimen 5 was wetted to saturation under a stress of 310 kPa, it collapsed. However, if specimen 5 was unloaded to an equivalent preconsolidation pressure (saturated) of 165 kPa, the specimen started to swell.

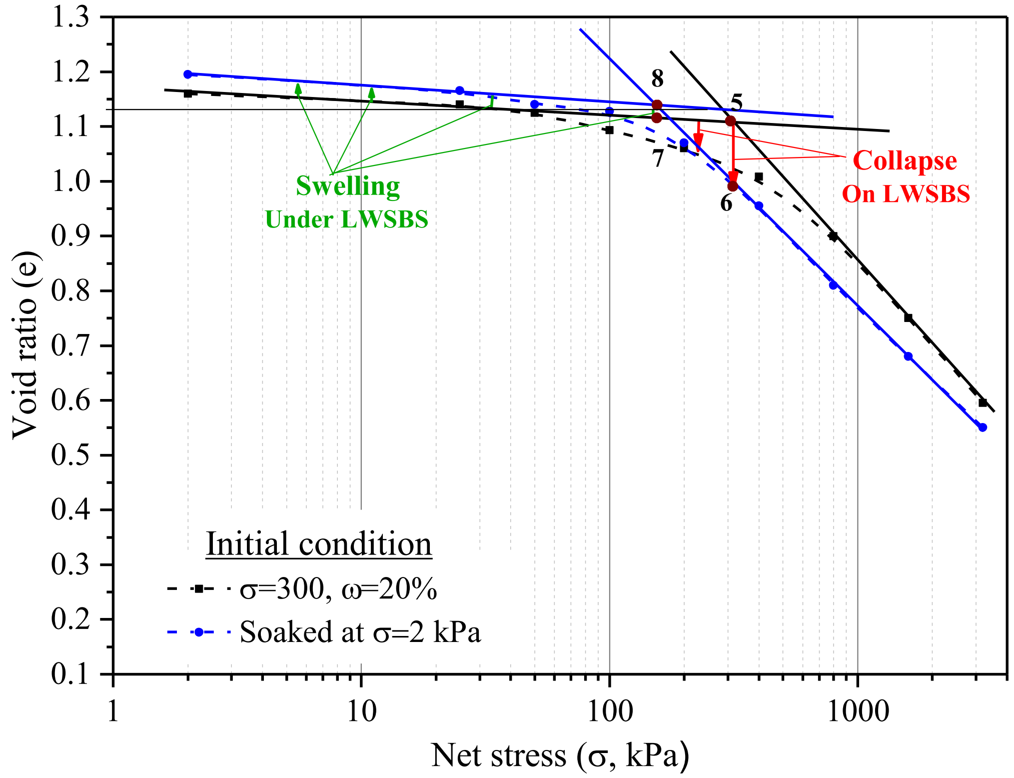

Figure 5.46. Preconsolidation stresses for saturated and unsaturated specimens and mechanism of collapse and swelling according to Alonso et al. (1990) model (lime-treated soil)

To represent the model of Alonso et al. (1990), the preconsolidation pressures (yield) were specified in the σ-s space, as shown in Figure 5.45 (points 5 & 8). The values of suction were also measured using tensiometers (Hyprop) or a chilled mirror hygrometer (WP4C). To investigate the behaviour of lime-treated soil in the σ-s space, a third specimen was tested. The third specimen was initially compacted to 300 kPa at a moisture content of 20%, then wetted to a moisture content of 29.5%, under a stress of 2 kPa. The specimen was covered with plastic wrap and left for 4-8 hrs for equilibrium then cured for 7 days. As the moisture content of the specimen was 29.5%, the degree of saturation was approximately 70%, and subsequently, the specimen was close to the LOO. Therefore, to obtain the preconsolidation pressure, the rate of loading needed to be low to keep the pore air pressure equivalent to the atmospheric pressure. As mentioned in Section 3.5, the rate of stress was 4 kPa/min. The preconsolidation pressure was found to be 210 kPa. From Figure 5.45, it can be noticed that the behaviour of stabilised soil (Loading-Collapse) in σ-s space is represented as an approximately linear line. Furthermore, the Loading-Collapse path for untreated soil occurred at a range of suction higher than that for lime-treated soil.

To represent the points in Figures 5.44 & 5.46 (from Alonso's model) onto the MPK framework, a new equivalent plot was developed, as shown in **Figures 5.47** & **5.48**. As the MPK framework considered the moisture content as the main variable instead of suction, Figure 5.45 (in σ-s space) was converted to **Figure 5.49** (σ-e_w space). These results were matched with the findings of this study (see section 5.4).

To compare the collapse and swelling potential according to the Alonso et al. (1990) model and the MPK framework, **Figure 5.50** was plotted. Figure 5.50 shows that the MPK framework obtained collapse and swelling values that were close to the results obtained using the Alonso et al. (1990) model.

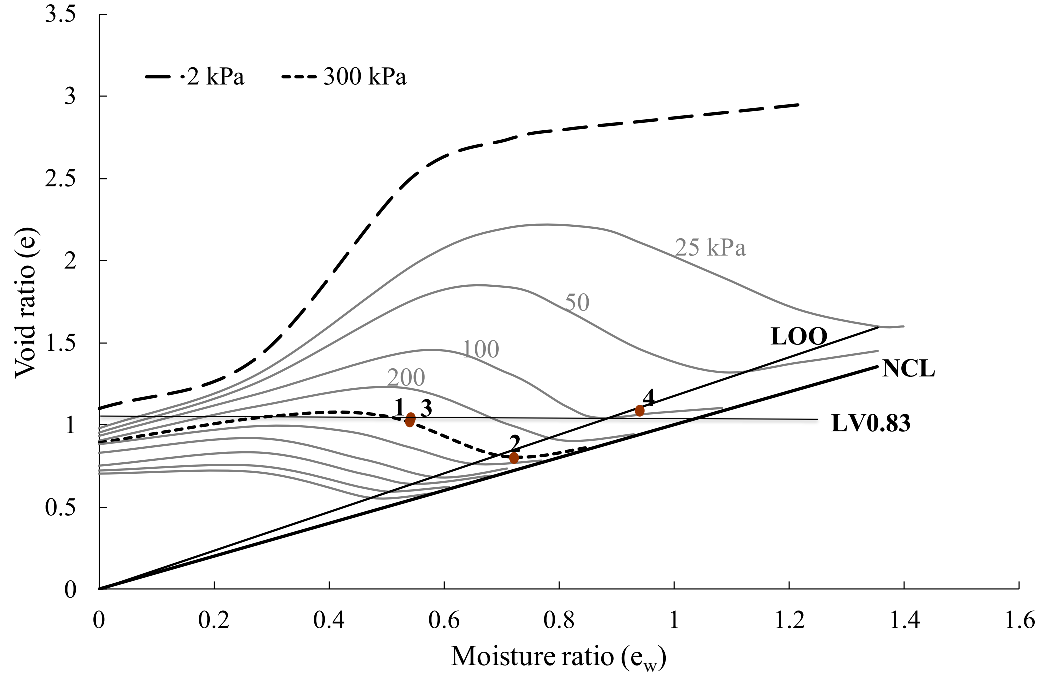

Figure 5.47. Preconsolidation stresses for saturated and unsaturated specimens and mechanism of collapse and swelling according to the MPK framework (untreated soil)

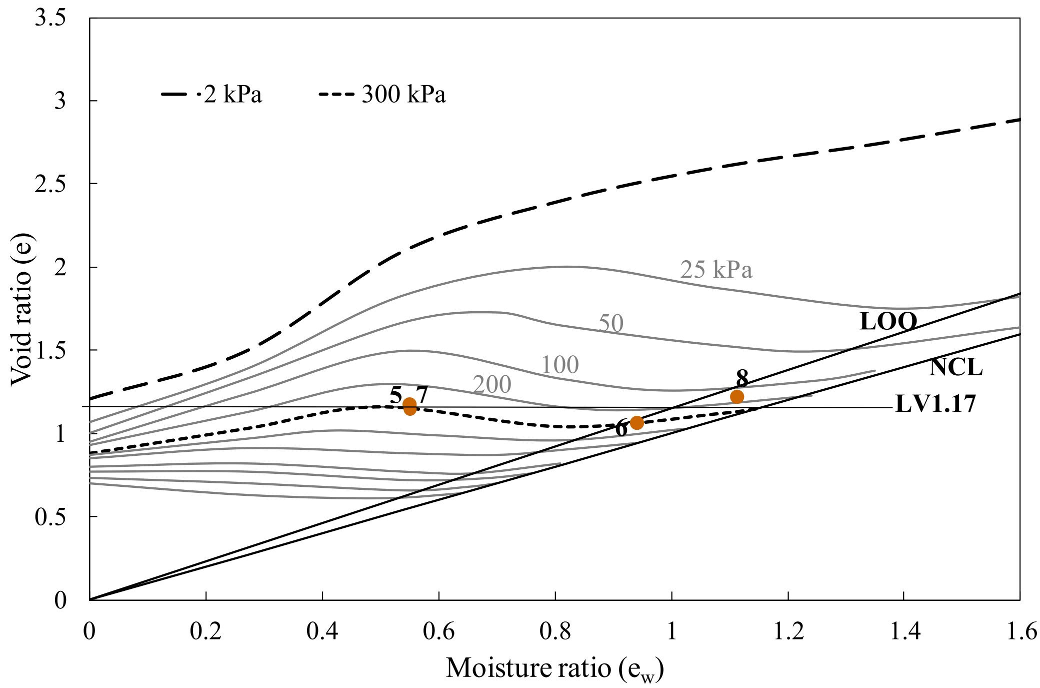

Figure 5.48. Preconsolidation stresses for saturated and unsaturated specimens and mechanism of collapse and swelling according to the MPK framework (lime-treated soil)

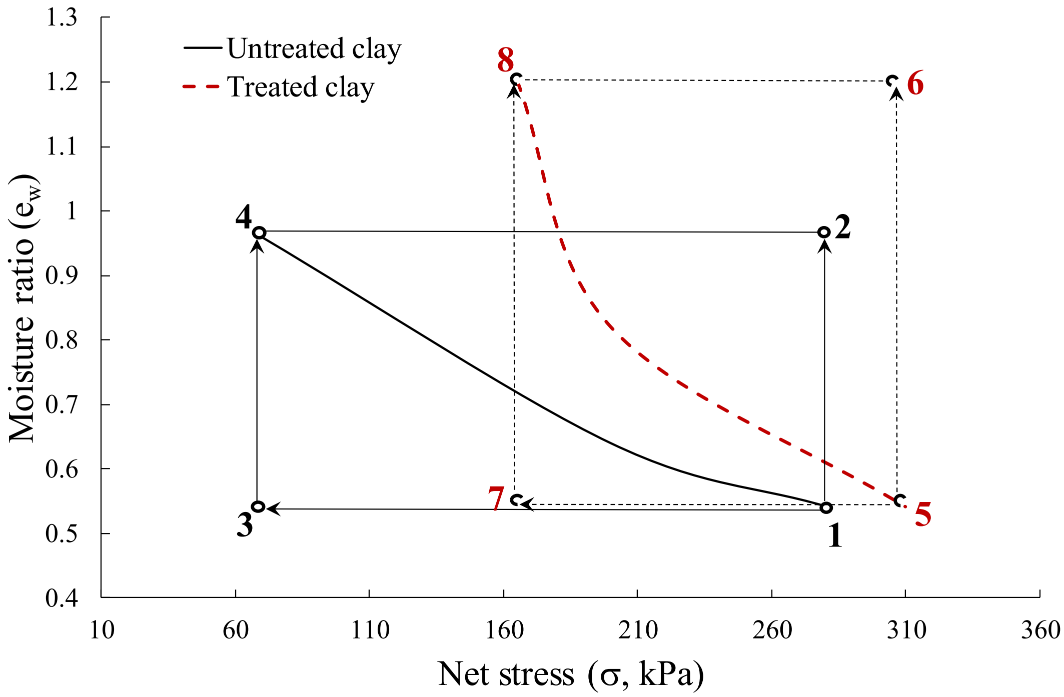

Figure 5.49. Yield curves for the untreated and lime-treated soils in σ-e_w space

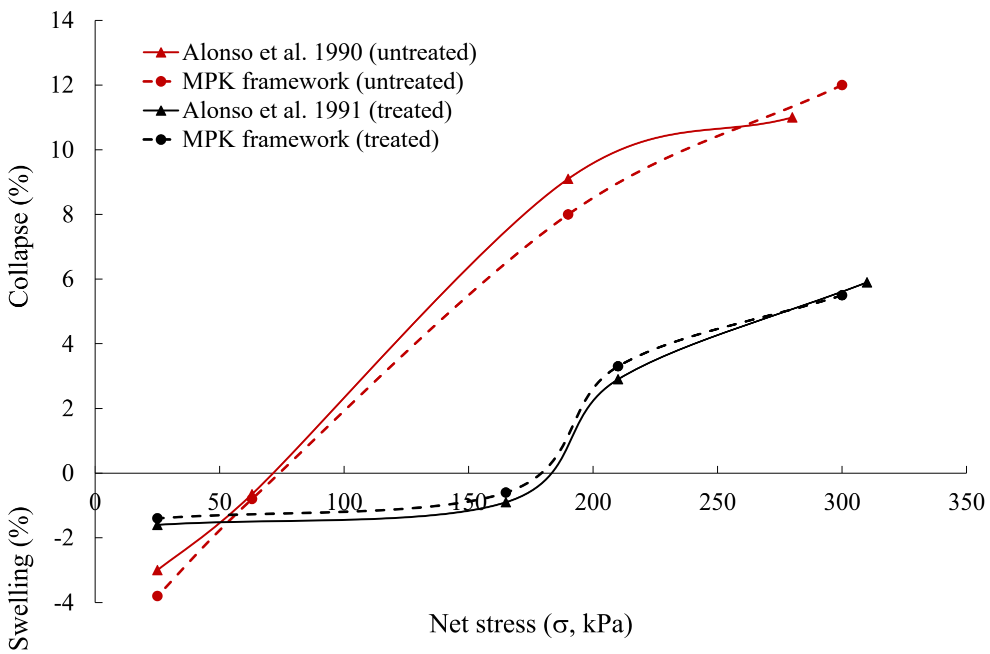

Figure 5.50. Collapse and swelling potentials for untreated and lime-treated soil according to Alonso et al. (1990) and the MPK models

5.9 Conclusions

A series of laboratory tests were performed to investigate the volumetric behaviour of an unsaturated compacted expansive clay, as well as an expansive clay stabilised with lime at the OLC. The expansive clay material selected was a residual soil derived from a Quaternary Basalt deposit located in Victoria, Australia. The suitability and validity of the MPK framework were examined by applying different state paths, such as loading-wetting, loading-wetting-loading, loading-unloading-wetting, loading-unloading-wetting-unloading-wetting, collapse potential and swelling potential. Furthermore, the swelling and collapse potential were tested under a wide range of moisture contents and stress levels, with special attention given to the effect of stress history and operational stress on the swelling and collapse behaviour. The following conclusions were reached:

1- The behaviour of all soil specimens tested during loading, unloading and wetting closely followed the MPK framework proposed by Kodikara (2012). However, the outcome of the current research suggests that the MPK framework did not extend to specimens prepared at a degree of saturation less than 37% for untreated and 33% for lime-treated soil, then wetted under stress levels less than 1000 kPa and 500 kPa for untreated and lime-treated soil, respectively. Therefore, the Loading Wetting State Boundary Surface (LWSBS) can be divided into two parts. Part A, where the MPK was valid, can be represented as a cosine function. However, part B, where the MPK did not extend, was found to be represented as an exponential function.
2- For all specimens tested, it was noted that the void ratio value decreased as the moisture content increased for all stress levels due to the macroscopic structure build-up. However, this relation reversed for very low moisture contents (when the degree of saturation was less than 37% for untreated soils and 33% for lime-treated soils). The occurrence of this feature is similar to having compaction curves with multiple peaks, and appears to be related to the weakening of the effect of suction to form stronger contacts among aggregates that give larger macro void space.

3- Static compaction curves for the untreated expansive clay showed that the void ratio varied within a narrow range of moisture content (under a constant stress level), whereas, for the specimens treated with lime, the void ratio varied over a much greater range of moisture content.
4- The variation of the void ratio (at constant stress level) for the untreated clay specimens was higher than that of the lime-treated specimens. In addition, the void ratio variation decreased as the stress increased. This means that the collapse potential of the untreated clay was higher than the lime-treated clay. Furthermore, the treated specimens required more water to achieve maximum collapse.
5- For any specimen, by identifying the compaction stress and corresponding void ratio, a constant void ratio line (LV) can be plotted on the LWSBS. It is then straightforward to predict the collapse for any condition. The value of swelling can be neglected for each point located on the LV, and therefore the important behaviour that can be measured from the LV is a collapse.
6- If a specimen was unloaded to a stress above the LV, the specimen swelled only. The path of swelling depends on the gradient of the swelling path.
7- A certain LV for the untreated soil specimens involved a range of stress contours more than what this certain LV covers for lime-treated soil, which is evidence of soil property improvement.
8- At a constant moisture content, the value of collapse increased as the void ratio increased, whereas the initial dry density decreased and the compaction stress decreased. Furthermore, at the constant void ratio, the collapse potential increased as the moisture content decreased.
9- Maximum collapse values were achieved when a specimen was wetted under a stress equivalent to the compaction stress.
10- Hydrated lime contributed to improving the collapsibility of the expansive soil specimens tested from very high to high collapsibility, or from high to medium collapsibility. This means that the collapse potentials were significantly reduced after stabilisation and that these values should be considered.

The theory of one-dimensional consolidation was applied to the MPK framework to evaluate swelling and collapse potential. One-dimensional consolidation theory for unsaturated soil required the measurement of swelling and collapse potential under suction control. Suction produced hydraulic hysteresis between wetting and drying cycles (Fleureau et al. 1993); however, this issue did not appear when water was used (Fleureau et al. 2002). Therefore, the MPK framework was recommended to predict swelling and collapse potential. To achieve that for a specimen compacted at a planned moisture content and compaction stress level, the following steps should be considered:

1- The void ratio of the compacted specimen (at a planned condition) is measured (e_{com}),
2- Another specimen is prepared at a moisture content equivalent to the OMC, and then compacted to the planned stress level,
3- The corresponding void ratio (for the specimen in item 2) is calculated (e_{omc}),
4- By applying the values of e_{com} and e_{omc} in equation 5-13, the collapse potential can be predicted:

$$\textbf{Collapse potential}\ (\%) = \frac{\boldsymbol{e_{com}-e_{omc}}}{\boldsymbol{1+e_{com}}} \times \mathbf{100} \qquad 5\text{-}13$$

The mechanism of collapse and swelling according to the MPK framework was applied to the study of Alonso et al. (1990). The results showed that the collapse and swelling values obtained from these theories were very close to each other. To identify the specimen state (untreated or lime-treated) after wetting, the following steps should be considered:

1- The initial condition of that specimen should be identified (moisture content, void ratio and preconsolidation pressure (Pc_1)),
2- An identical specimen is saturated under a very small vertical stress (for example: 2 kPa) and subsequently, the preconsolidation pressure of the saturated soil (Pc_2) will be obtained,

3- If a specimen was prepared at the initial condition and then wetted under a stress level (Pc) between Pc_1 and Pc_2 ($Pc_2 < Pc \leq Pc_1$), the specimen will collapse,

4- However, for a specimen prepared at the initial condition and then wetted under a stress level lower than the preconsolidation pressure of the saturated soil Pc_2 ($Pc \leq Pc_2$), the specimen will swell.

CHAPTER 6. INFLUENCE OF LIME STABILISATION OF AN EXPANSIVE CLAY BASED ON VOLUMETRIC BEHAVIOUR AND SWCC

Although suction is not essential for the application of the modified MPK framework in many practical problems, the suction profile within the $e-e_w-\sigma$ space is important to complete the hydro-mechanical picture in the volumetric space. This extension will allow the development of constitutive models and the Soil Water Characteristic Curves (SWCC) more rationally in the future.

6.1 Introduction

This chapter presents the influence of lime stabilisation of an expansive clay soil based on volumetric behaviour and the Soil Water Characteristic Curve (SWCC). In this study, suction was used as a dependent variable on moisture content to describe swelling and collapse behaviour for untreated and lime-treated (4% lime) compacted expansive clay. This was achieved by using the Soil Water Characteristic Curve (SWCC), which represents the suction-moisture content relationship. The Loading Wetting State Boundary Surface (LWSBS) proposed by Kodikara (2012) was adopted as a yield surface to represent the volumetric behaviour of the unsaturated soil in void ratio vs. moisture ratio vs. net stress space. The expansive clay studied was the Braybrook soil (found in a western suburb of Melbourne, Australia). A series of laboratory tests were performed to interpret the influence of lime stabilisation of an expansive clay soil based on volumetric behaviour and the Soil Water Characteristic Curve (SWCC). As mentioned in Chapter 4, the standard Proctor compaction and one-dimensional swell tests were conducted to obtain the Optimum Lime Content (OLC) based on swelling potential. Static compaction tests were conducted to establish compaction curves at different net stresses, and subsequently, the LWSBS was generated as mentioned in Section 3.5 and Chapter 5. The Hyprop, filter paper and chilled mirror hygrometer (WP4C) equipment were used to measure the SWCC at and below the LWSBS at different net stress levels for untreated and lime-treated expansive clay. Finally, collapse and swelling potential were measured at various initial moisture contents and stress levels.

6.2 Test Results

6.2.1 Optimum lime content (OLC) and Loading Wetting State Boundary Surface (LWSBS) generation

A set of 1-D swell tests were conducted on both untreated and lime-treated samples, which were prepared at OMC and MDD based on standard Proctor compaction tests. The lime-treated specimens were cured for 1, 7 and 28 days (Zhao et al. 2014b). The specimens were placed in an oedometer device and saturated with distilled water under a pressure of 25 kPa, simulating field stress conditions. The swell results showed that a significant drop occurred for specimens that were treated with 2% lime, and reached zero with the addition of 4% lime (section 4.4.6).

For both untreated and 4% lime-treated specimens, the Loading Wetting State Boundary Surface (LWSBS) was obtained by generating compaction curves at various net stresses. Static compaction tests were conducted at different moisture contents to develop each compaction curve. The specimens were compacted statically with a moisture content varying from 0 to 50%, while the static compaction stress varied from 2 kPa to 4000 kPa. The stress of 2 kPa was considered as the loosest stress resulting from the weight of the loading cap. Figures 5.1 & 5.2 show the LWSBS for the untreated and 4% lime-treated specimens in the e-e_w, e-log(σ), and e-e_w-log(σ) spaces.

6.2.2 Interpretation of volumetric behaviour of unsaturated clay using the SWCC (untreated and lime-treated)

In this study, the SWCC was investigated at and below the yield surface of the LWSBS to interpret the volumetric behaviour. To obtain the SWCC at the LWSBS, suction values were measured under compaction stress (loading zone) at different moisture ratios. At a particular suction, the collapse value was obtained after adding water to a moisture content close to the LOO. The SWCC below the LWSBS was obtained by measuring suction values under a stress level lower than the compaction stress (unloading zone) at different moisture ratios. The corresponding swell was measured after the specimen was saturated.

6.2.2.1 Suction distribution at the LWSBS

The procedure to identify the suction distribution of the untreated and lime-treated clays at the LWSBS in e-e_w space was followed (see sections 3.6.4 & 3.6.5). **Figures 6.1** & **6.2** present the SWCC at the yield surface for the untreated and 4% lime-treated clay samples, respectively. The osmotic suction for the untreated clay was measured and was found to vary from 80 to 100 kPa. As the increase in cation concentration in the water leads to an increase in osmotic suction (Zhao et al. 2014a), the osmotic suction for the lime-treated clay was found to vary from 340 to 380 kPa.

By measuring void ratio values after compaction, the relationship between void ratio and matric suction is presented in **Figure 6.3**. It is important to note that the range of this relation started from a moisture ratio corresponding to the maximum void ratio. For the expansive clay used in this study, it was necessary to identify the moisture ratio range where the void ratio started from a maximum to minimum value for a certain net stress level. Figures 5.1 & 5.2 show that the maximum void ratio value occurred approximately at a degree of saturation of 37% and 33% for the untreated and lime-treated clay, respectively. Hence, for a certain net stress, the relationship between suction and void ratio was studied for the degree of saturation range starting from 37% and 33% to the Line of Optimums (LOO), as presented in Figure 6.3.

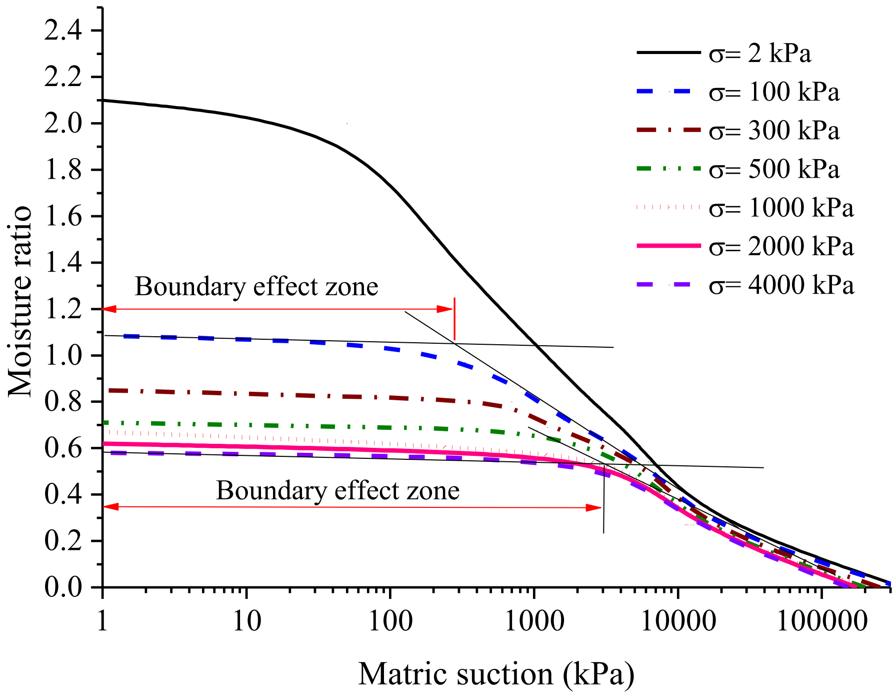

Figure 6.1. SWCC at the yield surface (untreated clay)

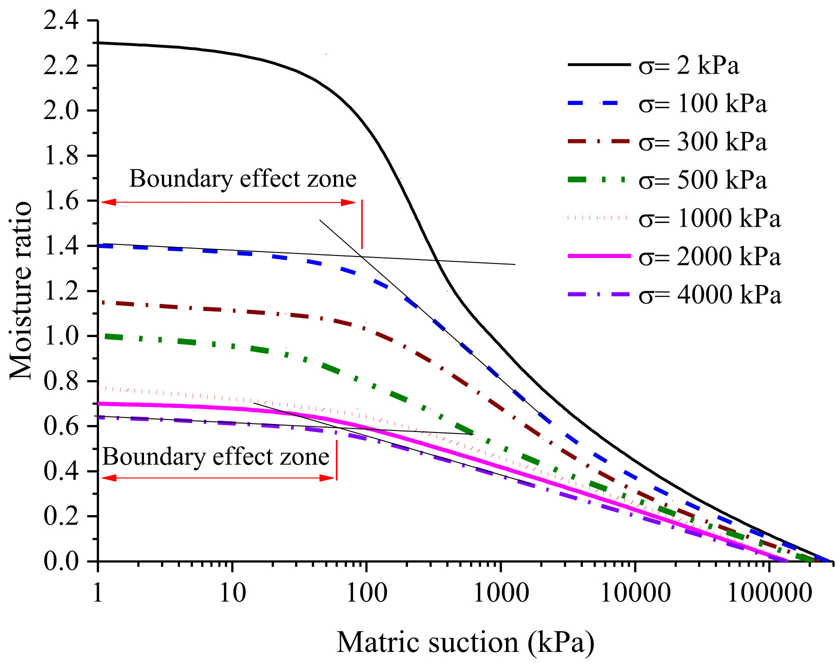

Figure 6.2. SWCC at the yield surface (4% lime-treated clay)

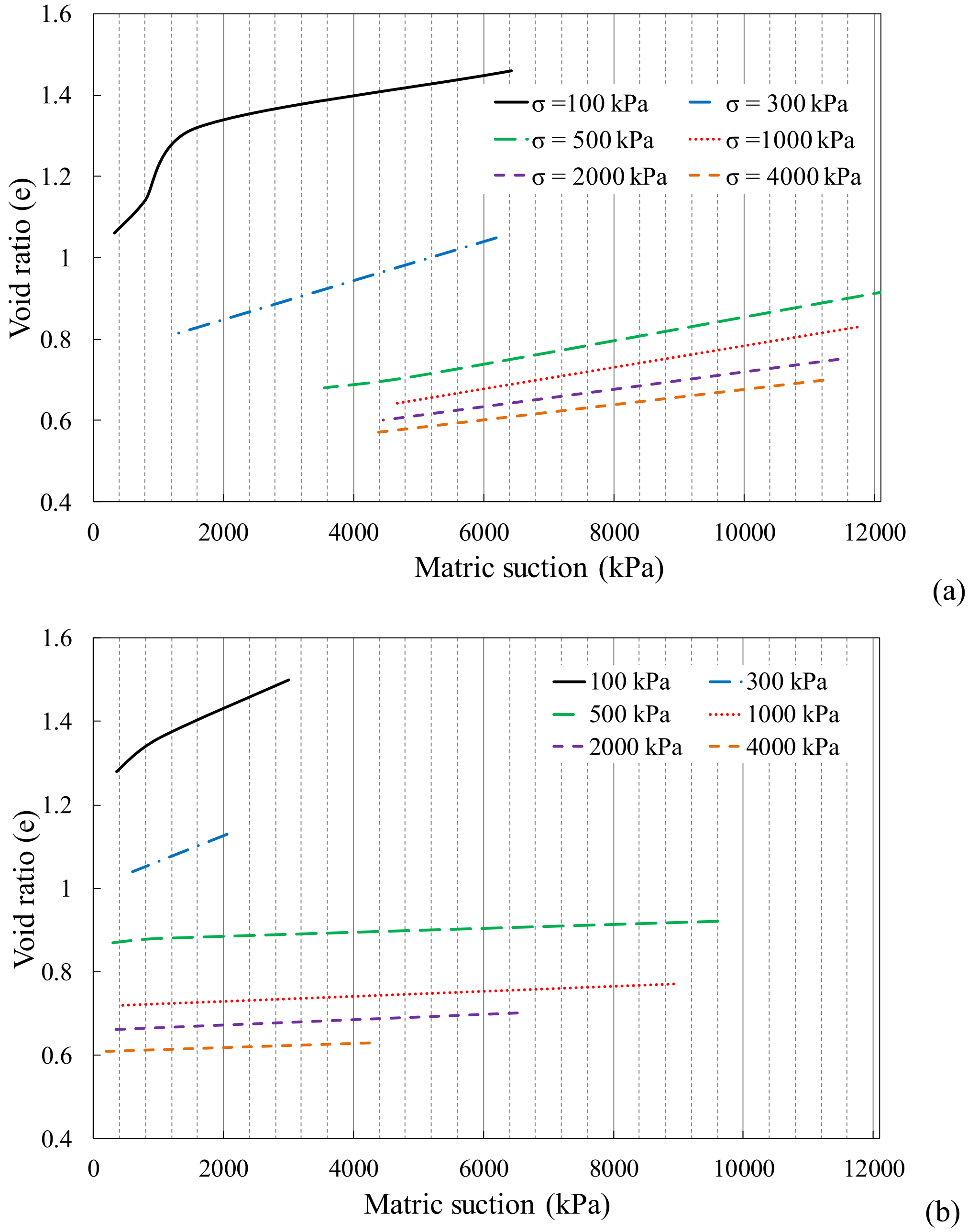

Figure 6.3. Void ratio-suction relationship at equal total vertical stress (at the LWSBS) (a) untreated clay (b) 4% lime-treated clay

By identifying the moisture ratio, void ratio, net stress and suction for each untreated and 4% lime treated specimen, the suction distribution at the LWSBS was plotted as shown in **Figures 6.4 & 6.5**.

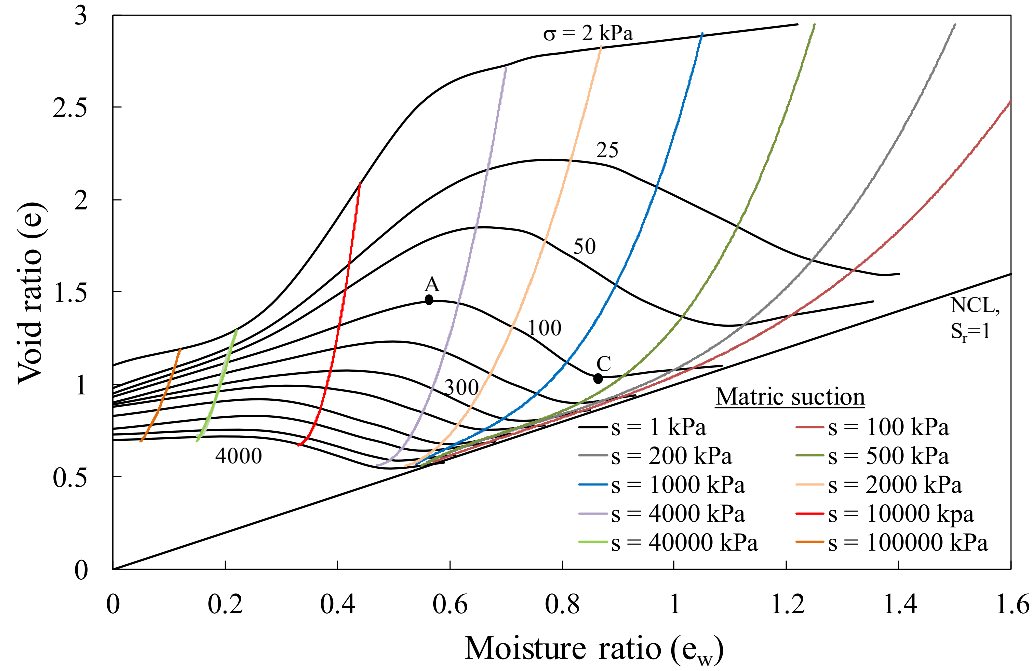

Figure 6.4. Suction distribution at the LWSBS (untreated clay)

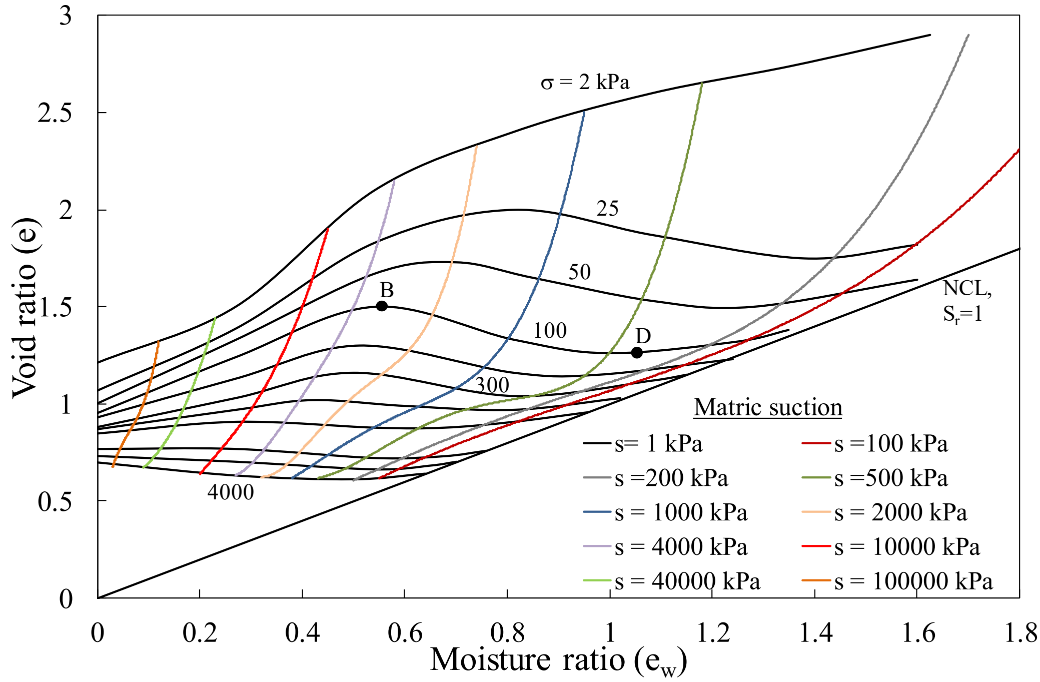

Figure 6.5. Suction distribution at the LWSBS (4% lime-treated clay)

As the slopes of the transition zone, presented in Figure 6.1, become closer after a suction value of 4000 kPa for the untreated soil, it can be noticed in Figure 6.4 (suction contours at the LWSBS for the untreated soil) that the void ratio-moisture ratio relationship followed the quadratic polynomial function (Equation 6-1) for suctions higher than 4000 kPa. However, it followed the cubic polynomial function (Equation 6-2) for suction below 4000 kPa.

$$\boldsymbol{e = ae_w{}^2 + be_w + c} \qquad 6\text{-}1$$

$$\boldsymbol{e = ae_w{}^3 + be_w{}^2 + ce_w + d} \qquad 6\text{-}2$$

where a, b, c and d are fitting parameters.

However, for lime-treated soil (Figure 6.5), the relationship between void ratio and moisture ratio for each suction contour was found to become more complex, as the slopes of the transition zone become closer after reaching a high suction (approximately after suction of 10000 kPa in Figure 6.2). Figure 6.5 shows that this relation followed a cubic polynomial function (Equation 6-2) for suction contours higher than 10000 kPa, while it followed the quartics polynomial (Equation 6-3) function for suction contours below 10000 kPa.

$$\boldsymbol{e = ae_w{}^4 + be_w{}^3 + ce_w{}^2 + de_w + f} \qquad 6\text{-}3$$

where a, b, c, d and f are fitting parameters.

6.2.2.2 Collapse Measurement

To interpret the influence of suction on the collapse behaviour of untreated and lime-treated soil, five sets of 1-D testing was conducted based on compaction stress values of 100, 300, 500, 1000, and 4000 kPa. **Figure 6.6** shows the collapse potential for specimens (untreated and lime-treated) compacted to different compaction and matric suction values, and then wetted to saturation.

To investigate the relationship between suction and the volumetric behaviour of untreated and lime-treated clays, two identical specimens were prepared at a certain moisture content and compacted statically to a certain compaction stress. For example, two identical untreated specimens were prepared at a moisture content of 21% (e_w =

0.57) and then compacted to a compaction stress of 100 kPa. The first specimen was used to measure suction, which was found to be 5300 kPa (point 1 in Figure 6.6). The second specimen was wetted under the same compaction stress to reach saturation condition. After wetting, the specimen volume reduced (i.e. collapsed) and volume changes were recorded until they became negligible. The collapse value was then calculated, which was found to be 17% (point 1 in Figure 6.6).

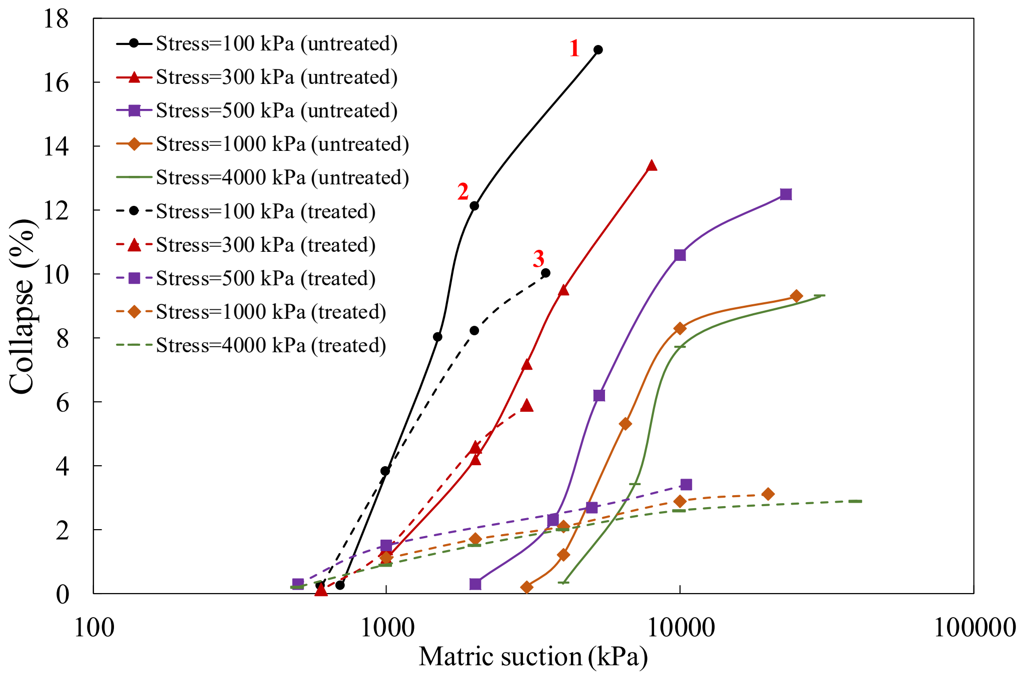

Figure 6.6. Influence of suction change on collapse value for the untreated and 4% lime-treated specimens

The other two untreated specimens were prepared at a moisture content of 26% (e_w = 0.704) and compacted to a compaction stress of 100 kPa. The first specimen was used to measure suction, which was found to be 2000 kPa (point 2 in Figure 6.6). The other specimen was wetted under the same compaction stress to reach saturation condition. After wetting, the specimen collapsed, and the collapse value was found to be 12.1% (point 2 in Figure 6.6). The same procedure was followed for the untreated specimens, which were prepared at different moisture contents and then compacted statically to the stress of 100, 300, 500, 1000, and 4000 kPa.

For the lime-treated specimens, the same process was followed, except that the specimens were cured for 7 days before suction and collapse values were obtained. For example, two identical specimens were prepared at a moisture content of 20.4% (e_w = 0.553) and then compacted to the compaction stress of 100 kPa. The suction and corresponding collapse values were found to be 3500 kPa and 10%, respectively (point 3 in Figure 6.6).

6.2.2.3 Suction distribution below the LWSBS for Untreated and Lime-Treated Clay

In order to develop the suction contours below the LWSBS, it was necessary to first measure and plot the SWCCs below the LWSBS. To achieve this, three groups of specimens were tested based on three different initial moisture ratios (**Figure 6.7)**. The first group included at least six identical dry specimens (moisture content of zero, e_w =0) compacted statically to a net stress of 1000 kPa, which were then unloaded to an operational stress of 2 kPa. The lime-treated specimens were cured for 7 days. Subsequently, each specimen was wetted with different amounts of water (S_r from 0 to 100%) at the operational stress of 2 kPa. After wetting, the volume changes were recorded and suction values were measured until the volume change became negligible. The SWCCs for the first group of untreated and lime-treated clay specimens are shown in Figure 6.7 (LU 0 1000 2).

The same procedure was repeated to obtain the SWCC for the second and third groups, with the difference being that the specimens were prepared at moisture contents 10% (e_w =0.271) and 20% (e_w =0.542) for the second and third groups, respectively. After unloading, the specimens were wetted from the moisture content equivalent to 10% for group 2 and 20% for group 3 to full saturation as shown in Figure 6.7 (LU 10 1000 2 & LU 20 1000 2). To cover a wide range of the SWCCs below the LWSBS, specimens were compacted under different initial moisture ratios to the compaction stress of 1000 kPa and then unloaded to different operational stresses, such as 25 kPa and 100 kPa, as shown in **Figures 6.8** & **6.9**.

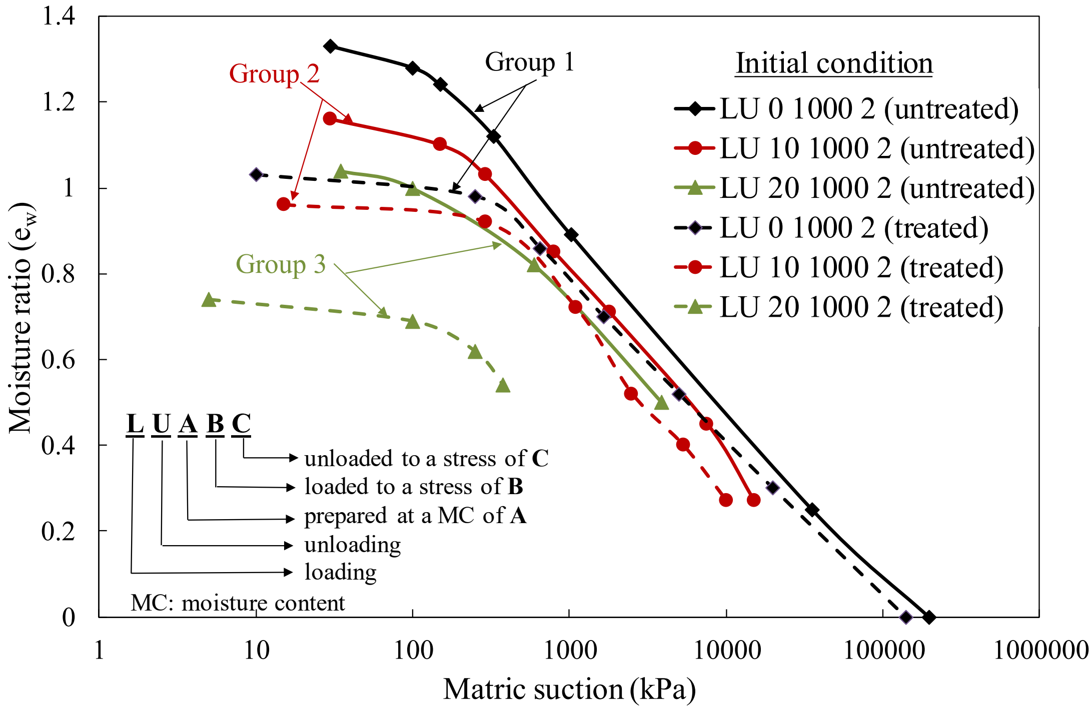

Figure 6.7. SWCC below the LWSBS for the untreated and 4% lime-treated specimens prepared at moisture contents 0, 10 & 20%, loaded to 1000 kPa, unloaded to 2 kPa, and then wetted

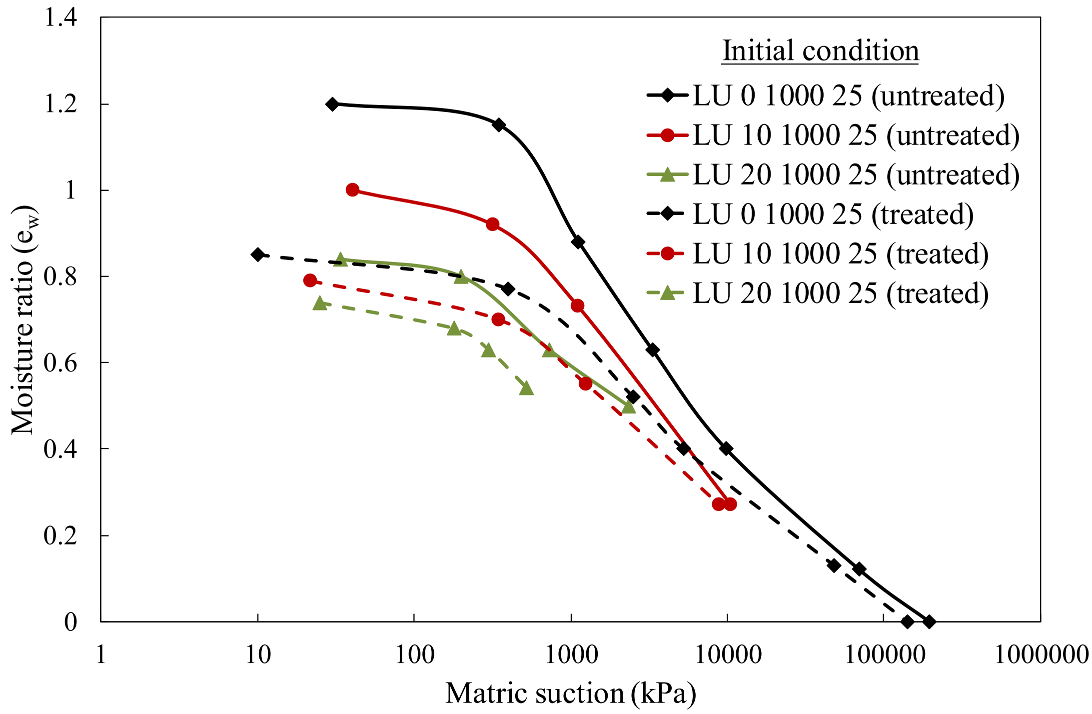

Figure 6.8. SWCC below the LWSBS for the untreated and 4% lime-treated specimens prepared at moisture contents 0, 10 & 20%, loaded to 1000 kPa, unloaded to 25 kPa, and then wetted

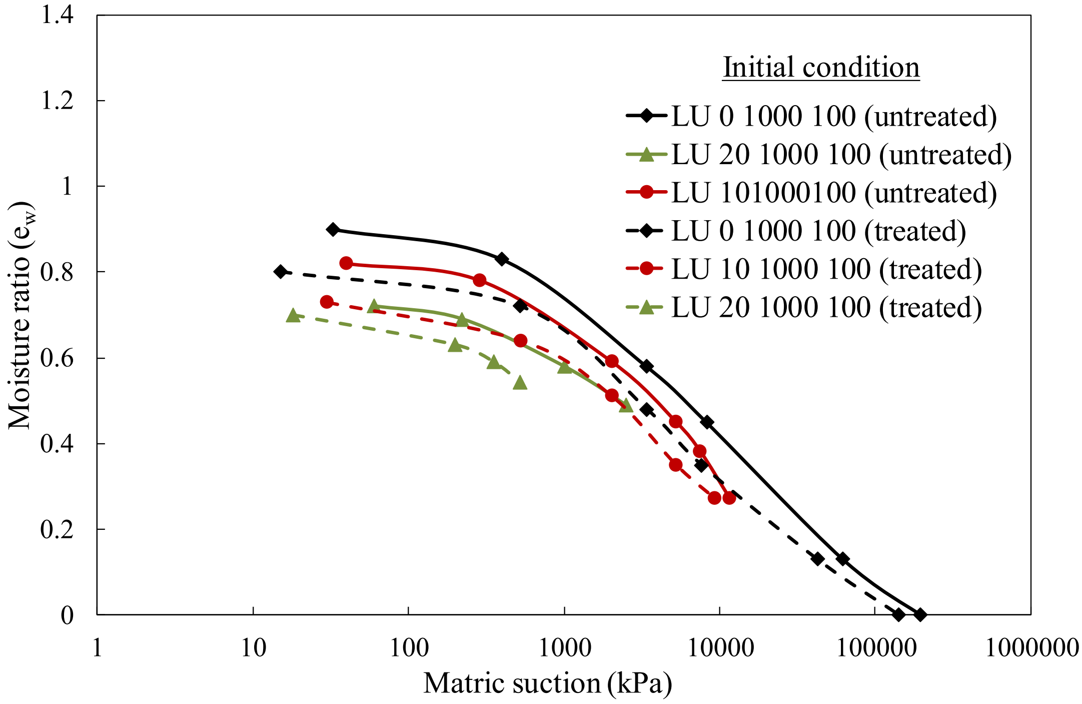

Figure 6.9. SWCC below the LWSBS for the untreated and 4% lime-treated specimens prepared at moisture contents 0, 10 & 20%, loaded to 1000 kPa, unloaded to 100 kPa, and then wetted

For the untreated and lime-treated specimens that were prepared at 0% moisture ratio and compacted to 1000 kPa, then subsequently wetted with different amounts of water under the operational stresses of 2, 25, 100 kPa, the specimen volume changes were measured after water was added. The void ratios were then calculated, and consequently, the relationship between void ratio and suction at a certain operational stress was obtained, as shown in **Figure 6.10**. By identifying the moisture ratio, void ratio, and suction for each untreated and lime-treated specimen, the suction contours in the e-e_w and e-e_w-log(σ) spaces at operational stresses of 2 kPa, 25 kPa, and 100 kPa were plotted (**Figures 6.11**, **6.12** & **6.13**).

From Figures 6.11, 6.12 & 6.13, it was obvious that for high suction contours, the e-e_w relationship followed an exponential function path (Equation 6-4). However, as soon as the suction contours approached the normally consolidated line (NCL), where the degree of saturation is equal to 100%, the e-e_w relation followed the quadratic polynomial function (Equation 6-1).

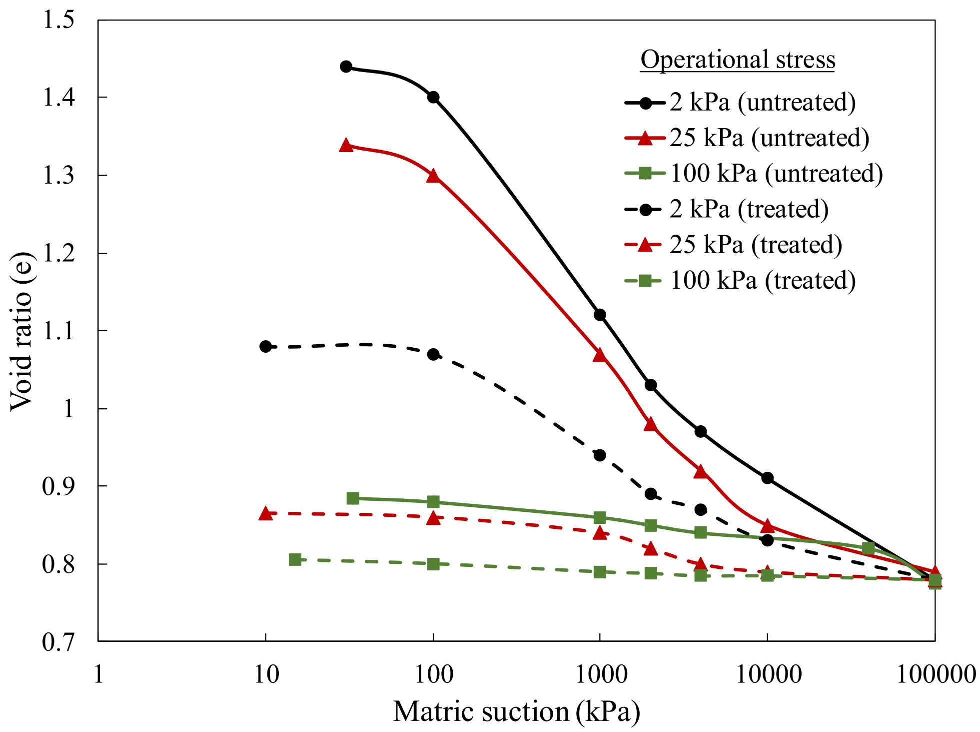

Figure 6.10. Void ratio-suction relationship at equal total vertical stress (below the LWSBS) for the untreated and 4% lime-treated clay

$$\boldsymbol{e = e_0 + a e^{\left(\frac{e_w - e_{w0}}{b}\right)}} \qquad 6\text{-}4$$

where e_0 and e_{w0} are the initial void ratio and moisture ratio, respectively, and a and b are fitting parameters. The proposed Equations (6-1) & (6-4) were compared to the experimental curves obtained from Figure 6.11 for the untreated clay. This comparison showed the validity of the proposed equations in describing the suction contours below the LWSBS, as shown in **Figure 6.14**.

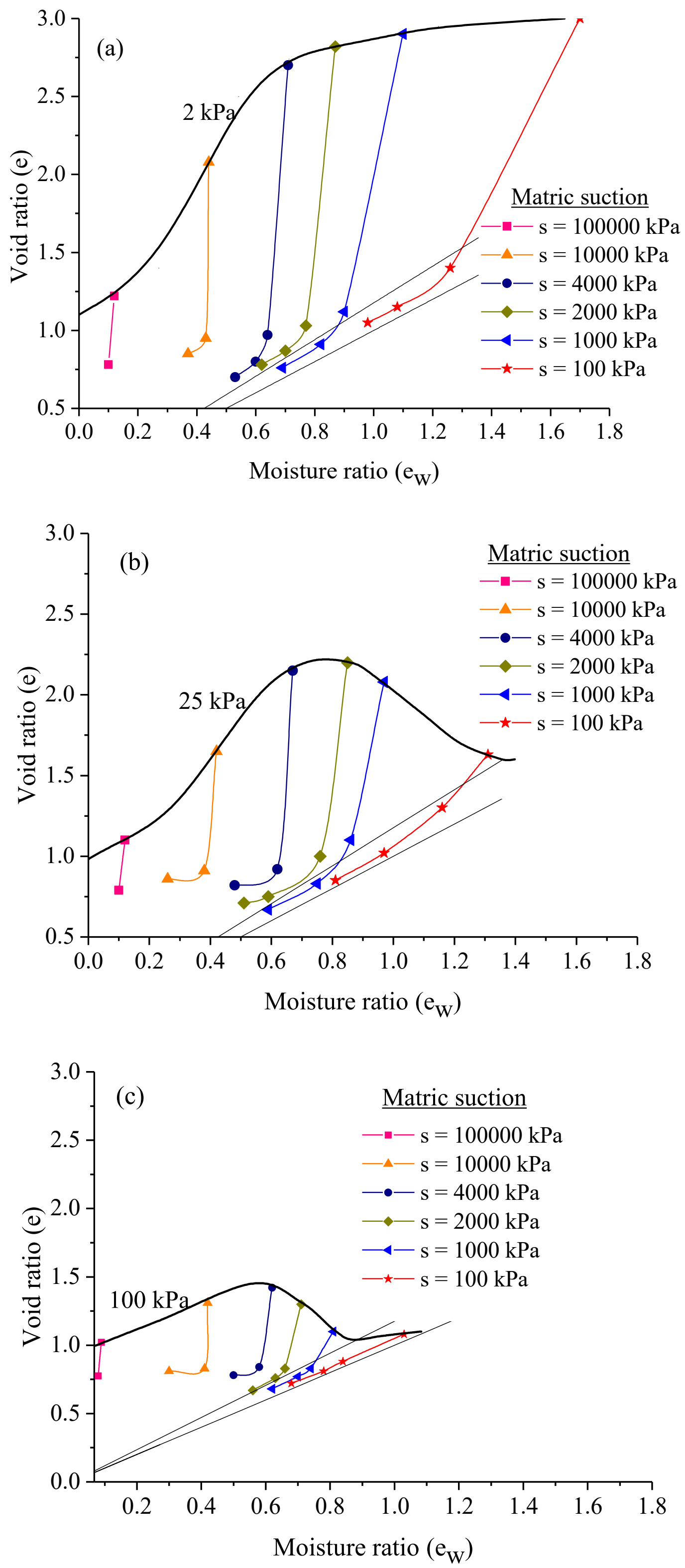

Figure 6.11. Suction contours below the LWSBS for untreated clay in e-e_w space at stress (a) 2 kPa (b) 25 kPa (c) 100 kPa

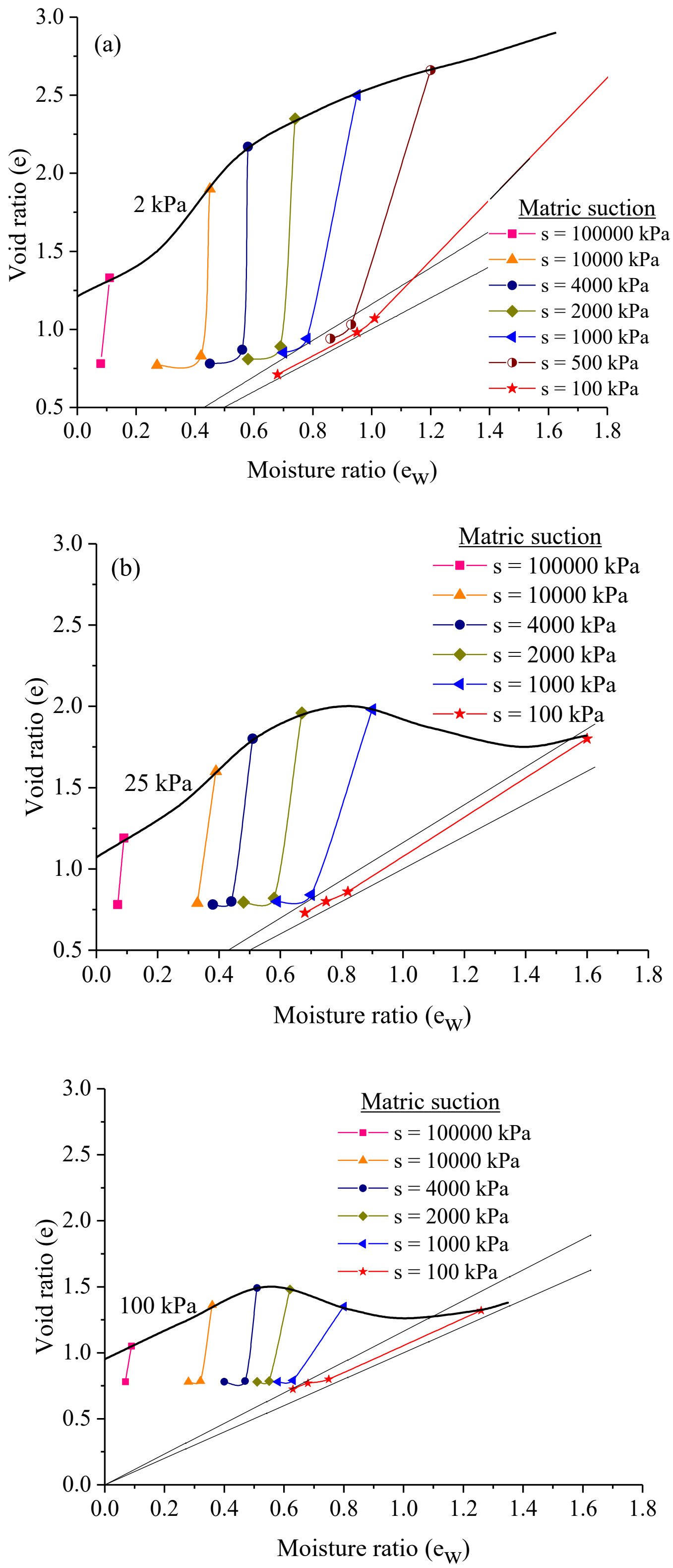

Figure 6.12. Suction contours below the LWSBS for 4% lime-treated clay in the *e*-e_w space at stress (a) 2 kPa (b) 25 kPa (c) 100 kPa

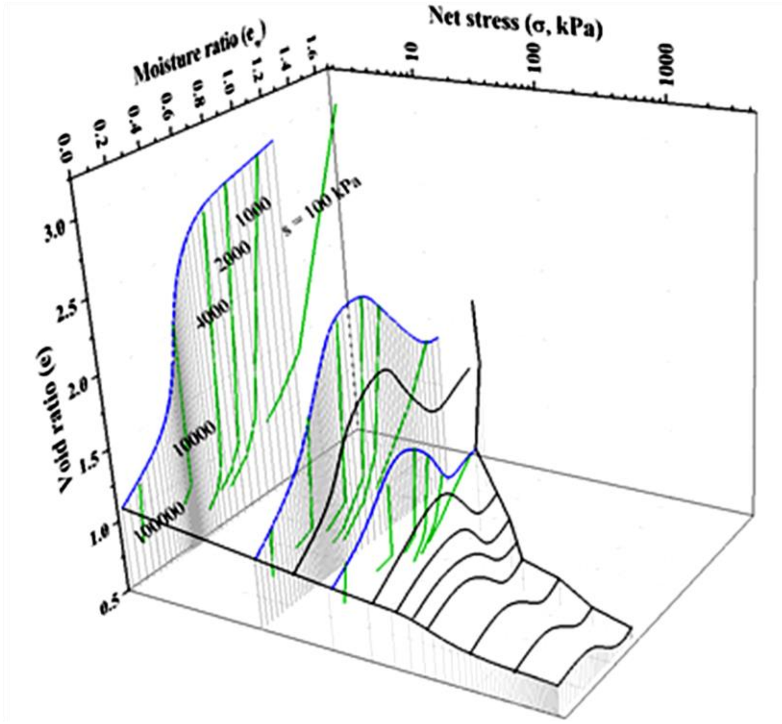

(a)

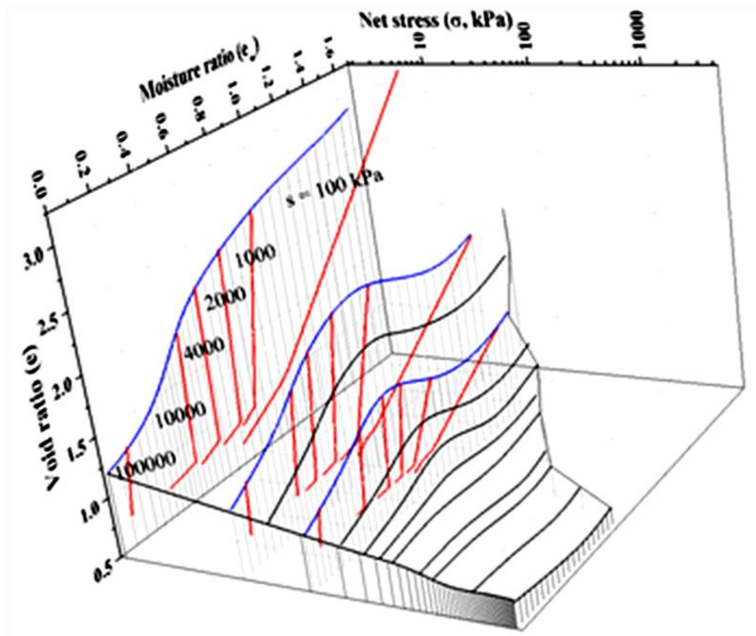

(b)

Figure 6.13. Suction contours below the LWSBS in the *e*-e_w-log(σ) space (a) untreated clay (b) 4% lime-treated clay

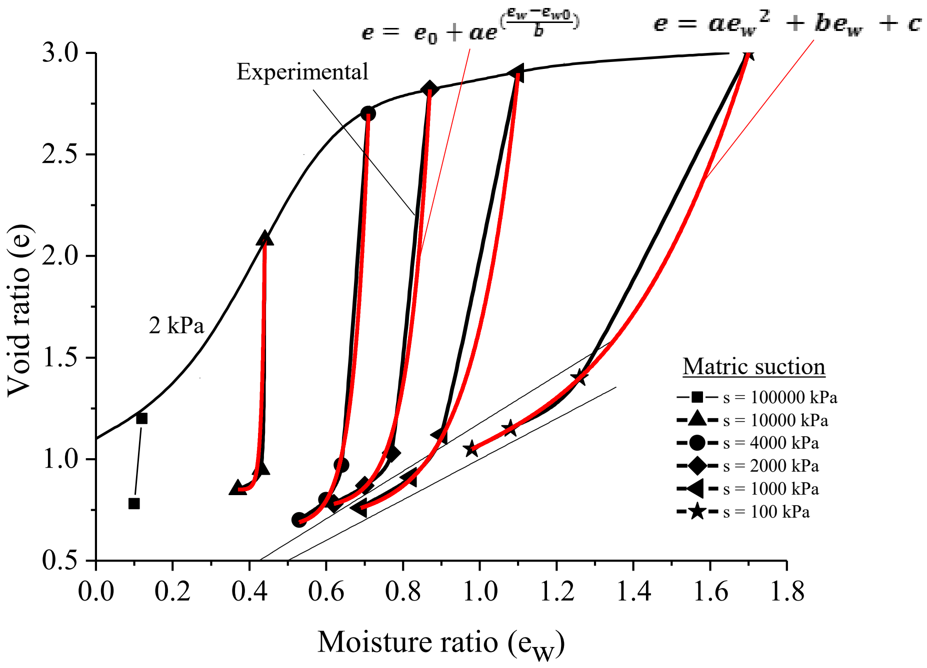
$e = e_0 + ae^{\left(\frac{e_w - e_{w0}}{b}\right)}$
$e = ae_w^{\ 2} + be_w + c$
Experimental
2 kPa
Void ratio (e)
Moisture ratio (e_W)
Matric suction
s = 100000 kPa
s = 10000 kPa
s = 4000 kPa
s = 2000 kPa
s = 1000 kPa
s = 100 kPa

(a)

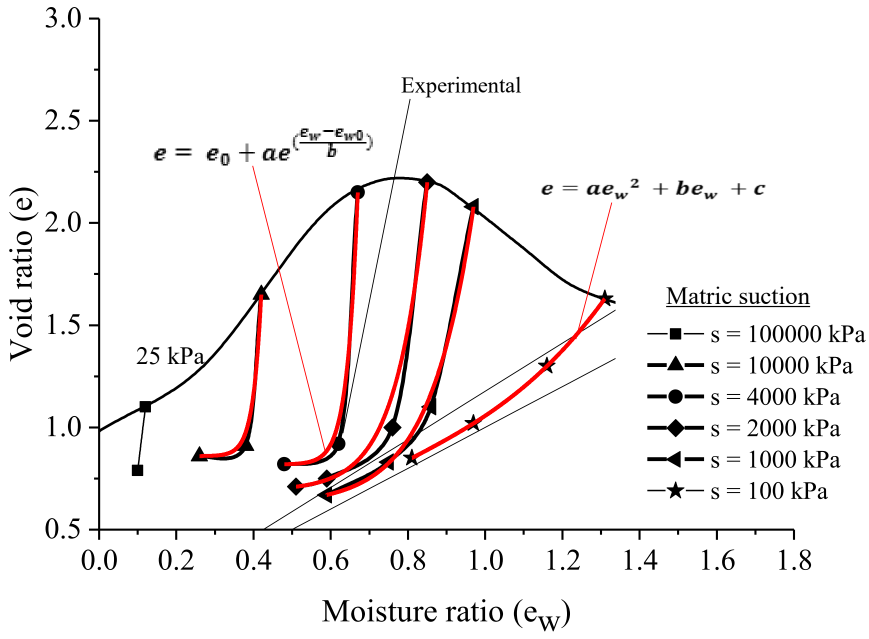
Experimental
$e = e_0 + ae^{\left(\frac{e_w - e_{w0}}{b}\right)}$
$e = ae_w^{\ 2} + be_w + c$
25 kPa
Void ratio (e)
Moisture ratio (e_W)
Matric suction
s = 100000 kPa
s = 10000 kPa
s = 4000 kPa
s = 2000 kPa
s = 1000 kPa
s = 100 kPa

(b)

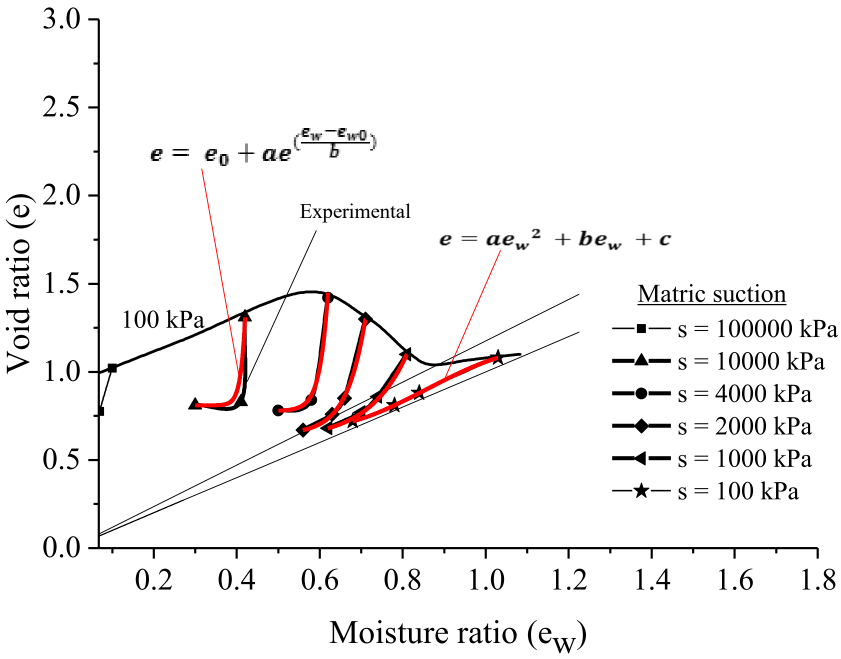

(c)

Figure 6.14. Validation of the proposed equations to describe the suction contours below the LWSBS

6.2.2.4 Swelling Measurement

To investigate the effect of suction on swelling behaviour for the untreated and lime-treated soils, specimens were again prepared and tested. These specimens were prepared in the same manner as previously for the collapse (section 6.2.2.2). The only exception was that the specimens were unloaded to a stress level less than the compaction stress (after loading), and then wetted to reach saturation.

The results of three sets of 1-D testing conducted based on operational stresses of 2, 25, and 100 kPa is presented in **Figure 6.15**. The first set included three groups based on moisture contents of 0%, 10%, and 20% (e_w =0, 0.271 and 0.542). The first group included preparing two identical specimens for the untreated and another two for the lime-treated soils at 0% moisture content (points 1 & 4 in Figure 6.15). The untreated and lime-treated specimens were compressed statically to 1000 kPa, and then unloaded to 2 kPa. The lime-treated specimens were cured for 7 days. Subsequently, one specimen (untreated or lime-treated specimens) was used to measure the suction by using the Hyprop or WP4C, and the values were found to be 190,000 kPa and 140,000 kPa for the untreated and lime-treated specimens, respectively (points 1 & 4 in Figure 6.15). The other specimen (untreated or lime-treated specimens) was then wetted until it reached saturation stage. After wetting, the volume of the specimen increased and the increase in volume change (i.e. swell) was recorded. Once this change became negligible, the test was stopped and the final swelling value was obtained. The final swelling value was found to be 30.1% for the untreated specimen and 14.8% for the lime-treated specimen (points 1 & 4 in Figure 6.15).

The same procedure was followed for the second and third groups with the change being that the specimens were prepared at moisture contents of 10%, $e_w = 0.271$ (points 2 & 5 in Figure 6.15) and 20%, $e_w = 0.542$ (points 3 & 6 in Figure 6.15), respectively. The same steps were repeated for the second and the third set of tests, with exception being that the operational stress was changed to 25 kPa and 100 kPa, respectively.

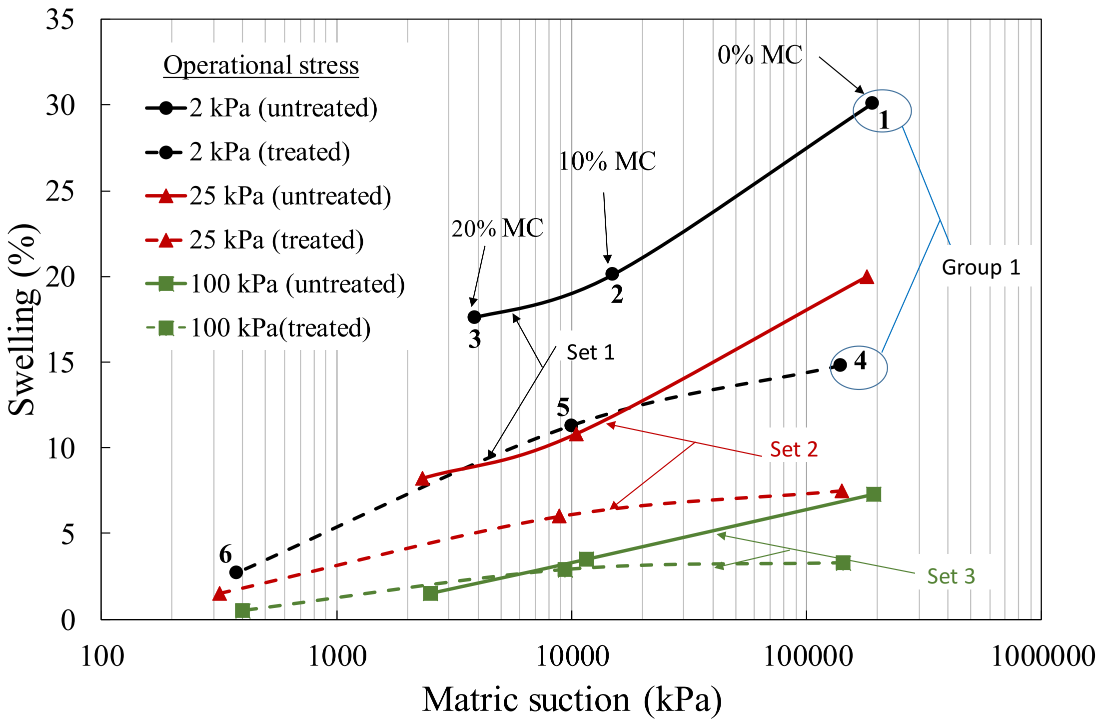

Figure 6.15. Influence of suction change on swelling behaviour (untreated and 4% lime-treated specimens were prepared at various moisture content, then loaded to 1000 kPa and then unloaded to different operational stresses)

6.3 Discussion

A large number of tests were performed on both untreated and lime-treated (4% lime content) residual expansive clay soil to investigate the influence of lime stabilisation (at the OLC) based on volumetric behaviour and the Soil Water Characteristic Curve (SWCC).

By measuring suction values for the untreated and lime-treated specimens after compacting them at different moisture contents and stress levels, the SWCCs at the yield surface were obtained, as shown in Figures 6.1 & 6.2. From these figures, it was evident that as the net stress increased, the SWCC moved downward. Figure 6.1 (for untreated soil) showed that the range of the boundary effect zone increased as compaction stress increased, with this zone extended from a suction value of 300 kPa (for a compaction stress of 100 kPa) to a suction value of 3000 kPa (for a compaction stress of 4000 kPa). This means that as the compaction stress increased, the void ratio decreased, and, consequently, higher suction was required to cause air to enter the pores of the soil. However, for the lime-treated soil in Figure 6.2, the average range of the boundary effect zone extended to the suction value of 80 kPa. This value, if compared with the untreated soil, indicated that the suction required to cause air to enter the pores of soil was less after treatment. The reason for this is the fact that the cation exchange process requires water to progress. The reduction in void ratio after stabilisation is less than that of the untreated soil (void ratio after stabilisation will be higher than that of untreated soil). Consequently, the suction force required to cause air to enter the pores of the treated soil is less than that of the untreated soil. To explain this point clearly, in Figures 6.4 & 6.5, for untreated and lime-treated specimens which were prepared at a moisture content of 20% (e_w =0.542) and compacted to 100 kPa (points **A** and **B**, respectively), the void ratios of untreated and lime-treated specimens were approximately 1.5. After wetting to the LOO, the void ratio reduced to 1 and 1.25 for untreated and lime-treated specimens (point **C** and **D**), respectively. The moisture ratio required to produce this reduction was 0.83 and 1 for untreated and lime-treated specimens, respectively. Hence, the suction required to enter the pores for untreated soil was higher than that required for the lime-treated soil.

For the untreated soil, the SWCCs in the boundary effect zone became closer for stresses higher than 500 kPa (Figures 6.1). However, the SWCCs became closer for stresses higher than 1000 kPa for the lime-treated soil (Figures 6.2). At a certain stress, the treated soil needed higher moisture content to reach full saturation compared to the untreated soil. The reason for this behaviour can be explained by the fact that the cation exchange process for lime-treated clay requires water to progress.

By focusing on the relationship between void ratio and suction for the untreated and lime-treated soils (Figure 6.3), it was obvious that the void ratio increased as suction increased for both the untreated and treated soils. Furthermore, the change in void ratio decreased as net stresses increased for both. In addition, the change in void ratio values for the untreated soil was higher than the lime-treated soil which is evidence of improvement.

The influence of suction on the volumetric behaviour of the untreated and lime-treated soils is presented in Figure 6.6. The figure shows that all specimens collapsed after wetting, and that the collapse values increased as specimen suction (directly after compaction) increased. Furthermore, the collapse values increased as compaction stress decreased. Although the expansive clay was treated with lime at the OLC, the lime-treated clay was considered to be categorised as highly collapsible (ASTM-D5333 2003; Rafie et al. 2008) when it was prepared at a suction higher than 2000 kPa and wetted under a compaction stress less than 300 kPa.

The SWCCs under the yield surface (LWSBS) for the untreated and lime-treated soils were presented in Figures 6.7, 6.8 & 6.9. It was evident that the first part of the SWCC (boundary effect zone) of the untreated specimen started with a moisture ratio higher than the lime-treated specimen. The reason for this behaviour was that the soil's behaviour below the LWSBS described the swelling path after adding water. This path either remained below the LWSBS after reaching saturation or reached the yield surface, which depended on the gradient of this path (α) (this will be further explained in Chapter 7). The swelling path gradient of the untreated soil was steeper than that of the lime-treated soil, meaning that the change in void ratio values for the untreated soil was higher than the lime-treated soil (evidence of improvement). Therefore, it was expected that the untreated specimen reached the saturation condition with a moisture content higher than that of the lime-treated specimen, and subsequently, the air entry value for the untreated specimen was less than that for lime-treated specimen. Furthermore, Figures 6.7, 6.8 & 6.9 showed that the difference in moisture content at saturation condition, for both untreated and lime-treated soils, decreased as operational stress increased. This was an indication that the drop in the swelling path gradient for the untreated soil was more than that of the lime-treated soil.

The relationship between void ratio and suction for specimens prepared at zero moisture ratio and compacted to 1000 kPa, then wetted at operational stresses of 2, 25, and 100 kPa for the untreated and lime-treated clays, was presented in Figure 6.10. It was evident that the void ratio decreased as the suction increased, and that the change in void ratio decreased as operational stress increased for both untreated and lime-treated soils. As the soil was treated with lime at the OLC and the OLC was measured under a surcharge pressure equivalent to 25 kPa, it was noted that the effect of suction could be neglected at operational stresses higher than 25 kPa.

The effect of suction below the yield surface on the volumetric behaviour of the untreated and lime-treated clays is shown in Figure 6.15. It showed that the specimens swelled after adding water, and the swelling values increased as the suction of the specimens (directly after unloading) increased at a constant operational stress. Furthermore, the swelling values decreased as the operational stress increased. It is also important to mention that significant swelling did occur when the lime-treated specimen was prepared at a suction ≥10000 kPa (moisture content ≤ 10%), then compacted to 1000 kPa, and then wetted under operational stresses ≤ 25 kPa, as shown in Figure 6.15. To check these results, two identical specimens were prepared at a suction of 10000 kPa

(10% moisture content), then loaded to 1000 kPa. One specimen was unloaded to 25 kPa, and then wetted to saturation. The swelling value was then obtained. The other specimen was cured for 7 days, and the same procedure was then followed to obtain the swelling value. It was noticed that the difference in swelling values was small and can be neglected. This behaviour can be attributed to the mechanism of the reaction between lime and clay. The first reaction began after adding water to the clay-lime mixture. The hydrated lime dissociated to Ca^{+2} and $2(OH)^{-1}$ ions, and consequently, the cation exchange, flocculation, and agglomeration started. That means enough water must be provided to start the stabilisation process. As a result, adding a small amount of water to the clay (the clay is still dry) does not affect the stabilisation process during curing. However, the OLC was obtained at OMC, and thus there was enough water to start the stabilisation process during curing.

6.4 Conclusions

The aim of studying the influence of lime stabilisation of an expansive clay based on volumetric behaviour and the SWCC was to develop the full profile of the soil suction for wetting and loading within the $e\!-\!e_w\!-\!\sigma$ space. A series of laboratory tests were performed to investigate the influence of lime stabilisation of an expansive clay soil based on volumetric behaviour and the Soil Water Characteristic Curve (SWCC). The yield surface was established for both untreated and lime-treated clays. The SWCCs were obtained at and below the surface at different stress levels. Furthermore, the collapse and swelling potential were tested under a wide range of moisture content and stress levels. By identifying the moisture ratio, void ratio, net stress and suction for each untreated and lime-treated specimen, the suction distribution at and below the LWSBS were represented mathematically. By measuring the SWCCs at the yield surface for untreated and lime-treated clays, the following conclusions were reached:

1- For untreated soil, the range of the boundary effect zone increased as the compaction stress increased. The air entry value varied from 300 kPa (for a compaction stress of 100 kPa) to 3000 kPa (for a compaction stress of 4000 kPa). Furthermore, the slopes of the SWCCs in the transition zone became closer to each other after a suction value of 4000 kPa.

2- The average range of the boundary effect zone extended to a suction value of 80 kPa for the lime-treated specimens. When compared to the untreated soil, this indicates that the air entry value reduced after treatment. The slopes of the SWCCs in the transition zone became closer to each other after high suction was reached (i.e. 10000 kPa).

3- At a certain stress, the lime-treated soil needed more moisture content to reach the full saturation condition than the untreated soil. The reason for this is the fact that the cation exchange process requires water to progress.

4- The void ratio increased as suction increased for both untreated and lime-treated soils. Furthermore, the change in void ratio decreased as net stresses increased for both. In addition, the change in void ratio values for untreated soil was higher than the lime-treated soil, showing evidence of improvement.

5- The suction contour paths in the e-e_w space were represented as a polynomial function for untreated and lime-treated clays.

6- After wetting under a certain compaction stress, the untreated and lime-treated specimens collapsed, and the collapse values increased as the specimen suction (directly after compaction) increased. Furthermore, the collapse values increased as compaction stress decreased.

7- Although the lime-treated specimens were stabilised with lime at the optimum lime content, these specimens were categorised as highly collapsible when the specimens were prepared at a suction higher than 2000 kPa and wetted under a compaction stress less than 300 kPa.

However, by measuring the SWCCs below the yield surface for both untreated and treated clays, the following conclusions were reached:

1- The first part of the SWCC (boundary effect zone) of the untreated specimen started with a moisture content higher than that of the lime-treated specimen.

2- The difference in moisture content at the saturation condition, for untreated and lime-treated soils, decreased as operational stress increased.
3- The e-e_w relations were represented as an exponential function for high suction contours, while a polynomial function represented the e-e_w relations for low suction contours.
4- After wetting under a stress less than the compaction stress, the untreated and lime-treated specimens swelled, and these values increased as the suction of the specimens (directly after unloading) increased at constant operational stress. Moreover, the swelling values decreased as the operational stress increased.
5- A significant swelling occurred when the lime-treated specimen was prepared at suction ≥10000 kPa (moisture content ≤ 10%) and compacted to 1000 kPa, then wetted under operational stresses ≤ 25 kPa.

As the MPK framework is not dependant on the suction parameter, any volumetric behaviour related to the loading and/or wetting of compacted unsaturated expansive clay, as well as an expansive clay stabilised with lime, can be explained by the LWSBS in the $e-e_w-\sigma$ space. However, knowledge of the suction profile within the $e-e_w-\sigma$ space can be useful to complete the hydro-mechanical picture in the volumetric space. Therefore, any future research can be directed to explain the suction according to the modified framework (incorporating the suction within the modified MPK framework) for an unsaturated compacted expansive clay, as well as an expansive clay stabilised with lime.

CHAPTER 7. BEHAVIOUR OF LIME-STABILISED AND COMPACTED EXPANSIVE SOILS UNDER CYCLES OF SWELL-SHRINK

To investigate the climatic effect on volumetric behaviour (for long-term) and consequently on the structural design, a set of cycles of swell-shrink tests were conducted on the untreated and lime-stabilised clays at different initial lime contents, moisture contents and net stress levels.

7.1 Introduction

This chapter investigates the swell-shrink behaviour of lime-stabilised compacted expansive soil from weathered quaternary volcanic geological deposits located in Western Victoria, Australia. These soils were stabilised with varying percentages of hydrated lime (2%, 3% and 4%), and the swell-shrink paths of both untreated and treated soils were studied. Two sets of specimens were prepared based on the initial moisture content, dry density and lime content. The first set included specimens with different lime content, compacted at the optimum moisture content and maximum dry density, and then subjected to cycles of swell and shrink tests under pressures of 6.25 kPa and 25 kPa. The second set included specimens prepared at optimum lime content and compacted at a moisture content lower than optimum moisture content, then subjected to cycles of swell and shrink tests below a pressure of 25 kPa. Vertical deformation and swell-shrink cycle relationships for the untreated and treated samples were obtained and analysed.

7.2 Experimental Program

A series of laboratory tests were performed to identify the behaviour of lime-stabilised and compacted expansive soils under cycles of swell-shrink. The first series of tests were conducted to classify the expansive clay characteristics before stabilisation, and included specific gravity, organic content, Atterberg limit and linear shrinkage, as mentioned in Chapter 3. The second series was conducted to find the optimum lime content based on swelling potential that included pH concentration, standard Proctor compaction and one-dimensional swell, as mentioned in Chapter 4. The third series was performed to investigate the effect of lime stabilisation on the swell-shrink path under cyclic conditions, which is the focus of this chapter.

7.3 Test Results

Two sets of specimens were prepared based on initial moisture content, dry density and lime content. To verify the results of this study, the data provided by Tripathy et al. 2012 was analysed.

7.3.1 Specimens prepared at OMC and MDD and lime content less than OLC

7.3.1.1 Swell- Shrink Cycles

Cycles of swell-shrink tests were conducted on untreated and lime-treated specimens, with 2% and 3% lime content (less than the optimum lime content of 4%). The specimens were compacted to the optimum moisture content and maximum dry density. The lime-treated specimens were all cured for 7 days. All specimens were then subjected to cycles of swell and shrink tests under pressures of 6.25 and 25 kPa. These tests were conducted using the oedometer device with some modifications, as shown in Figure 3.31, and following the procedure mentioned in Section 3.7. The swell-shrink tests were stopped when the vertical movement of swelling and shrinkage became equal to each other for each cycle (equilibrium).

It was noticed that shrinkage cracks were present in the specimens, which also caused a reduction in sample diameter. The cracks and reduction in diameter decreased as the lime content increased, as shown in **Figure 7.1**. This is a further indication that lime stabilisation contributed to reducing the plasticity and swelling of the expansive soils. The measured vertical deformations were converted to strain ($\Delta H/ H_o$) where ΔH was the change in height due to swelling or shrinkage and H_o was the initial height. The paths of vertical deformation for the untreated and lime-treated specimens under pressures of 6.25 and 25 kPa are presented in **Figures 7.2**. From this data, the variations in vertical swelling and shrinkage with swell-shrink cycles were then calculated, and have been presented in **Figure 7.3**.

0% Lime content

3% Lime content

Figure 7.1. States of the untreated and lime-treated specimens after four cycles of shrinkage

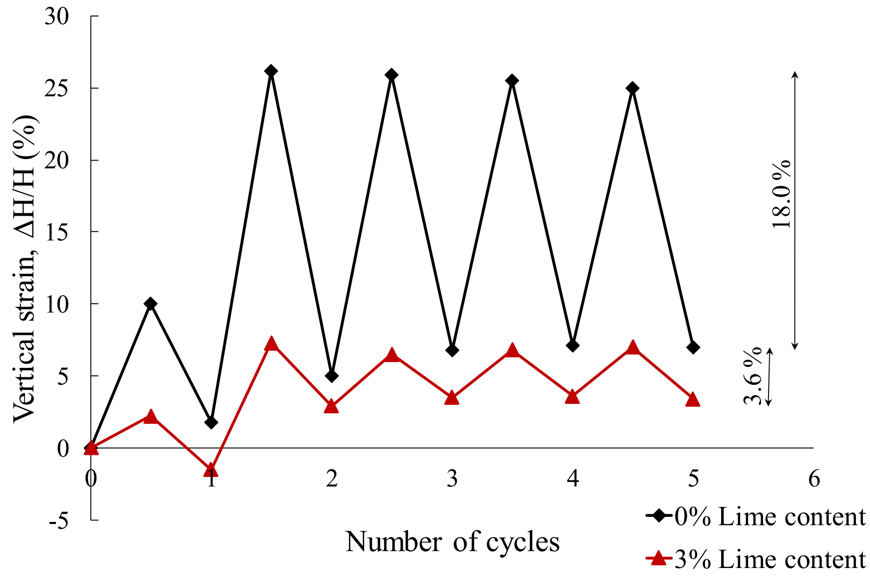

(a)

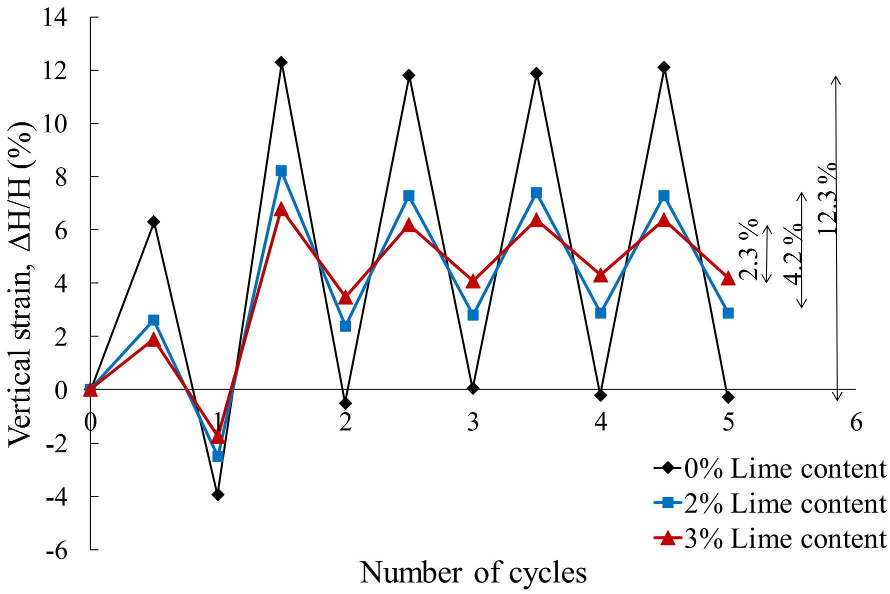

(b)

Figure 7.2. Vertical strain and swell-shrink cycles' relationship at pressure of (a) 6.25 kPa (b) 25 kPa

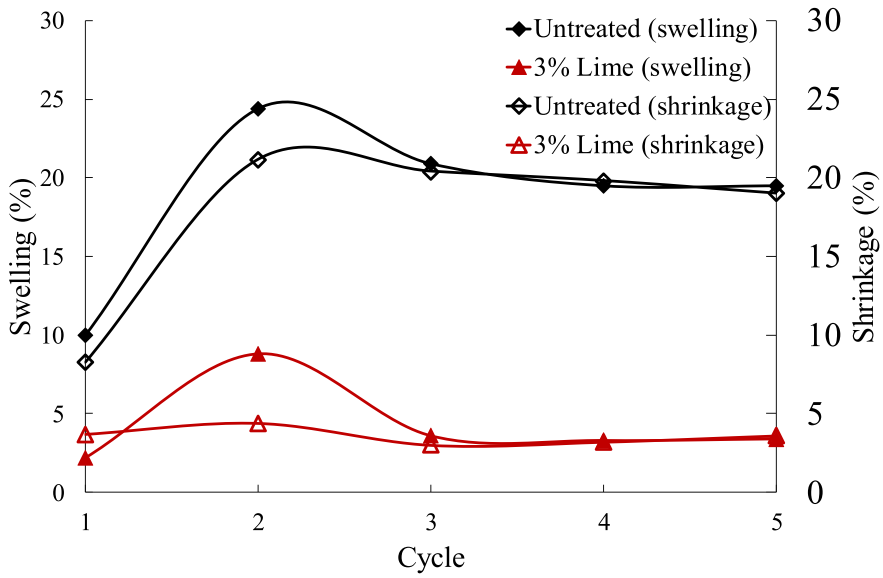

(a)

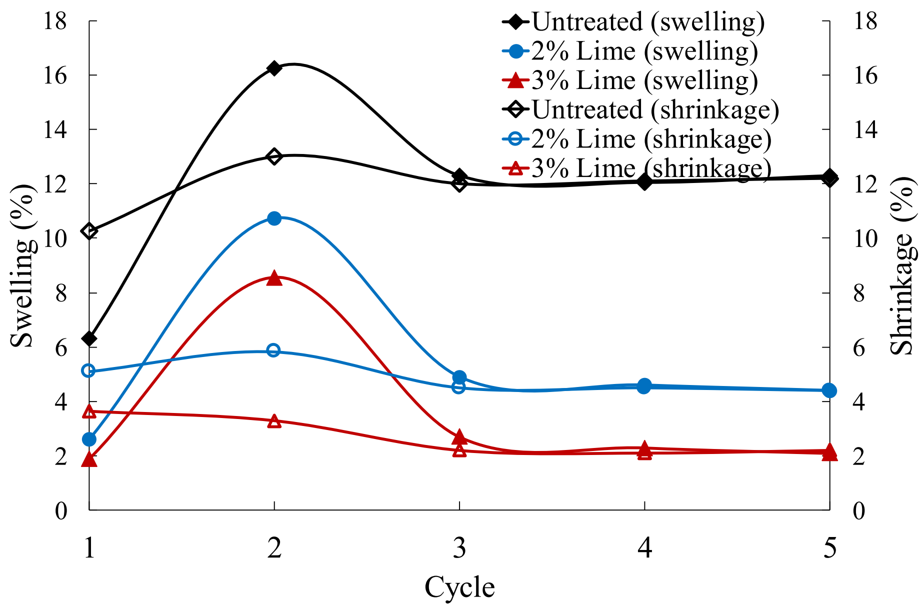

(b)

Figure 7.3. Variation in vertical swelling and shrinkage with swell-shrink cycles at a pressure of (a) 6.25 kPa (b) 25 kPa

7.3.1.2 Paths of Void Ratio- Moisture Content

At equilibrium condition and following the procedure mentioned in Section 3.7.2, after five cycles, the change in void ratio with moisture content was measured for both untreated and lime-treated specimens under pressures of 6.25 kPa and 25 kPa. By using the mathematical model proposed by Gould et al. (2011), the relationship of void ratio and moisture content for both samples at the equilibrium condition were plotted as shown in **Figure 7.4**. Each point represents an individual specimen.

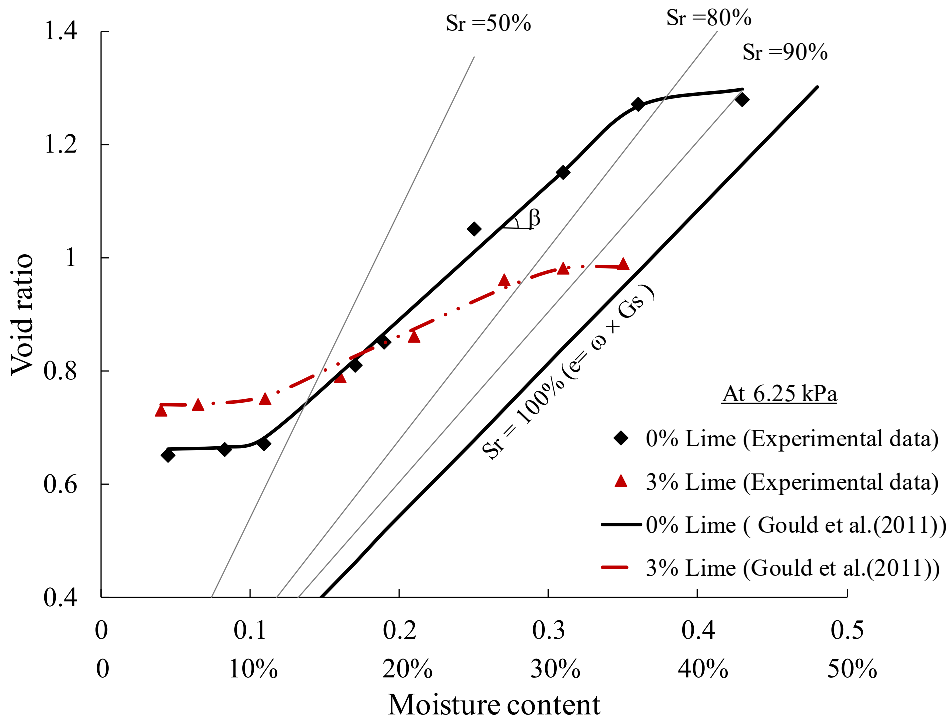

(a)

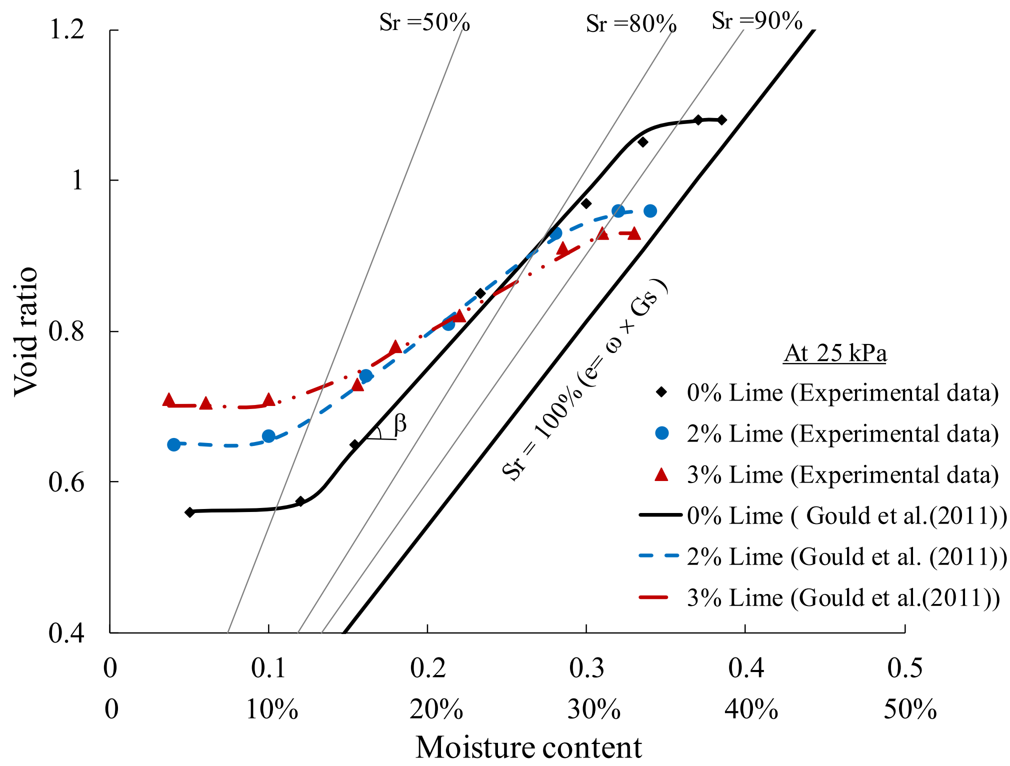

(b)

Figure 7.4. Void ratio-moisture content relation at equilibrium condition at (a) 6.25 kPa (b) 25 kPa

7.3.2 Specimens prepared at OLC and moisture contents less than OMC

7.3.2.1 Swell- Shrink Cycles

Cycles of swell-shrink tests were conducted on lime-treated specimens prepared at the OLC (4%) and moisture contents less than the OMC. Two specimen groups were prepared at 10% and 20% moisture content and 4% lime content, then compacted to stresses of 1000 kPa and 300 kPa, respectively. The specimens were allowed to cure for 7 days and then subjected to cycles of swell and shrink tests at 25 kPa. The procedure mentioned in Section 3.7 was followed to measure the vertical strain with swell-shrink cycles' relationship, as shown in **Figure 7.5**. From this data, the variations in vertical swelling and shrinkage with swell-shrink cycles were then calculated and have been presented in **Figure 7.6**.

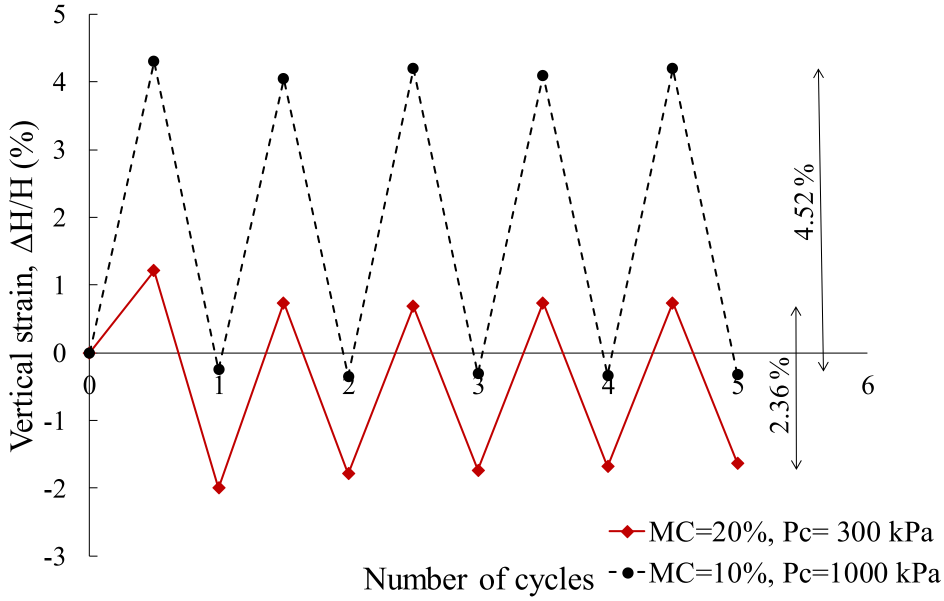

Figure 7.5. Vertical strain and swell-shrink cycles' relationship for specimens compacted at OLC (4%)

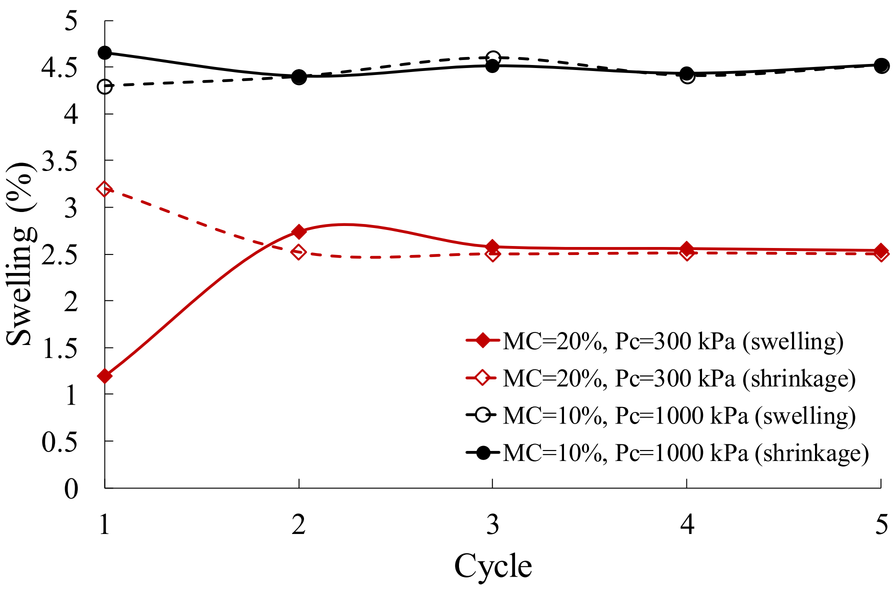

Figure 7.6. Variation in vertical swelling and shrinkage with swell-shrink cycles for specimens compacted at OLC (4%)

7.3.2.2 Paths of Void Ratio- Moisture Content

At the equilibrium condition and following the procedure mentioned in Section 3.7.2, after five cycles, the change in void ratio with moisture content was measured for each group under a pressure of 25 kPa. By using the mathematical model proposed by Gould et al. (2011), the relationship between void ratio and moisture content at the equilibrium condition were plotted as shown in **Figure 7.7**. Each point represents an individual specimen.

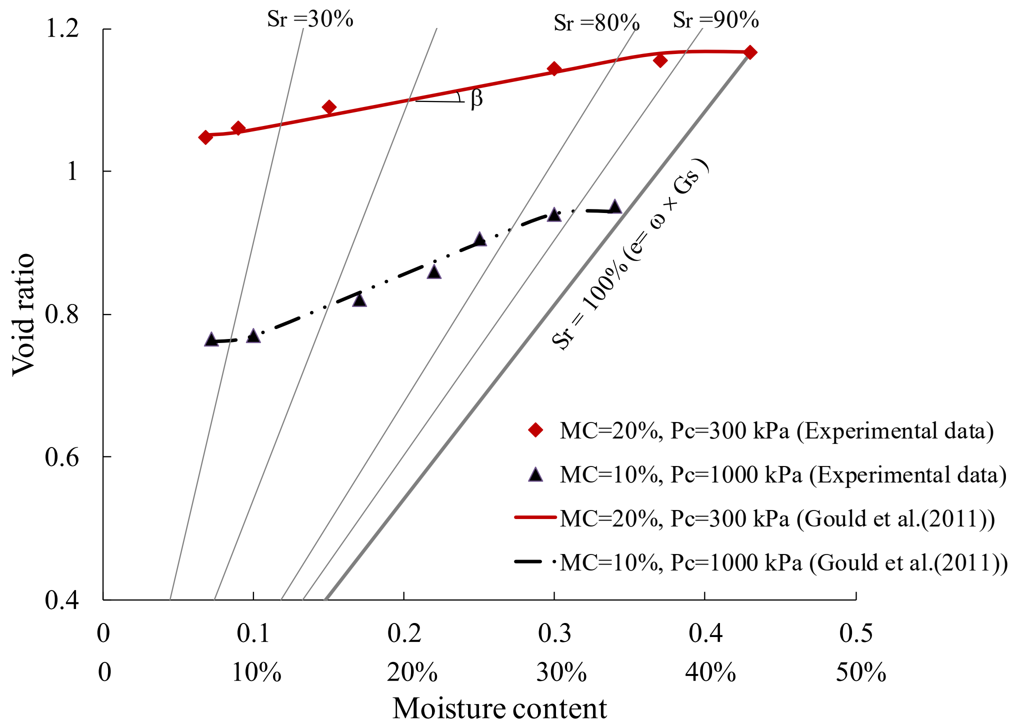

Figure 7.7. Void ratio-moisture content relation at equilibrium condition for specimens prepared at OLC (4%) under a pressure of 25 kPa

7.3.3 Study of Tripathy et al. 2012

To verify the results of the current study, the data provided by Tripathy et al. 2012 was analysed. Tripathy et al. (2002) studied the behaviour of compacted expansive soils under swell-shrink cycles. In this study, cyclic swell-shrink tests were performed on two compacted expansive soils at surcharge pressures of 6.25, 50, and 100 kPa until reaching an equilibrium condition. These soils were collected from the Northern

Karnataka State of India and named as **A** and **B**. The physical properties of these soils are shown in Table 7.1. These soils were compacted using standard Proctor compaction at different initial moisture contents and dry densities.

Table 7.1. Soil properties of the soils tested by Tripathy et al. (2002)

Characteristics	**Soil A**	**Soil B**
Specific gravity (G_s)	2.68	2.73
Grain size analysis Passing No. 200 sieve Sand content % Silt content % Clay content %	 98 2 36 62	 80 20 28 52
Atterberg limit Liquid limit (LL)% Plastic Limit (PL) Plasticity index (PI)	 100 42 58	 74 32 42
Free swell %	340	225
Standard Proctor Compaction Maximum Dry Density (MDD) kN/m^3 Optimum Moisture Content (OMC) %	 12.63 35	 14.13 30

A3 and **B3** specimens represented soils **A** and **B**, which were compacted at OMC and MDD (**Table 7.2**). **A1** and **B1** specimens represented soils **A** and **B**, which were compacted at moisture contents less than the OMC (at the dry side of the OMC). The moisture contents of **A1** and **B1** were 26% and 21%, respectively. The dry densities were 12.15 and 13.62 kN/m^3 for **A1** and **B1**, respectively. **A6** and **B6** represented soils **A** and **B**, which were compacted at moisture contents higher than the OMC (at the wet side of the OMC). The specimen **A6** was compacted at 41% moisture content and 12.15 kN/m^3 dry density, while specimen **B6** was compacted at 34.5% moisture content and 13.62 kN/m^3 dry density. All specimens were subjected to swell-shrink cycles under different surcharge pressures until reaching the equilibrium condition. Specimen **A3** was tested under surcharge pressures of 6.25, 50, and 100 kPa, whereas specimen **B3** was tested under surcharge pressures of 6.25 and 50 kPa. The specimens **A1**, **A6**, **B1**, and **B6** were tested under a surcharge pressure of 6.25 kPa. Moisture content–void ratio paths were then measured. This study concluded that the specimens reached the equilibrium condition after four swell-shrink cycles.

Table 7.2. Moisture content and dry density of soils tested by Tripathy et al. (2002)

Specimen	Moisture content (%)	Dry density (kN/m^3)
A3	35 (OMC)	12.63 (MDD)
B3	30 (OMC)	14.13 (MDD)
A1	26	12.15
B1	21	13.62
A6	41	12.15
B6	34.5	13.62

The data results of their study were analysed to investigate the effective or minimum cycles sufficient to achieve the equilibrium condition. The variation of vertical swelling and shrinkage with swell-shrink cycles were measured for specimens **A3**, **B3**, **A1**, **B1**, **A6**, and **B6**, as shown in **Figures 7.8**, **7.9**, **7.10**, and **7.11**, respectively.

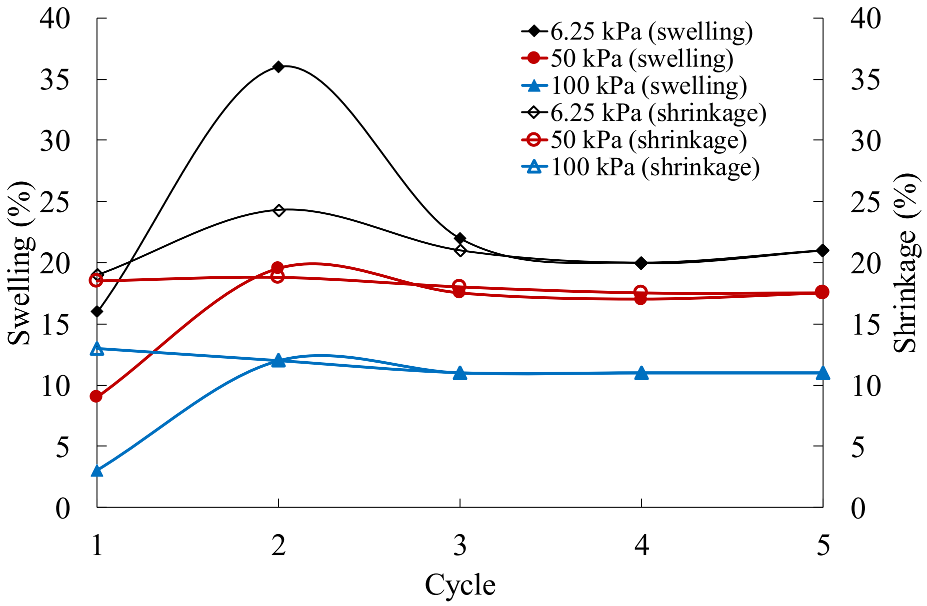

Figure 7.8. Variation in vertical swelling and shrinkage with swell-shrink cycles for specimen A3, from Tripathy et al. (2002) test data

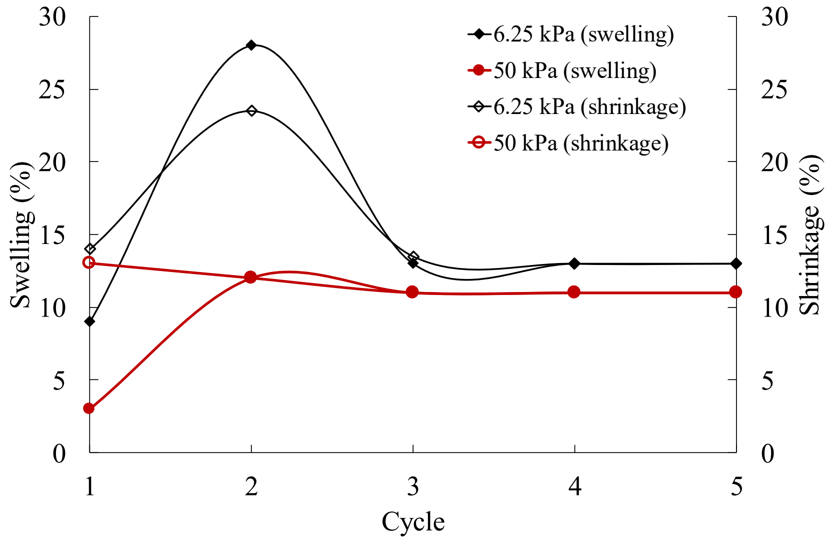

Figure 7.9. Variation in vertical swelling and shrinkage with swell-shrink cycles for specimen B3, from Tripathy et al. (2002) test data

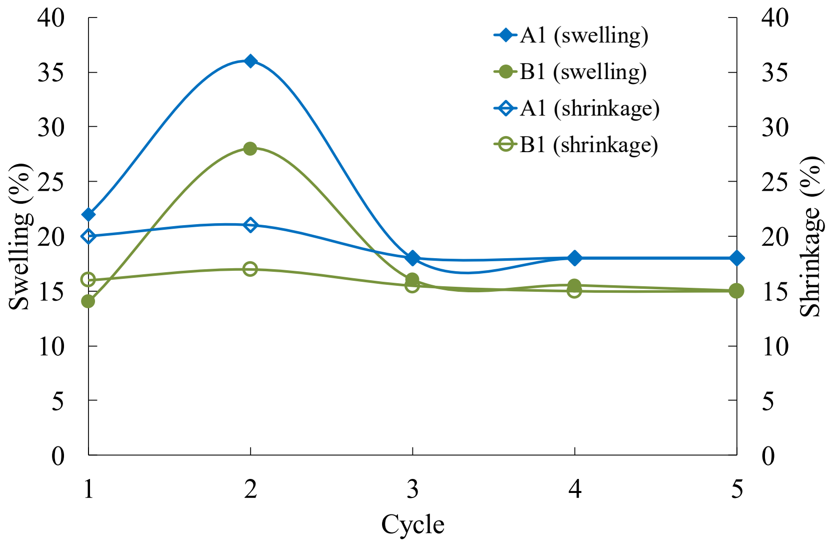

Figure 7.10. Variation in vertical swelling and shrinkage with swell-shrink cycles for A1 and B1, from Tripathy et al. (2002) test data

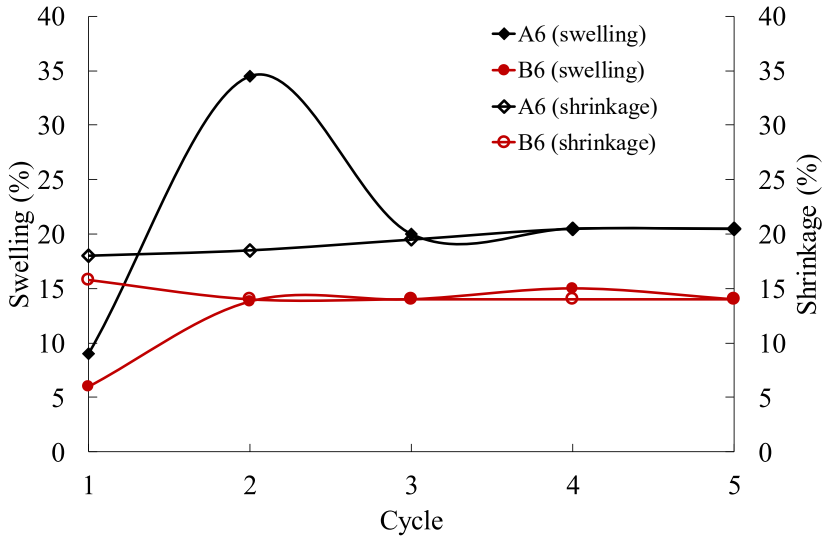

Figure 7.11. Variation in vertical swelling and shrinkage with swell-shrink cycles for A6 and B6, from Tripathy et al. (2002) test data

The study of Tripathy et al. (2002) also concluded that the specimens reached the equilibrium condition after four swell-shrink cycles, and that the variation in vertical swelling and shrinkage with swell-shrink cycles for all specimens prepared at different moisture contents and stress levels showed that the equilibrium condition occurred at either cycle three or four. However, based on the small swell-shrink difference after cycle three, one can assume the equilibrium occurred practically at the end of cycle three.

7.4 Discussion

According to the one-dimensional swelling test results, the optimum lime content for the expansive soil used in this study was 4%, with a minimum required curing time of 7 days. The effect of subjecting untreated and lime-treated specimens to cycles of swell-shrink was studied below and at the optimum lime content (after 7 days of curing) at different moisture contents and stress levels.

The vertical deformation during the swell-shrink cycle for the untreated and lime-treated specimens, prepared with lime contents below the OLC and at OMC and MDD, under surcharges of 6.25 kPa and 25 kPa, was presented in Figure 7.2. This figure showed that the maximum swelling occurred in the second cycle. This means that if a pavement is designed to rely on the results of a single swell-shrink test, it will be exposed to high swelling in the second cycle, which can result in premature damage or roughness.

The variation in vertical swelling and shrinkage with swell-shrink cycles at pressures of 6.25 kPa and 25 kPa, as presented in Figure 7.3, showed that the equilibrium condition occurred at either cycle three or four for both untreated and lime-treated specimens. However, based on a small swell-shrink difference after cycle three, one can assume that the equilibrium practically occurred at the end of cycle three. The study of Tripathy et al. (2002) showed that for all specimens prepared at different moisture contents and stress levels, the active cycle was cycle three, as shown in Figures 7.8, 7.9, 7.10 and 7.11.

It is evident from Figure 7.4 that the shape of the swell-shrink path for the untreated and lime-treated soil is an **S** curve, where the middle phase is almost linear. For the untreated sample, the swell-shrink path was approximately parallel to the saturation line. The gradient of this path (α) was 0.82 (Equation 7-1) for both surcharges of 6.25 kPa and 25 kPa. The gradient of the swell-shrink path in terms of void ratio and moisture content is β (Equation 7-2), as shown in Figure 7.4.

$$\alpha = \left(\frac{\partial e}{\partial e_w}\right)_\sigma = \beta / G_s \qquad 7\text{-}1$$

$$\beta = \left(\frac{\partial e}{\partial w}\right)_\sigma \qquad 7\text{-}2$$

However, the swell-shrink path for the lime-treated sample, compared to the untreated sample, became smaller and moved toward the saturation line with a smaller gradient (α). In addition, as the lime content increased, the swell-shrink path became flatter. The values of α for samples stabilised with 2% and 3% lime were 0.50 and 0.33, respectively.

The major volume change shown in Figure 7.4 occurred through the linear portion of the **S**-shaped curve. For the untreated sample surcharged under 6.25 kPa, the major volume change started when the sample reached approximately 45% saturation, and the volume change became minimal at 80% saturation. However, for the sample surcharged under 25 kPa, the major volume change started when the sample reached approximately 60% saturation, and the volume change became minimal at 85% saturation. On average, the major volume change occurred between 50% and 82% saturation. For the lime-treated sample, the significant and major portion of the volume change began at approximately 45% saturation, with the volume change becoming minimal at 90% saturation. The reason for this behaviour is due to structural changes in the pore structure of the lime-treated clay after adding lime. The value of swelling of the untreated sample is higher than that of the lime-treated sample, which means that the void ratio of the untreated sample is higher than that of the lime-treated sample. The relationship of void ratio and degree of saturation is an inverse relationship. This means that the same amount of water causes a different degree of saturation. Hence, the degree of saturation of the lime-treated samples will be higher than that of the untreated sample.

The vertical deformation during swell-shrink cycles for the lime-treated specimens prepared at the OLC and moisture contents less than the OMC (10% and 20%) was displayed in Figure 7.5. These specimens were compacted to 1000 kPa and 300 kPa, then exposed to swell-shrink cycles under a surcharge of 25 kPa. This figure showed that the maximum swelling occurred at the conclusion of the first cycle. This means the effect of swell-shrink cycles can be neglected for lime-treated specimens prepared at the dry side of OMC. The reason for this behaviour can be attributed to the reaction mechanism between lime and clay. The first reaction began after adding water to the clay-lime mixture, and consequently, the cation exchange, flocculation, and agglomeration started. This means that initially, the treated specimens did not have sufficient water to start the stabilisation process (curing can be neglected). Therefore, after adding water during the first cycle, the stabilisation process started; consequently, the swelling potential decreased (if it was compared with the untreated soil). The stabilisation process continued for the second and third cycles (curing is considered), and thus the swelling potential decreased with a value less than that obtained from the first cycle. Figure 7.5 also shows that the swell potential increased as compaction stress increased and moisture content decreased.

The variation in vertical swelling and shrinkage with swell-shrink cycles for specimens compacted at the OLC is presented in Figure 7.6. It is evident from the figure that the equilibrium condition occurred at cycle three as well. The void ratio-moisture content relation at the equilibrium condition for specimens prepared at the OLC under a pressure of 25 kPa (Figure 7.7) showed that as compaction stress decreased, the gradient of swelling decreased and the **S** shape became flatter.

7.5 Conclusion

A set of cycles of swell-shrink tests were conducted on untreated and lime-stabilised expansive clays at different initial lime contents, moisture contents and stress levels. These tests were performed under surcharge pressures of 6.25 kPa and 25 kPa. For specimens prepared at the OMC, MDD and lime contents less than the OLC, the results showed the following:

1- As soon as the untreated and treated soils reached equilibrium, the swell-shrink path became elastic, where the vertical displacement due to swelling and shrinkage became the same.
2- Both untreated and lime-stabilised samples reached an equilibrium condition after three swell-shrink cycles.
3- The maximum swelling occurred at the second cycle for all samples tested. This suggests a review of current design procedures is required for those that do not consider cyclic movements, as these procedures are underestimating the swell-shrink potential.

4- The gradient of the swelling and shrinkage path for the untreated expansive soil reached 0.82, while this gradient reduced to approximately a sixth and third when it was treated with 2% and 3% lime, respectively. This means that the shape of swelling and shrinkage became flattened after lime was added.
5- For the untreated samples, the critical volume change occurred between 50% and 82% saturation, whereas the critical volume change occurred between 45% and 90% saturation for the lime-treated samples. Therefore, the treated samples reached maximum swelling at a higher degree of saturation than the untreated samples.
6- For the untreated and treated samples, it is important to measure the swelling value from the first cycle, for short-term, to simulate the field condition after compaction. It is also important to consider the climate cycles to simulate the field condition for the long-term.

For specimens prepared at the OLC and moisture contents less than the OMC, the results showed the following:

1- The lime-stabilised specimens reached an equilibrium after three cycles.
2- The maximum swelling occurred at the first cycle for all samples tested. This suggests the climatic effect can be neglected for such design procedures.
3- The gradient of swelling and the shrinkage path increased as compaction stress increased.

CHAPTER 8. CONCLUSIONS AND RECOMMENDATIONS

This chapter presents the outcomes of the current research program and lists recommendations for future work.

8.1 Conclusions

The aim of this research project was to extend the understanding and develop a new model in relation to the volumetric behaviour of an unsaturated expansive clay after lime stabilisation (at the optimum lime content) by using net stress, void ratio and moisture ratio, and by using suction as a dependent variable on moisture ratio. The clay selected for this study was a residual soil derived from a weathered quaternary basalt deposit located in Victoria, Australia. The MPK framework proposed by Kodikara (2012) was adopted as the starting point for the development of a new model. To achieve the aim of this research, four objectives were planned. The first objective was to develop a new method to estimate the optimum lime content for the selected expansive clay in order to reduce the swell potential, while taking into account the reduction in pH concentration during the curing. ASTM-D6276 (1999) recommends using the method by Eades and Grim (1966), which depends on measuring the pH 1 hr after stabilisation. This method has been adopted and used in many studies. However, it does not consider the time effect of curing, which causes a reduction in pH concentration over time. The second objective was to improve the MPK framework by describing the volumetric behaviour of an unsaturated compacted expansive clay, as well as the behaviour of his expansive clay stabilised with lime. This research also sought to propose a new method to estimate the collapse and swelling potential after wetting using the developed framework. To achieve this, the suitability and validity of the MPK framework were assessed on the untreated and lime-treated expansive clay by applying different state paths. The third objective of this research was to then describe the volumetric behaviour of the untreated and lime-treated expansive clay in terms of suction via the developed

MPK framework (i.e. complete the hydro-mechanical picture in the volumetric space). This objective was achieved by investigating the Soil Water Characteristic Curve (SWCC) for the selected untreated and lime-treated soil at and below the virgin compression surface (LWSBS). The fourth objective included identification of the behaviour of lime-stabilised and compacted expansive soils under cycles of swell-shrink (climatic effect).

8.1.1 New method to estimate the optimum lime (OLC) content for expansive clay

The Eades and Grim (1966) method is currently recommended by ASTM-D6276 (1999) to estimate the optimum lime content for expansive soils, and depends on measuring the pH 1 hr after stabilisation. However, this method does not consider the time effect of curing, which can cause a reduction in pH concentration over time.

To investigate the effect of curing on estimating the optimum lime content for the selected residual expansive soil (Braybrook clay), a range of tests, including the Atterberg limit, linear shrinkage, pH concentration, standard Proctor compaction, Unconfined Compressive Strength (UCS), and swelling potential complemented by XRD and SEM, were conducted. From these results, a new method was suggested. This method relies on the purpose of soil improvement. If the purpose of improvement is to reduce the deformation (swell-shrinkage potential), then the OLC is the lime percentage that keeps the pH level at approximately 12.4 for 7 days. However, if increasing soil strength is the main objective of soil improvement, then the lime percentage maintaining the pH level at approximately 12.4 for 28 days should be selected. To check the validity of the new method, another basaltic soil was collected from the Whittlesea site, and the test results confirmed the suitability of the method.

It is important to mention that the purpose of this study was not to suggest that the Eades and Grim method or the new method proposed in this research should be used in place of traditional tests, such as strength or deformation tests. More importantly, this study recommends that for the preliminary determination of the required lime content, taking into account the purpose of soil improvement, different curing periods for pH measurements should be considered.

8.1.2 Improvement of the MPK framework and proposal of a new method to estimate of collapse and swelling potential

To investigate the volumetric behaviour of an unsaturated compacted expansive clay, as well as an expansive clay stabilised with lime, the suitability and validity of the MPK framework were examined by applying different state paths, such as loading-wetting, loading-wetting-loading, loading-unloading-wetting, loading-unloading-wetting-unloading-wetting, collapse potential and swelling potential. It was discovered that the behaviour of all clay specimens tested followed the MPK framework proposed by Kodikara (2012). However, the MPK framework was found to not be valid for specimens prepared at a degree of saturation less than 37% for the untreated clay and less than 33% for the lime-treated clay, especially when wetted under stress levels below 1000 kPa for the untreated clay and 500 kPa for the lime-treated clay. As a result of this finding, the MPK framework was improved by dividing the virgin compression surface (LWSBS) into two parts: Part A, where the MPK framework was valid, and Part B, where the MPK framework did not extend. For Part A, the variation of e with e_w can be expressed as a cosine function (Equation 8-1) taking into account the degree of saturation S_r and the upper boundary condition as follows:

$$\frac{e}{e_s'} = \left[\left(\frac{e_0'}{e_s'} - 1\right) \cos\left(\frac{\varphi(e_w - e_{w0})}{e_s' - e_{w0}}\right) + \left(1 - \frac{e_0'}{e_s'}\cos(\varphi)\right)\right] \frac{1}{1 - \cos(\varphi)} \qquad \text{8-1}$$

$$e_0' = \frac{e_{w0}}{S_r}$$

$$\sigma = \left(e^{(e_0^{*\prime} - e_0')/\lambda_0}\right) \times \sigma_i$$

$$e_s' = e_{so}^{*} - \lambda_1 ln\left(\frac{\sigma}{\sigma_i}\right)$$

where:

e_{w0}: the initial moisture ratio at stress σ and degree of saturation S_r,

e_0': the initial void ratio at stress σ, moisture ratio e_{w0} and degree of saturation S_r,

e_{w0i}^{*} = moisture ratio at S_r and $\sigma = \sigma_i$,

$e_0^{*\prime}$: the initial void ratio at stress $\sigma = \sigma_i$, moisture ratio e_{w0} ($e_{w0} < e_{w0i}^{*}$),

λ_0: the gradient of compression line at $e_w = e_{w0}$ ($\lambda = ae_w + b$),

e_s': the void ratio on normally consolidated line (NCL) and at stress σ,

e_{so}^{*}: the void ratio on NCL and at stress σ_i,

The domain of the cosine function starts from $e_w = e_{wo}$ to $e_w = e_s$ (on NCL).

For Part B, the variation of e with e_w can be expressed as an exponential function (Equation 8-2). This function is valid from e_w=0 to $e_w = e_{w0}$.

$$\boldsymbol{e = e_0\, e^{ce_w}} \qquad \text{8-2}$$

$$\boldsymbol{c = \frac{1}{e_{w0}} ln \frac{e_0'}{e_0}}$$

The results also showed that for all untreated and lime-treated specimens, the void ratio value decreased as the moisture content increased at all stress levels tested due to the macroscopic structure build-up. However, this relation reversed when a specimen with very low moisture content (S_r < 37% for untreated clay and S_r < 33% for lime-treated clay) was wetted under low-stress conditions (i.e. σ< 1000 kPa for untreated clay and < 500 kPa for lime-treated clay). The occurrence of this feature is similar to having compaction curves with multiple peaks, and appears to be related to the weakening of the effect of suction to form stronger contacts among aggregates that give larger macro void space.

Furthermore, the swelling and collapse potentials were tested under a wide range of moisture contents and stress levels, with special attention given to the effect of stress history and operational stress on the swelling and collapse behaviour. From the results, a new method to predict the swelling and collapse values using the modified framework was proposed. By identifying the compaction stress and corresponding void ratio, a constant void ratio line (LV) could be plotted on the LWSBS. From there, it is straightforward to predict collapse at any condition. The value of swelling can be neglected for each point located on the LV; therefore, the important behaviour that can be measured from the LV is a collapse. The maximum collapse values were achieved when a specimen was wetted under a stress equivalent to the compaction stress. At constant moisture content, the value of collapse increased as the void ratio increased, initial dry density decreased, and compaction stress decreased. Furthermore, at the constant void ratio, the collapse potential increased as the moisture content decreased. If a specimen was unloaded to a stress above the LV, the specimen would swell only. The path of swelling depended on the gradient of the swelling path. The swelling magnitude increased as the operational stress decreased, and compaction stress increased.

It is also important to mention that although the expansive clay was treated with lime at the optimum lime content (according to swelling potential), this study showed significant swelling had occurred when the specimen was prepared at a very low moisture content (i.e. dry side of the LOO) (10%) and compacted to 1000 kPa, then wetted under an operational stress of 25 kPa. This behaviour could be attributed to the mechanism of reaction between the lime and clay. The first reaction began after adding water to the clay-lime mixture. The hydrated lime dissociated to Ca^{+2} and $2(OH)^{-1}$ ions, and consequently cation exchange, flocculation, and agglomeration started. That meant enough water was needed to start the stabilisation process. As a result, adding only a small amount of water to the clay (the clay is still dry) would not affect the stabilisation process during curing. However, the OLC was obtained at the OMC, meaning that there was enough water to start the stabilisation process during curing.

Finally, this study concluded that the presence of the hydrated lime contributed to improving the collapsibility of the expansive soil specimens tested from a state of very high down to high collapsibility, or from a state of high to medium collapsibility. This means that the collapse potentials were significantly reduced after stabilisation with lime and that these values should be considered.

8.1.3 Incorporating suction within the modified MPK framework

As the modified MPK framework is not dependant on the suction parameter, any volumetric behaviour related to the loading and/or wetting of the compacted unsaturated expansive clay and an expansive clay stabilised with lime can be explained by the LWSBS in the $e{-}e_w{-}\sigma$ space. However, knowledge of the suction profile within the $e{-}e_w{-}\sigma$ space was necessary to complete the hydro-mechanical picture in the volumetric space.

In order to develop the suction contours at and below the LWSBS, it was necessary to first measure and plot the SWCC at and below the LWSBS. The Hyprop, filter paper and chilled mirror hygrometer (WP4C) were all used to measure suction and develop the SWCC at and below the virgin compression surface at different net stress levels for the untreated and lime-treated expansive clay samples. By identifying the moisture ratio, void ratio, net stress and suction for each untreated and lime-treated specimen, the suction distribution at and below the LWSBS were represented mathematically. Using these measurements, the soil suction of an unsaturated compacted expansive clay, as well as an expansive clay stabilised with lime, could be explained using the LWSBS (in the $e{-}e_w{-}\sigma$ space). This study also concluded that although the soil specimens were treated with lime at the optimum lime content, the lime-treated specimens were considered to be categorised as highly collapsible when the specimens were prepared at a suction higher than 2000 kPa and wetted under a compaction stress less than 300 kPa. Furthermore, a significant swelling occurred when the treated specimen was prepared at high suction (≥10000 kPa).

8.1.4 Identification of the soil behaviour under cycles of swell-shrink

To investigate the climatic effect on volumetric behaviour (for long-term), and consequently, on the structural design for the untreated and lime-stabilised expansive clays, a set of cycles of swell-shrink tests were conducted at different initial lime contents, moisture contents and stress levels. The results showed that all specimens tested reached an equilibrium condition after three swell-shrink cycles. For specimens prepared at the OMC, MDD and with lime contents less than the OLC, the maximum swelling occurred on the second cycle. This finding suggests that a review of current design procedures is required for those that do not consider cyclic movements, as they are underestimating the swell-shrink potential. Therefore, it is important to measure the swelling value from the first cycle, for the short-term, to simulate the field condition after compaction. It is also important to consider the climate cycles to simulate the field condition for the long term. However, for specimens prepared at the OLC and moisture contents less than OMC, the results showed that the maximum swelling occurred at the first cycle for all specimens tested. This suggests the climatic effect can be neglected for such design procedures.

8.2 Recommendations

The current research program has completed the interpretation of volumetric behaviour related to the loading and/or wetting of compacted unsaturated expansive clay, as well as an expansive clay stabilised with lime (at the OLC), using the modified MPK framework. This study has also incorporated the suction profile within the e−e_w−σ space to complete the hydro-mechanical picture in the volumetric space. The following studies are recommended to be undertaken in future research:

1- The extension of volumetric behaviour to drying and loading state paths, including suction. This thesis emphasised the state paths involving loading and wetting. However, some appraisals, including drying and loading state paths, were implemented on the basis of some available data. These results were encouraging to explain the change in yield stress due to drying using the LWSBS. However, these appraisals were preliminary, and more research needs to be undertaken to fully address this area.

2- Extension to model shear behaviour: this thesis established the volumetric space of e, e_w, σ and s. Naturally, the next step is to model shear behaviour requiring the inclusion of a combination of deviatoric stress (q). In the Barcelona Basic

Model (BBM), this behaviour is based on the loading/wetting collapse (LC) curve, which corresponds to the constant plastic part of volume change in q, σ, and s space incorporation, with the volumetric space given by υ (1+e), σ and s. A similar approach may be followed to incorporate shear behaviour using either q, σ, υ, υ_w or q, p, υ, s as constitutive variables.

3- Development of basic numerical models to simulate volumetric and shear models. The constitutive models for volumetric and shear behaviour can be used to implement the numerical models, which could be considered as basic models for use in routine applications.

REFERENCES

AASHTO-M145-91 2004, *Standard specification for classification of soils and soil-aggregate*, American Association of State Highway and Transportation Officials, www.aashto.org.

Al-Homoud, AS, Khedaywi, T & Al-Ajlouni, AM 1995, 'Studies on the Control of Swell and Collapse Potential of Selected Jordanian Soils Using Asphalt Stabilization', *Soils and Foundations*, vol. 35, no. 2, pp. 15-23.

Al-Mukhtar, M, Khattab, S & Alcover, JF 2012, 'Microstructure and geotechnical properties of lime-treated expansive clayey soil', *Engineering Geology*, vol. 139–140, 6/22/, pp. 17-27.

Al-Rawas, AA, Hago, AW & Al-Sarmi, H 2005, 'Effect of lime, cement and Sarooj (artificial pozzolan) on the swelling potential of an expansive soil from Oman', *Building and Environment*, vol. 40, no. 5, 5, pp. 681-687.

Al-Taie, A, Disfani, MM, Evans, R, Arulrajah, A & Horpibulsuk, S 2016, 'Swell-shrink Cycles of Lime Stabilized Expansive Subgrade', *Procedia Engineering*, vol. 143, pp. 615-622.

Al-Taie, A, Disfani, MM, Evans, R, Arulrajah, A & Horpibulsuk, S 2018, 'Impact of curing on behaviour of basaltic expansive clay', *Road Materials and Pavement Design*, vol. 19, no. 3, pp. 624-645.

Alonso, E, Gens, A & Hight, D 1987, 'Special problem soils. General report,' *Proceedings of the 9th European conference on soil mechanics and foundation engineering, Dublin*, 1087-1146.

Alonso, EE, Gens, A & Josa, A 1990, 'A constitutive model for partially saturated soils', *Géotechnique*, vol. 40, no. 3, pp. 405-430.

AS1289.3.4.1 2008, *Methods of Testing of Testing Soils for Engineering Purposes - Soil classification tests - Determination of the linear shrinkage of a soil - Standard method*, Sydney, Australia: Standards Association of Australia.

AS1289.5.1.1 2017, *Methods of Testing of Testing Soils for Engineering Purposes- Soil compaction and density tests- Determination of the dry density/ moisture content* *relation of a soil using standard compactive effort*, Sydney, Australia: Standards Association of Australia.

AS1289.5.2.1 2017, *Methods of Testing of Testing Soils for Engineering Purposes- Soil compaction and density tests- Determination of the dry density/ moisture content relation of a soil using modified compactive effort*, Sydney, Australia: Standards Association of Australia.

AS2870 2011, *Residential slabs and footings*, Sydney: Australia: Standards Association of Australia.

AS5101.4 2008, *Method for preparation and testing of stabilized material: Unconfined compressive strength of compacted materials*, Sydney, Australia: Standards Association of Australia.

ASTM-25 2006, *Standard Test Method for Chemical Analysis of Limestone, Quicklime, and Hydrated Lime*, West Conshohocken, ASTM International.

ASTM-D422 2007, *Standard Test Method for Particle Size Analysis of Soils*, West Conshohocken, ASTM International.

ASTM-D427 1998, *Standard Test Method for Shrinkage Factors of Soils by the Mercury Method*, West Conshohocken, ASTM International.

ASTM-D698 2000, *Standard Test Methods for Laboratory Compaction Characteristics of Soil Using Standard Effort (12,400 ft-Ibf/ft^3)*, West Conshohocken, ASTM International.

ASTM-D854 2010, *Standard Test Methods for Specific Gravity of Soil Solids by Water Pycnometer*, West Conshohocken, ASTM International.

ASTM-D2435 1996, *Standard Test Method for One-Dimensional Consolidation Properties of Soils*, West Conshohocken, ASTM International.

ASTM-D2487 2006, *Standard Practice for Classification of Soils for Engineering Purposes (Unified Soil Classification System)*, West Conshohocken, ASTM International.

ASTM-D2487 2011, *Standard Practice for Classification of Soils for Engineering Purposes (Unified Soil Classification System)*, West Conshohocken, ASTM International.

ASTM-D2974 2000, *Standard Test Methods for Moisture, Ash, and Organic Matter of Peat and Other Organic Soils*, West Conshohocken, ASTM International.

ASTM-D4318 2000, *Standard Test Method for Liquid Limit, Plastic Limit, and Plasticity Index of soils*, West Conshohocken, ASTM International.

ASTM-D5298 1994a, *Standard Test Method for Measurement of Soil Potential (Suction) Using Filter Paper*, West Conshohocken, ASTM International.

ASTM-D5298 1994b, *Standard Test Methods for Measurement of Soil Potential (Suction) Using Filter Paper*, West Conshohocken, ASTM International.

ASTM-D5298 2016, *Standard Test Method for Measurement of Soil Potential (Suction) Using Filter paper*, West Conshohocken, ASTM International.

ASTM-D5333 2003, *Standard Test Method for Measurement of Collapse Potential of Soils*, West Conshohocken, ASTM International.

ASTM-D6276 1999, *Standard Test Methods for Using pH to Estimate the Soil-Lime Proportion Requirement for Soil Stabilization*, West Conshohocken, ASTM International.

ASTM-D6836 2016, *Standard Test Methods for Determination of the Soil Water Characteristic Curve for Desorption Using Hanging Column, Pressure Extractor, Chilled Mirror Hygrometer, or Centrifuge*, West Conshohocken, ASTM International.

Attom, MF & Al-Sharif, MM 1998, 'Soil stabilization with burned olive waste', *Applied Clay Science*, vol. 13, no. 3, 9, pp. 219-230.

AustStab 2002, *Lime stabilisation practice,* AustStab Technical Note, pavement recycling and stabilisation association, 1.

AustStab 2008, *Lime stabilisation practice,* AustStab Technical Note, pavement recycling and stabilisation association, 1.

AustStab 2010, *What is Lime?,* AustStab Technical Note, pavement recycling and stabilisation association, 4.

Avsar, E, Ulusay, R & Sonmez, H 2009, 'Assessments of swelling anisotropy of Ankara clay', *Engineering Geology*, vol. 105, no. 1-2, pp. 24-31.

Baghabra Al-Amoudi, OS & Abduljauwad, SN 1995, 'Compressibility and collapse characteristics of arid saline sabkha soils', *Engineering Geology*, vol. 39, no. 3–4, 6, pp. 185-202.

Basha, EA, Hashim, R, Mahmud, HB & Muntohar, AS 2005, 'Stabilization of residual soil with rice husk ash and cement', *Construction and Building Materials*, vol. 19, no. 6, 7, pp. 448-453.

Bell, FG 1996, 'Lime stabilization of clay minerals and soils', *Engineering Geology*, vol. 42, no. 4, 7, pp. 223-237.

Bell, G, Bowen, K, Douglas, J, Hancock, J, Jenkin, J, Kenley, P, Knight, J, Neilson, J, Spencer-Jones, D & Talent, J 1967, 'Geology of the Melbourne district, Victoria', *Geological survey of Victoria, bulletin*, no. 59.

Bishop, AW 1959, 'The principle of effective stress', *Teknisk Ukeblad*, vol. 39, pp. 859-863.

Bolzon, G, Schrefler, BA & Zienkiewicz, OC 1996, 'Elastoplastic soil constitutive laws generalized to partially saturated states', *Géotechnique*, vol. 46, no. 2, pp. 279-289.

Bulut, R, Lytton, RL & Wray, WK 2001, 'Soil suction measurements by filter paper', in *Expansive clay soils and vegetative influence on shallow foundations*, pp. 243-261.

Cabalar, AF, Karabash, Z & Mustafa, WS 2014, 'Stabilising a clay using tyre buffings and lime', *Road Materials and Pavement Design*, vol. 15, no. 4, pp. 872-891.

Cai, Y, Shi, B, Ng, CWW & Tang, C-s 2006, 'Effect of polypropylene fibre and lime admixture on engineering properties of clayey soil', *Engineering Geology*, vol. 87, no. 3–4, 11/3/, pp. 230-240.

Cameron, D & Walsh, P 1997, *The design of residential slabs and footings,* Standard Australia.

Chen, D-H, Si, Z & Saribudak, M 2009, 'Roadway heaving caused by high organic matter', *Journal of Performance of Constructed Facilities*, vol. 23, no. 2, pp. 100-108.

Chen, FH 1998, *Foundation on expansive soils,* Elsevier Science, New York, USA.

Chen, FH 2012, *Foundations on expansive soils,* Elsevier, New York, USA.

Chen, H & Wang, Q 2006, 'The behaviour of organic matter in the process of soft soil stabilization using cement', *Bulletin of Engineering Geology and the Environment*, vol. 65, no. 4, pp. 445-448.

Chen, L & Lin, D-F 2009, 'Stabilization treatment of soft subgrade soil by sewage sludge ash and cement', *Journal of Hazardous Materials*, vol. 162, no. 1, pp. 321-327.

Chen, S-H 2015, 'Embankment Dams', in *Hydraulic Structures*, Springer, pp. 497-592.

Ciancio, D, Beckett, CTS & Carraro, JAH 2014, 'Optimum lime content identification for lime-stabilised rammed earth', *Construction and Building Materials*, vol. 53, 2/28/, pp. 59-65.

Clare, K & Cruchley, A 1957, 'Laboratory Experiments in The Stabilization of Clays With Hydrated Lime', *Geotechnique*, vol. 7, no. 2, pp. 97-111.

Colmenares Montanez, JE 2002, *Suction and volume changes of compacted sand-bentonite mixtures*, thesis, Imperial College London (University of London).

Corporation, TE 2006, *Orion Star™-Series Meter-User's Guide*, viewed <http://web.unideb.hu/uh9v32/muszer2/orionstar.pdf. [Accessed 14-03-2017]>.

Costa, WDSM 2010, *Study of desiccation cracking and fracture properties of clay soils*, thesis, Monash University. Faculty of Engineering. Department of Civil Engineering.

Crescimanno, G & Provenzano, G 1999, 'Soil shrinkage characteristic curve in clay soils: Measurement and prediction', *Soil Science Society of America Journal*, vol. 63, no. 1, pp. 25-32.

Dahlhaus, P & O'Rourke, M 1992, 'The Newer Volcanics', *Engineering Geology of Melbourne*, pp. 205-212.

Dasog, GS, Acton, DF, Mermut, AR & Jong, ED 1988, 'Shrink-swell potential and cracking in clay soils of Saskatchewan ', *Canadian Journal of Soil Science*, vol. 68, no. 2, 1988/05/01, pp. 251-260.

Day, RW 1994, 'Swell-shrink behavior of compacted clay', *Journal of geotechnical engineering*, vol. 120, no. 3, pp. 618-623.

Day, RW & Hager, L 1999, *Geotechnical and foundation engineering: design and construction,* McGraw-Hill New York.

de Brito Galvão, TC, Elsharief, A & Simões, GF 2004, 'Effects of lime on permeability and compressibility of two tropical residual soils', *Journal of environmental engineering*, vol. 130, no. 8, pp. 881-885.

de Melo Ferreira, SR & Fucale, S 2014, 'Evaluation of the Collapsibility of Soils in the Semiarid Region of Pernambuco, Brazil', *Journal of Civil Engineering and Architecture*, vol. 8, no. 10

Decagon 2012, *WP4C dewpoint Potentiameter*, [on line], viewed <http://www.decagon.com/products/environmental-instruments/water-potential-instruments/wp4c-dewpoint-potentiameter/. [Accessed 05-24- 2014]>.

Decagon, D 2010, 'WP4C Dewpoint PotentiaMeter operator's manual, Version 2', Decagon Devices, Pullman, WA.

Delaney, M, Li, J & Fityus, S 2005, 'Field monitoring of expansive soil behaviour in the Newcastle-hunter region', *Journal of Australian Geomechanics*, vol. 40, no. 2, pp. 3-14.

Der Merwe, V 1964, 'DH The Prediction of heave from the Plasticity Index and Percentage Clay Fraction', *Trans. SA Ins. Civ. Eng*, no. 6.

Dermatas, D, Xu, X, Cao, X, Shen, G, Menounou, N, Arienti, P & Delaney, J 2005, 'An evaluation of pozzolanic lead immobilization mechanisms in firing range soils', *Stabilisation/Solidification Treatment and Remediation: Advances in S/S for Waste and Contaminated Land. London: Taylor and Francis*, pp. 45-56.

Dineen, K, Colmenares, J, Ridley, A & Burland, J 1999, 'Suction and volume changes of a bentonite-enriched sand', *Proceedings of the Institution of Civil Engineers-Geotechnical Engineering*, vol. 137, no. 4, pp. 197-201.

Du, Y, Li, S & Hayashi, S 1999, 'Swelling–shrinkage properties and soil improvement of compacted expansive soil, Ning-Liang Highway, China', *Engineering Geology*, vol. 53, no. 3, 1999/07/01/, pp. 351-358.

Eades, JL & Grim, RE 1966, 'A quick test to determine lime requirements for lime stabilization', *Highway research record*, no. 139, pp. 61-72.

Echlin, P 2009, 'Sample Embedding and Mounting', in *Handbook of Sample Preparation for Scanning Electron Microscopy and X-Ray Microanalysis*, Springer, New York, USA., pp. 47-63.

Elkady, TY 2015, 'The effect of curing conditions on the unconfined compression strength of lime-treated expansive soils', *Road Materials and Pavement Design*, pp. 1-18.

EN459-1 2010, *Building Lime-Part 1: Definitions, specifications and conformity criteria*, NSAI Standard, Northwood, Ireland.

EN459-2 2010, *Building Lime-Part 2: Test Methods*, NSAI Standard, Northwood, Ireland.

Fattah, MY, Al-Ani, MM & Al-Lamy, MTA 2012, 'Treatment of collapse of gypseous soils by grouting', *Proceedings of the ICE-Ground Improvement*, vol. 166, no. 1, pp. 32-43.

Fattah, MY, Al-Ani, MM & Al-Lamy, MTA 2014, 'Studying collapse potential of gypseous soil treated by grouting', *Soils and Foundations*, vol. 54, no. 3, 6//, pp. 396-404.

Fattah, MY, Yahya, AY, Al-Hadidi, MT & Ahmed, BA 2013, 'Effect of salt content on total and matric suction of unsaturated soils', *European Scientific Journal, ESJ*, vol. 9, no. 9.

Feidenhans'l, R 1989, 'Surface structure determination by X-ray diffraction', *Surface Science Reports*, vol. 10, no. 3, 5, pp. 105-188.

Ferber, V, Auriol, J-C, Cui, Y-J & Magnan, J-P 2009, 'On the swelling potential of compacted high plasticity clays', *Engineering Geology*, vol. 104, no. 3-4, pp. 200-210.

Fityus, S, Smith, D & Allman, M 2004, 'Expansive soil test site near Newcastle', *Journal of Geotechnical and Geoenvironmental Engineering*, vol. 130, no. 7, pp. 686-695.

Fleureau, J-M, Kheirbek-Saoud, S, Soemitro, R & Taibi, S 1993, 'Behavior of clayey soils on drying-wetting paths', *Canadian geotechnical journal*, vol. 30, no. 2, pp. 287-296.

Fleureau, J-M, Verbrugge, J-C, Huergo, PJ, Correia, AG & Kheirbek-Saoud, S 2002, 'Aspects of the behaviour of compacted clayey soils on drying and wetting paths', *Canadian Geotechnical Journal*, vol. 39, no. 6, 2002/12/01, pp. 1341-1357.

Fredlund, D 2000, 'The Implementation of Unsaturated Soil Mechanics into Geotechnical Engineering Practice', *National Research Council of Canada*.

Fredlund, D & GAN, J 1996, 'The collapse mechanism of a soil subjected to one-dimensional loading and wetting,' *International Journal of Rock Mechanics and Mining Sciences and Geomechanics Abstracts*, Elsevier, 157A-157A.

Fredlund, DG 2006, 'Unsaturated soil mechanics in engineering practice', *Journal of geotechnical and geoenvironmental engineering*, vol. 132, no. 3, pp. 286-321.

Fredlund, DG & Morgenstern, NR 1976, 'Constitutive relations for volume change in unsaturated soils', *Canadian Geotechnical Journal*, vol. 13, no. 3, pp. 261-276.

Fredlund, DG & Rahardjo, H 1993, *Soil mechanics for unsaturated soils,* John Wiley & Sons, New York.

Fredlund, DG & Vu, HQ 2003, 'Numerical Modelling of Swelling and Shrinking soils around slabs-on-ground,' *Proceeding, Post-Tensioning Institute Annual Technical Conference, Huntington Beach, CA, USA*.

Fredlund, DG & Xing, A 1994, 'Equations for the soil-water characteristic curve', *Canadian Geotechnical Journal*, vol. 31, no. 4, 1994/08/01, pp. 521-532.

Gallipoli, D, Gens, A, Sharma, R & Vaunat, J 2003a, 'An elasto-plastic model for unsaturated soil incorporating the effects of suction and degree of saturation on mechanical behaviour', *Géotechnique*, vol. 53, pp. 123-135.

Gallipoli, D, Wheeler, S & Karstunen, M 2003b, 'Modelling the variation of degree of saturation in a deformable unsaturated soil', *Géotechnique.*, vol. 53, no. 1, pp. 105-112.

Gilbert, OH 1959, *The influence of negative pore water pressures on the strength of compacted clays*, M. Sc. thesis, Massachusetts Institute of Technology, Cambridge, Mass.

Gould, SJF, Kodikara, J, Rajeev, P, Zhao, X-L & Burn, S 2011, 'A void ratio - water content - net stress model for environmentally stabilized expansive soils', *Canadian Geotechnical Journal*, vol. 48, no. 6, pp. 867-877.

Groenevelt, P & Bolt, G 1972, 'Water retention in soil1', *Soil Science*, vol. 113, no. 4, pp. 238-245.

Gueddouda, M, Goual, I, Lamara, M, Smaida, A & Mekarta, B 2011, 'Chemical stabilization of expansive clays from Algeria', *Global Journal of Researches in Engineering*, vol. 11, no. 5, pp. 1-7.

Habibagahi, G & Taherian, M 2004, 'Prediction of collapse potential for compacted soils using artificial neural networks', *Scientia Iranica*, vol. 11, no. 1-2, pp. 1-20.

Haines, WB 1923, 'The volume-changes associated with variations of water content in soil', *The Journal of Agricultural Science*, vol. 13, no. 03, pp. 296-310.

Hamza, O 2014, *Treatment of Expansive Subgrade Soils Using Lime and Fly Ash*, thesis, Department of Civil Engineering, University of Khartoum, Sudan.

Hansen, W 1967, 'Basic chemistry of reactions of aggregates in portland cement concrete', *Journal Materials*, vol. 2, no. 2, pp. 408-431.

Harris, P, Harvey, O, Puppala, A, Sebesta, S & Rao, S 2009, *Mitigating the Effects of Organics in Stabilized Soils: Technical Report,* Research Report No. FHWA/TX-09/0-5540-1 Texas Transportation Institute, Texas A&M University, College Station, Texas.

Hasan, J & Fredlund, D 1980, 'Pore pressure parameters for unsaturated soils', *Canadian geotechnical journal*, vol. 17, no. 3, pp. 395-404.

Hazelton, PA & Murphy, BW 2007a, *Interpreting soil test results: What do all the numbers mean?,* CSIRO Publishing, Collingwood, Australia.

Hazelton, PA & Murphy, BW 2007b, *Interpreting soil test results: What do all the numbers mean?, CSIRO publishing*.

Hilf, JW 1956, *An investigation of pore water pressure in compacted cohesive soils*, thesis, US Department of the Interior, Bureau of Reclamation.

Ho, DYF, Fredlund, DG & Rahardjo, H 1992, 'Volume change indices during loading and unloading of an unsaturated soil', *Canadian Geotechnical Journal*, vol. 29, no. 2, 1992/04/01, pp. 195-207.

Horpibulsuk, S, Phetchuay, C, Chinkulkijniwat, A & Cholaphatsorn, A 2013, 'Strength development in silty clay stabilized with calcium carbide residue and fly ash', *Soils and Foundations*, vol. 53, no. 4, pp. 477-486.

Houlsby, G 1997, 'The work input to an unsaturated granular material', *Géotechnique*, vol. 47, no. 1, pp. 193-6.

Houston, S, Houston, W, Zapata, C & Lawrence, C 2001, 'Geotechnical engineering practice for collapsible soils', *Geotechnical & Geological Engineering*, vol. 19, no. 3-4, 2001/09/01, pp. 333-355.

Huat, BB, Maail, S & Mohamed, TA 2005, 'Effect of chemical admixtures on the engineering properties of tropical peat soils', *American Journal of Applied Sciences*, vol. 2, no. 7, pp. 1113-1120.

Islam, M 2015, *A study of volumetric behaviour of compacted clayey soils in the void ratio, moisture ratio and net stress space*, thesis, Monash University. Faculty of Engineering. Department of Civil Engineering, Melbourne, Australia.

Islam, T & Kodikara, J 2015, 'Interpretation of the loading–wetting behaviour of compacted soils within the "MPK" framework. Part I: Static compaction 1', *Canadian Geotechnical Journal*, vol. 53, no. 5, pp. 783-805.

Ismaiel, H 2006, *Treatment and improvement of the geotechnical properties of different soft fine-grained soils using chemical stabilization,* Shaker, Thesis Mathematisch -Naturwissenschaftlich-Technischen Fakultät der Martin – Luther-Universität Halle-Wittenberg.

ISO-14688 2002, *Geotechnical investigation and testing–Identification and classification of soil–Part 1: Identification and description*, International Standard, Switzerland.

James, RW 1982, *The Optical Principles of the Diffraction of X-rays* Ox Bow, Woodbridge, Connecticut.

Jones, DE & Holtz, WG 1973, *Expansive Soils -- the Hidden Disaster,* National Emergency Training Center.

Jones, EW, Koh, YH, Tiver, BJ & Wong, MA 2009, 'Modelling the behaviour of unsaturated, saline clay for geotechnical design', *School of Civil Environment and Mining Engineering, University of Adelaide, Australia*,

Jones, LD & Jefferson, I 2012, *Expansive soils,* ICE Publishing, London, UK.

Jotisankasa, A, Ridley, A & Coop, M 2007, 'Collapse behavior of compacted silty clay in suction-monitored oedometer apparatus', *Journal of Geotechnical and Geoenvironmental Engineering*, vol. 133, no. 7, pp. 867-877.

Joy, DC 2006, *Scanning electron microscopy,* Wiley Online Library.

Kampala, A & Horpibulsuk, S 2013, 'Engineering properties of calcium carbide residue stabilized silty clay', *J Mater Civ Eng ASCE*, vol. 25, no. 5, pp. 632-644.

Kampala, A, Horpibulsuk, S, Prongmanee, N & Chinkulkijniwat, A 2014, 'Influence of Wet-Dry Cycles on Compressive Strength of Calcium Carbide Residue–Fly Ash

Stabilized Clay', *Journal of Materials in Civil Engineering*, vol. 26, no. 4, pp. 633-643.

Karlsson, R & Hansbo, S 1989, *Soil Classification and Identification: Byggforskningsrädet,* Swedish Geotechnical Soc.

Karunarathne, A, Sivanerupan, S, Gad, E, Disfani, M, Rajeev, P, Wilson, J & Li, J 2014a, 'Field and laboratory investigation of an expansive soil site in Melbourne', *Australian Geomechanics Journal*, vol. 49, no. 2, pp. 85-93.

Karunarathne, A, Sivanerupan, S, Gad, EF, Disfani, MM, Wilson, JL & Li, J 2014b, 'Field monitoring of seasonal ground movements in expansive soils in Melbourne,' *Unsaturated Soils: Research and Applications - Proceedings of the 6th International Conference on Unsaturated Soils, UNSAT 2014, London*, 1359-1365.

Kerrane, JP 2005, 'What are Expansive Soils?', *Notes by Benson & Associates PC, Golden Colorado*, USA.

Khalili, N, Khabbaz, M & Valliappan, S 2000, 'An effective stress based numerical model for hydro-mechanical analysis in unsaturated porous media', *Computational mechanics*, vol. 26, no. 2, pp. 174-184.

Kodikara, J 2012, 'New framework for volumetric constitutive behaviour of compacted unsaturated soils', *Canadian Geotechnical Journal*, vol. 49, no. 11, pp. 1227-1243.

Kodikara, J., Islam, T., Wijesooriya, S., Bui, H., and Burman, B. 2014, 'On controlling influence of the line of optimums on the compacted clayey soil behavior', *Proceedings of the Sixth International Conference on Unsaturated Soils, UNSAT2014. Edited by N. Khalili, AR Russell, and A. Khoshghalb. Sydney, Australia*, 219-225.

Kodikara, JK & Choi, X 2006, 'A simplified analytical model for desiccation cracking of clay layers in laboratory tests,' 2558-2569.

Krahn, J & Fredlund, D 1972, 'On total, matric and osmotic suction', *Soil Science,* vol. 114, no. 5, pp. 339-348.

Kurucuk, N 2011, *Compaction behaviour of soils*, thesis, Department of Civil Engineering Monash University, Victoria, Australia.

Langroudi, AA & Yasrobi, SS 2009, 'A micro-mechanical approach to swelling behavior of unsaturated expansive clays under controlled drainage conditions', *Applied Clay Science*, vol. 45, no. 1-2, pp. 8-19.

Leong, E-C, Tripathy, S & Rahardjo, H 2003, 'Total suction measurement of unsaturated soils with a device using the chilled-mirror dew-point technique', *Geotechnique*, vol. 53, no. 2, pp. 173-182.

Li, J & Cameron, DA 2002, 'Case study of courtyard house damaged by expansive soils', *Journal of performance of constructed facilities*, vol. 16, no. 4, pp. 169-175.

Li, J, Cameron, DA & Ren, G 2014, 'Case study and back analysis of a residential building damaged by expansive soils', *Computers and Geotechnics*, vol. 56, 3, pp. 89-99.

Likos, WJ & Lu, N 2003, 'Automated humidity system for measuring total suction characteristics of clay', *Geotechnical Testing Journal,* vol. 26, no. 2, pp. 179-190.

Lim, YY & Miller, GA 2004, 'Wetting-induced compression of compacted Oklahoma soils', *Journal of Geotechnical and Geoenvironmental Engineering*, vol. 130, no. 10, pp. 1014-1023.

Lin, ZG & Wang, SJ 1988, 'Collapsibility and deformation characteristics of deep-seated loess in China', *Engineering Geology*, vol. 25, no. 2, 1988/06/01, pp. 271-282.

Little, DN 1999, *Evaluation of structural properties of lime stabilized soils and aggregates,* National Lime Association.

Little, DN & Nair, S 2009, *Recommended practice for stabilization of subgrade soils and base materials,* National Cooperative Highway Research Program, Transportation Research Board of the National Academies.

Liu, J, Shi, B, Jiang, H, Huang, H, Wang, G & Kamai, T 2011, 'Research on the stabilization treatment of clay slope topsoil by organic polymer soil stabilizer', *Engineering Geology*, vol. 117, no. 1–2, 1/10/, pp. 114-120.

Liu, MD, Indraratna, B, Horpibulsuk, S & Suebsuk, J 2012, 'Variations in strength of lime-treated soft clays', *Proceedings of the ICE-Ground Improvement*, vol. 165, no. 4, pp. 217-223.

Lloret, A, Villar, MV, Sànchez, M, Gens, A, Pintado, X & Alonso, EE 2003, 'Mechanical behaviour of heavily compacted bentonite under high suction changes', *Geotechnique*, vol. 53, no. 1, pp. 27-40.

Loret, B & Khalili, N 2002, 'An effective stress elastic–plastic model for unsaturated porous media', *Mechanics of Materials*, vol. 34, no. 2, pp. 97-116.

Lu, N. 2008, 'Is matric suction a stress variable?', *Journal of Geotechnical and Geoenvironmental Engineering*, vol. 134, no. 7, 899-905.

Manasseh, J & Olufemi, AI 2008, 'Effect of lime on some geotechnical properties of Igumale shale', *Electronic Journal of Geotechnical Engineering*, vol. 13, no. 6, pp. 1-12.

Mann, A 2003, *The identification of road sections in Victoria displaying roughness caused by expansive soils,* School of Engineering and Science, Swinburne University of Technology.

Maps 2015, *Energy and Earth Resources-Earth resources online store [online]* viewed 08-08-2017, <http://dpistore.efirst.com.au/categories.asp?cID=4>.

Marinho, F & Stuermer, M 2000, 'The Influence of the Compaction Energy on the SWCC of a Residual Soil', in *Advances in Unsaturated Geotechnics*, American Society of Civil Engineers, pp. 125-141.

Matyas, EL & Radhakrishna, H 1968, 'Volume change characteristics of partially saturated soils', *Géotechnique*, vol. 18, no. 4, pp. 432-448.

McDowell, C 1959, c*Board Bulletin*, no. 231

Mitchell, AR & van Genuchten, MT 1992, 'Shrinkage of Bare and Cultivated Soil', *Soil Sci. Soc. Am. J.*, vol. 56, no. 4, 1992, pp. 1036-1042.

Mitchell, P & Avalle, D 1984, 'A technique to predict expansive soil movements,' *Fifth International Conference on Expansive Soils 1984: Preprints of Papers,* Institution of Engineers, Australia, pp. 124.

Mohamed, A 2013, 'Improvement of swelling clay properties using hay fibers', *Construction and Building Materials*, vol. 38, pp. 242-247.

Muhmed, A & Wanatowski, D 2013, 'Effect of Lime Stabilisation on the Strength and Microstructure of Clay', *IOSR Journal of Mechanical and Civil Engineering (IOSR-JMCE)*, vol. 6, pp. 87-94.

Murray, EJ & Sivakumar, V 2010, *Unsaturated Soils: A fundamental interpretation of soil behaviour,* John Wiley & Sons, UK.

Nalbantoğlu, Z 2004, 'Effectiveness of Class C fly ash as an expansive soil stabilizer', *Construction and Building Materials*, vol. 18, no. 6, pp. 377-381.

Nalbantoglu, Z & Gucbilmez, E 2001, 'Improvement of calcareous expansive soils in semi-arid environments', *Journal of arid environments*, vol. 47, no. 4, pp. 453-463.

Nelson, JD, Chao, KC, Overton, DD & Nelson, EJ 2015, *Foundation engineering for expansive soils,* John Wiley & Sons, USA.

Nelson, JD & Miller, DJ 1992, *Expansive soils: problems and practice in foundation and pavement engineering,* John Wily & Sons, Inc., New York, NY.

Nelson, JD, Overton, DD & Chao, K 2003, 'Design of foundations for light structures on expansive soils,' *California Geotechnical Engineers Association Annual Conference*, Carmel, California.

Northcote, KH 1962, *Atlas of Australian Soils: Explanatory Data for Sheet 2: Melbourne-Tasmania Area,* Commonwealth Scientific and Industrial Research Organization, Australia.

Nwakanma, CA 1979, *The use of red tropical soils as pozzolanas: reactions, products and properties*, thesis, University of Leeds.

Onitsuka, K, Modmoltin, C, Kouno, M & Negami, T 2003, 'Effect of organic matter on lime and cement stabilized Ariake clays', *土木学会論文集*, no. 729, pp. 1-13.

Ouhadi, V & Yong, R 2003, 'The role of clay fractions of marly soils on their post stabilization failure', *Engineering geology*, vol. 70, no. 3-4, pp. 365-375.

Pan, H, Qing, Y & Pei-yong, L 2010, 'Direct and indirect measurement of soil suction in the laboratory', *Electronic Journal of Geotechnical Engineering*, vol. 15, no. 3, p. 1.

Popescu, M 1980, 'Behaviour of expansive soils with a crumb structure,' *Expansive Soils*, ASCE, 158-171.

Qiu, XM & Bian, HB 2013, 'Experimental study of remolded unsaturated soil subjected to wetting load under constant compression,' *Applied Mechanics and Materials*, Trans Tech Publ, 2657-2661.

Rafie, B, Moayed, RZ & Esmaeli, M 2008, 'Evaluation of soil collapsibility potential: A case study of Semnan railway station', *Electronic Journal of Geotechnical Engineering*, vol. 13, pp. 1-7.

Rajeev, P & Kodikara, J 2011, 'Numerical analysis of an experimental pipe buried in swelling soil', *Computers and Geotechnics*, vol. 38, no. 7, pp. 897-904.

Ramesh, H, Krishnaiah, A & Supriya, M 2012, 'Effect of Lime on the Compaction and Strength Behaviour of Red Earth treated with Mine tailings', *IOSR Journal of Mechanical and Civil Engineering (IOSRJMCE) ISSN*, pp. 2278-1684.

Richards, B, Peter, P & Emerson, W 1983, 'The effects of vegetation on the swelling and shrinking of soils in Australia', *Geotechnique*, vol. 33, no. 2, pp. 127-139.

Richards, B, Peter, P & Martin, R 1984, 'The determination of volume change properties in expansive soils,' *Fifth International Conference on Expansive Soils 1984: Preprints of Papers*, Institution of Engineers, Australia, pp. 179.

Ridley, A & Burland, J 1993, 'A new instrument for the measurement of soil moisture suction', *Géotechnique*, vol. 43, no. 2, pp. 321-4.

Ridley, A & Wray, W 1996, 'Suction measurement: a review of current theory and practices,' *Proceedings of the First International Conference on Unsaturated Soils/UNSAT'95/Paris/France/6-8 September 1995,* pp. 1293-1322.

Rogers, C & Roff, T 1997, 'Lime modification of clay soils for construction expediency', *Proceedings of the ICE-Geotechnical Engineering*, vol. 125, no. 4, pp. 242-249.

Romero Morales, E 1999, 'Characterisation and thermo-hydro-mechanical behaviour of unsaturated Boom clay: an experimental study', Universitat Politiecnica de Catalunya.

Santagiuliana, R & Schrefler, B 2006, 'Enhancing the Bolzon–Schrefler–Zienkiewicz constitutive model for partially saturated soil', *Transport in porous media*, vol. 65, no. 1, pp. 1-30.

Saride, S, Puppala, AJ & Chikyala, SR 2013, 'Swell-shrink and strength behaviors of lime and cement stabilized expansive organic clays', *Applied Clay Science*, vol. 85, pp. 39-45.

Schanz, T & Elsawy, MB 2015, 'Swelling characteristics and shear strength of highly expansive clay–lime mixtures: A comparative study', *Arabian Journal of Geosciences*, pp. 1-9.

Schofield, R 1935, 'The pF of the water in soil,' *Transactions of 3rd International Congress of Soil Science*, 37-48.

Seco, A, Ramírez, F, Miqueleiz, L & García, B 2011, 'Stabilization of expansive soils for use in construction', *Applied Clay Science*, vol. 51, no. 3, pp. 348-352.

Sharp, KD, Improvement, ASoCECoS & Geosynthetics 1993, *Fly ash for soil improvement: proceedings of sessions sponsored by Committees on Soil Improvement and Geosynthetics of the Geotechnical Engineering Division of the American Society of Civil Engineers in conjunction with the ASCE Convention in Dallas, Texas, October 24-28, 1993,* American Society of Civil Engineers.

Sheng, D, Fredlund, DG & Gens, yyA 2008, 'A new modelling approach for unsaturated soils using independent stress variables', *Canadian Geotechnical Journal*, vol. 45, no. 4, pp. 511-534.

Sheng, D & Zhou, A-N 2011, 'Coupling hydraulic with mechanical models for unsaturated soils', *Canadian Geotechnical Journal*, vol. 48, no. 5, pp. 826-840.

Shroff, AV 2003, *Soil Mechanics and Geotechnical Engineering,* Taylor & Francis.

Singh, D & Kuriyan, SJ 2003, 'Estimation of unsaturated hydraulic conductivity using soil suction measurements obtained by an insertion tensiometer', *Canadian Geotechnical Journal*, vol. 40, no. 2, pp. 476-483.

Sitharam, T, Sivapullaiah, P & Subba Rao, K 1995, 'Shrinkage behaviour of compacted unsaturated soils,' *Proceedings of the First International Conference on Unsaturated Soils/UNSAT'95/Paris/France/6-8 September 1995.* vol. 1, pp. 195-200.

Sivakumar, V, Sivakumar, R, Murray, E, MacKinnon, P & Boyd, J 2010, 'Mechanical behaviour of unsaturated kaolin (with isotropic and anisotropic stress history). Part 1: wetting and compression behaviour', *Géotechnique*, vol. 60, no. 8, pp. 581-594.

Sivakumar, V & Wheeler, SJ 2000, 'Influence of compaction procedure on the mechanical behaviour of an unsaturated compacted clay. Part 1: Wetting and isotropic compression', *Géotechnique*, vol. 50, pp. 359-368.

Songyu, L, Heyuan, L, Peng, J & Yanjun, D 1998, 'Approach to cyclic swelling behaviour of compacted clays,' *Proceedings of the 2nd International Conference on Unsaturated Soils, Beijing, China*, 219-225.

Stirk, G 1954, 'Some aspects of soil shrinkage and the effect of cracking upon water entry into the soil', *Crop and Pasture Science*, vol. 5, no. 2, pp. 279-296.

Subba Rao, K & Satyadas, G 1987, 'Swelling potential with cycles of swelling and partial shrinkage,' *6th Inter. Conf. Expansive soils*, 137-142.

Sukmak, P, Horpibulsuk, S & Shen, SL 2013a, 'Strength development in clay-fly ash geopolymer', *Construction and Building Materials*, vol. 40, pp. 566-574.

Sukmak, P, Horpibulsuk, S, Shen, SL, Chindaprasirt, P & Suksiripattanapong, C 2013b, 'Factors influencing strength development in clay-fly ash geopolymer', *Construction and Building Materials*, vol. 47, pp. 1125-1136.

Sun, DA, Matsuoka, H & Xu, YF 2004, 'Collapse behavior of compacted clays in suction-controlled triaxial tests', *Geotechnical Testing Journal*, vol. 27, no. 4, pp. 362-370.

Tadepalli, R & Fredlund, DG 1991, 'The collapse behavior of a compacted soil during inundation', *Canadian Geotechnical Journal*, vol. 28, no. 4, pp. 477-488.

Tarantino, A & Col, ED 2008, 'Compaction behaviour of clay', *Géotechnique*, vol. 58, pp. 199-213.

Tarantino, A & Mongiovì, L 2001, 'Experimental procedures and cavitation mechanisms in tensiometer measurements', in *Unsaturated Soil Concepts and Their Application in Geotechnical Practice*, Springer, pp. 189-210.

Tarantino, A, Romero, E & Cui, YJ 2009, *Laboratory and field testing of unsaturated soils,* Amsterdam, The Netherlands, Springer.

Tarantino, A & Tombolato, S 2005, 'Coupling of hydraulic and mechanical behaviour in unsaturated compacted clay', *Geotechnique*, vol. 55, no. 4, pp. 307-317.

Thompson, M 1968, 'Lime stabilization of soils for highway purposes', *Ill Univ Hwy Res Lab Civil Eng Studies*.

Tripathy, S, Subba Rao, KS & Fredlund, DG 2002, 'Water content - Void ratio swell-shrink paths of compacted expansive soils', *Canadian Geotechnical Journal*, vol. 39, no. 4, pp. 938-959.

UMS 2010, *Infield 7-Operation manual* [online], viewed <http://www.ums-muc.de/assets-ums/00E0L.pdf>.

UMS 2013, *Hyprop-Laboratory evaporation method for the determination of pF-curves and unsaturated conductivity*, [Online], viewed <http://www.ums-muc.de/en/products/soil_laboratory/hyprop.html. [Accessed 08-29- 2014]>.

UMS 2015, *Hyprop-Operational manual*, [online], viewed <https://tp.dresden-concept.de/userdata/e2e7fda78c954ee94c5e2c4a81b07326.pdf. [Accessed 28-02-2017]>.

Viswanadham, BVS, Phanikumar, BR & Mukherjee, RV 2009, 'Swelling behaviour of a geofiber-reinforced expansive soil', *Geotextiles and Geomembranes*, vol. 27, no. 1, pp. 73-76.

Warkentin, BP & Bozozuk, M 1961, 'Shrinking and swelling properties of two Canadian clays-Propriétés de retrait et de gonflement de deux argiles canadiennes', *Technical Memorandum, Division of Building Research, National Research Council Canada*, no. 72-7, pp. 1-5.

Wheeler, S, Sharma, R & Buisson, M 2003, 'Coupling of hydraulic hysteresis and stress–strain behaviour in unsaturated soils', *Géotechnique*, vol. 53, no. 1, pp. 41-54.

Wheeler, SJ & Sivakumar, V 1995, 'An elasto-plastic critical state framework for unsaturated soil', *Géotechnique*, vol. 45, pp. 35-53.

Yi, Y, Li, C & Liu, S 2015, 'Alkali-Activated Ground-Granulated Blast Furnace Slag for Stabilization of Marine Soft Clay', *Journal of Materials in Civil Engineering,* vol 27, no. 4: 04014146, *DOI: 10.1061/(ASCE)MT.1943-5533.0001100*.

Yilmaz, I & Civelekoglu, B 2009, 'Gypsum: An additive for stabilization of swelling clay soils', *Applied Clay Science*, vol. 44, no. 1–2, 4, pp. 166-172.

Yong, RN & Ouhadi, VR 2007, 'Experimental study on instability of bases on natural and lime/cement-stabilized clayey soils', *Applied clay science*, vol. 35, no. 3-4, pp. 238-249.

Yunus, NM, Wanatowski, D & Stace, L 2011, 'Effect of humic acid on physical and engineering properties of lime-treated organic clay', *Engineering and Technology*, vol. 59, no. 201, pp. 1.

Zhang, X & Lytton, RL 2008, 'Discussion of “A new modelling approach for unsaturated soils using independent stress variables” Appears in Canadian Geotechnical Journal, 45 (4): 511–534', *Canadian Geotechnical Journal*, vol. 45, no. 12, pp. 1784-1787.

Zhang, X & Lytton, RL 2009, 'Modified state-surface approach to the study of unsaturated soil behavior. Part I: Basic concept', *Canadian Geotechnical Journal*, vol. 46, no. 5, pp. 536-552.

Zhao, H, Ge, L, Petry, TM & Sun, Y-Z 2014a, 'Effects of chemical stabilizers on an expansive clay', *KSCE Journal of Civil Engineering*, vol. 18, no. 4, pp. 1009-1017.

Zhao, H, Liu, J, Guo, J, Zhao, C & Gong, B 2014b, 'Reexamination of Lime Stabilization Mechanisms of Expansive Clay', *Journal of Materials in Civil Engineering*, pp. 7.